Physical Experiments and Numerical Modeling to Determine Critical Requirements for Monitored Natural Attenuation of Methyl tert-Butyl Ether

Illa Lyn Amerson
B.S. Massachusetts Institute of Technology
M.S. Arizona State University

A dissertation presented to the faculty of the
OGI School of Science & Engineering
at Oregon Health & Science University
in partial fulfillment of the
requirements for the degree
Doctor of Philosophy
in
Environmental Science and Engineering

August 2002

The dissertation "Physical Experiments and Numerical Modeling to Determine Critical Requirements for Monitored Natural Attenuation of Methyl tert-Butyl Ether" by Illa Lyn Amerson has been examined and approved by the following Examination Committee:

Dr. Richard L. Johnson, Thesis Advisor
Associate Professor

Dr. Patricia L. Toccalino
Assistant Professor

Dr. Paul G. Tratnyek
Associate Professor

Dr. John T. Wilson
U.S. Environmental Protection Agency

DEDICATION

To my father, with whom I gladly share this degree

We are both doctors now.

To my mother, the first (and still the best) teacher I ever had

ACKNOWLEDGMENTS

Many people have shaped my experience here at OGI. First, I must thank my advisor, Rick Johnson, for providing the opportunity to pursue this research as well as his financial and professional support along the way. I would also like to thank my committee, Patty Toccalino, Paul Tratnyek, and John Wilson for the time, energy, and many valuable insights they contributed to this work.

The American Petroleum Institute Soil and Groundwater Technical Task Force provided funding and guidance for the Large Experimental Aquifer Program study and the natural gradient tracer test at Port Hueneme, California. The staff at the Naval Facilities Engineering Service Center at Ventura Naval Base, Port Hueneme, California provided critical logistical support for the tracer test. I would like to thank Karen Miller, Dorothy Cannon, and James Osgood, in particular.

I am grateful to the ESE staff for helping in so many ways over the last four years. Lorne Isabelle helped solve countless problems with the GC/MS. Linda Wolf and Therese Young guided me through OGI administrative procedure flawlessly. Jim Mohan saved my computer from itself on several occasions, a huge contribution during the dissertation days. Thank you all.

My fellow students in ESE and throughout OGI have made my experience here both challenging and fun. Thank you for your insights, camaraderie, laughter, and encouragement. To my friends among the students, staff, and faculty, thank you for all of the support from beginning to end.

Finally, I want to acknowledge my parents for so many years of patience, energy, time, and support without which this goal would have been unreachable.

TABLE OF CONTENTS

LIST OF TABLES

LIST OF FIGURES

ABSTRACT

Physical Experiments and Numerical Modeling to Determine Critical Requirements for Monitored Natural Attenuation of Methyl tert-Butyl Ether

Illa Lyn Amerson B.S., M.S.

Ph.D., OGI School of Science & Engineering
at Oregon Health & Science University

August 2002

Thesis Advisor: Dr. Richard L. Johnson

Methyl tert-butyl ether (MTBE) is a common fuel additive found in oxygenated gasoline at concentrations up to 15% by volume. Releases of oxygenated fuels from underground storage tanks have resulted in MTBE becoming a potentially long-term groundwater contamination problem because the compound is more soluble, more mobile, and slower to degrade than other gasoline constituents of concern. This is significant because corrective actions for MTBE-containing releases may necessarily differ from those used for other gasoline constituents. This is particularly true for monitored natural attenuation (MNA), an approach that relies on demonstrating that naturally occurring processes such as dispersion, sorption, and biodegradation will control and mitigate groundwater contamination.

Physical experiments and numerical modeling have been conducted to identify and quantify the critical components of MTBE behavior as it relates to MNA and determine what data must be collected to illuminate that behavior. The work presented here includes a three-dimensional dissolution study, a natural gradient tracer test, and numerical modeling. The dissolution study began with a gasoline spill of known composition and volume and monitored the evolution of the dissolved plume through water table fluctuations and flow through the source. The natural gradient tracer test involved a dissolved plume of perdeuterated-MTBE and demonstrated the influence of

dominant flow paths and heterogeneity on plume structure and migration. The numerical modeling began with the simple scenario of a constant source in a homogeneous aquifer. Subsequent scenarios added increasing complexity in hydrogeology and source function to identify factors that complicate the demonstration of natural attenuation of MTBE. Analysis of the experimental and modeling results identified tracer compounds, the source function, hydrogeology, and the sampling network as critical factors for monitored natural attenuation of MTBE and quantified their respective impacts on making an effective demonstration that natural attenuation is occurring.

CHAPTER 1
INTRODUCTION

1.1 Overview

Methyl *tert*-butyl ether (MTBE) has become increasingly prevalent as a fuel additive beginning in the late 1970s. Originally, MTBE was used at low concentration (1-3% by volume) to replace alkyl lead compounds as an octane enhancer. The oxygenated fuels and reformulated gasoline programs mandated under the Clean Air Amendments of 1990 have increased those concentrations in gasoline to 10-15% by volume in areas using MTBE. Releases of oxygenated gasoline from underground storage tanks have now made MTBE a critical and pervasive groundwater contaminant and a long-term problem (Johnson et al. 2000). This is due in part to its prevalent use and in part to its chemical properties. MTBE is more soluble, slower to degrade, and more mobile in the subsurface compared to other gasoline constituents such as benzene, toluene, ethylbenzene, and the xylenes (BTEX) (Squillace et al. 1997). This is significant because corrective actions for MTBE-containing releases may necessarily differ from those used for other gasoline constituents. This is particularly true for monitored natural attenuation (MNA). Because of MTBE's current usage and potential future impacts on water resources (Johnson et al. 2000), it is necessary to evaluate the role of natural attenuation of MTBE.

The U.S. Environmental Protection Agency (USEPA) defines natural attenuation processes as those that "act without human intervention to reduce the mass, toxicity, mobility, volume, or concentration of contaminants in soil or groundwater" including "biodegradation, dispersion, dilution, sorption, volatilization, radioactive decay, and chemical or biological stabilization, transformation, or destruction of contaminants" (USEPA 1999). MNA is

appropriate at a site when characterization and ongoing groundwater monitoring data can be used to demonstrate that contaminant plumes are being controlled or mitigated by these naturally occurring processes.

Monitored natural attenuation has become a popular component of groundwater restoration strategies. Several standards and protocols have been written to address MNA for petroleum hydrocarbons (ASTM 1998, AFCEE 1995, USEPA 1999). The Air Force Center for Environmental Excellence (AFCEE) has also prepared a report for MNA of MTBE that draws heavily on its petroleum hydrocarbon protocol (AFCEE 1999). In general, these approaches follow the lines of evidence outlined by the National Research Council (NRC): 1) demonstrated loss of contaminants of concern, 2) geochemical indicators of degradation and/or estimated attenuation rates, and 3) microbiological data and/or assimilative capacity estimates. Specific demonstration methods include concentration versus time data, contour maps, attenuation rates, changes in geochemical indicators, and reaction by-product formation (ASTM 1998, USEPA 1999).

While these lines of evidence are valid for MNA of MTBE, their application to MTBE may require more complex sampling networks, more time, and more expense to demonstrate. In the case of MTBE, the degradation rate may be slow enough that plume expansion due to advective transport could mask any losses due to degradation. Other hydrocarbons present in gasoline plumes (e.g. BTEX) will likely be degraded before MTBE, causing changes in geochemical indicators such as DO, sulfate, or methane concentrations. In such a case, it may be difficult to differentiate a geochemical signal due to upgradient BTEX degradation from local MTBE degradation. The main MTBE degradation by-product, tert-butyl alcohol (TBA), is often present in oxygenated fuels as well and cannot confirm degradation assuming TBA degrades slower than MTBE. For these reasons, MTBE poses unique challenges to identifying natural attenuation and implementing MNA.

The latest recommendations from the NRC concerning natural attenuation (NRC 2000) as a groundwater-remediation strategy have significant implications for all contaminants but will place particularly high demands for site-specific knowledge on demonstrations involving MTBE. According to their

recommendations, MNA should be considered acceptable only when a biotransformation or immobilization mechanism is scientifically recognized, is documented to be working, and is sustainable until remediation is complete. Furthermore, the recommendations are more focused on direct field evidence of contaminant degradation rather than evidence that merely suggests contaminant degradation in the field. Considering the site knowledge and supporting data required to meet these recommendations, a conceptual model of MNA of MTBE was an important addition to our scientific knowledge and a key step to evaluating the future role of MNA in addressing MTBE plumes.

1.2 Fate and Transport Mechanisms

Dissolution from a residual gasoline source, advection, dispersion, sorption, and biodegradation will control the migration of MTBE plumes. It is the interaction of these processes that ultimately determines the longevity and complexity of contaminant plumes and whether they expand, stabilize, or shrink over time.

1.2.1 Dissolution

In areas where oxygenated fuels are used, MTBE frequently has the highest concentration of any component in gasoline on a volume/volume basis. It is also considerably more water-soluble than other chemicals present in gasoline. Table 1.1 gives an example of volume fraction and solubility data for several constituents of a well-characterized oxygenated gasoline. Given the relatively high percentage of MTBE in oxygenated fuels and its high relative solubility, the dissolution of MTBE from gasoline source zones is a key factor affecting the development and attenuation of MTBE plumes. It follows, therefore, that understanding the role of dissolution from the source is critical to implementing an MNA protocol for MTBE.

The aqueous concentration of MTBE in equilibrium with residual gasoline is related to its fraction in the gasoline. The equilibrium water solubility (C_s) of MTBE can be calculated from equation (1.1) where γ is the activity coefficient of MTBE in gasoline, X_m is the mole fraction of MTBE and c_s^0 is the pure compound solubility in water.

$$C_s\ (mg/L) = \gamma X_m c_s^0 \qquad (1.1)$$

The activity coefficient for MTBE in gasoline has been reported to be close to 1 (Barker et al. 1991). Using the example fuel in Table 1.1, the expected equilibrium aqueous concentration of MTBE is on the order of 5000 mg/L.

Table 1.1: Representative Volume Fraction and Solubility Data for Oxygenated Gasoline Components

Compound	% of Gasoline by Volume	Pure-Phase Solubility in Water (mg/L)
MTBE[a]	11.09	43,000 - 54,300
Benzene[b]	0.79	1,000 – 2,170
Toluene[b]	5.91	485.6 – 616
Hexane[b]	2.40	12.3 – 16.2
1,2,4-trimethylbenzene[b]	2.53	50.3 – 58.8
Isooctane[b]	1.77	1.36 – 2.29

[a]Howard et al. 1991; [b]Montgomery et al. 1996

Despite the theoretical possibility of achieving this aqueous concentration, field observations are typically more than an order of magnitude lower.

1.2.2 Advection and Dispersion

Advection drives bulk fluid flow in the subsurface. The average linear velocity at which a contaminant moves depends on the hydraulic conductivity of the medium (K), the gradient (the change in elevation per unit length, dh/dL), and the effective porosity (i.e., the porosity through which water can flow, n_e). For field-scale problems, it is often convenient to use average properties for these values to estimate a velocity. With respect to evaluating natural attenuation and implementing a monitoring program, however, it is important to recognize that each of the dependent parameters can change substantially with location at a site. For example, K can vary spatially in lenses of different types of material. Gradients can vary seasonally in both magnitude and direction as seen at a site in Elizabeth City, NC (USEPA 2000). Of these parameters, varying K will have the greatest impact on plume characteristics and the process of assessing natural attenuation.

Dispersion causes the aqueous plume to spread longitudinally, laterally, and vertically as it moves downgradient due to advective transport. Dispersion results from velocity variations at several scales caused by heterogeneity in the subsurface medium. At the microscopic scale, dispersion occurs due to varying path lengths in soil pores. Macroscale dispersion is caused by differing K values in soil layers or regions of differing soil type as seen in Sudicky (1986). Regional or dominant site-specific features are responsible for megascale dispersion. The contributions of all three scales cause contaminant plumes to develop increasingly complex structures as they travel.

1.2.3 Sorption

Sorption of contaminants onto aquifer materials generally serves as a means of retarding the bulk transport of organic contaminants. Gasoline-derived contaminants partition from the aqueous phase onto organic material associated with most aquifer materials. The process is reversible so migration is not stopped but merely slowed by sorption. The extent to which this occurs depends on the partitioning coefficient, K_d, which relates the equilibrium concentration of sorbed contaminant to dissolved contaminant. K_d is estimated as $K_d = f_{oc}*K_{oc}$ where f_{oc} is the fraction of organic carbon in the medium and K_{oc} is the organic carbon partition coefficient (Squillace et al. 1997). K_{oc} in turn can be estimated from chemical properties such as octanol-water partitioning coefficients or solubility data. Sorption, therefore, is dependent on both the subsurface environment and the chemical properties of the contaminants.

The effect of sorption on contaminant migration can be expressed using a retardation factor, $R=1+(\rho_b K_d/n)$, where ρ_b is the bulk solid density, n is the porosity, and K_d is as above. The velocity of the contaminant then becomes $v_c = v_x/R$, indicating that the contaminant travels slower than the bulk fluid (Domenico and Schwartz 1998). The K_{oc} value of MTBE is ~11 (Squillace et al., 1997). Using f_{oc} = 0.001 for a sand aquifer, the retardation factor for MTBE is calculated to be ~1, indicating that it essentially moves at the velocity of the groundwater. This value was confirmed in the Borden aquifer, Ontario, Canada where R=1.01 for MTBE

(versus 1.1 for benzene). This becomes more significant given the previous discussion of dispersion. It follows that if dispersion is proportional to velocity, a contaminant that travels faster will be more impacted by dispersion and the plume complexities associated with it.

1.2.4 Biodegradation

Because biodegradation is a mass-reducing mechanism, the biodegradability of MTBE has received much research attention, both in the context of MNA and as a key to engineered remediation solutions. Several researchers have demonstrated aerobic degradation of MTBE in microcosm studies using natural aquifer or stream-bed sediments (Schirmer et al., 1999, Bradley et al., 2001). Salanitro et al. (1994) and Hanson et al. (1999) report the isolation of two distinct bacteria capable of degrading MTBE under aerobic conditions. Church et al. (1999) also demonstrated aerobic degradation of MTBE using model column aquifers. Two additional findings are common among these studies. In general, MTBE degradation lagged until other sources of organic carbon (including BTEX) were removed. In addition, these researchers saw little to no degradation under anaerobic conditions.

Despite those findings, anaerobic degradation mechanisms are suggested by a few microcosm studies under specific environmental conditions. Mormile et al. (1994) saw partial (but limited) degradation of MTBE under nitrate-reducing concentrations in one microcosm. Yeh and Novak (1994) saw anaerobic degradation at one of three sites investigated and suggested that it was pH dependent. Anaerobic degradation was seen in soil microcosms from Elizabeth City, NC (USEPA 2000) under methanogenic conditions. Finneran and Lovley (2001) recently reported anaerobic degradation of MTBE in microcosms amended with humic substances when Fe(III) was present.

In the majority of the aerobic and anaerobic studies, tert-butyl alcohol (TBA) was observed as a degradation product. Presumably, TBA could be used as an indicator of MTBE degradation in an MNA protocol. Unfortunately, TBA is also used as a fuel oxygenate and is a by-product of MTBE synthesis so its presence at a

site could be from source-zone contamination as well as degradation of MTBE. More recent work by Hunkeler (2001) has focused on using compound-specific carbon isotope analysis to differentiate sources of MTBE and its degradation products. This technique has potential applications in MNA as a means of demonstrating whether or not observed TBA is a degradation product.

1.3 Research Objectives and Experimental Approach

The objectives of this work were to identify the critical components of MTBE behavior as it relates to MNA and determine what data must be collected to illuminate that behavior. The work presented here includes a three-dimensional dissolution study, a natural-gradient tracer test, and numerical modeling. The dissolution study began with a gasoline spill of known composition and volume and monitored the evolution of the dissolved plume through water-table fluctuations and flow through the source. The natural gradient tracer test involved a dissolved plume of perdeuterated-MTBE and demonstrated the influence of dominant flow paths and heterogeneity on plume structure and migration. The numerical modeling began with the simple scenario of a constant source in a homogeneous aquifer. Subsequent scenarios added increasing complexity in hydrogeology and source function to identify factors that complicate the demonstration of natural attenuation of MTBE. The knowledge gained through the experiments and modeling are then brought together in an analysis of MNA of MTBE for the complex simulated site to identify critical knowledge gaps.

1.4 Organization

The thesis is presented in five chapters corresponding to the experimental approach described above. Specifically, the contents are:

- Chapter 2 – A natural gradient tracer test that examined natural attenuation of MTBE in an existing gasoline plume under anaerobic conditions.
- Chapter 3- A numerical modeling study to illuminate critical knowledge gaps through increasingly complex site scenarios.

- Chapter 4 - Dissolution of MTBE from a residual gasoline source in an Oregon Health & Science University (OHSU) Large Experimental Aquifer Program (LEAP) three-dimensional physical model.
- Chapter 5 – An analysis of MNA of MTBE in the complex modeling scenario given common techniques and field limitations.

1.5 References

ASTM. 1998. Standard Guide for Remediation of Groundwater by Natural Attenuation at Petroleum Release Sites. ASTM E 1943 – 98. American Society for Testing and Materials, West Conshohocken, PA.

AFCEE. 1995. Technical Protocol for Implementing Intrinsic Remediation with Long-Term Monitoring for Natural Attenuation of Fuel Contamination Dissolved in Groundwater. Air Force Center for Environmental Excellence, Technology Transfer Division. San Antonio, TX. Available: http://www.afcee.brooks.af.mil/er/ert/techprotocols.htm [Viewed: August 20, 2002]

Barker, J.F., R.W. Gillham, L. Lemon, C.I. Mayfield, M. Poulson, and E.A. Sudicky. 1991. Chemical Fate and Impact of Oxygenates in Groundwater: Solubility of BTEX from Gasoline-Oxygenate Compounds. Publication 4531. American Petroleum Institute. Washington, DC.

AFCEE. 1999. Methyl *tert*-Butyl Ether (MTBE) Its Movement and Fate in the Environment and Potential for Natural Attenuation. Air Force Center for Environmental Excellence, Technology Transfer Division. San Antonio, TX. Available: http://www.afcee.brooks.af.mil/er/ert/natural.htm [Viewed: August 20, 2002]

Bradley, P.M., J.E. Landmeyer, and F.H. Chappelle. 2001. Widespread Potential for Microbial MTBE Degradation in Surface-Water Sediments. *Environmental Science and Technology*. 35(4):658-662.

Church, C.D., P.G. Tratnyek, J.F. Pankow, J.E. Landmeyer, A.L. Baehr, M.A. Thomas, and M. Schirmer. 1999. Effects of Environmental Conditions on MTBE Degradation in Model Column Aquifers. *Proceedings*, U.S. Geological Survey, Toxic Substances Hydrology Program Technical Meeting, Charleston, SC, March 7-12, 1999. pp. 93-101.

Domenico, P.A. and F.W. Schwartz. 1998. *Physical and Chemical Hydrogeology*. John Wiley & Sons, Inc. New York City, NY.

Finneran, K.T. and D.R. Lovley. 2001. Anaerobic Degradation of Methyl *tert*-Butyl Ether (MTBE) and *tert*-Butyl Alcohol (TBA). *Environmental Science and Technology*. 35(9):1785-1790.

Hanson, J.R., C.E. Ackerman, and K.M. Scow. 1999. Biodegradation of Methyl *tert*-Butyl Ether by a Bacterial Pure Culture. *Applied and Environmental Microbiology.* 65(11): 4788-4792.

Howard, P.H., G.W. Sage, W.F. Jarvis, and D.A. Gray. 1991. *Handbook of Environmental Fate and Exposure Data for Organic Chemicals.* Vol. 2. Lewis, Chelsea, MI.

Hunkeler, D., B.J. Butler, R. Aravena, and J.F. Barker. 2001. Monitoring Biodegradation of Methyl *tert*-Butyl Ether (MTBE) Using Compound-Specific Carbon Isotope Analysis. *Environmental Science and Technology.* 35(4): 676-681.

Johnson, R.L., J. Pankow, D. Bender, C. Price, and J. Zogorski. 2000. MTBE, To What Extent Will Past Releases Contaminate Community Supply Wells? *Environmental Science and Technology.* 34(9):210A-216A.

Montgomery, J.H. 1996. *Groundwater Chemicals Desk Reference.* CRC Press, Inc., New York City, NY.

Mormile, M.R, S. Liu, and J.M. Suflita. 1994. Anaerobic Biodegradation of Gasoline Oxygenates: Extrapolation of Information to Multiple Sites and Redox Conditions. *Environmental Science and Technology.* 28(9): 1727-1732.

Salanitro, J.P., L.A. Diaz, M.P. Williams, and H.L. Wisniewski. 1994. Isolation of a Bacterial Culture the Degrades Methyl *t*-Butyl Ether. *Applied Environmental Microbiology.* 60: 2593-2596.

Schirmer, M., B.J. Butler, J.F. Barker, C.D. Church, and K. Schirmer. 1999. Evaluation of Biodegradation and Dispersion as Natural Attenuation Processes of MTBE and Benzene at the Borden Field Site. *Physics and Chemistry of the Earth, Part B: Hydrology, Oceans & Atmosphere.* 24(6): 557-560.

Squillace, P.J., J.F. Pankow, N.E. Korte, and J.S. Zogorski. 1997. Review of the Environmental Behavior and Fate of Methyl *tert*-Butyl Ether. *Environmental Toxicology and Chemistry.* 16(9): 1836-1844.

Sudicky, E.A. 1986. A Natural Gradient Experiment on Solute Transport in a Sand Aquifer: Spatial Variability of Hydraulic Conductivity and Its Role in the Dispersion Process. *Water Resources Research.* 22(13): 2069-2082.

USEPA. 1999. *Use of Monitored Natural Attenuation at Superfund, RCRA Corrective Action, and Underground Storage Tank Sites.* Directive 9200.4-17P. U.S. Environmental Protection Agency, Office of Solid Waste and Emergency Response.

USEPA. 2000. *Natural Attenuation of MTBE in the Subsurface under Methanogenic Conditions.* Research Report. EPA 600/R-00/006. U.S. Environmental Protection

Agency, National Risk Management Research Laboratory, Office of Research and Development, Cincinnati, OH.

Yeh, C.K. and J.T. Novak. 1994. Anaerobic Biodegradation of Gasoline Oxygenates in Soils. *Water Environment Research.* 66(5): 744-752.

CHAPTER 2

A NATURAL GRADIENT TRACER TEST TO EVALUATE NATURAL ATTENUATION OF A DISSOLVED MTBE PLUME UNDER ANAEROBIC CONDITIONS

2.1 Introduction

A key aspect of demonstrating natural attenuation is to quantify field attenuation rates and specifically field degradation rates. Laboratory studies conducted using discrete soil samples and groundwater from a site can provide degradation-rate information as well as mechanisms and daughter products, but these are not directly transferable to field conditions. Several field studies have been conducted to quantify field attenuation and degradation rates for MTBE and to assess its behavior relative to BTEX. A variety of techniques have been used including monitoring of a plume footprint and distribution of concentrations (Schirmer and Barker 1998, Landmeyer et al. 1998, Pavne et al. 1997), determining mass flux past "fences" installed perpendicular to groundwater flow (Borden et al. 1997), and concentration changes along longitudinal transects (USEPA 2000).

Although field-degradation rates were estimated, these studies demonstrated some of the complicating factors inherent in plume studies. For example, changes in groundwater velocity, hydrogeology and water table elevation were often documented. Such changes impact not only the actual plume structure but also the data provided by sampling networks. Over several years of plume monitoring, Landmeyer et al. (1998) documented substantial changes to BTEX and MTBE distribution. Although the aquifer they studied was naturally aerobic, they ultimately concluded that reductions in MTBE concentrations were due to dilution and dispersion rather than degradation. Other than the Schirmer and Barker study, the field examples listed above resulted from accidental leaks or spills, allowing only

estimation of the initial volume and composition of the sources. In all cases, TBA was not useful as indicator of degradation, either due to its suspected presence in the original gasoline or its absence from the groundwater altogether.

Natural gradient tracer tests involve letting a tracer travel with the flow of groundwater at a site and provide a solution to some of the complications in plume studies. Natural gradient tracer tests have been used by researchers to investigate physical transport processes (Julian et al. 2001, Boggs et al. 1992, Sudicky 1986) as well as chemical fate (Schirmer and Barker 1998). They are particularly useful because they yield field-scale data on specific fate and transport processes, given tracers with known properties and initial concentrations. Tracer tests can illustrate hydrogeologic features that may be difficult and resource intensive to determine with discrete approaches, such as localized gradients or geologic features. Using a combination of tracers, changes in concentration due to dilution, sorption, dispersion, or volatilization can be differentiated from the effects of biodegradation. Given the importance and challenge of estimating field attenuation rates, natural gradient tracer tests in different hydrogeologic and geochemical environments can provide a database of field information on natural attenuation to supplement laboratory measurements and plume studies on accidental releases.

In the natural gradient tracer test described here, aqueous perdeuterated MTBE ($^2H_{12}$-MTBE) tracer was added into an existing, anaerobic MTBE-containing groundwater plume. Known initial tracer conditions and detailed sampling after one year of transport provided a clear assessment of the advection, dispersion, and degradation of the $^2H_{12}$-MTBE tracer under sulfate-reducing conditions. The results of this study illustrated important considerations for implementing MNA for MTBE.

2.2 Study Location and Characterization

The tracer test was conducted at the United States Naval Base Ventura County, Port Hueneme Site, Port Hueneme, CA, an active military base located approximately 60 miles (96 km) north of Los Angeles, CA. The base is underlain by three distinct hydrogeologic units. An upper unit extending from 0-3 m below

ground surface (bgs) is fine-grained, clayey-silt which was added as fill across much of the base. The bottom 0.3-m of this unit is typically water saturated. An intermediate unit extending from 3-6 m bgs is fine- to medium-grained sand. Below ~6-7 m bgs is an underlying silty-clay unit (Salanitro et al., 2000). Recent data suggest that coarser sands exist just above the contact with the silty-clay layer in some parts of the aquifer (Johnson 2002). The tracer study took place in the semi-perched fine to medium sand aquifer at 3-6 m bgs. The regional hydraulic gradient was approximately 0.003 m/m and groundwater flows to the southwest at a rate of approximately 0.3 m/day.

An existing plume of BTEX and MTBE-impacted groundwater resulted from a gasoline release from the Navy Exchange (NEX) service station around 1984. The plume, as delineated by wells and direct-push sampling, is long and narrow and extends approximately 1.5 kilometers downgradient from the source. Contaminant concentrations suggest that residual non-aqueous phase liquid (NAPL) is still present at this site. The dissolved plume can be divided into two areas: one area where both BTEX and MTBE are present and one where MTBE is the sole contaminant of concern.

Dissolved oxygen concentrations at this site are naturally low and generally measure <2 mg/L inside and outside the NEX plume. Groundwater at the site is pH neutral (average pH of 6.9 in measurements taken for this study). The aquifer has a noticeable salt content with chloride and sulfate concentrations exceeding 50 mg/L and 500 mg/L, respectively.

2.3 Experimental

2.3.1 Cross-Gradient Sampling Transect

A cross-gradient sampling transect through the existing plume (shown on Figure 2.1) was completed using a Geoprobe® to characterize hydraulic conductivity (K), contaminant concentrations, and geochemical conditions prior to the tracer test. K measurements were used to locate an area of higher values in which to inject the tracer plume. Contaminant concentrations, as well as presence/absence of sheen on the samples, were needed to help differentiate between

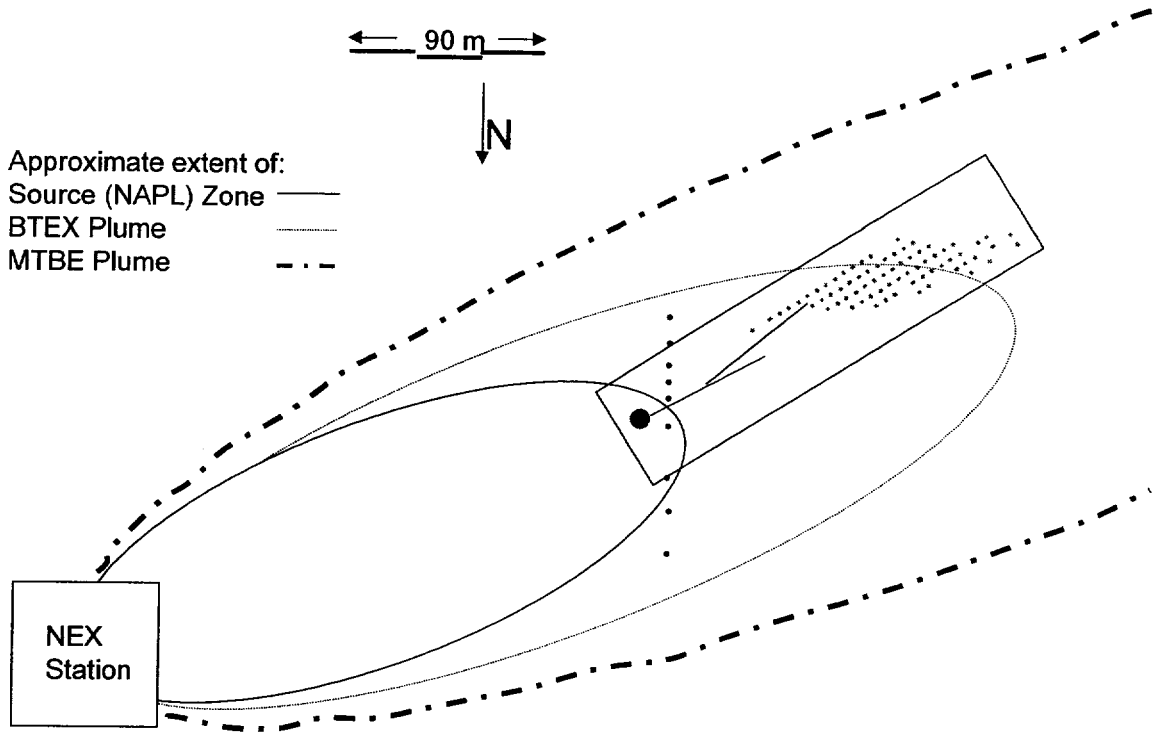

(a)

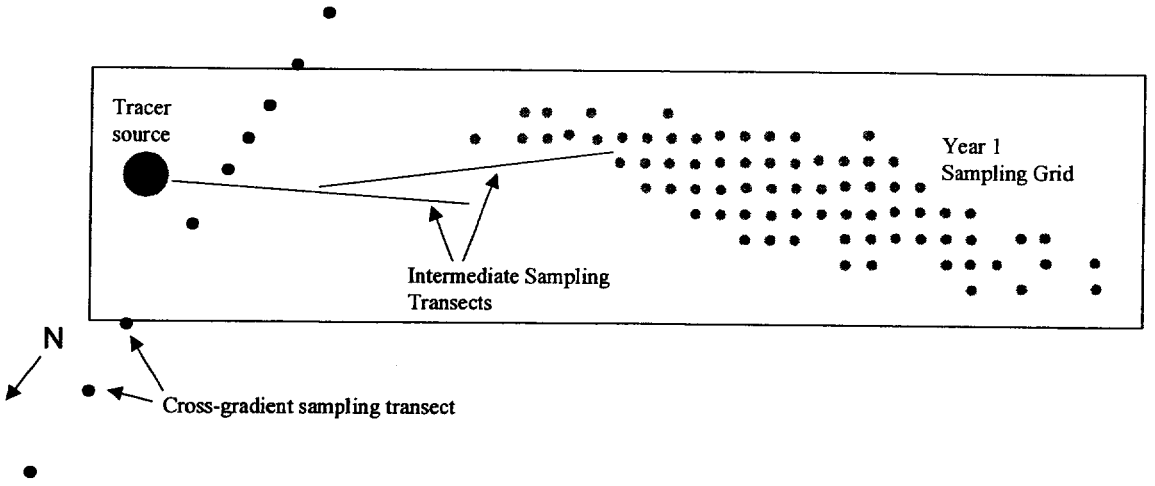

(b)

Figure 2.1: (a) Schematic of Port Hueneme Plume, Tracer Source, and Sampling Points, (b) Close up of Sampling Points

the source zone and dissolved plume, which were adjacent to each other in the area desired for the tracer test. Geochemical data were used to understand the groundwater characteristics at the chosen injection location.

2.3.1.1 Groundwater Characteristics

Groundwater sampling was conducted prior to the K measurements in order to collect samples that were not affected by water introduced during the slug tests. At each transect location, a Geoprobe® equipped with ¾" rod was used to push a stainless steel sampling tip with a 10 cm screened interval to the desired depth. Sampling locations were at 0.5-m vertical intervals from 3 m to 6 m bgs. At each location, dissolved oxygen and pH were measured by pumping water at a low flow rate through a flow-through cell equipped with microelectrodes in series attached to a digital voltmeter. Measurements were recorded once the readings stabilized, which indicated that ambient conditions had been reached at that location. The tubing was then disconnected from the flow-through cell and samples for chemical analysis were collected in triplicate in 40-ml volatile organic analysis (VOA) vials with Teflon coated septa.

MTBE and BTEX were analyzed on-site using an SRI 8610C gas chromatograph/flame ionization detector (GC/FID) with a 15-m Restek MXT-1 column. The temperature program was: initial temperature 45°C; ramp at 10°C/minute to 150°C. Standard solutions contained MTBE, benzene, toluene, ethylbenzene, m-, p-, and o-xylene. Standards and samples were prepared by transferring 10-mL of water from the sample vial to a clean VOA and injecting 500 µL of the resulting headspace onto the column after shaking for approximately 30 seconds. Response factors were determined based on aqueous concentration. m- and p-xylene could not be separated and were recorded as a single concentration.

Several ions were measured to determine redox conditions and available electron acceptors at the site. Ferrous iron [Fe(II)] was determined by the phenanthroline method using a Hach field colorimeter. A standard 1 mg-Fe(II)/L solution prepared by Hach was used to calibrate the colorimeter. For each standard and sample, a 5-mL volume of solution was placed in the reaction vial with a pre-

measured amount of powdered reagent and left to react for 2 minutes before being analyzed. A distilled water blank was used to zero the colorimeter before each standard or sample measurement. Samples with Fe(II) concentrations exceeding 5 mg/L required dilution to stay within the method range. In this case, samples were diluted to 20% strength with distilled water before the reaction and measurement steps. Particulate matter was allowed to settle before colorimetric analysis.

Nitrate, sulfate, and chloride were analyzed on a Dionex DX 500 Ion Chromatograph (IC) at Arizona State University within two weeks of sample collection. The IC is equipped with an Ionpac® AS12A analytical column, Ionpac® AG12A guard column, and ECD. The IC utilizes a 2.7 mM sodium carbonate/0.3 mM sodium bicarbonate mobile phase. Standard solutions contained nitrate, sulfate, and chloride in distilled water. The response factor was determined based on aqueous concentration.

2.3.1.2 Hydraulic Conductivity

Hydraulic conductivity was measured using the apparatus shown in Figure 2.2. The water reservoir was connected to a ¾" Geoprobe® rod ending in a stainless-steel tip with a 10-cm screened interval. The in-line pressure transducer at the bottom of the water reservoir was used to monitor the change in head with time. The transducer signal was measured at known hydraulic heads to calibrate the output prior to starting K measurements. At each location, the Geoprobe® was used to advance the tip to the desired depth and the apparatus was attached to the top of the rod.

Before each test, the valve to the pump was opened and groundwater was pumped into the reservoir from the depth to be tested. This allowed the full length of the rod and apparatus to be filled with water so the pressure change reflected flow to the aquifer only. If the point did not yield water readily, groundwater was supplemented with distilled water. When the water reservoir was full, the pump was stopped. The datalogging software started to collect data from the pressure transducer once the reservoir was full. Both control valves were switched at the same time to start the test. Although the apparatus is unique, this test is essentially a

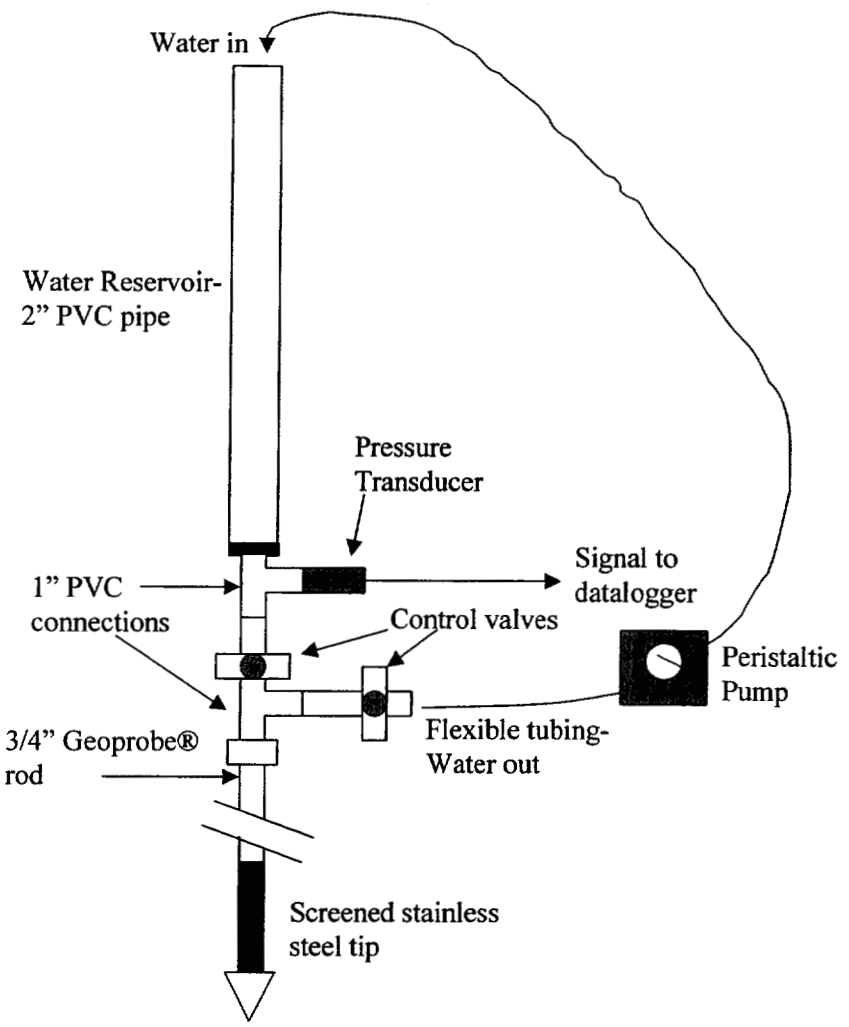

Figure 2.2: Apparatus for Hydraulic Conductivity Measurements

slug test in a point piezometer and can be evaluated using the method by Hvorslev (Freeze and Cherry, 1979).

The rate of flow, q, through the screened interval can be related to the K, K, and head difference, H-h, according to

$$q(t) = \pi r^2 dh/dt = FK(H-h) \quad (2.1)$$

where r = radius of the reservoir

H = head at $t = \infty$

h = head at any time $0<t<\infty$

F = a shape factor based on the dimensions of the screened interval

The basic lag time, T_0 is defined as

$$T_0 = \pi r^2/FK \quad (2.2)$$

Making the substitution into equation 2.1, solving equation 2.1 with the initial condition

$h = H_0$ at $t = 0$, and taking the natural log of both sides yields

$$\ln (H-h/H-H_0) = -t/T_0 \quad (2.3)$$

When the left-hand side is plotted against t, $T_0 = t$ when $\ln (H-h/H-H_0) = -1$, as shown in Figure 2.3. For a screened interval having a length, L, and radius, R, when $L/R>8$, the expression for K becomes

$$K = r^2 \ln(L/R)/2LT_0 \quad (2.4)$$

2.3.2 Tracer Placement and Initial Sampling

2.3.2.1 Well Placement and Preparation

The tracer injection location was in an area of higher K and mid-range organics concentrations approximately 60-65 m from the northern end of the transect. The well network consisted of 5 injection wells, 10 extraction wells, and 81 sampling wells arranged within a 8-m x 8-m area as shown in Figure 2.4. The wells were constructed of 1" PVC. The injection and extraction wells were screened from 3 m to 4 m bgs. The sampling wells were screened from 3 m to 5.5 m below ground surface. The screened interval of the sampling wells represents the full thickness of the perched aquifer in this area of the site.

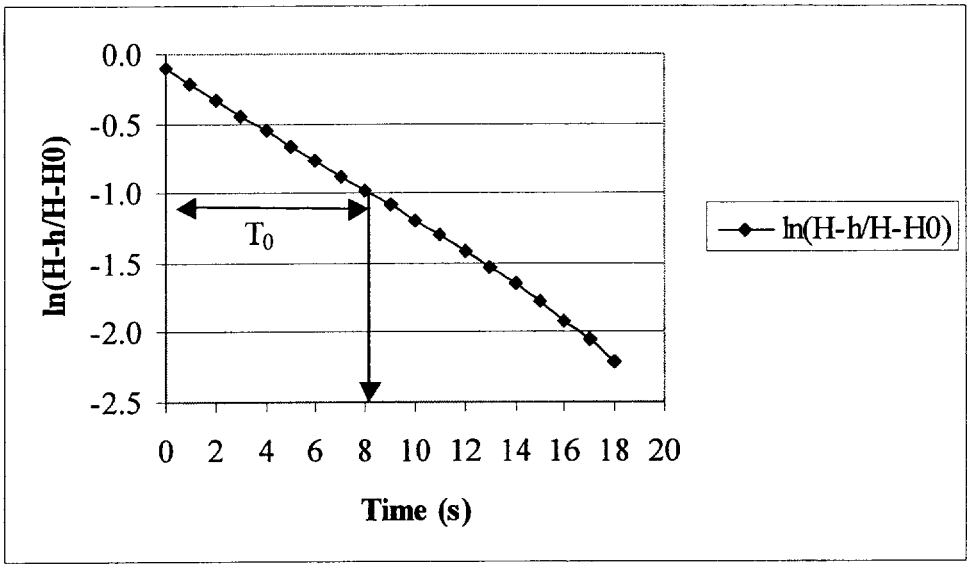

Figure 2.3: Graphical Determination of Hydraulic Conductivity from a Slug Test

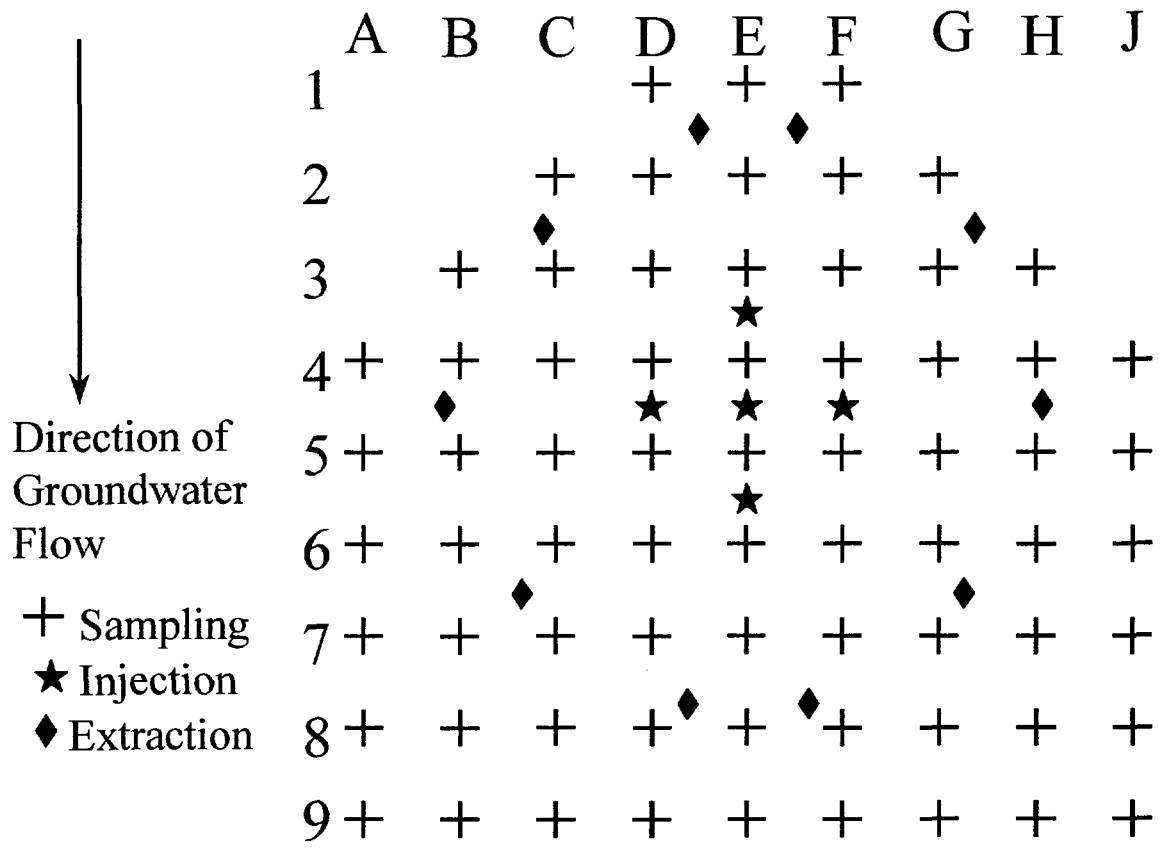

Figure 2.4: Layout of Tracer Injection, Extraction, and Sampling Wells

Wells were installed in sections using a direct push technique. Geoprobe® rod was extended down the center of the well and attached to a stainless steel tip that was also sealed to the well. The screened interval of each well was installed as a full section with 1-m lengths of solid 1" PVC pipe to bring the well to ground surface. Once a well was in place, the rod was unscrewed from the drive tip, which remained in place and served as the bottom of the well. After installation, the wells and wells screens were cleared of sediment and pumped until the extracted water was clear.

2.3.2.2 Tracer Preparation, Injection, and Sampling

Perdeuterated MTBE ($^2H_{12}$-MTBE), synthesized by Cambridge Isotopes (Cambridge, MA), served as an MTBE analog for the tracer study. Its partitioning and degradation characteristics were assumed to be similar to those of the less deuterated compound. The $^2H_{12}$-MTBE tracer, therefore, allowed MTBE to be placed within the
gasoline plume while providing an analytical mechanism to distinguish the tracer plume from the existing plume. Thierrin et al. 1995 documented the usefulness of perdeuterated compounds in natural gradient tracer tests to determine field-degradation rates. Sodium bromide was chosen as a conservative tracer because bromide would not volatilize or partition into any residual NAPL in the injection zone. The initial bromide mass balance provided confirmation for the initial mass balance on $^2H_{12}$-MTBE since bromide would not be subject to volatilization during injection. Naturally occurring bromide, if present at the site, was at concentrations below the method detection limit; therefore, the potential for interference with the tracer was small. Because hydraulic control was critical during the initial plume placement, fluorescein, a bright green fluorescent dye, was used as a visual method of monitoring the injection process.

The $^2H_{12}$-MTBE and bromide tracer plume was injected at a location slightly upgradient from a point approximately 60-65 m along the cross-gradient sampling transect. A concentrated tracer stock solution was introduced over a 1-m interval (3 to 4 m bgs) using five central injection wells surrounded by a circle of ten extraction

wells. The wells were installed by direct push using a Geoprobe®. Each of the five peristaltic pumps used for tracer introduction was connected to two extraction wells and one injection well. This approach was used to maintain hydraulic control during tracer placement and to prevent changing the dissolved oxygen concentration and geochemistry of the groundwater. The groundwater and stock solution injection rates were 1 L/min and 2 mL/min, respectively, for each pump. Tracer injection was completed in approximately 24 hours.

The stock solution containing the three tracers was mixed with site groundwater injected into the subsurface. The target *in situ* concentrations of the $^{2}H_{12}$-MTBE and bromide were 1 mg/L and 500 mg/L, respectively. Because fluorescein was present purely as a visual tool, there was no specific target concentration for the dye. A stock solution containing 250 g/L bromide ion and 2,500 ppmv fluorescein was prepared to account for a 500 fold dilution factor expected in the initial tracer plume in groundwater. Since $^{2}H_{12}$-MTBE losses to volatilization had to be minimized, the stock solution was placed in Tedlar bags in 0.8-L increments for a total of 20 stock bags. Prior to injecting each bag of stock into the subsurface, 0.4-g of $^{2}H_{12}$-MTBE was injected into each Tedlar bag. This allowed airtight containment without any headspace. A shortage of $^{2}H_{12}$-MTBE resulted in a smaller injection volume in the last set of bags. In addition, a small volume of stock was left in each bag to avoid drawing air into the injection tubing and groundwater. A total of 7 g of $^{2}H_{12}$-MTBE and 3750 g of bromide ion were injected into approximately 7000 L of groundwater.

Immediately following tracer injection, the initial plume was sampled to determine its structure and to check the initial mass balance. An inflatable packer assembly with sampling ports at 0.5-m vertical intervals was inserted into each well to provide discrete vertical sampling. When a visual assessment of the fluorescein dye indicated that sample concentrations might vary significantly within the 0.5-m interval, the sampler was shifted 25 cm and 0.25-m samples were collected. Duplicate samples were collected at each location in 40-mL VOA vials with Teflon coated septa. Samples were packed in ice and driven to Oregon Graduate Institute (OGI) where they were placed in a 4°C cold room until analyzed. Samples were

analyzed from highest concentration to lowest based on visual assessment of fluorescein concentration within one and half weeks of collection.

2.3.2.3 Sample Analysis

Samples were analyzed for $^{2}H_{12}$-MTBE, MTBE, and BTEX by headspace injection on a HP 5890/5971A GC/MS with a 50-m Petrocol column. Each sample was injected using the "splitless" mode. The injector temperature was 280°C. The temperature program was: initial temperature -40°C; ramp 40°C/minute to 40°C; ramp 10°C/min to 150°C. Liquid nitrogen was used to cool the oven to an initial temperature of -40°C. The MS temperature was held at 290°C. The MS was operated in selective ion mode. The Standard solutions contained $^{2}H_{12}$-MTBE, MTBE, benzene, toluene, ethylbenzene, m-, p-, and o-xylene. A 1-mL volume of each standard or sample was transferred by syringe into a clean, helium-purged VOA vial with a Teflon coated septum. A 2-µL volume of perdeuterated benzene (D_6B) was added as an internal standard to all standards and samples.

Bromide was analyzed at OGI by high pressure liquid chromatography with a Gilson pump and LDC/Milton Roy Conductomonitor III ECD set at 0.1 µS conductance. Separation was achieved on a Metrosep Anion Dual1 packed column with an 8 mmol othallic acid/2% acetonitrile mobile phase at a flow rate of 0.5 mL/min.

2.3.3 Interim Sampling

Interim sampling trips were made to Port Hueneme at 4 and 8 months after injection (November 1998 and March 1999, respectively) to track the plume and help determine a starting location for the plume characterization after one year of transport. Direct push groundwater samples were obtained using a van-mounted Geoprobe® equipped with a special stainless steel tip for water sampling. The sampling tip had a ¾" outer diameter and a 10-cm screened interval. A peristaltic pump was used to bring groundwater to the surface. Water was pumped until it was clear of sediment before taking a sample. The November 1998 sampling included 8 sampling locations at 5-m intervals in the longitudinal direction and 2 transverse

sampling locations 5-m to either side of the longitudinal transect midpoint. Samples were collected in duplicate at 0.5-m vertical intervals between 3 m and 6 m bgs. The March 1999 sampling began at the last point sampled in November 1998. This transect was angled slightly south of the previous transect (Figure 2.2) because results from November indicated that only the edge of the tracer plume was sampled. The longitudinal transect included 7 locations at 7.5-m intervals. Transverse sampling locations were 5-m to either side of the 5th longitudinal transect point. Samples were collected in duplicate at 0.5-m vertical intervals between 3 m and 7 m bgs. Chemical analyses for $^{2}H_{12}$-MTBE and bromide were conducted as discussed above for the initial plume.

2.3.4 Characterization After 1 Year of Transport

The Geoprobe® sampling method described above was used to characterize the tracer plume after 1 year of transport. The last sampling location of the March 1999 transect was the starting point of the sampling grid at 1 year. Sampling locations were based on a 5-m grid. Subsurface samples were collected at 0.5-m intervals from 3 m to 7 m bgs at each push location. The results of on-site GC/MS analyses were used to select each day's sampling locations. A total of 81 push locations were required to characterize the $^{2}H_{12}$-MTBE tracer plume after 1 year of transport. The layout of the grid and its relation to the initial plume location and interim transects is shown on Figure 2.1(b).

Analytes for the full characterization were similar to those of the initial plume. Samples were analyzed for $^{2}H_{12}$-MTBE, MTBE, BTEX, Fe(II), and bromide. In addition, dissolved oxygen and pH were also measured before each sample was collected. The analytical methods for bromide and Fe(II) are identical to those used for the cross-gradient sampling transect. The GC/MS method for the organics was modified to include a HP 7694 automated headspace sampler so that analyses could be completed during afternoon sampling and overnight. The autosampler equilibrated each sample for 1 minute at an oven temperature of 70°C. The sample loop and transfer line temperatures were 80°C and 90°C, respectively. A 1-minute injection to a "splitless" injector was performed by the autosampler. In order to

detect lower concentrations of $^2H_{12}$-MTBE, 5-mL of sample were added to each autosampler vial along with 10 μL of D_6B as an internal standard. The vials were not purged with helium before adding the sample because of field constraints so a solvent delay (1-3 min) was introduced to miss the air peak.

2.3.5 Method of Moments for Mass Balance and Plume Parameter Calculations

Mass balances on the initial and Year 1 tracer plumes were calculated using the method of moments discussed in Freyberg (1986). The method was also used to calculate descriptive parameters of the tracer plume at Year 1. Moments are spatially-integrated functions defined by the following expression for a concentration distribution

$$M_{ijk}(t) = \int_{-\infty}^{\infty}\int_{-\infty}^{\infty}\int_{-\infty}^{\infty} nC(x,y,z,t)x^i y^j z^k \, dx\, dy\, dz$$

The zeroth, first, and second (i+j+k = 0, 1, and 2, respectively) allow the total mass, center of mass location, and plume spread to be calculated. When discrete data points are used as in the tracer study, the integrals can be replaced with summations to yield

$$M_{ijk}(t) = \sum_{-\infty}^{\infty}\sum_{-\infty}^{\infty}\sum_{-\infty}^{\infty} nC(x,y,z,t)x^i y^j z^k \, \Delta x\, \Delta y\, \Delta z$$

The moments of interest for estimating plume characteristics are, therefore, written as follows

Zeroeth Moment: $M_{000} = \sum_{-\infty}^{\infty}\sum_{-\infty}^{\infty}\sum_{-\infty}^{\infty} nC(x,y,z,t)\Delta x\, \Delta y\, \Delta z$

First Moment: $M_{100} = \sum_{-\infty}^{\infty}\sum_{-\infty}^{\infty}\sum_{-\infty}^{\infty} nC(x,y,z,t)x\Delta x\, \Delta y\, \Delta z$

Second Moment: $M_{200} = \sum_{-\infty}^{\infty}\sum_{-\infty}^{\infty}\sum_{-\infty}^{\infty} nC(x,y,z,t)x^2\Delta x\, \Delta y\, \Delta z$

Equivalent equations can be written for the y and z directions. Plume parameters can be estimated from the following relationships (Freyberg 1986)

Total Mass = M_{000}

Center of Mass Location: $x_c = M_{100}/M_{000}$; $y_c = M_{010}/M_{000}$; $z_c = M_{001}/M_{000}$

Dispersion Coefficient: $D_x = \frac{M_{200}}{M_{000}} - x_c^2 \Big/ 2t$ (and equivalent for y and z directions)

The dispersion coefficient calculation is only valid if the initial dimensions of the plume are small in comparison to the "final" dimensions.

2.4 Results and Discussion

2.4.1 Cross-Gradient Sampling Transect

Hydaulic conductivity along the transect (Table 2.1) ranged from 0.002 to 0.45 cm/s. This represents a greater than 2 order of magnitude difference in K in the transect measurements. This range differed somewhat from previously reported values at this site (Salanitro et al. 2000) and may have reflected the short vertical interval tested and consequently a different scale of heterogeneity. A scatterplot of the K with distance along the transect is shown in Figure 2.5. There was a region of generally higher K in the center of the transect that was bracketed by lower values at 0.0 m and 83.4 m along the transect. The distribution of higher and lower values of K showed considerable variability with depth. This indicated that there may be areas of localized higher K in the direction perpendicular to groundwater flow, but the presence of a preferential flow path at a specific depth was not evident.

Dissolved oxygen, nitrate, sulfate, ferrous iron, and chloride were analyzed to examine water quality and dominant microbial activity in relation to the contaminant plume. Table 2.2 shows the distribution of inorganics along the transect. Dissolved oxygen concentrations in the aquifer were ≤1 mg/L at 56 of 63 sampling locations and just above 1 mg/L at the remaining locations. Nitrate ranged from below detection limits to 12.5 mg/L with the higher values at the far south of the transect; therefore, nitrate reduction did not appear to play a role in biodegradation at the time of the tracer test. Iron(II) was present at 0.3-12 mg/L but did not show any correlation to the contaminant distribution. Sulfate concentrations ranged from 10.3 to 1230 mg/L. A significant (1-2 order of magnitude) decrease in sulfate was observed in the most contaminated section of the transect. This indicated that sulfate-reducing bacteria may be present and active at this site.

Table 2.1: Hydraulic Conductivity Along the Cross-Gradient Transect

K (cm/s)									
	North to South Distance Along Transect (m)								
Depth (m)	0.0	20.4	42.7	52.8	63.3	73.7	83.4	94.4	106.0
3.0	0.020	0.057	0.114	0.140	0.320	0.182	0.021	0.084	0.160
3.5	0.026	0.177	0.198	0.160	0.198	0.160	0.044	0.259	0.164
4.0	0.072	0.085	0.292	0.015	0.306	0.102	0.071	0.116	0.140
4.5	0.041	0.003		0.153	0.129	0.116	0.077	0.110	0.036
5.0	0.075	0.002	0.116	0.192	0.065	0.116	0.017	0.156	0.073
5.5	0.041	0.035	0.008	0.172	0.075	0.012	0.060	0.052	0.028
6.0	0.028	0.056	0.056	0.192	0.056		0.055	0.029	0.020

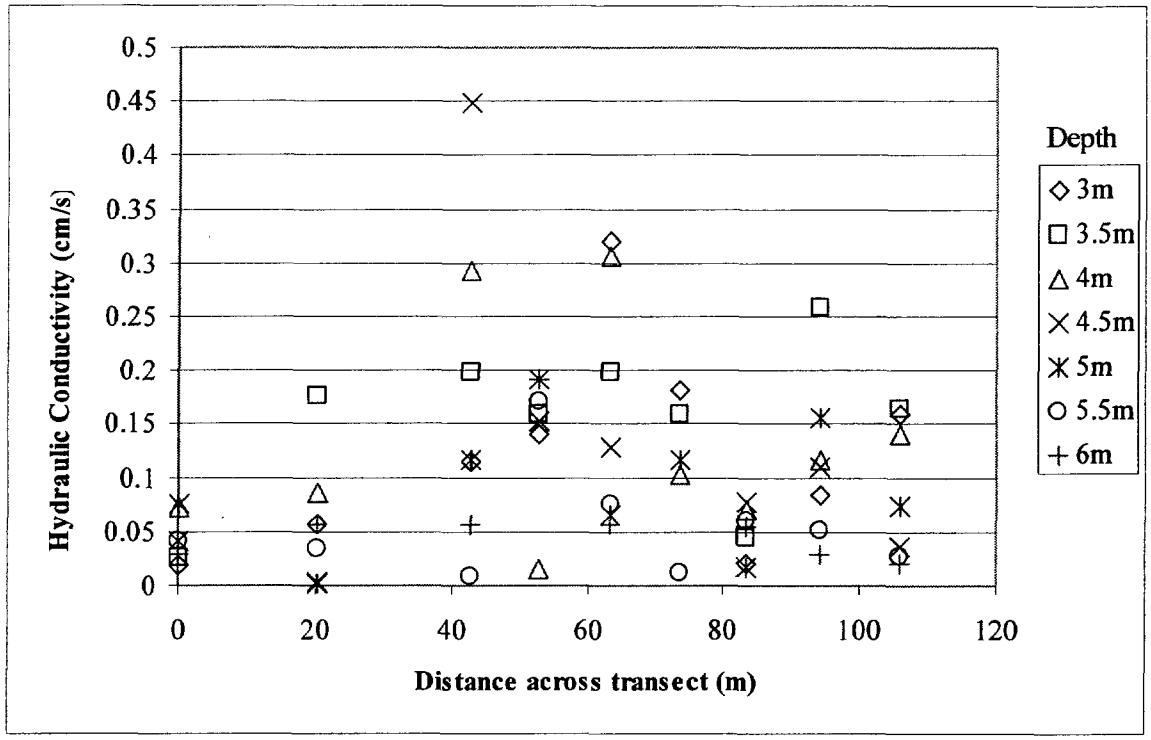

Figure 2.5: Scatterplot of Hydraulic Conductivity Distribution

Table 2.2: Inorganic Compound Concentrations in the Cross-Gradient Transect

Depth (m)	North to South Distance Along Transect (m)								
	0.0	20.4	42.7	52.8	63.3	73.7	83.4	94.4	106.0
Iron(II) (mg/L)									
3.0	0.3	12.2	8.1	12.1	3.3	3.3	2.2	1.0	0.3
3.5	1.6	9.6	10.2	10.4	3.3	2.8	3.3	1.9	0.4
4.0	2.36	2.9	10.8	9.2	3.7	3.3	3.4	1.0	0.5
4.5	7.0	5.3	6.3	5.1	3.3	0.5	3.4	3.6	0.6
5.0	9.4	6.5	3.2	5.8	6.8	3.1	6.1	10.5	3.2
5.5	7.4	9.0	0.7	8.7	4.2	3.4	3.4	3.7	4.7
6.0	6.7	4.2	0.9	6.6	3.3	0.3	3.4	3.6	5.1
Sulfate (mg/L)									
3.0	546	452	40.3	10.3	18.5	57.0	995	NA	1230
3.5	351	747	540	206	90.9	513	531	1100	633
4.0	791	NA	335	533	501	674	NA	861	643
4.5	751	NA	345	617	545	NA	783	716	660
5.0	681	636	338	546	669	743	789	684	711
5.5	899	2.9	413	686	586	806	660	721	539
6.0	700	730	628	531	734	791	800	799	604
Nitrate (mg/L)									
3.0	<0.01	<0.01	0.07	<0.01	0.06	0.20	0.04	NA	7.57
3.5	<0.01	0.04	<0.01	0.06	<0.01	<0.01	<0.01	1.33	12.5
4.0	<0.01	NA	<0.01	<0.01	<0.01	<0.01	NA	6.07	5.46
4.5	0.02	0.06	<0.01	0.04	<0.01	NA	<0.01	1.53	0.04
5.0	<0.01	<0.01	<0.01	<0.01	<0.01	<0.01	<0.01	<0.01	0.07
5.5	<0.01	<0.01	<0.01	<0.01	<0.01	<0.01	0.03	<0.01	<0.01
6.0	0.025	0.40	<0.01	<0.01	<0.01	<0.01	<0.01	<0.01	<0.01
Chloride (mg/L)									
3.0	91.6	81.3	87.7	72.6	98.7	84.3	72.3	NA	118
3.5	62.2	110	69.4	83.5	73.8	94.1	77.5	99.4	73.9
4.0	99.6	NA	79.3	81.4	92.9	99.3	NA	86.3	82.4
4.5	106	1.5	80.3	86.1	88.4	NA	87.7	79.9	86.0
5.0	86.5	89.9	69.3	65.2	88.5	93.0	87.6	77.1	86.5
5.5	109	2.2	69.1	70.2	75.1	95.2	70.5	82.9	61.8
6.0	80.8	75.0	70.1	58.1	78.4	85.8	85.4	84.4	66.3

BDL – Below Detection Limit
NA – Not Analyzed

MTBE and BTEX data for the NEX plume were used to place the tracer plume in a location away from the source zone but within the flowpath of the existing MTBE plume. Table 2.3 gives the MTBE and BTEX transect data. MTBE concentrations exceeded 100 mg/L at 3 m bgs at and around the transect midpoint. Total BTEX concentrations at these same locations ranged from 251.3 to 577.4 mg/L. The sample with the highest BTEX concentrations appeared to have a sheen on the surface, indicating that residual gasoline may be present at that location. Both MTBE and BTEX concentrations drop with increasing depth and increasing distance from the transect midpoint. At the ends of the transect, MTBE and total BTEX are generally below 1 mg/L. Despite these general trends there is not a strong correlation between the K and MTBE concentrations at the transect sampling points, although the highest concentrations of MTBE do occur at points where K exceeds 0.1 cm/s (Figure 2.6). Based on the contaminant concetrations, the K measurements, and site logistics, the tracer plume was injected 60-65 m from the northern end of the transect.

2.4.2 Initial Tracer Plume

The plan view of the vertically-averaged initial $^{2}H_{12}$-MTBE distribution is shown in Figure 2.7(a). The figure shows that the target concentration was closely met in the center of the plume. Furthermore, hydraulic control was maintained during the injection procedure as the tracer plume was contained within the bounds of the extraction wells. Figure 2.7(b) shows the vertical transect through the center wells in the longitudinal direction. Although the injection and extraction wells were only screened to 4 m bgs, the tracer plume extends to a depth of 5.5 m.

Mass balance calculations were performed for both $^{2}H_{12}$-MTBE and bromide. Because of its conservative behavior under the site conditions, the bromide mass balance was used to confirm the quality of the $^{2}H_{12}$-MTBE mass balance. The calculated masses were 6.25 g (89.3%) of $^{2}H_{12}$-MTBE and 3,388 g (90.3%) of bromide. Given that the percentages of the tracers accounted for in the mass balances were similar, losses of $^{2}H_{12}$-MTBE to volatilization or partitioning into residual NAPL were minimal. The rest of the tracer mass may exist in the part of

Table 2.3: MTBE and BTEX Concentrations Along the Cross-Gradient Transect

Depth (m)	North to South Distance Along Transect (m)								
	0.0	20.4	42.7	52.8	63.3	73.7	83.4	94.4	106.0
MTBE (mg/L)									
3.0	1.3	16.6	272	102	146	72.5	14.7	0.5	0.5
3.5	0.1	21.6	45.7	17.6	21.2	60.1	0.2	0.8	0.4
4.0	<0.1	5.2	78.1	18.1	14.6	9.7	4.1	<0.1	0.1
4.5	0.8	10.8	38.0	33.7	7.9	9.7	1.8	0.4	0.4
5.0	0.8	6.7	25.7	4.4	0.2	3.8	0.1	0.5	0.2
5.5	0.8	1.5	31.5	5.1	3.4	0.4	<0.1	0.2	0.1
6.0	0.7	0.6	8.1	1.6	1.2	2.6	0.8	0.5	0.3
Total BTEX (mg/L)									
3.0	0.1	0.5	577	262	368	251	1.8	0.3	0.1
3.5	1.1	0.2	47.0	28.5	66.4	89.4	0.7	0.6	0.3
4.0	1.0	0.4	19.2	17.9	33.6	18.7	0.6	0.6	0.2
4.5	0.5	0.3	6.0	18.2	9.0	28.3	0.7	0.3	0.1
5.0	0.6	0.4	1.4	1.7	3.4	8.2	0.1	0.4	0.3
5.5	0.6	0.1	4.4	3.3	8.7	6.6	0.1	0.5	1.0
6.0	0.6	0.1	1.4	2.0	2.2	6.7	0.6	1.3	0.2

BDL – Below Detection Limit

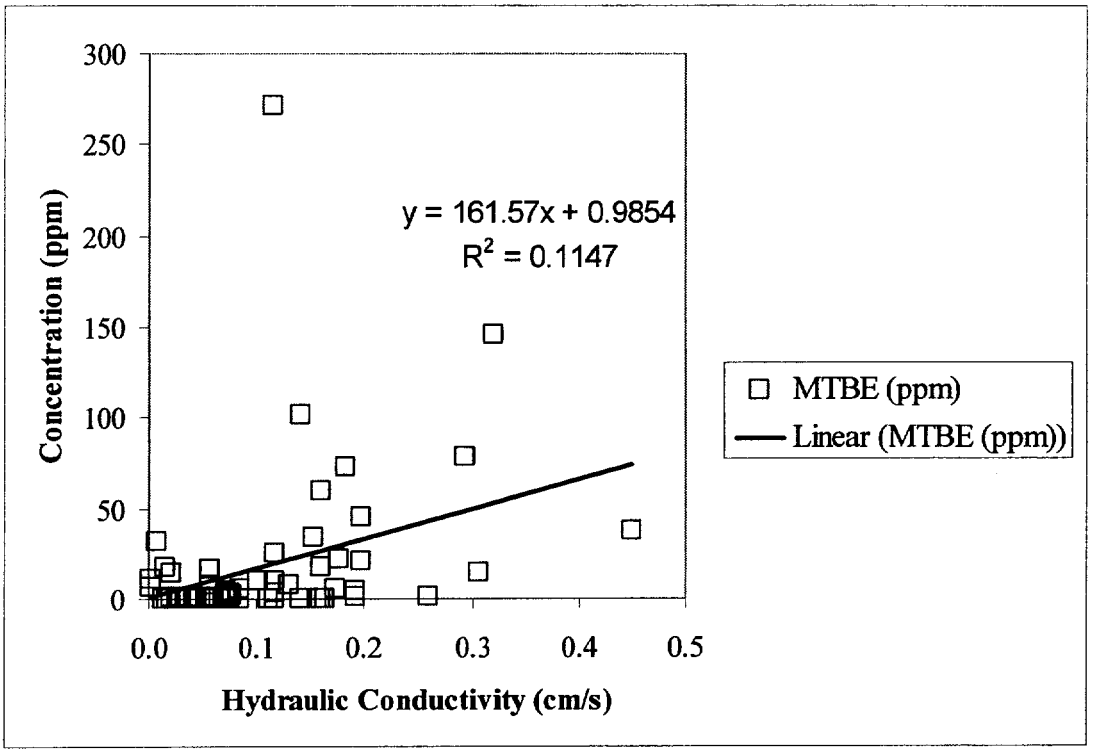

Figure 2.6: Relationship Between MTBE and Hydraulic Conductivity in Transect Samples

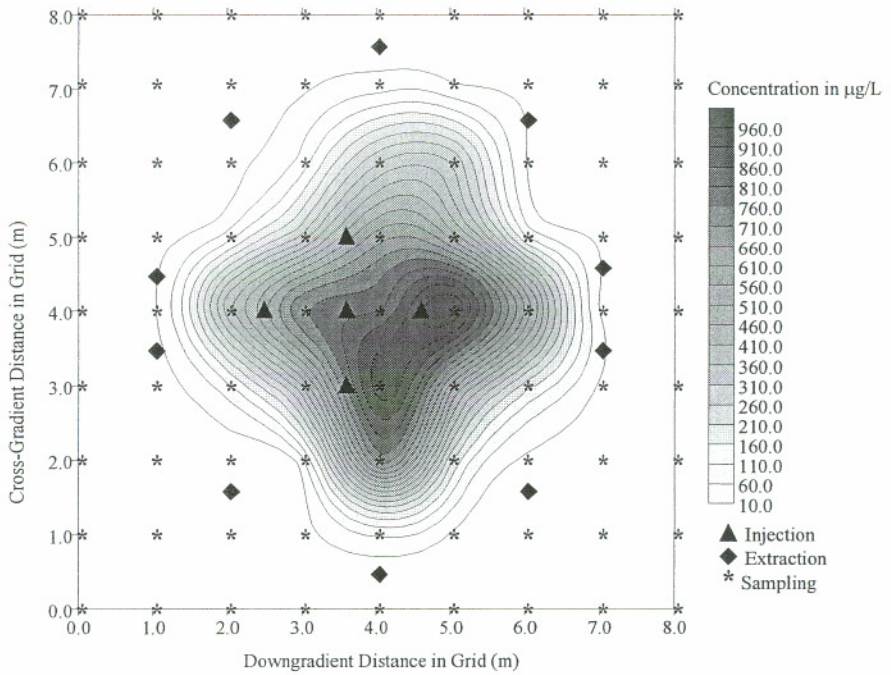

(a)

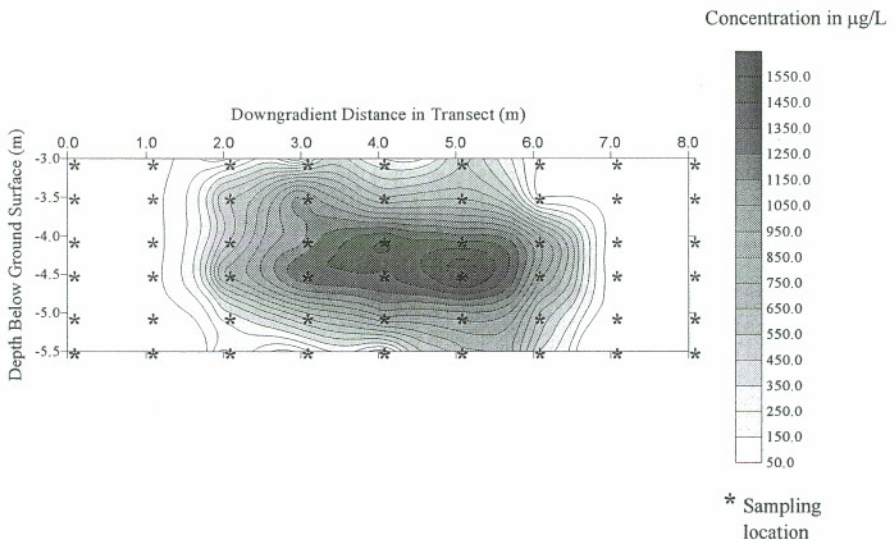

(b)

Figure 2.7: a) Plan View of Initial (Vertically-Averaged) $^{2}H_{12}$-MTBE Distribution; b)Vertical Cross-Section of the Initial $^{2}H_{12}$-MTBE Distribution in the Longitudinal Direction

the plume between sampling wells or in the underlying confining layer and was, therefore, not able to be accounted for in the sample data.

2.4.3 Intermediate Sampling

The first intermediate sampling transect, completed 4 months after injection, showed 1-2 order of magnitude reductions from the initial concentrations of $^{2}H_{12}$-MTBE and bromide. These values were lower than expected and, in retrospect, occurred because the transect sampled only the edge of the tracer plume. The second transect showed concentrations that were equal to and up to 4 times higher than the values observed in the first transect, supporting the conclusion that the first transect sampled only the edge of the tracer plume. These data also indicated that the tracer flow path deviated from the expected direction of groundwater flow based on the hydraulic gradient at the site and the overall flow direction of the existing MTBE plume. The data acquired from these transects provided the starting location for the detailed tracer plume characterization at the conclusion of one year of transport.

2.4.4 Plume Characterization After 1 Year

Due to the significantly lower tracer concentrations after 1 year of transport and the detection limit of the HPLC, the bromide concentration in the majority of samples had fallen below the detection limit by July 1999. Consequently, plume parameters can be reported for $^{2}H_{12}$-MTBE only. Furthermore, the effect of sorption on plume behavior could not be assessed for this study since the bromide data were not available for comparison.

Plan views of the vertically-averaged initial and 1-year tracer plume data are shown in Figure 2.8. Two features are particularly noteworthy. First, the length of the plume had grown from 6 m in 1998 to over 90 m in 1999. The plume widened from 6 m to approximately 25 m at its widest part. Second, the plume has several "pockets" of higher concentrations surrounded by low concentrations, indicating the impact of regions of high and low K within the tracer placement area and along the flow path. Referring back to Table 2.1 and Figure 2.5, the measurements at the

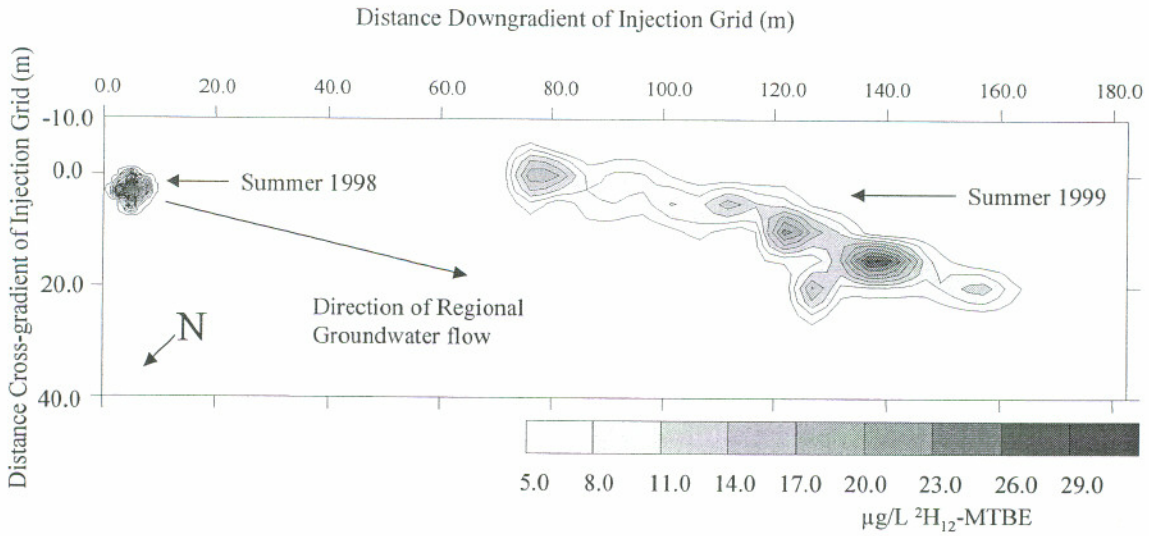

Figure 2.8: Plan View of the Tracer Plume After 1 Year of Transport

direct push locations 63.3 m and 73.7 m along the transect give an idea of the K values at the injection location and along the flow path.

A vertical cross-section down the centerline of the plume was constructed from the concentration data along transect B-B' on Figure 2.9(a). The contoured concentration data are shown with the bounding soil layers on Figure 2.9(b). The non-uniform distribution of $^{2}H_{12}$-MTBE was quite apparent in this view, and portions of the plume had clearly moved at different velocities. There did not appear to be a strong correlation between velocity and depth based on the vertical cross-section; that is, at no depth did groundwater appear to move consistently faster than at any other. The tracer was originally placed 3-5.5 m bgs. The presence of $^{2}H_{12}$-MTBE at lower depths indicates that there was a vertical component to groundwater flow at this site. Downward movement was limited, however, by the underlying clay layer. This was also observed in the existing MTBE plume. During sampling it was evident that the depth of the confining layer increased with distance from the source and, as shown in Figure 2.9(b), the plume movement conformed to the upper and lower limits of the aquifer. It is believed, therefore, that the tracer and existing MTBE plume were simply following the stratigraphy at this site.

The total calculated mass of $^{2}H_{12}$-MTBE was 7.69 g after one year of transport, compared to the injected mass of 7 g. The slightly higher mass calculated at year 1 was not surprising given sampling and analysis errors and the large volume over which the integration occurred. The mass balance at year 1 was within 10 % of the $^{2}H_{12}$-MTBE mass known to have been injected.

The mass balance after 1 year of transport suggested that no $^{2}H_{12}$-MTBE mass was lost during the study. This was consistent with the high-sulfate, anaerobic character of the aquifer and the behavior of the NEX MTBE plume, which appears to be migrating without significant attenuation. Recent work published by USEPA (2000) suggests a possible mechanism for biodegradation of MTBE under methanogenic conditions, but it requires very low sulfate concentrations (<4 mg/L). Natural sulfate concentrations at the site were on the order of 500-1000 mg/L, thus the lack of biodegradation was not surprising given other published results.

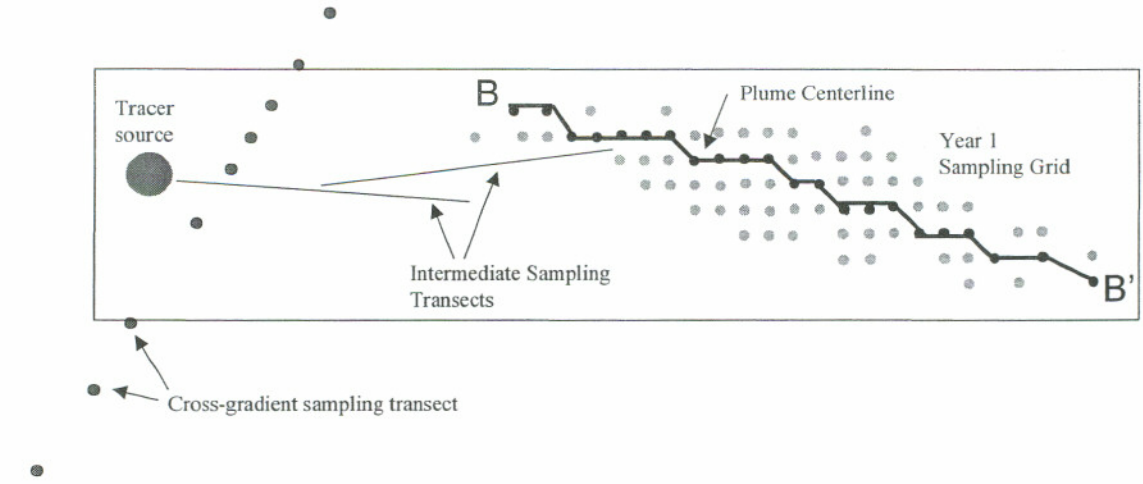

(a)

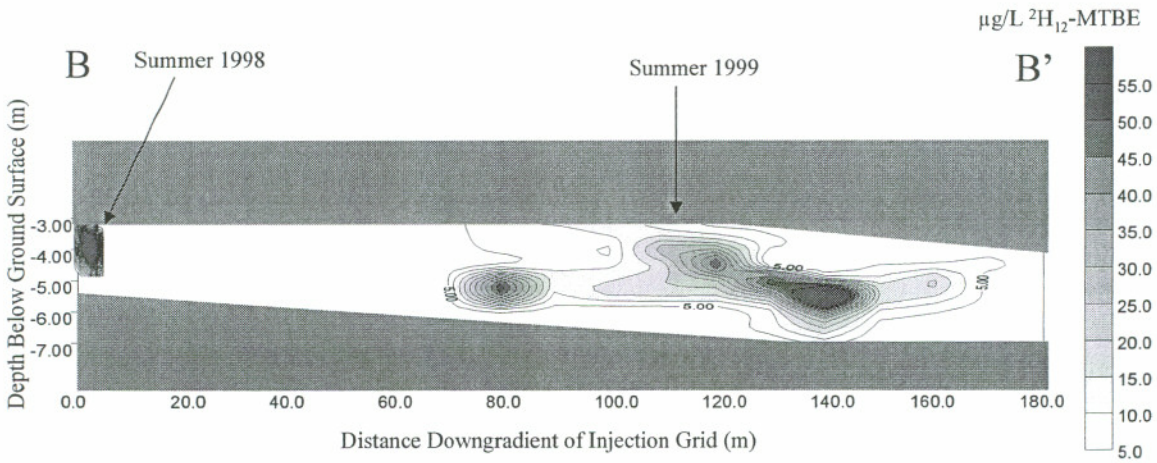

(b)

Figure 2.9: Vertical Cross-Section of the Tracer Plume Along the Center Line after 1 Year of Transport, (a) Transect Location in Grid, (b) Contoured $^2H_{12}$-MTBE Data

Dispersion was the dominant mechanism resulting in lower aqueous $^{2}H_{12}$-MTBE concentrations. The method of moments was also used to calculate the center of mass displacement and dispersion coefficients for the tracer plume. After 1 year of transport, the center of mass of the tracer plume was displaced 120.3 m downgradient of the initial tracer center of mass. The vertical location was 5.1 m bgs, compared to 4.3 m bgs in the initial plume. The lateral and longitudinal dispersion coefficients (D_x and D_y) were 0.08 m^2/d and 0.85 m^2/d, respectively. Using the center of mass displacement calculation and the transport time, the average velocity of the tracer plume was calculated to be 0.32 m/d. Consequently, average longitudinal and transverse dispersivities were calculated to be 2.69 m and 0.25 m, respectively. It is worth noting that the dispersivities and dispersion coefficients alone were not sufficient to describe the complexity of the plume.

Comparison of the tracer plume and the MTBE plume at the site showed both important similarities and differences. Both plumes indicated that biodegradation of MTBE was probably not an important process at the site. As discussed above, longitudinal dispersion played an important role in the shape of the tracer plume. That same process was undoubtedly at work in the larger plume, but the size and duration of the gasoline source tend mask the dispersion process and the aquifer structure that controls the dispersion process. One implication of this is that the role of the higher-velocity zones within the MTBE plume was masked by the overall plume shape. As discussed below, this has significant implications for the correct interpretation of monitored natural attenuation at the site.

2.5 Implications for MNA

There was a dramatic drop in tracer concentrations in the year of transport. Based on the $^{2}H_{12}$-MTBE mass balance, MTBE mass lost due to degradation was negligible under the anaerobic, high-sulfate conditions at Port Hueneme. This is important because degradation of other gasoline components may result in oxygen depletion in an otherwise aerobic system. Anaerobic MTBE degradation has been documented under nitrate-reducing, sulfate-reducing, and methanogenic conditions (Mormile et al. 1994, USEPA 2000), but this study provides cautionary evidence

that degradation may not occur at some sites. Even if microcosm studies indicate that degradation is possible at a site, a defensible field demonstration that MNA is a viable strategy may still be difficult.

This study yielded important considerations for such a demonstration. MNA protocols (e.g., USEPA 1999) frequently rely on evidence from an "appropriate" monitoring well (or wells) to demonstrate that MNA, and more specifically biodegradation, is occurring. These wells often take the form of transects down the "center" of the groundwater plume or as pairs of "fences" made up of wells across the width of the plume. The applicability and potential pitfalls of these approaches can be examined in the context of the tracer test reported here.

An accurate assessment of biodegradation from a longitudinal transect requires knowledge of the source strength over time and placement of the transect along the centerline of the plume *on a mass transport basis*. The interpretation of longitudinal transect data often involves plotting contaminant concentrations against downgradient distance. A macroscopic velocity allows the distance measurement to be equated to travel time, from which degradation rates can be calculated. The data from the Port Hueneme tracer test indicate that there is a preferential flow path that is not co-located with the apparent centerline of the NEX MTBE plume. The presence of such channels in a plume will cause some of the contaminant mass to move at a different velocity than the overall plume characteristics would suggest. Consequently, the travel time along the apparent centerline may not accurately reflect the travel time of contaminant mass in the aquifer and may lead to errors in the calculated degradation rate. The existence of preferential flow paths may also make locating the actual plume centerline on a mass transport basis very difficult. If the transect and the actual plume centerline diverge with distance from the source, reduced contaminant concentrations due to dispersion and dilution could support an erroneous conclusion that degradation is occurring.

Likewise, estimates of MNA using fences across a plume rely on understanding changes in source strength with time. Quantifying the change in contaminant flux between a pair of fences also requires knowledge of the

groundwater velocity as well as contaminant concentrations. The tracer test data suggest that the flux distribution along fences at the Port Hueneme site would be complicated due the presence of the preferential flow path. The contaminant flux along this path would be different than that calculated using the macroscopic velocity and measured concentrations. Furthermore, the velocity along the preferential flow path would need to be accounted for at each fence for mass fluxes to be compared. This means that the location of the preferential flow path needs to be known at each fence. In order to overcome this difficulty it is important to understand the distribution of K and local hydraulic gradients along the fences. Often these can be determined in a cost-effective manner using current direct-push technologies. Concurrent groundwater samples would provide the necessary contaminant distribution data. Using this approach could result in a significant improvement in the robustness of MNA demonstrations.

2.6 Conclusions

Degradation was not a significant mechanism controlling the attenuation of $^{2}H_{12}$-MTBE in this study. Due to the complexity of the aquifer, dispersion was responsible for the two order of magnitude reduction in $^{2}H_{12}$-MTBE concentrations observed after one year of transport. Both aquifer heterogeneity and the presence of a preferential flow path would have precluded an accurate understanding of transport at the site without the large number of samples collected in this study.

An understanding of the plume structure was a prerequisite for assessing the potential mechanisms of natural attenuation of the tracer plume. Hydrogeology controlled the detailed structure of the tracer plume during the year of transport. The effects of higher and lower K regions along the flow path were apparent in the tracer plume after one year. In addition, the presence of a preferential flow path clearly impacted the tracer behavior.

Because the tracer plume was injected as a dissolved point source, its behavior was expected to differ from that of a plume dissolving from a NAPL source (e.g. the Port Hueneme MTBE plume). Consequently, the tracer test was not perfectly analogous to groundwater plumes resulting from gasoline releases. In

particular, due to the long-term nature of the gasoline source, MTBE concentrations would not have been as significantly reduced due to longitudinal dispersion as was the case for the pulse tracer injection. Nevertheless, the tracer test demonstrated the existence of a complex velocity field, which was not apparent from observations of the existing plume. Thus, an understanding of preferential flow fields at this and other sites would be critical to correctly assess the processes controlling natural attenuation of MTBE.

2.7 References

Boggs, J.M., S.C.Young, L.M. Beard, L.W. Gelhar, K.R.Rehfeldt, and E.E. Adams. 1992. Field Study of Dispersion ina Heterogeneous Aquifer 1. Overview and Site Description. *Water Resources Research.* 28(12):3281-3291.

Borden, R.C., R.A. Daniel, L.E. LeBrun, IV, and C.W. Davis. 1997. Intrinsic Biodegradation Rates of MTBE and BTEX in a Gasoline-Contaminated Aquifer. *Water Resources Research.* 33(5):1105-1115.

Freeze, R.A. and J.A. Cherry.1979. *Groundwater.* Prentice-Hall, Inc. Englewood Cliffs, NJ.

Freyberg, D.L. 1986. A Natural Gradient Experiment on Solute Transport in a Sand Aquifer 2. Spatial Moments and the Advection and Dispersion of Nonreactive Tracers. *Water Resources Research.* 22(13): 2031-2046.

Johnson, P.C. 2002. Personal Communication. May 16, 2002. Port Hueneme, California.

Julian, H.E., J.M. Boggs, C. Zheng, and C.E. Feehley. 2001. Numerical Simulation of a Natural Gradient Tracer Experiment for the Natural Attenuation Study: Flow and Physical Transport. *Groundwater.* 39(4):534-545.

Landmeyer, J.E., F.H. Chapelle, P.M. Bradley, J.F. Pankow, C.D. Church, and P.G. Tratnyek. 1998. Fate of MTBE Relative to Benzene in a Gasoline-Contaminated Aquifer (1993-98). *Groundwater and Monitoring Remediation.* Fall 1998: 93-102.

Mormile, M.R., S. Liu, and J.M. Suflita. 1994. Anaerobic Biodegradation of Gasoline Oxygenates: Extrapolation of Information to Multiple Sites and Redox Conditions. *Environmental Science and Technology.* 28(9): 1727-1732.

Pavne, R.E., N.J. Novick, and M.N. Gallagher. 1997. Demonstrating Intrinsic Bioremediation of MTBE and BTEX in Groundwater at a Service Station Site.

Preprints of Extended Abstracts, 213th American Chemical Society National Meeting, Division of Environmental Chemistry, San Francisco, CA. pp. 418-419.

Salanitro, J.P., P.C. Johnson, G.E. Spinnler, P.M. Maner, H.L. Wisniewski, and C. Bruce. 2000. Field-Scale Demonstration of Enhanced MTBE Bioremediation through Aquifer Bioaugmentation and Oxygenation. *Environmental Science and Technology*. 34: 4152-4162.

Schirmer, M. and J.F. Barker. A Study of Long-Term MTBE Attenuation in the Borden Aquifer, Ontario, Canada. *Groundwater and Monitoring Remediation*. Spring 1998: 113-122.

Sudicky, E.A. 1986. A Natural Gradient Experiment on Solute Transport in a Sand Aquifer: Spatial Variability of K and Its Role in the Dispersion Process. *Water Resources Research*. 22(13): 2069-2082.

USEPA. 1999. Office of Solid Waste and Emergency Response. *Use of Monitored Natural Attenuation at Superfund, RCRA Corrective Action, and Underground Storage Tank Sites*. Directive 9200.4-17P. Washington, District of Columbia: U.S. E.P.A.

USEPA. 2000. Office of Research and Development. *Natural Attenuation of MTBE in the Subsurface under Methanogenic Conditions*, Research Report, EPA 600/R-00/006. Cincinnati, Ohio: U.S. E.P.A.

CHAPTER 3
NUMERICAL MODELING TO EVALUATE CRITICAL FACTORS FOR MONITORED NATURAL ATTENUATION OF MTBE

3.1 Introduction

Monitored natural attenuation (MNA) demonstrations must often rely, in part, on assumptions about the contaminant source and the field site. Because it is impractical, if not impossible, to characterize a field site to an absolute certainty, MNA will always involve some uncertainty. The goals of the modeling work presented here were to investigate how knowledge about the source function and hydrogeology, as well as the choice of sampling network and evaluation method, impact the data collected and their interpretation.

Field demonstrations of natural attenuation utilize a number of approaches to show that mass removal mechanisms such as degradation are containing and reducing the contaminant plume. These might include concentration versus time or concentration versus distance data from longitudinal transects along the centerline of the plume, mass fluxes through fences of monitoring wells across the plume perpendicular to groundwater flow, mass budgets, mass balances, or contaminant and geochemical footprints (ASTM 1998, USEPA 1999, NRC 2000). As sites become more complicated, analytical or numerical modeling may be needed to adequately interpret the field data and make additional site characterization decisions (ASTM 1998). In the case of numerical modeling, a site conceptual model including hydrogeologic, geochemical, and contaminant distribution data is developed in an iterative process in order to understand the important physical and chemical processes at a site (NRC 2000). All of these of these approaches have a common reliance on making reasonable assumptions about and collecting appropriate data on the specific contaminant(s) of interest.

The modeling cases described herein began with a simple hydrogeologic system and then incorporated increasingly complicated transport and fate scenarios. The baseline case evaluated three sampling networks in a simple, completely homogeneous aquifer with a constant contaminant source. Subsequent cases introduced more aquifer heterogeneity, an exponentially decaying source function, and biodegradation with multiple electron acceptors. This sequential addition of complexity allowed sources of error to be attributed to specific mechanisms and analyzed in a way that is impossible under field conditions.

Benzene and MTBE were both included as contaminants of concern in all modeling cases. Including benzene is important for two reasons. First, the current MNA protocols may be more effective for benzene than MTBE because of benzene's degradability and retardation due to sorption. Including both compounds, therefore, provides a basis for comparison linked to chemical properties. Second, several researchers have shown that MTBE may not degrade while BTEX compounds are present (Church et al. 1999, Deeb et al. 2001, USEPA, 2000). The degradation case needed to account for this observation to provide a more realistic scenario for natural attenuation of MTBE.

A total of 5 cases were evaluated to illuminate critical factors for developing the conceptual model. The site characteristics used in each case were based on the Port Hueneme field site (Chapter 2). The source concentrations were based on the aqueous concentrations observed in the dissolution study discussed in the next chapter, which represented aqueous data in the immediate vicinity of an MTBE-containing gasoline source. Each case is summarized briefly below.

- *Case 1: Constant source, uniform hydrogeology, mean hydraulic conductivity*

  This is the baseline case. The differences in observed concentrations were attributable only to the limitations of the sampling networks and the differences in chemical properties.

- *Case 2: Constant source at three locations, sinusoidal higher permeability zone, mean hydraulic conductivity for each zone*

This step introduced curvature in the hydrogeology similar to that found during the tracer test at Port Hueneme without any detailed smaller scale heterogeneity. Since a uniform hydraulic gradient was imposed on the sinusoidal feature, this set of simulations demonstrated the effect of source position relative to dominant hydrogeologic features on the observed plume structure.

- *Case 3: Exponentially decaying source, sinusoidal higher permeability zone included, average characteristics for each zone*

  This case considered an exponentially decaying source zone in the same hydrogeology as the previous scenario.

- *Case 4: Exponentially decaying source, sinusoidal higher permeability zone, permeability distribution taken from site characterization transect data, full 3-D representation*

  This case introduced a three-dimensional permeability field based on characteristics measured in the tracer test site characterization.

- *Case 5: Source and hydrogeology characteristics of Experiment 4 with biodegradation added*

  In this case biodegradation was introduced as a mass-removal mechanism. The initial condition was aerobic but oxygen depletion was allowed and an anaerobic electron acceptor was available.

3.2 Experimental

The modeling was performed using the Department of Defense's Groundwater Modeling System (GMS) as a pre- and post-processing tool for U.S. Geological Survey's (USGS) Modular Three-Dimensional Finite-Difference Ground-Water Flow Model (MODFLOW) and Battelle Pacific Northwest National Laboratory's Reactive Transport in 3-Dimensions (RT3D). MODFLOW is a finite-difference model used to simulate groundwater flow in three-dimensional, heterogeneous, and anisotropic media for a constant-density fluid (Harbaugh and McDonald 1996). The version used in these simulations is MODFLOW-96, the most

recent release of the model. RT3D is able to simulate reactive flow and transport of multiple mobile and/of immobile species. RT3D has several standard reaction packages that are designed to support natural attenuation demonstrations (Clement 1997). RT3D uses the groundwater head distribution from MODFLOW as input to its flow-related calculations.

3.2.1 Relevant Equations

The governing equations for MODFLOW and RT3D are described in detail in McDonald and Harbaugh (1988) and Clement (1997) respectively. An abridged listing of the relevant equations is presented here as an aid to understanding the input approach for the modeling experiments.

MODFLOW solves the equation for three dimensional groundwater flow given by Equation 3.1.

$$\frac{\partial}{\partial x}\left(K_{xx}\frac{\partial h}{\partial x}\right) + \frac{\partial}{\partial y}\left(K_{yy}\frac{\partial h}{\partial y}\right) + \frac{\partial}{\partial z}\left(K_{zz}\frac{\partial h}{\partial z}\right) - W = S_S\frac{\partial h}{\partial t} \qquad (3.1)$$

where K_{xx}, K_{yy}, and K_{zz} are hydraulic conductivity values along the x, y, and z coordinate axes (LT^{-1}), respectively, h is the potentiometric head (L), W is a volumetric flux per unit volume representing sources and/or sinks (T^{-1}), S_S is the specific storage of the porous media (L^{-1}) and t is time (T).

RT3D uses an operator split to solve the macroscopic fate and transport equation, thus separating the equation into four components:

advection: $$\frac{\partial C}{\partial t} = -\frac{\partial(v_i C)}{\partial x_i} \qquad (3.2)$$

dispersion: $$\frac{\partial C}{\partial t} = \frac{\partial}{\partial x_i}\left(D_{ij}\frac{\partial C}{\partial x_i}\right) \qquad (3.3)$$

source/sink-mixing: $$\frac{\partial C}{\partial t} = \frac{q_s}{\phi}C_S \qquad (3.4)$$

and reaction: $$\frac{\partial C}{\partial t} = r \qquad (3.5)$$

where C is concentration (ML^{-3}), v is pore velocity (LT^{-1}), D_{ij} is the hydrodynamic dispersion coefficient (L^2T^{-1}), q_s is the volume flux of water per unit volume

representing sources and/or sinks (T^{-1}), ϕ is the soil porosity, C_s is the concentration of the source/sink (ML^{-3}), and r is any possible reaction term. The first three equations apply only to mobile species. For these experiments all species were assumed to be mobile.

3.2.2 Three-Dimensional Grid Setup

Cases 1 through 3 were run in a 2,000 m (X) x 500 m (Y) x 4 m (Z) domain on a 640,000 cell three-dimensional rectangular grid. The grid dimensions were 400 cells (X) by 200 cells (Y) by 8 cells (Z). Cases 4 and 5 used a domain size of 1,500 m (X) x 300 m (Y) x 4 m (Z) 72,000 cell grid. The grid dimensions were 150 cells (X) by 60 cells (Y) by 8 cells (Z). The X and Y dimensions represent a scale up of the Port Hueneme tracer test domain. The Z dimension corresponds to the vertical extent of the uppermost Port Hueneme aquifer in the vicinity of the tracer test.

Observation points were used to "monitor" chemical concentrations in selected cells over time. Points were placed in the center of each cell. Observation points were grouped conceptually into four distinct "sampling" networks to be used in the data evaluation: 1) a detailed three-dimensional grid, 2) five cross-gradient fences, 3) a cross-gradient source zone fence, and 4) a longitudinal transect. The five cross-gradient fences were a subset of the detailed grid. Each cross-gradient fence consisted of points at 15-m and 0.5-m spacings in the Y and Z directions, respectively. The longitudinal transect consisted of observation points located at a100-m spacing in the X direction and 0.5-m spacing in the Z direction. The location of the transect along the Y dimension changed with the location of the source zone as discussed later in this chapter.

Observation points in the three-dimensional grid were located at a 10 to15-m spacing in the X direction, a 15-m spacing in the Y direction and at 0.5-m intervals in the Z direction. The grid points began at 200 m into the domain and continued to the end of the grid. The downgradient fences were located 200 m, 400 m, 800 m, 1200 m, and 1600 m into the domain. The source zone fence bisected the source in the longitudinal direction. The longitudinal transect points began at 200 m into the domain and continued to the end of the grid.

A 10-year simulation period was used for each model run. Output data were recorded at 90-day intervals throughout each simulation. A FORTRAN program, PostRT3D (Thoms, 2002), was used to extract data at each observation point from the concentration files.

3.2.3 General Input Parameters

MODFLOW was operated with the Preconditioned Conjugate Gradient (PCG2) solver. Assigned units for all simulations were length in meters, time in days, mass in kilograms, and concentration in parts per million. Constant head boundaries were assigned at the first and last columns in the grid. Hydraulic heads at the boundaries were 50.0 m and 44.0 m, respectively, for a gradient of 0.003 m/m in Cases 1 through 3 and 0.004 m/m in Cases 4 and 5. All other cells were defined as variable head cells with a starting hydraulic head of 47.0 m.

The GMS true layer method was used to assign values to each layer. All layers were designated as confined, ensuring water saturation through each simulation. The vertical hydraulic conductivity was set to 6.65 m/d. This value was taken from the average hydraulic conductivity of soil cores taken from Port Hueneme as measured with a falling head permeameter. The horizontal hydraulic conductivity input data were based on results of the cross-gradient transect hydraulic conductivity measurements at Port Hueneme, CA. The exact input for horizontal hydraulic conductivity changed with each block of simulations as complexity in hydrogeology increased as described later.

RT3D was run with the advection, dispersion, source mixing, and chemical reaction packages activated. A 3-day transport step size was used for Cases 1 through 3. Cases 4 and 5 used a transport step of 0.1 days to accommodate the chemical reaction package needed in Case 5. Porosity was set to 0.3. The advection package specified the Modified Method of Characteristics (MMOC) as the solution method. The MMOC is a mixed Eulerian-Lagrangian solution scheme that uses a backward particle-tracking mechanism to approximate advective transport. Longitudinal dispersivity varied among simulation blocks; however, ratios of transverse and vertical dispersivity to longitudinal dispersivity were constant for all

runs at 0.1 and 0.001, respectively. The values were similar to the values observed for the tracer plume in the natural gradient tracer test. The effective molecular diffusion coefficient was 8 x 10^{-5} m^2/d . Bulk density for the material was 1,700 kg/m^3.

The source zone in each simulation was 50 m x 100 m x 2 m (W x L x H). The specific location varied with each experiment and is discussed in detail below. In all experiments the source was located in layers 1 through 4, corresponding to the uppermost 2 m of the model domain. Three species were modeled in all simulations: MTBE, benzene, and a generic conservative tracer. Linear sorption was assumed for all three species. Sorption coefficients were 0.000011 m^3/kg for MTBE, 0.00008 m^3/kg for benzene, and 0 m^3/kg for the tracer (Squillace et al. 1997). These values correspond to retardation factors of 1.06 for MTBE, 1.5 for benzene, and 1.0 for the tracer.

3.2.4 Specific Experimental Details

3.2.4.1 Case 1 – Baseline Scenario

The first experiment was a constant source in a homogeneous hydraulic conductivity field. Differences in species behavior were due entirely to chemical properties in this scenario. Figure 3.1 shows the layout of this scenario. The hydraulic conductivity equaled the average value of 91.58 m/d from the Port Hueneme transect. The value was assigned to all cells in the grid. The average groundwater velocity was 0.92 m/d.

In Case 1 the source concentrations of MTBE, benzene, and tracer were set at constant values of 300 ppm, 10 ppm, and 300 ppm, respectively. The source was placed at X = 100 – 200 m and Y = 225 – 275 m. Longitudinal dispersivity was set at 1.5 m for this scenario.

3.2.4.2 Case 2 – Block Hydraulic Conductivity Field with a Constant Source

The scenarios modeled in Case 2 are shown on Figure 3.2. The hydraulic conductivity profile was divided into two blocks of higher and lower hydraulic conductivity values. In addition, a sinusoidal channel based on the curvature of the

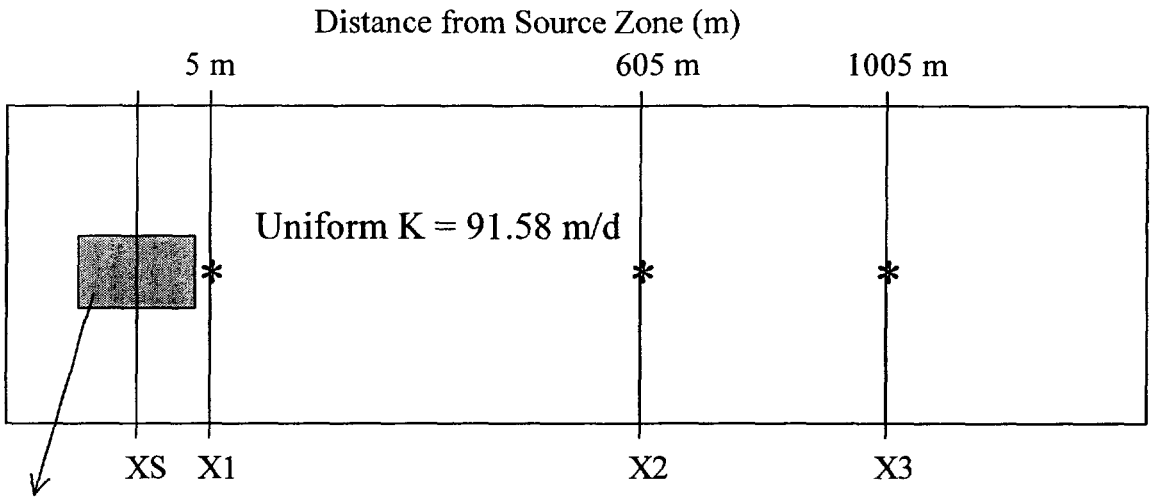

Figure 3.1: Schematic of Domain in Case 1 – Constant Source in Homogeneous Flow Field

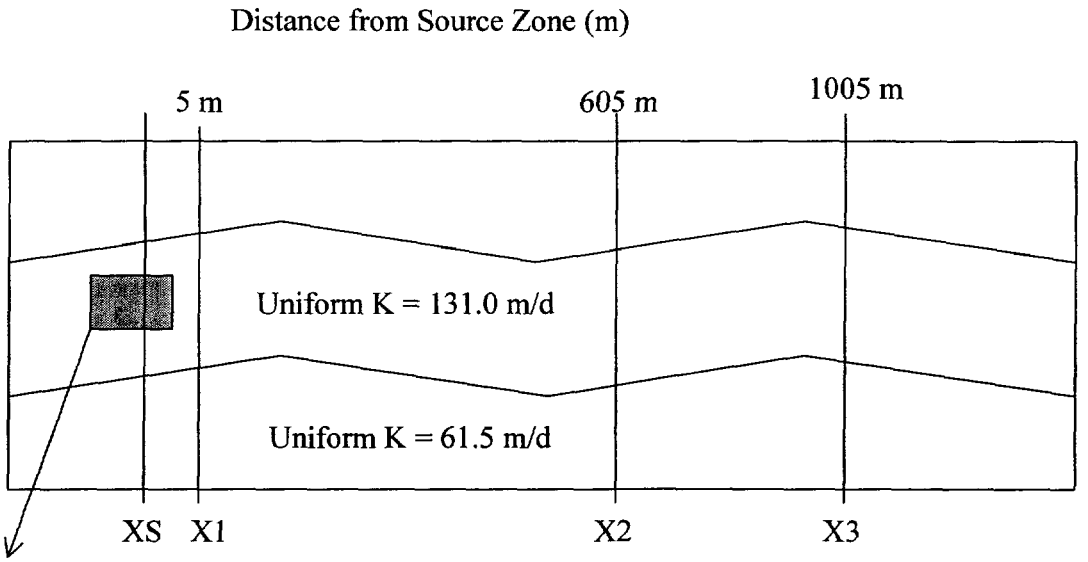

Source Zone: 50 m wide x 100 m long
XS, X1, X2, X3 = Cross-gradient fences of monitoring wells

Figure 3.2: Schematic of Domain in Case 2 – Constant Source at Three Locations in Zigzag Block Flow Field

Port Hueneme tracer plume was built into the model. Figure 2.6 showed an area of slightly higher hydraulic conductivity in the center of the Port Hueneme transect. Values from the 42.7 m to 73.7 m transect locations were averaged and assigned to the higher hydraulic conductivity channel. Values from the 0 m, 20.4 m, 83.4 m, 94.4 m, 106.0 m transect locations were averaged and assigned to the surrounding lower hydraulic conductivity region. The values in the higher and lower hydraulic conductivity blocks were 131.04 m/d and 61.50 m/d, respectively. Groundwater velocities in the two regions were 1.3 m/d and 0.62 m/d with an average velocity over the domain of 0.89 m/d. The estimated amplitude of the channel curvature was 25 m and the frequency was 160 m. The curved channel was approximated by a zigzag pattern formed by shifting the hydraulic conductivity field one cell in the Y direction every 4 cells in the X direction. The direction of the shift was reversed after every 20 shifts. Longitudinal dispersivity was input as 1 m for Case 2.

The source function and chemical concentrations were the same in Case 2 as those in Case 1. The source was moved to four different locations in relation to the channel to evaluate the effect of source position relative to hydrogeologic features on plume structure and concentration profiles. The four source locations were (1) centered along the Y axis as in Case 1, (2) in the lower hydraulic conductivity block upgradient of any curvature, (3) in the higher hydraulic conductivity block near curvature and (4) in the lower hydraulic conductivity block near curvature. Three of the four scenarios were evaluated further in this chapter. Since scenarios 2-3 and 2-4 both involve source placement near the channel boundary, only one of these two scenarios was chosen for further evaluation. Scenario 2-4 was potentially more interesting because the source was in a lower hydraulic conductivity zone just upgradient of the higher hydraulic conductivity zone.

3.2.4.3 Case 3 – Exponentially Decaying Source

An exponentially decaying source represented the next level of complexity added in Case 3. All other parameters were identical to those in Case 2. The initial concentrations of the MTBE, benzene, and the tracer were 300 ppm, 10 ppm, and

300 ppm, respectively. A first-order source decay rate with a 3-year half-life was used to generate the source concentration profiles for the three species. Although this was a simplification of actual source behavior, it was a useful means of evaluating the importance of knowing the source function when interpreting monitoring data. The source function input was accomplished by dividing a 3,660-day simulation period into 122 stress periods of 30 days each. The source zone was then modeled as a block of specified concentration point sources with a different concentration in each stress period.

3.2.4.4 Case 4 – Exponentially Decaying Source in a Three-Dimensional Hydraulic Conductivity Field

Cases 4 and 5 placed the exponentially decaying source function from Case 3 into a computer-generated three-dimensional spatially correlated random hydraulic conductivity field. The source was placed at X = 90 - 190 m and Y = 125 – 175 m. This location was centered along the Y axis as in Cases 1, 2-1, and 3.

The three-dimensional hydraulic conductivity fields were generated with FGEN (University of Waterloo, Waterloo, Ontario, Canada), a FORTRAN program designed to generate cross-correlated random fields from simple geostatics using a direct Fourier transform method (Robin et al. 1993). The input parameters required by FGEN are given in Table 3.1. The cross-correlated G field was not generated, so values pertaining to the G field and its relationship to the H field were dummy variables required to run the program.

The nodal dimensions for the fields were chosen to generate a larger field than the model domain so that a smaller a hydraulic conductivity field could be sub-sampled. The dimensions for the FGEN grid were twice the size of the grid used by MODFLOW and RT3D in all directions. The spatial step sizes were chosen to correspond to the grid cell dimensions used by MODFLOW and RT3D. The mean and variance of the Port Hueneme transect hydraulic conductivity data calculated to be 0.106 cm/s and 0.0079 $(cm/s)^2$, respectively. The power spectrum used for field generation assumed an exponential decay in the covariance with increasing distance between to points. Only one realization was generated per FGEN run.

Table 3.1: FGEN Input Used to Generate the Three-Dimensional Hydraulic Conductivity Field

Parameter	Description	Value 1	Value 2	Value 3
ISEEDH, ISEEDG	First seeds for H,G	10	10	
NFULL	Nodal dimensions of full field	300	120	16
NTRUNC	Nodel dimensions of truncated field	300	120	16
SSTEP	Spatial step size	10	5	0.5
HMEAN, GMEAN	Mean of H,G	0.106	0.106	
HVAR, GVAR	Variance of H,G	0.0079	0.0079	
HNUG, GNUG	Nugget of H,G	0.0	0.0	
ITYPE	Power spectrum type (2 = Exp. Covariance)	2		
ICROSS	Cross spectrum type (1 = linear)	1		
COHER	Coherency Squared	1.0		
HLAMDA	Correlation lengths H	1000	5	0.5
GLAMDA	Correlation lengths G	1000	5	0.5
ASLOPE	Slope linear spectrum	1.0		
DELAY	Delay vector for G rel. to H	0.0	0.0	0.0
DOGFLD	Generate G Field	F		
IPSCRN, ICAUTO	Print option/covariance option	1	1	
IWBIN, IWASC	Binary/ASCII options	0	1	
NFOUT	Number of realization to output	1		
MFOUT()	Sorted array of output	1		
NREAL	Number of realizations to generate	1		

The nugget and correlation length data were estimated by constructing variograms for the Port Hueneme data. Since the model was not an attempt to match Port Hueneme but rather to invoke similar characteristics, the variogram data were used to select reasonable input data rather than construct a rigorous hydrogeologic model of the site. The variogram [$\gamma(\mathbf{h})$] provides a characterization of spatial variability in a population (or a sample) and is defined by:

$$\gamma(\mathbf{h}) = 1/2E\{[K(\mathbf{x}) - K(\mathbf{x}+\mathbf{h})]^2\} \quad (3.6)$$

where:

$\mathbf{h}$ = separation vector or lag

$K(\mathbf{x})$ = hydraulic conductivity at $\mathbf{x}$

$K(\mathbf{x}+\mathbf{h})$ = hydraulic conductivity at $\mathbf{x}+\mathbf{h}$

$E\{\}$ = expected value operator

If the mean and covariance are assumed to be stationary the variogram can be related to the variance (σ^2) and covariance [$C_v(\mathbf{h})$] by

$$\gamma(\mathbf{h}) = \sigma^2 - C_v(\mathbf{h}) \quad (3.7)$$

$C_v(\mathbf{h})$ is defined by

$$C_v(\mathbf{h}) = 1/N \Sigma (k_i(\mathbf{x})k_i(\mathbf{x}+\mathbf{h}) - \mu_v^2 \quad (3.8)$$

where N is the number of data pairs of measured hydraulic conductivity (k_i) at locations $\mathbf{x}$ and $\mathbf{x}+\mathbf{h}$ and and μ_v is the mean.

Variograms for the Port Hueneme transect data were constructed for the cross-gradient and vertical directions. For the variogram in the vertical direction only pairs located in the same sampling location were considered. For the variogram in the cross-gradient direction, only sampling locations from 42.7 m to 106.0 m were included to have more regular spacing at 10-m intervals. The first two direct push locations are at a 20-m interval. Variograms for the Port Hueneme data are shown in Figure 3.3(a) and (b). The correlation length should be taken from the rising portion of each variogram (Rehfeldt et al., 1992); however, the Port Hueneme data present some complications. On the vertical direction variogram, there appears to be a slight inversion point at lag 3 and again at lag 4 and selection of the correlation length may be somewhat arbitrary. Since one goal of the model was to investigate

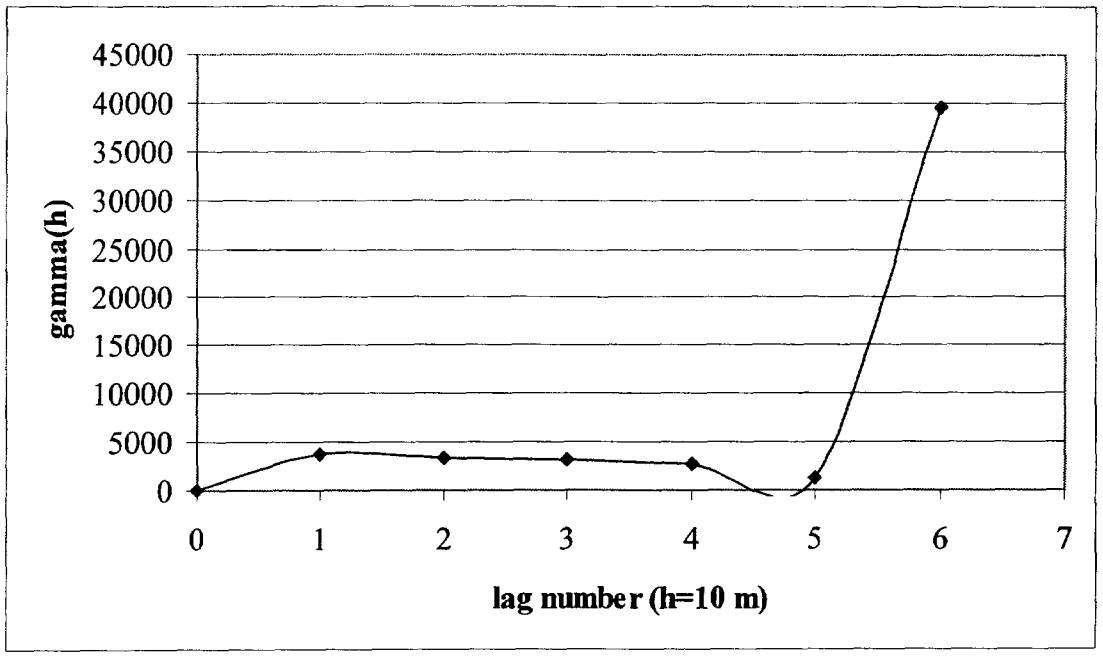

(a)

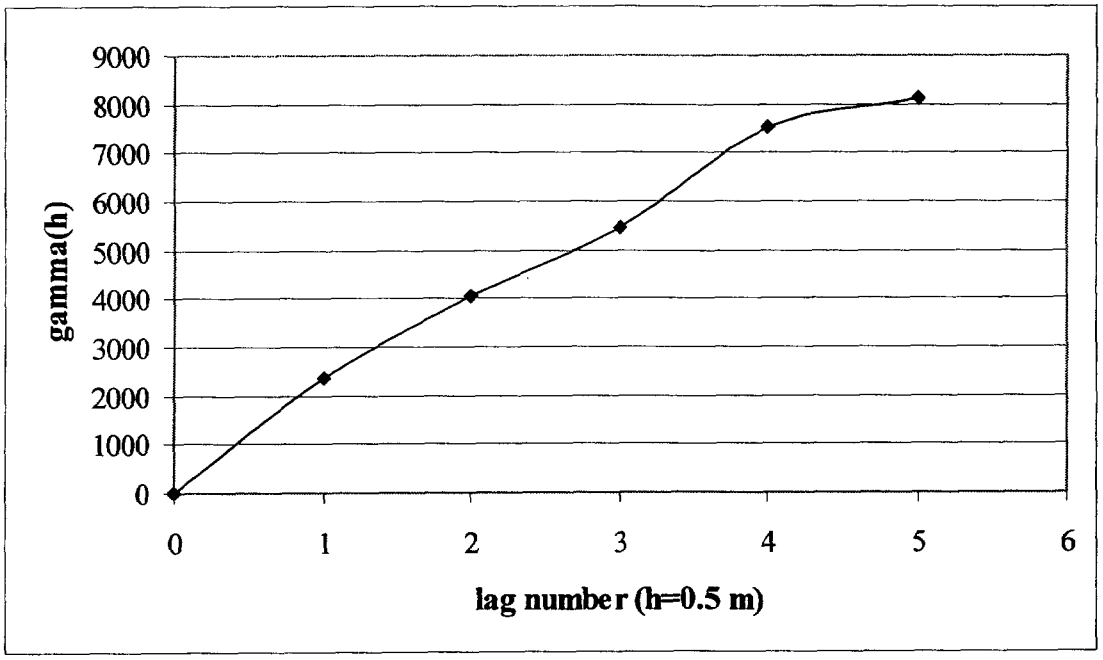

(b)

Figure 3.3: Variograms Generated from the Port Hueneme Sampling Transect Hydraulic Conductivity Data in the (a) Cross-gradient and (b) Vertical Directions

the impact of increasing heterogeneity, a vertical correlation length of 0.5 m was chosen for all simulations. The cross-gradient variogram is nearly asymptotic at one lag and exhibits irregular behavior at the greatest lags. This may be due to the presence of heterogeneity at different scales along the transect. The rising portion of the variogram occurs between 0 and 1 lag (0-10 m). Consequently, hydraulic conductivity fields used in the simulations were generated with a correlation length of 5 m . The correlation length in the longitudinal direction was not determined from field data. The long, narrow structure of the tracer plume in the natural gradient tracer test suggests that although lenses of finer or coarser material may exist, the correlation length of the dominant material could be quite large. The hydraulic conductivity field was generated with longitudinal correlation lengths of 1000 m.

Once the hydraulic conductivity fields were generated, two additional operations were required before importing the field to GMS. The same hydraulic conductivity curvature built into Cases 2 and 3 was imposed using a FORTRAN program, FGENCV (Thoms, 2002). After these modifications were made, the dataset was imported into GMS using its data browser and read into MODFLOW.

The hydraulic conductivity field generated by FGEN was statistically consistent with the input data. The output mean and variance were 0.106 cm/s and 0.0064 $(cm/s)^2$, respectively. Figure 3.4 (a) – (d) shows the Y-Z cross-sections corresponding to the source fence and cross-gradient fences 1, 3, and 4. The average groundwater velocity in this field was 0.92 m/d.

3.2.4.5 Case 5 – Biodegradation of MTBE

Case 5 incorporated an exponentially decaying source function, a three-dimensional hydraulic conductivity field, and biodegradation of MTBE by multiple electron acceptors and inhibition by the presence of BTEX compounds. The hydraulic conductivity field, MODFLOW input parameters, and source function were identical to those in Case 4. The species characteristics for Case 5 differed somewhat from previous simulations because the degradation parameters were

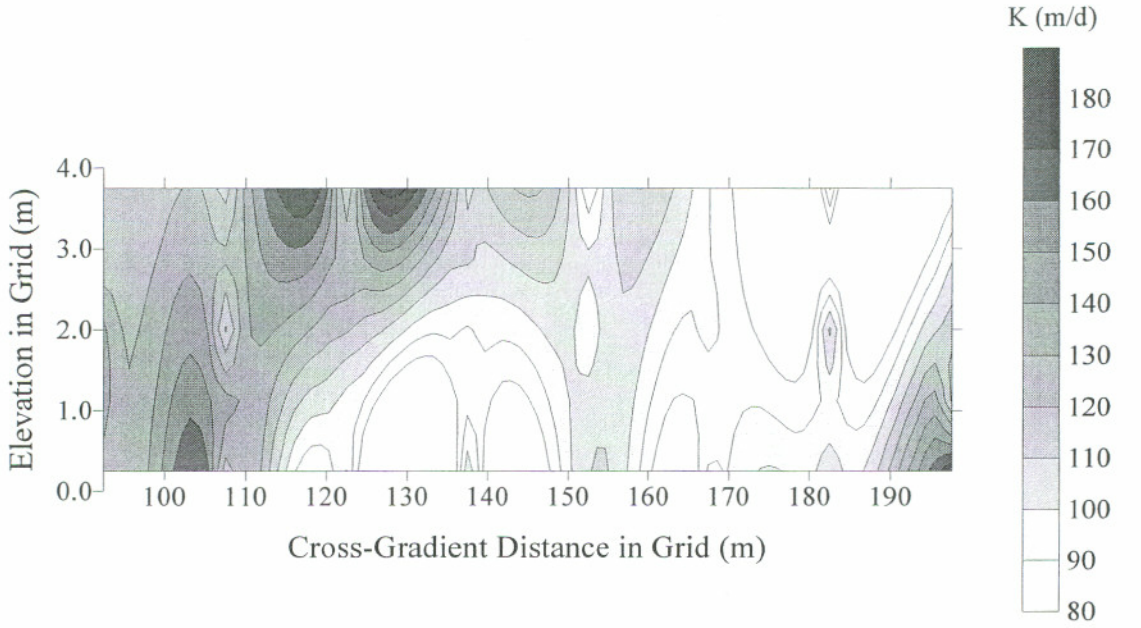

(a)

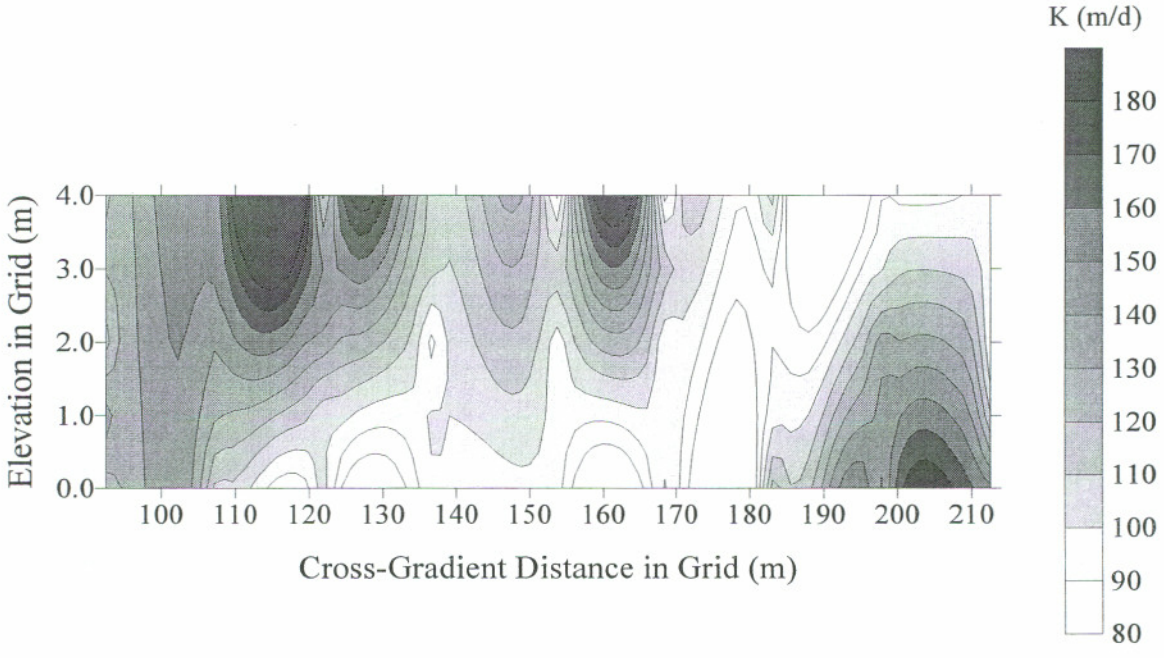

(b)

Figure 3.4: Hydraulic Conductivity in (a) Source Fence, (b) Fence X1 at 5 m from Source, (c) Fence X3 at 605 m from Source, (d) Fence X4 at 1005 m from Source

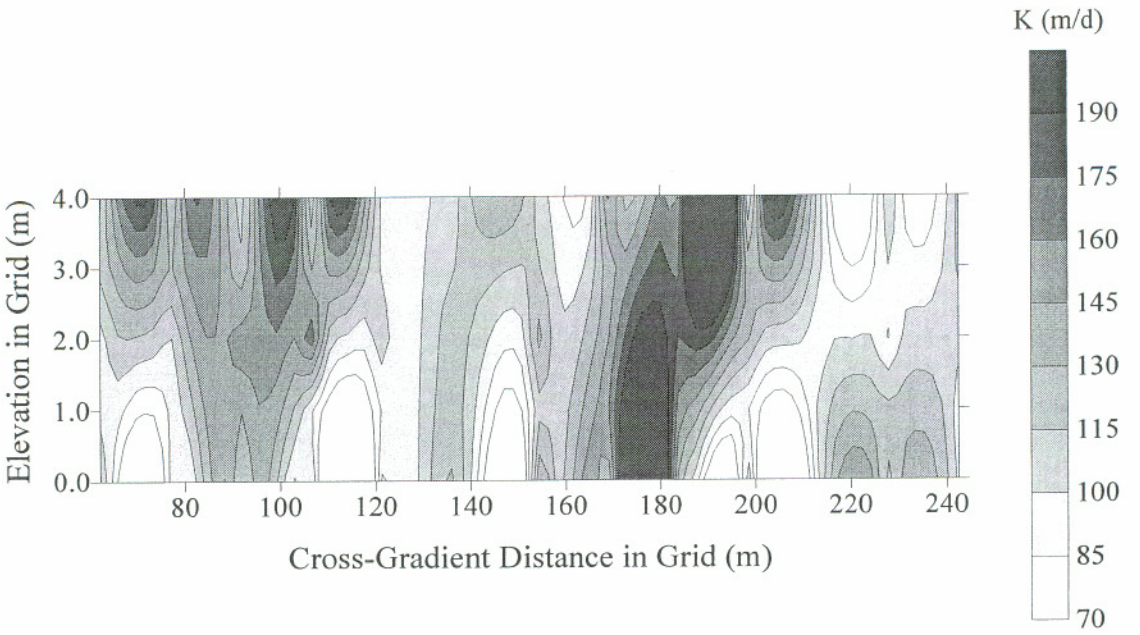

(c)

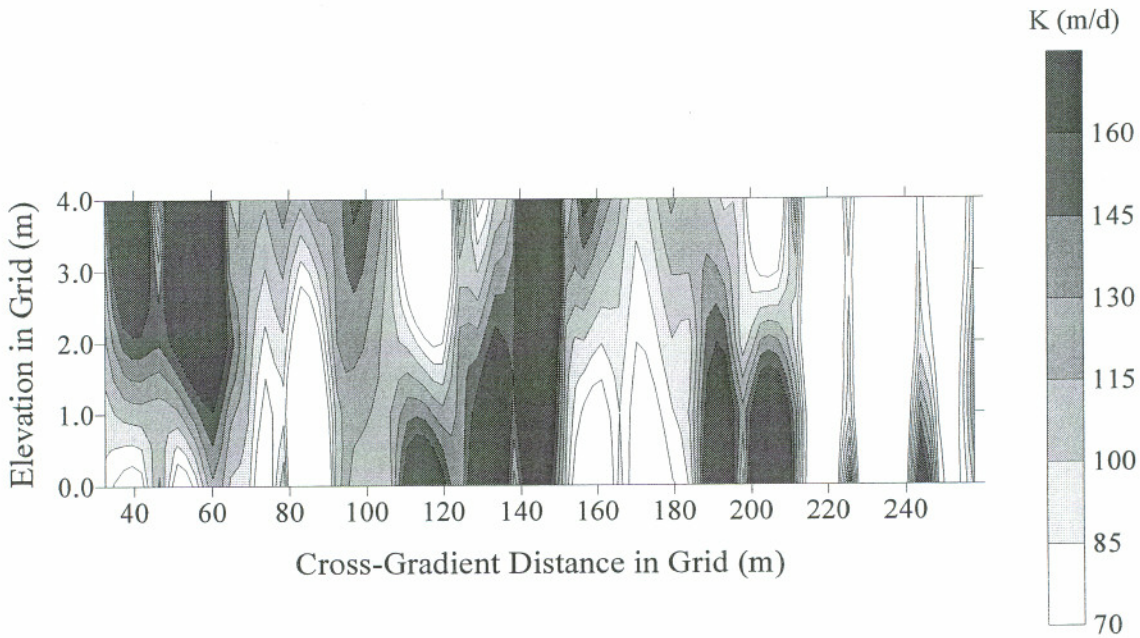

(d)

Figure 3.4 (continued): Hydraulic Conductivity in (a) Source Fence, (b) Fence X1 at 5 m from Source, (c) Fence X3 at 605 m from Source, (d) Fence X4 at 1005 m from Source

reflective of a BTEX mixture rather than just benzene. This modification was made because degradation of MTBE, and consequently the evaluation of natural attenuation, will be impacted by preferential degradation of all BTEX compounds not just benzene. The remaining species-related parameters were unchanged to allow some similarity to previous experiments.

Biodegradation was modeled using a modification of an existing RT3D reaction package for degradation of BTEX with multiple electron acceptors. The custom reaction package limited the electron acceptors to oxygen (O_2) and anaerobic electron acceptor (An). It also included MTBE as a second hydrocarbon species with a dependence on the absence of benzene for MTBE degradation to occur. The last modification was substitution of zero-order rate constants for MTBE based on the available published data on MTBE degradation. The kinetic expressions used in Case 5 were as follows:

$$\frac{d[B]}{dt} = -k_{B,O_2}[B]\frac{[O_2]}{K_{O_2}+[O_2]} - k_{B,SO_4}[B]\frac{[An]}{K_{An}+[An]}\frac{K_{i,O_2}}{K_{i,O_2}+[O_2]} \tag{3.9}$$

$$\frac{d[M]}{dt} = -k_{M,O_2}\frac{[O_2]}{K_{O_2}+[O_2]}\frac{K_{i,B}}{K_{i,B}+[B]} - k_{M,An}\frac{[An]}{K_{An}+[An]}\frac{K_{i,O_2}}{K_{i,O_2}+[O_2]}\frac{K_{i,B}}{K_{i,B}+[B]} \tag{3.10}$$

$$\frac{d[O_2]}{dt} = -Y_{O_2/B}\,k_{B,O_2}[B]\frac{[O_2]}{K_{O_2}+[O_2]} - Y_{O_2/M}\,k_{M,O_2}\frac{[O_2]}{K_{O_2}+[O_2]}\frac{K_{i,B}}{K_{i,B}+[B]} \tag{3.11}$$

$$\frac{d[An]}{dt} = -Y_{An/B}\,k_{B,An}[B]\frac{[An]}{K_{An}+[An]}\frac{K_{i,O_2}}{K_{i,O_2}+[O_2]} - Y_{An/M}\,k_{M,An}\frac{[An]}{K_{An}+[An]}\frac{K_{i,O_2}}{K_{i,O_2}+[O_2]}\frac{K_{i,B}}{K_{i,B}+[B]} \tag{3.12}$$

where [ ] is concentration of the species [ML^{-3}], k is the first- (benzene) or zero- (MTBE) order rate constant for the hydrocarbon/electron acceptor pair [T^{-1} or $ML^{-3}T^{-1}$], K is the half-saturation constant [ML^{-3}], K_i is the inhibition factor [ML^{-3}],

which lessens a term's influence as the concentrations of species included drop to zero, and Y is the mass ratio of electron acceptor consumed to hydrocarbon degraded for each pair. Although the expressions appear somewhat cumbersome, the structure was necessary to model convergence when the reaction package was incorporated into the flow model.

The RT3D default aerobic rate of 0.05 d^{-1} was used for benzene. An anaerobic benzene degradation rate of 0.003 d^{-1} was selected based on default rates for anaerobic electron acceptors. The aerobic rate for MTBE was 0.01 mg/L/d based on published microcosm and model column aquifer data (Borden et al. 1997, Schirmer et al. 1999, Church et al. 1999). Although both zero-order and first-order aerobic degradation rates are available for MTBE, assuming zero-order kinetics with respect to MTBE was reasonable given the high concentrations used in the modeling. Kinetic data for anaerobic degradation of MTBE are still limited. Some evidence of MTBE degradation under nitrate-reducing and sulfate-reducing conditions was seen in microcosm studies by Mormile et al. (1994) but was not conclusive. Microcosm data in U.S. EPA (2000) indicated that first-order degradation rates under methanogenic conditions could be similar to reported first-order aerobic rates under favorable conditions. An anaerobic MTBE degradation rate of 0.01 mg/L/d was used in the model, again assuming zero-order kinetics with respect to MTBE given the high concentrations.

The default half-saturation constants were 0.5 mg/L. Inhibition factors for oxygen and benzene were 0.01 mg/L and 0.005 mg/L, respectively. The inhibition factors indicate values below which the corresponding term in the kinetic expression becomes increasingly insignificant. Yields for O_2/benzene and An/benzene were 3.13 and 4.7, respectively. Yields for O_2/MTBE and An/MTBE were 2.73 and 4.09, respectively. Prior to using the reaction package in the flow model it was tested for appropriate behavior using BATCHRXN, a program that simulates a batch reactor. The BATCHRXN output is plotted in Figure 3.5.

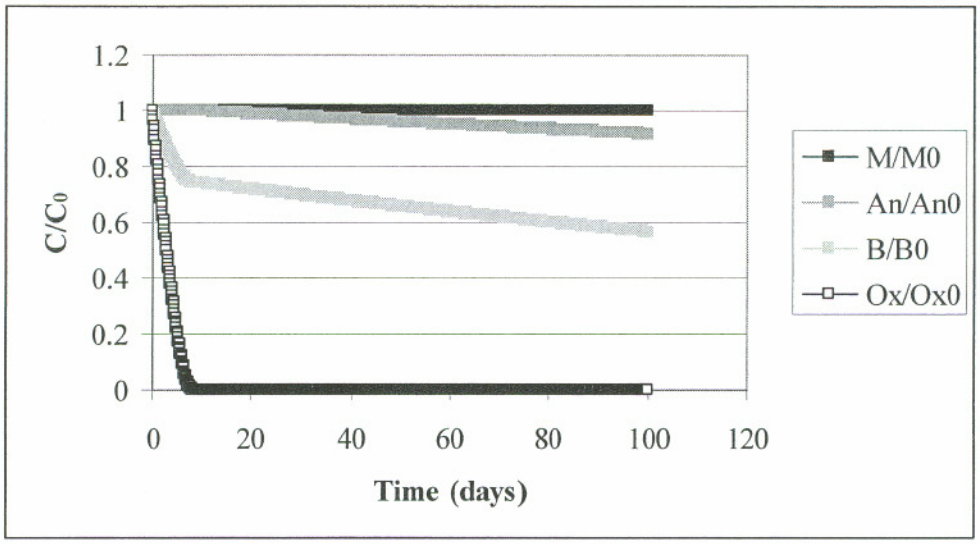

Figure 3.5: Reaction Package Output Showing MTBE, Anaerobic Electron Acceptor, Benzene, and Oxygen Profiles with Time Under Batch Reactor Conditions

3.2.5 Data Evaluation

3.2.5.1 Phase 1 – Relating model data to traditional sampling networks

To relate the data generated for the grid blocks to scenarios that have physical meaning for a field site, model data were put into sampling scenarios that could realistically occur at a site. The result was a series of concentration versus time (C vs. t) and distance (C vs. d) plots for the longitudinal transect, mass fluxes at snapshots in time for the fences, and plume contours over the model domain. In addition, mass balances were performed for each species at snapshots in time. The times chosen for snapshot calculations were 1,080 days, 2,070, and 3,060 days. These three times were selected to evaluate the use of fences and transects for assessing natural attenuation of expanding plumes.

In each experiment beyond the base case (Case 1), Surfer version 6.04 (Golden Software, Inc., 1996) was used to construct contour plots of the vertically-averaged plume data for each of the species at 1,080 days, 2,070 days, and 3,060 days using data from the full three-dimensional grid. Footprints of contaminant plumes and geochemical indicators of biodegradation are widely used to classify plumes and shrinking, stable or expanding (National Research Council, 2000). The plots also provided an excellent way to visually assess the impact of source function and hydrogeology on plume behavior over time.

The longitudinal transect represented a series of pairs of monitoring wells placed at 100-m intervals from the edge of the source zone to the end of the model domain oriented with the direction of groundwater flow. The wells reflected 2-m sampling intervals from 2 m to 4 m in elevation and 0 m to 2 m in elevation. This corresponded to the interval containing the source zone layers and the interval beneath the source zone layers. Because GMS produced data in 0.5-m vertical intervals, 2-m concentrations were calculated by averaging the 0.5-m concentrations for the appropriate layers. When layers were assigned different hydraulic conductivities (Cases 4 and 5), the concentrations were weighted according to the flow contribution to the well expected from each layer.

The fences were composed of sampling wells located at 15-m intervals across the plume. The flux associated with a given well and sampling interval in grams/day

was calculated by multiplying the measured concentration (g/m^3) by the groundwater velocity (m/d) and cross-sectional area perpendicular to groundwater flow (m^2). The cross-sectional area was equal to the length of the well sampling interval multiplied by the spacing between adjacent wells, taken from the midpoint between wells in either direction. To determine what, if any, effect well spacing has on the calculated attenuation rate, flux calculations were performed using 15-m and 30-m spacing. The fences located at ~5 m, ~600 m, and ~1000 m from the source were used for all flux calculations. In all cases the central well in the fence was in line with the source zone and the fence continued until the fluxes calculated on both sides of the plume were 0.0 g/d.

Data were evaluated to reflect two field sampling scenarios. The first assumed a uniform groundwater velocity based on the average hydraulic conductivity value for the grid. The second approach incorporated a local velocity calculated from hydraulic conductivity "measured" at the same sampling interval. The calculated velocity profile is assumed to apply over the cross-gradient interval associated with that well.

Flux calculations were performed using both 0.5-m and 2-m vertical intervals. Again, concentrations were averaged to obtain a 2-m concentration from the 0.5-m GMS grid spacing. In addition, an average hydraulic conductivity was calculated by taking the arithmetic mean to approximate the 2-m hydraulic conductivity data needed for the 2-m "measured" scenario. An arithmetic composition was chosen because the blocks of hydraulic conductivity are in parallel in relation to the direction of flow, although the true value would likely lie between the arithmetic and harmonic means (Marsily, 1986).

The method of moments (see Chapter 2) was used to calculate the total mass in the domain downgradient of the source zone at 1080 days, 2070 days, and 3060 days using data from the full three dimensional sampling grid. This provided a quantitative big-picture view of changes in the domain with time.

3.2.5.2 Phase 2 – Evaluation of Attenuation and Degradation Rates

The longitudinal transect data were evaluated as C versus d plots at 1080 days, 2070 days, and 3060 days. The plots were examined for obvious effects of hydrogeology, exponential source behavior and degradation on the contaminant profile. The contaminant velocity (seepage velocity divided by retardation factor) was used to convert the distance measurements into residence times in the system. In Cases

2-4, 4 and 5 several of velocities could be used to calculate residence times. In experiment 2-4 high and low velocities were calculated using the hydraulic conductivity values of the two material blocks, 131.04 m/d and 61.5 m/d, respectively. In Cases 4 and 5 the high and low velocities were calculated from hydraulic conductivity values at plus/minus one standard deviation from the mean value of the generated field,

160.7 mg/d and 22.5 m/d, respectively.

Apparent attenuation rates were calculated using the upper 2-m well data. Plots of log (C/C_0) versus residence time (RT) were generated for each compound and fitted with a linear trend line to estimate first-order attenuation rates. In all cases, C_0 is taken as the concentration of the compound in the source zone at the snapshot time. The attenuation rates generated by these plots encompass attenuation due to all mechanisms. To estimate a degradation rate, the measured contaminant concentrations were corrected using the source zone and measured tracer concentrations (T_0 and T_{meas}, respectively) such that

$$C_{corr} = \frac{C_{meas}}{\frac{T_{meas}}{T_0}} \qquad (3.13)$$

where C_{corr} and C_{meas} are respectively the corrected and measured concentrations of benzene or MTBE. The corrected values then reflected the concentrations that should have been measured if dispersion and sorption were not occurring. Because the tracer has a retardation factor of 1, it was a better correction factor for MTBE

than for benzene. Plots of log (C_{corr}/C_0) versus t then yielded estimated degradation rates.

An analysis was performed to evaluate whether or not accounting for the source function yielded improved attenuation rates from the longitudinal transect. Plotting C/C_{max} for benzene and MTBE provided an overall attenuation rate while accounting for the effect of the source function. C_{max} was defined as the source contaminant or tracer concentration that would have reached distance d if no attenuation had occurred. The correction procedure described above was repeated using T_{max} values. Plots of log (C_{corr}/C_{max}) versus t yielded an estimated degradation rate with the influence of the source function removed.

Natural attenuation rates based on mass fluxes through the fences were evaluated using the change in flux with time at a single fence and the change in flux between fences at a snapshot in time. The fences used in the analyses were located through the source zone (XS), 5 m downgradient (X1), 600 m downgradient (X3), and 1000 m downgradient (X4). Changes in flux with time were quantified at 1080 days, 2070 days, and 3060 days. Flux differences between fences were quantified for the six possible fence pairings to determine the changes in magnitude between fences and to evaluate the importance of fence spacing. The resulting differences for MTBE and benzene were compared to those for the conservative tracer. These calculations were performed at both 15-m and 30-m well spacing. In addition, attenuation rates were evaluated for both 0.5-m and 2-m vertical sampling intervals by considering the mass flux over the desired vertical interval.

Three additional evaluation methods were used when the exponential source function was included. The first related the change in flux with time observed at a given fence to the corresponding change in the source flux at the time that the parcel of water left the source based on each contaminant velocity. The second related the flux at a given fence and snapshot in time to the corresponding flux from the source, again accounting for the residence time in the system between the source and downgradient fences. The third was a comparison of fluxes from XS, X1 and X3 to that at X4 at 2070 days, accounting for residence time in the system. The required sampling times for a parcel of water arriving at X4 at 2070 days were not extracted

from the model output; therefore, the sampled times bracketing the actual times were used in the evaluation.

3.3 Results and Discussion

3.3.1 Cases 1 and 2 – Constant Source Function

Results for Experiments 1 and 2 have been grouped because the modeling scenarios differ only in the hydraulic conductivity field used and the source placement within that field. Consequently, differences in natural attenuation estimates can be readily attributed to relatively simple changes in site conditions. Benzene, MTBE, and tracer footprints were prepared for the three scenarios in Case 2 for which natural attenuation estimates were calculated. The results for scenario 2-1 are shown in Figures 3.6 through 3.8 as an example of the plume behavior with the curvature.

The C vs. d profiles in the upper wells at 1080 days and 2070 days show a gradual decrease in concentration followed by a drop corresponding to the toe of the plume. In the lower wells, there is a gradual rise followed by a drop at the toe of the plume. The behavior was consistent with spreading by dispersion. By 3060 days the MTBE and tracer plumes had moved through the farthest sampling point in the transect. Figures 3.9 through 3.11 show the C vs. d plots for the three species at 3060 days for all scenarios in Cases 1 and 2. The impact of the zigzag channel in Case 2 is evident in the oscillations in species concentrations between higher and lower values along the transect.

Attenuation of species' concentrations was due to dispersion once sorption effects were accounted for in the contaminant velocity. Apparent attenuation rates based on C vs. d data at t = 3060 days for all scenarios in Cases 1 and 2 are presented in Table 3.2. Multiple attenuation rates were presented for Case 2-4 to reflect the range of hydraulic conductivity encountered along the transect. Rates were listed as "not significant" if the $\log(C/C_0)$ or $\log(C/C_{max})$ vs. t plots showed scattered values with no observable trend. Apparent attenuation rates varied according to the contaminant velocity in each scenario.

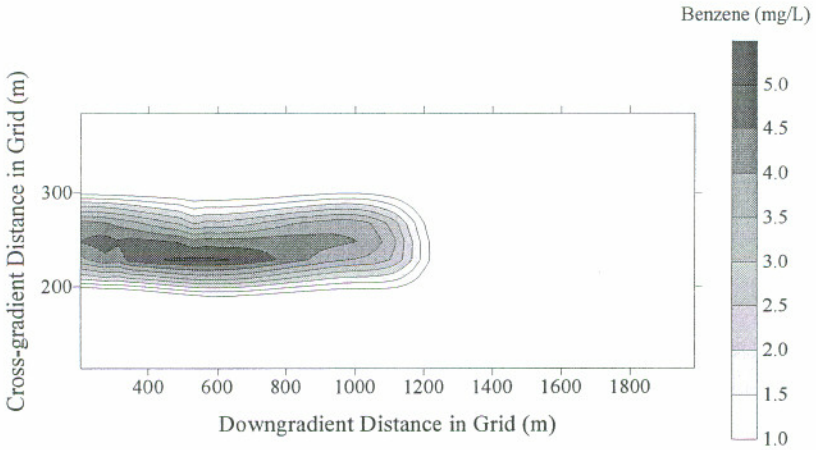

(a)

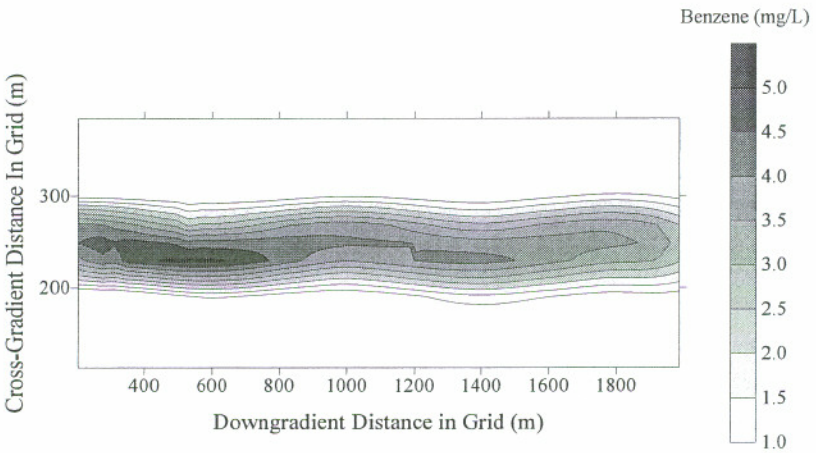

(b)

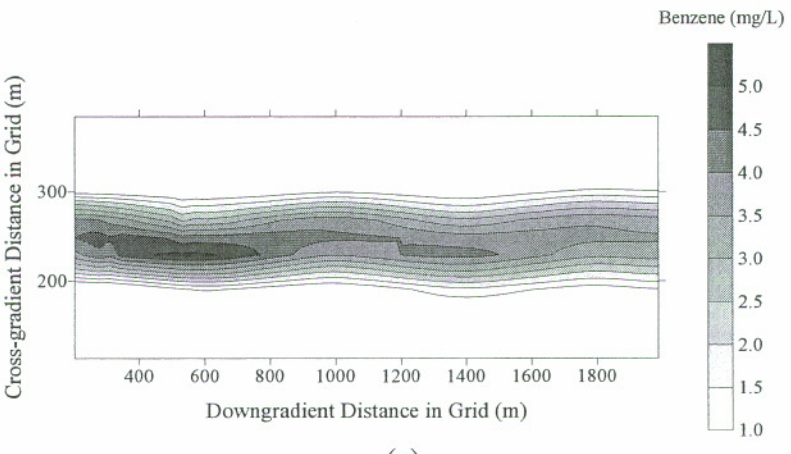

(c)

Figure 3.6: Case 2-1 Benzene Footprints at (a) 1080 Days, (b) 2070 Days, (c) 3060 Days

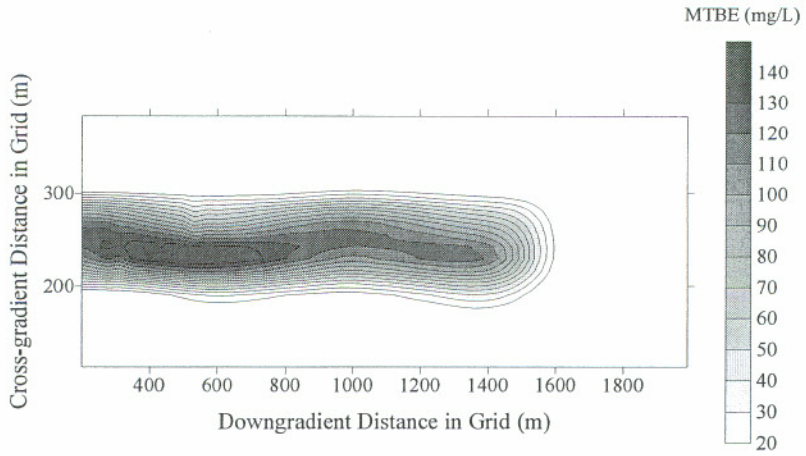

(a)

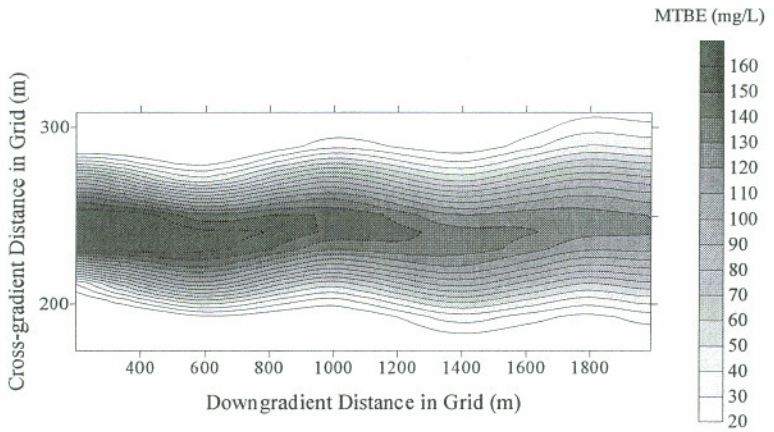

(b)

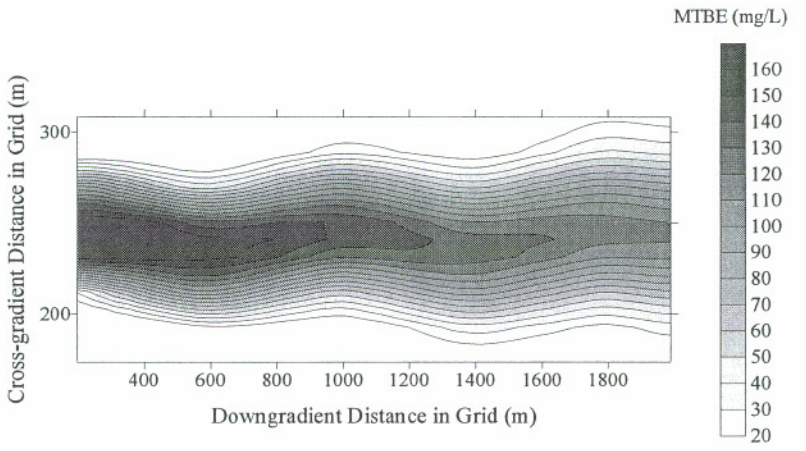

(c)

Figure 3.7: Case 2-1 MTBE Footprints at (a) 1080 Days, (b) 2070 Days, (c) 3060 Days

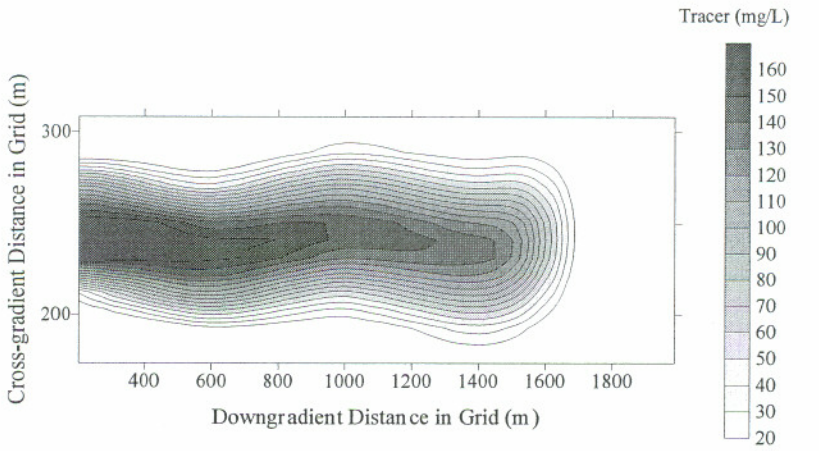

(a)

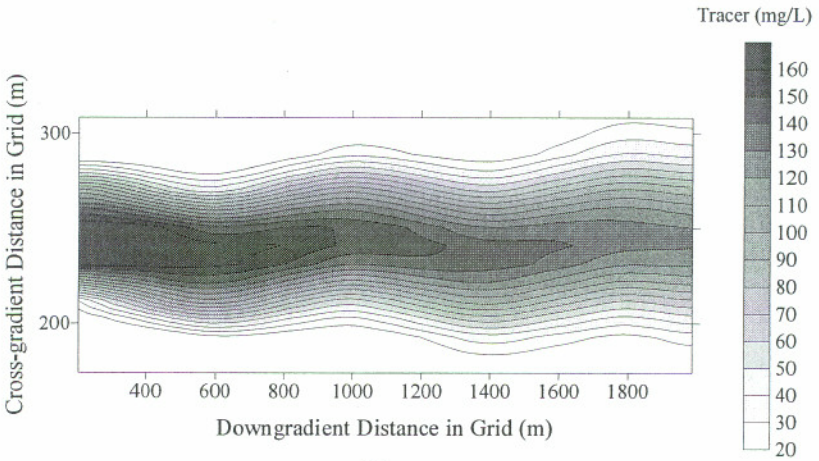

(b)

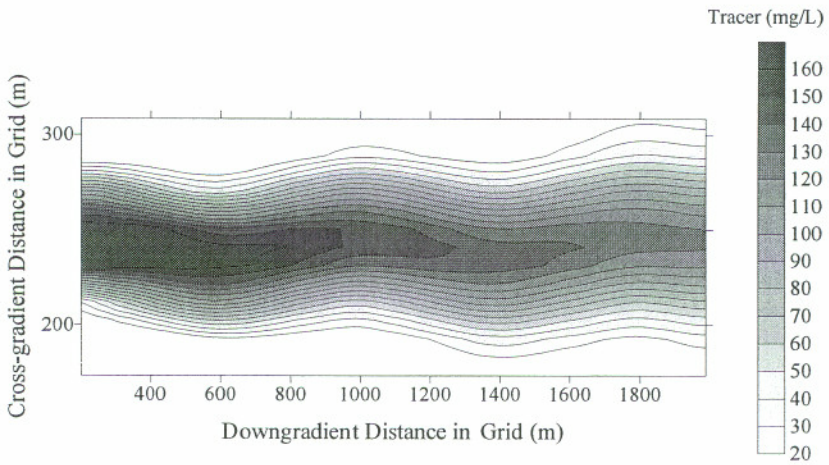

(c)

Figure 3.8: Case 2-1 Tracer Footprints at (a) 1080 Days, (b) 2070 Days, (c) 3060 Days

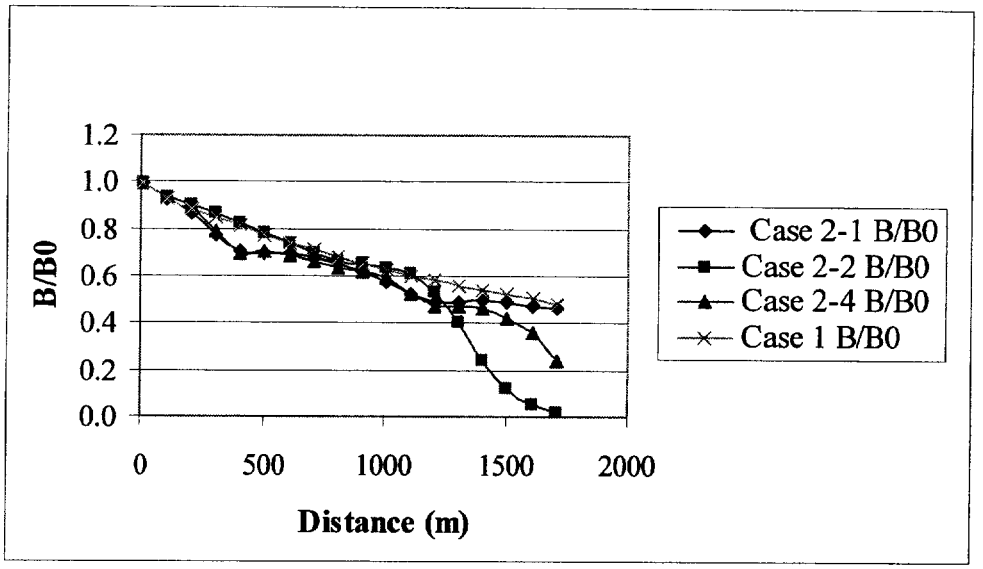

(a)

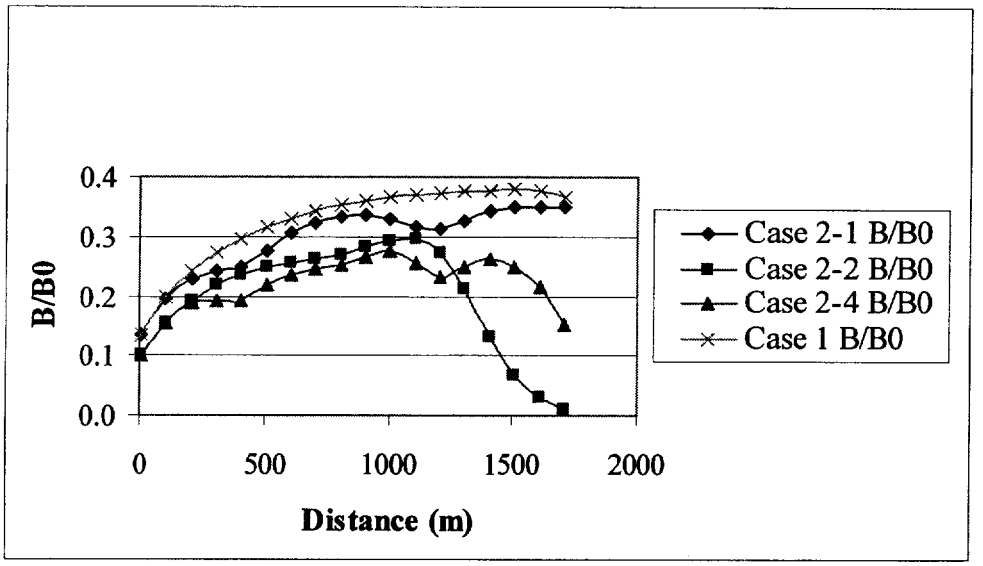

(b)

Figure 3.9: Benzene Concentrations along the Longitudinal Transect for the Four Constant Source Function Scenarios in (a) Upper 2-m Wells and (b) Lower 2-m Wells at 3060 Days

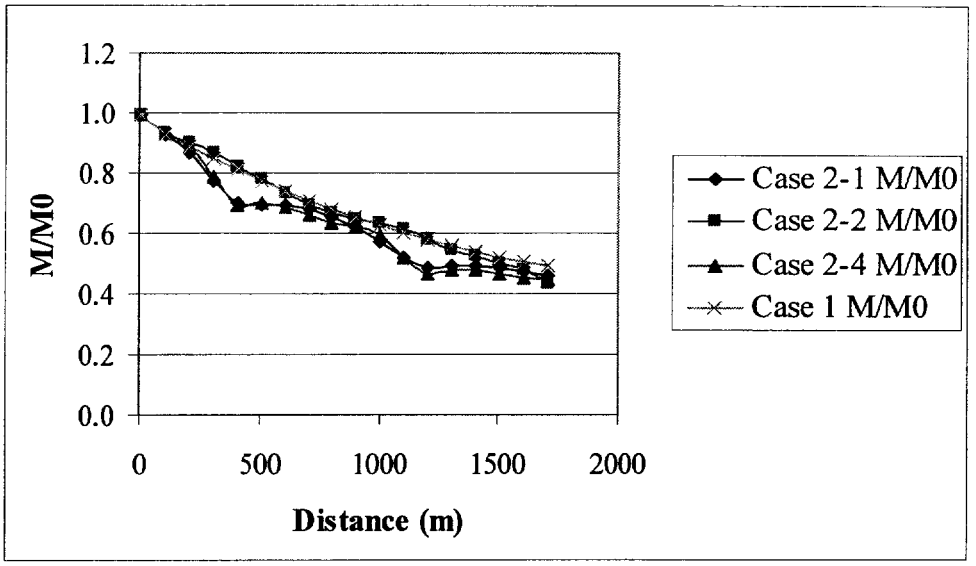

(a)

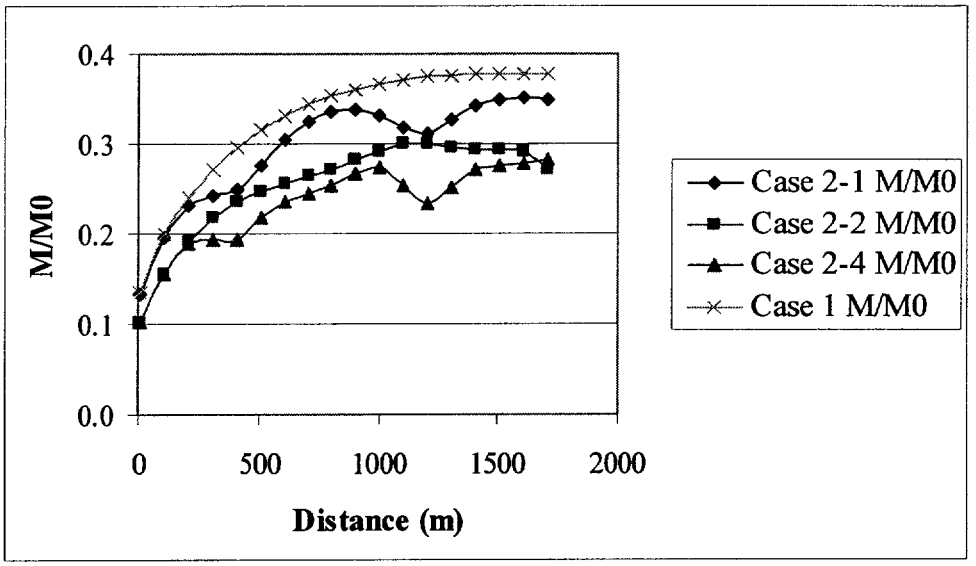

(b)

Figure 3.10: MTBE Concentrations along the Longitudinal Transect for the Four Constant Source Function Scenarios in (a) Upper 2-m Wells and (b) Lower 2-m Wells at 3060 Days

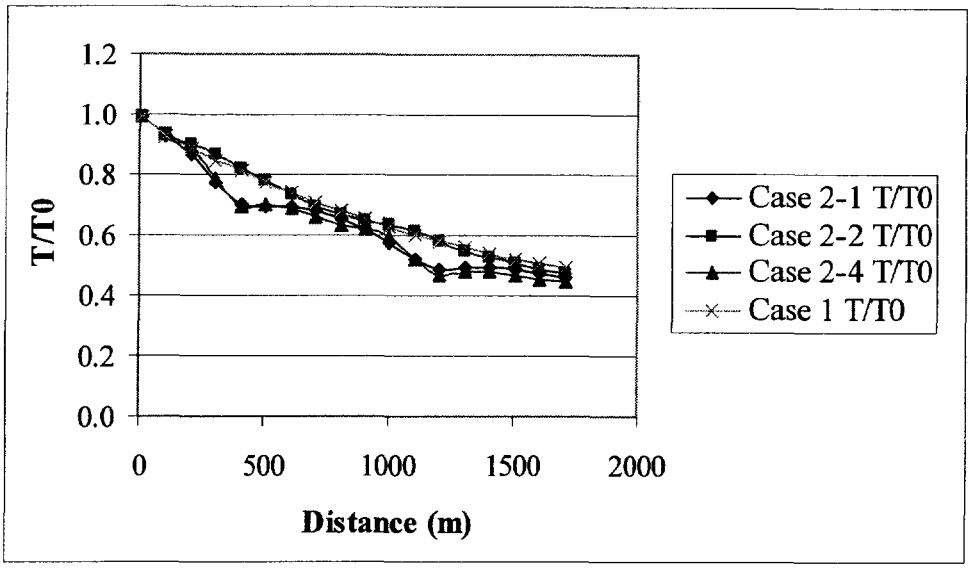

(a)

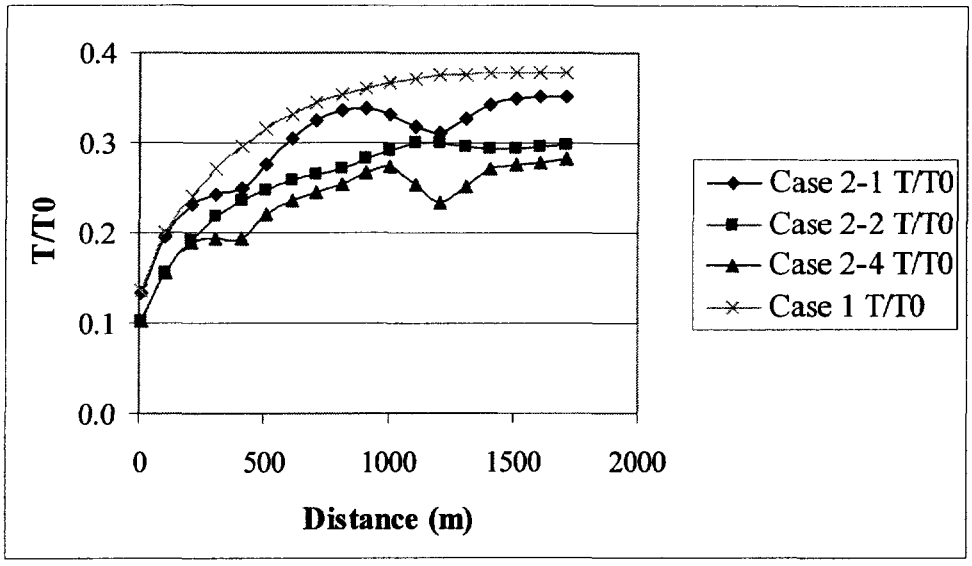

(b)

Figure 3.11: Tracer Concentrations along the Longitudinal Transect for the Four Constant Source Function Scenarios in (a) Upper 2-m Wells and (b) Lower 2-m Wells at 3060 Days

For example, the highest rates were calculated for MTBE and the tracer in Case 2-1 and 2-4 (high), which used the highest flow velocity.

In the constant source scenarios, changes in mass flux with time at a given fence demonstrated how the interaction of the source and the hydrogeology might impact a natural attenuation demonstration using this approach. The data showed that changes in mass flux with time only occurred at fences X3 and X4 while the plume was still expanding past those fence locations. Once the advective front of the plume had reached all four fences no changes in mass flux were observed with increasing time. The data for fence X4 in scenario 2-4 are shown in Figure 3.12 as an example.

An alternative use of fences was to observe changes in mass flux between fences using snapshots at t = 1080 days, t = 2070 days, and t= 3060 days. Data from Cases 1 and 2 are given in Table 3.3(a) – (d). The plume expansion shown in the footprints in Figures 3.6 – 3.8 can be seen in the large negative values between fences at t = 1080. Since the flux from the source is constant in each scenario, smaller differences between fence pairs represented smaller errors due to dispersive mass flux and well placement relative to the plume migration pathway. This is important in assessing natural attenuation with this approach because increases due to the dispersive mass flux could mask decreases due to degradation. Dispersive mass fluxes consistently increased with distance between fences. In general, the 15-m well spacing produced smaller differences than the 30-m spacing; however, there are several instances in the Case 2 scenarios where the opposite was true. In addition, the fluxes based on "measured" hydraulic conductivity values often produced in mass flux. These observations suggested that the curvature in the hydraulic conductivity field between the fences and the well placement in relation to that curvature ultimately affected the calculated flux differences between fences. This may have occurred because of the block hydraulic conductivity fields used in these scenarios. The effect was further evaluated with the three-dimensional hydraulic conductivity field in Case 4.

The total mass calculations quantified the movement of contaminants from the source into the sampling grid. These calculations provided a numerical

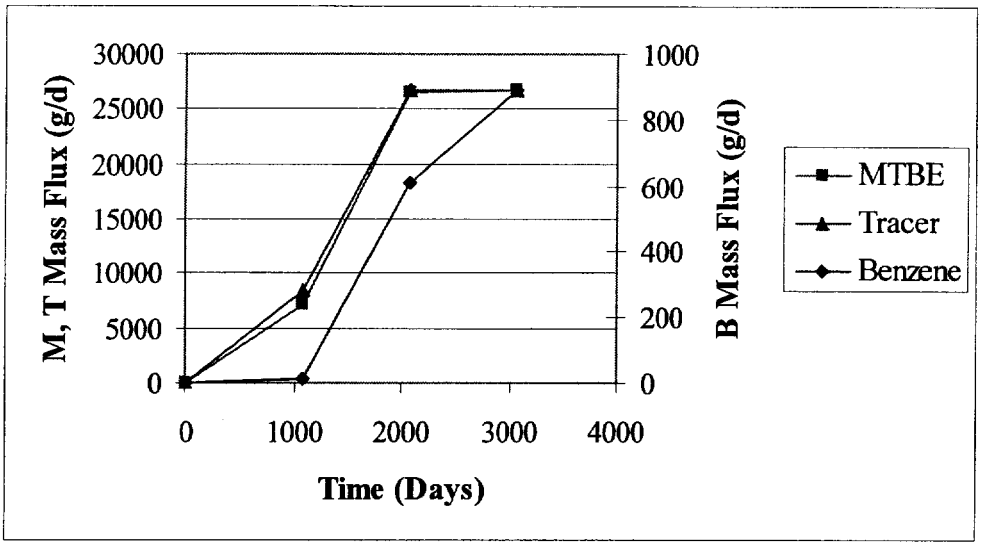

Figure 3.12: Change in Contaminant Mass Fluxes with Time for a Constant Source at the Far Downgradient Fence (X4) in Case 2-4

Table 3.2: First-Order Attenuation Rates (day^{-1}) for Constant Source Function Based on t = 3060 Days C versus Distance Data in Cases 1 and 2

Case	Calculated by:	Benzene	MTBE	Tracer	Attributed to:
1	C/C_0	-0.0001 R^2=0.99	-0.0002 R^2=0.98	-0.0002 R^2=0.98	Dsp
1	C_{corr}/C_0	NS	NS	NA	
2-1	C/C_0	-0.0002 R^2=0.91	-0.0003 R^2=0.91	-0.0003 R^2=0.91	Dsp
2-1	C_{corr}/C_0	NS	NS	NA	
2-2	C/C_0	-9E-5 R^2=0.99	-0.0001 R^2=0.99	-0.0001 R^2=0.99	Dsp
2-2	C_{corr}/C_0	NS	NS	NA	
2-4 high	C/C_0	-0.0002 R^2=0.92	-0.0003 R^2=0.94	-0.0003 R^2=0.94	Dsp
2-4 high	C_{corr}/C_0	NS	NS	NA	
2-4 average	C/C_0	-0.0002 R^2=0.92	-0.0002 R^2=0.94	-0.0002 R^2=0.94	Dsp
2-4 average	C_{corr}/C_0	NS	NS	NA	
2-4 low	C/C_0	-0.0001 R^2=0.92	-0.0001 R^2=0.94	-0.0001 R^2=0.94	Dsp
2-4 low	C_{corr}/C_0	NS	NS	NA	

NS = Not Significant; NA = Not Applicable
Dsp = Dispersion

Table 3.3(a): Changes in Benzene (B), MTBE (M), and Tracer (T) Mass Fluxes (g/day) Between Cross-gradient Fences for Case 1

			t = 1080 Days			t = 2070 Days			t = 3060 Days		
Fences	K Field	Distance (m)	B	M	T	B	M	T	B	M	T
X1-XS 15-m	Average	55	120	3607	3609	120	3607	3609	120	3607	3609
X1-XS 30-m	Average	55	188	5649	5651	188	5649	5651	188	5649	5651
X1-XS 15-m	Measured	55	120	3607	3609	120	3607	3609	120	3607	3609
X1-XS 30-m	Measured	55	188	5649	5651	188	5649	5651	188	5649	5651
X3-XS 15-m	Average	655	-16	5226	5227	174	5227	5227	174	5227	5227
X3-XS 30-m	Average	655	189	11561	11561	380	11561	11561	380	11561	11561
X3-XS 15-m	Measured	655	-16	5226	5227	174	5227	5227	174	5227	5227
X3-XS 30-m	Measured	655	189	11561	11561	380	11561	11561	380	11561	11561
X3-X1 15-m	Average	600	-136	1619	1618	54	1619	1618	54	1619	1618
X3-X1 30-m	Average	600	2	5911	5910	192	5912	5910	192	5912	5910
X3-X1 15-m	Measured	600	-136	1619	1618	54	1619	1618	54	1619	1618
X3-X1 30-m	Measured	600	2	5911	5910	192	5912	5910	192	5912	5910
X4-XS 15-m	Average	1055	-976	-25236	-17155	171	5175	5174	171	5175	5174
X4-XS 30-m	Average	1055	-768	-18983	-10904	380	11427	11427	380	11427	11427
X4-XS 15-m	Measured	1055	-976	-25236	-17155	171	5175	5174	171	5175	5174
X4-XS 30-m	Measured	1055	-768	-18983	-10904	380	11427	11427	380	11427	11427
X4-X1 15-m	Average	1000	-1096	-28844	-20764	51	1567	1565	51	1567	1565
X4-X1 30-m	Average	1000	-956	-24633	-16555	192	5778	5776	192	5778	5776
X4-X1 15-m	Measured	1000	-1096	-28844	-20764	51	1567	1565	51	1567	1565
X4-X1 30-m	Measured	1000	-956	-24633	-16555	192	5778	5776	192	5778	5776
X4-X3 15-m	Average	400	-960	-30463	-22382	-3	-52	-53	-3	-52	-53
X4-X3 30-m	Average	400	-957	-30544	-22465	0	-134	-134	0	-134	-134
X4-X3 15-m	Measured	400	-960	-30463	-22382	-3	-52	-53	-3	-52	-53
X4-X3 30-m	Measured	400	-957	-30544	-22465	0	-134	-134	0	-134	-134

Table 3.3(b): Changes in Benzene (B), MTBE (M), and Tracer (T) Mass Fluxes (g/day) Between Cross-gradient Fences for Case 2-1

			t = 1080 Days			t = 2070 Days			t = 3060 Days		
Fences	K Field	Distance (m)	B	M	T	B	M	T	B	M	T
X1-XS 15-m	Average	55	117	3518	3520	117	3518	3520	117	3518	3520
X1-XS 30-m	Average	55	184	5541	5545	184	5541	5545	184	5541	5545
X1-XS 15-m	Measured	55	172	5162	5165	172	5162	5165	172	5162	5165
X1-XS 30-m	Measured	55	270	8131	8137	270	8131	8137	270	8131	8137
X3-XS 15-m	Average	655	182	5464	5464	182	5464	5464	182	5464	5464
X3-XS 30-m	Average	655	381	11435	11437	381	11435	11437	381	11435	11437
X3-XS 15-m	Measured	655	268	8018	8018	268	8018	8018	268	8018	8018
X3-XS 30-m	Measured	655	559	16779	16782	559	16779	16782	559	16779	16782
X3-X1 15-m	Average	600	65	1946	1945	65	1946	1945	65	1946	1945
X3-X1 30-m	Average	600	197	5894	5892	197	5894	5892	197	5894	5892
X3-X1 15-m	Measured	600	96	2856	2854	96	2856	2854	96	2856	2854
X3-X1 30-m	Measured	600	289	8649	8646	289	8649	8646	289	8649	8646
X4-XS 15-m	Average	1055	-648	5349	5353	179	5355	5354	179	5355	5354
X4-XS 30-m	Average	1055	-449	11311	11316	377	11317	11317	377	11317	11317
X4-XS 15-m	Measured	1055	-952	7599	7606	254	7607	7607	254	7607	7607
X4-XS 30-m	Measured	1055	-662	16173	16181	539	16180	16182	539	16180	16182
X4-X1 15-m	Average	1000	-765	1832	1834	62	1838	1835	62	1838	1835
X4-X1 30-m	Average	1000	-633	5770	5771	193	5776	5772	193	5776	5772
X4-X1 15-m	Measured	1000	-1124	2438	2441	82	2445	2442	82	2445	2442
X4-X1 30-m	Measured	1000	-932	8042	8044	269	8049	8045	269	8049	8045
X4-X3 15-m	Average	400	-830	-115	-111	-4	-109	-110	-4	-109	-110
X4-X3 30-m	Average	400	-830	-124	-121	-14	-118	-119	-14	-118	-119
X4-X3 15-m	Measured	400	-1220	-418	-413	-20	-411	-412	-20	-411	-412
X4-X3 30-m	Measured	400	-1221	-607	-602	-11	-600	-600	-11	-600	-600

Table 3.3(c): Changes in Benzene (B), MTBE (M), and Tracer (T) Mass Fluxes (g/day) Between Cross-gradient Fences for Case 2-2

			t = 1080 Days			t = 2070 Days			t = 3060 Days		
Fences	K Field	Distance (m)	B	M	T	B	M	T	B	M	T
X1-XS 15-m	Average	55	26	763	763	26	763	763	26	763	763
X1-XS 30-m	Average	55	16	460	459	16	460	459	16	460	459
X1-XS 15-m	Measured	55	18	525	525	18	525	525	18	525	525
X1-XS 30-m	Measured	55	11	317	316	11	317	316	11	317	316
X3-XS 15-m	Average	655	-944	-10871	-7305	-127	-3815	-3816	-127	-3815	-3816
X3-XS 30-m	Average	655	-953	-10403	-7026	-123	-3721	-3726	-123	-3721	-3726
X3-XS 15-m	Measured	655	-598	-5515	-3061	-21	-654	-658	-21	-654	-658
X3-XS 30-m	Measured	655	-564	-3620	-1296	34	985	977	34	985	977
X3-X1 15-m	Average	600	-970	-11634	-8067	-152	-4578	-4579	-152	-4578	-4579
X3-X1 30-m	Average	600	-969	-10863	-7486	-139	-4182	-4186	-139	-4182	-4186
X3-X1 15-m	Measured	600	-615	-6041	-3586	-39	-1179	-1183	-39	-1179	-1183
X3-X1 30-m	Measured	600	-575	-3937	-1612	23	668	661	23	668	661
X4-XS 15-m	Average	1055	-1129	-33203	-32559	-851	-4402	-4207	-139	-4183	-4185
X4-XS 30-m	Average	1055	-1129	-32941	-32292	-852	-4862	-4668	-155	-4644	-4647
X4-XS 15-m	Measured	1055	-778	-22689	-22358	-583	-2958	-2824	-93	-2807	-2810
X4-XS 30-m	Measured	1055	-778	-22586	-22116	-582	-3211	-3078	-102	-3060	-3063
X4-X1 15-m	Average	1000	-1155	-33786	-33322	-876	-5164	-4969	-165	-4946	-4948
X4-X1 30-m	Average	1000	-1145	-32941	-32751	-868	-5323	-5127	-170	-5104	-5106
X4-X1 15-m	Measured	1000	-795	-22689	-22883	-601	-3483	-3350	-111	-3333	-3335
X4-X1 30-m	Measured	1000	-788	-22586	-22433	-593	-3528	-3394	-112	-3377	-3379
X4-X3 15-m	Average	400	-185	-22152	-25255	-724	-586	-391	-13	-367	-369
X4-X3 30-m	Average	400	-176	-22538	-25265	-729	-1141	-941	-31	-923	-920
X4-X3 15-m	Measured	400	-180	-17174	-19297	-562	-2304	-2167	-72	-2153	-2152
X4-X3 30-m	Measured	400	-214	-18966	-20820	-616	-4196	-4055	-136	-4045	-4041

Table 3.3(d): Changes in Benzene (B), MTBE (M), and Tracer (T) Mass Fluxes (g/day) Between Cross-gradient Fences for Case 2-4

			t = 1080 Days			t = 2070 Days			t = 3060 Days		
Fences	K Field	Distance (m)	B	M	T	B	M	T	B	M	T
X1-XS 15-m	Average	55	85	2546	2541	85	2546	2541	85	2546	2541
X1-XS 30-m	Average	55	125	3751	3746	125	3751	3746	125	3751	3746
X1-XS 15-m	Measured	55	-87	-2602	-2606	-87	-2602	-2606	-87	-2602	-2606
X1-XS 30-m	Measured	55	-209	-6261	-6264	-209	-6261	-6264	-209	-6261	-6264
X3-XS 15-m	Average	655	-512	-6474	-5598	-154	-4652	-4659	-154	-4652	-4659
X3-XS 30-m	Average	655	-425	-4784	-3835	-90	-2723	-2734	-90	-2723	-2734
X3-XS 15-m	Measured	655	-252	-1077	-479	7	179	168	7	179	168
X3-XS 30-m	Measured	655	-432	-7450	-6803	-200	-6030	-6045	-200	-6030	-6045
X3-X1 15-m	Average	600	-597	-9019	-8140	-239	-7197	-239	-239	-7197	-239
X3-X1 30-m	Average	600	-550	-8534	-7581	-215	-6474	-215	-215	-6474	-215
X3-X1 15-m	Measured	600	-166	1525	2127	94	2781	94	94	2781	94
X3-X1 30-m	Measured	600	-224	-1189	-539	9	231	9	9	231	9
X4-XS 15-m	Average	1055	-1038	-24304	-25619	-440	-4892	-4840	-160	-4824	-4834
X4-XS 30-m	Average	1055	-953	-22662	-25597	-362	-2201	-2147	-71	-2130	-2140
X4-XS 15-m	Measured	1055	-860	-20233	-16770	-418	-6840	-6809	-226	-6794	-6804
X4-XS 30-m	Measured	1055	-950	-24165	-17343	-534	-10071	-10036	-334	-10023	-10032
X4-X1 15-m	Average	1000	-1123	-26850	-25619	-525	-7438	-7382	-245	-7370	-7375
X4-X1 30-m	Average	1000	-1078	-26412	-25597	-487	-5951	-5893	-196	-5881	-5886
X4-X1 15-m	Measured	1000	-773	-17631	-16770	-332	-4238	-4203	-139	-4192	-4198
X4-X1 30-m	Measured	1000	-741	-17905	-17343	-326	-3810	-3772	-125	-3762	-3768
X4-X3 15-m	Average	400	-526	-17831	-17480	-286	-240	-181	-6	-173	-175
X4-X3 30-m	Average	400	-527	-17878	-18016	-272	523	587	19	593	594
X4-X3 15-m	Measured	400	-608	-19156	-18897	-425	-7019	-6977	-233	-6972	-6973
X4-X3 30-m	Measured	400	-518	-16716	-16803	-335	-4041	-3991	-134	-3992	-3986

assessment of plume behavior that compliments the visual assessment based on the footprints. Table 3.4 shows the total mass of each contaminant at the three snapshots in time for all four constant source scenarios in Cases 1 and 2. In addition, the changes in mass between sequential snapshots are shown. Based on total mass, the plume is expanding between 1080 days and 2070 days in all scenarios. Some plume expansion is seen between 2070 days and 3060 days in all scenarios except scenario 2-1, although the changes in total mass have become considerably smaller for MTBE and the tracer as the plumes move beyond the sampling grid. The results for Experiment 2-1 reflected the plume moving beyond the sampling grid by 2070 days, such that the amounts of contaminant mass entering and leaving the domain were equivalent for the last 990 days. The constant source results identify t = 3060 days as an appropriate snapshot to use for relatively steady plume behavior.

3.3.2 Case 3 – Exponentially Decaying Source

The results of Case 3 yielded the attenuation data necessary to understand the role of the exponential source function in the complex biodegradation assessment in Cases 4 and 5. Other than the source function, Case 3 was identical to Case 2-1, allowing a comparison of attenuation rates and associated complications attributed to the source function. The impact of the exponential source function can be seen in the species' footprints in Figures 3.13 through 3.15.

The C versus d data illustrated an interesting and potentially complicating result of the exponential source function. The concentration profiles with distance along the transect at t = 3060 days are shown in Figure 3.16. Along with the increases and decreases in concentration caused by the non-linear flow field, there is a slight upward trend along the transect in the upper wells. Although dispersion has reduced concentrations, the initial high source concentration has propagated downgradient, giving the impression of contaminant *production.* The effects were more pronounced with increasing retardation factor. When measured concentrations were related to C_{max}, the maximum concentration from the source that would be present at a downgradient location given the contaminant travel time,

Table 3.4: Total Mass (kg) and Change in Mass (kg/day) of Benzene, MTBE, and Tracer in the Plume at t = 1080 Days, 2070 Days, and 3060 Days

	Case 1			Case 2-1			Case 2-2			Case 2-4		
Time (Days)	B	M	T	B	M	T	B	M	T	B	M	T
1080	253	10432	11088	367	15101	16408	171	7031	7475	196	8067	8570
2070	489	19733	20187	677	20529	20527	330	13347	14073	376	14119	14582
3060	674	20307	20307	684	20529	20527	476	17561	17768	491	16131	16174
Kg/day 2070 -1080	0.24	9.4	9.2	0.31	5.5	4.5	0.16	6.4	6.7	0.18	6.1	6.1
Kg/day 3060 - 2070	0.19	0.6	0.1	0.01	0.0	0.0	0.15	4.3	3.7	0.12	2.0	1.6

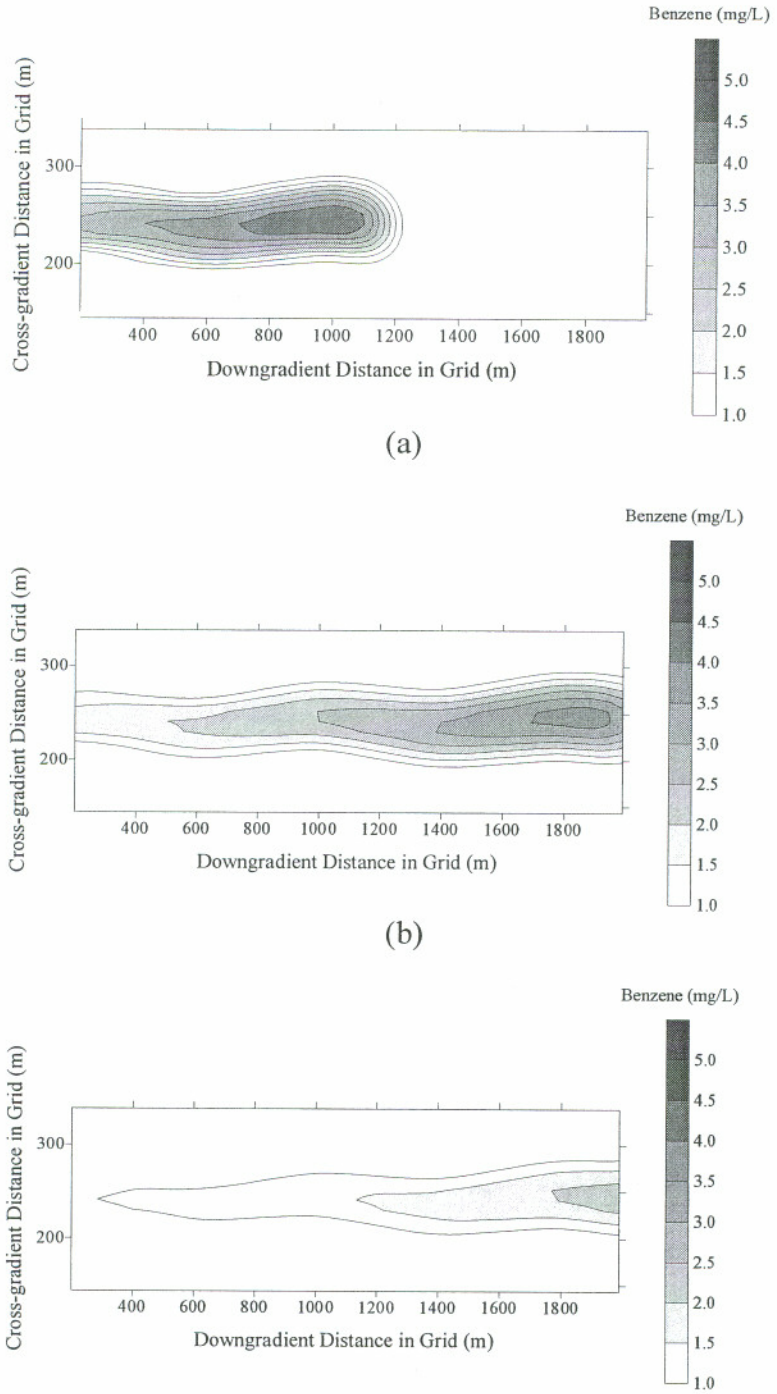

Figure 3.13: Case 3 Benzene Footprints at (a) t = 1080 Days, (b) 2070 Days, (c) 3060 Days

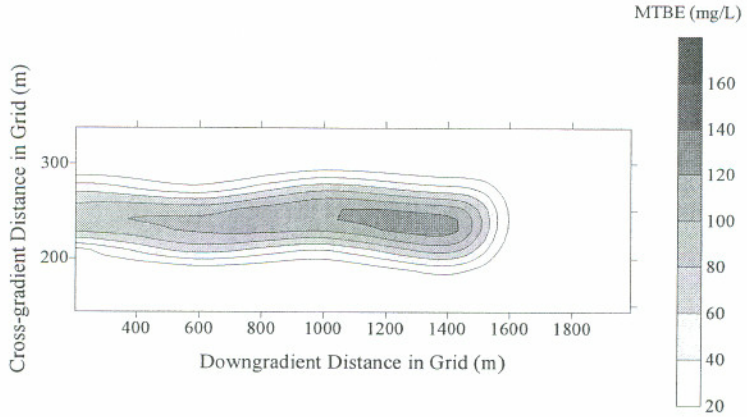

(a)

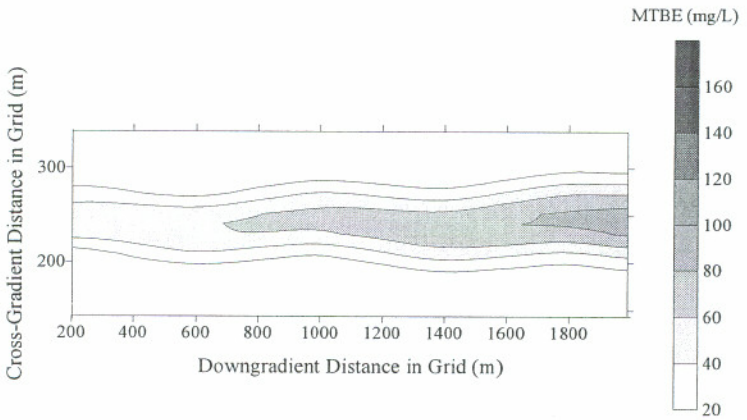

(b)

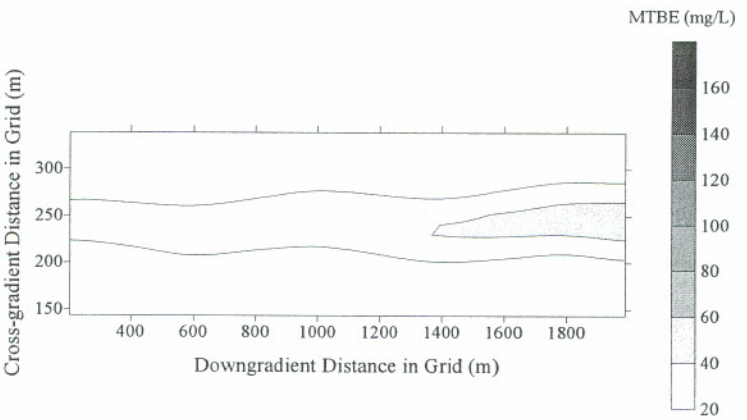

(c)

Figure 3.14: Case 3 MTBE Footprints at (a) t = 1080 Days, (b) 2070 Days, (c) 3060 Days

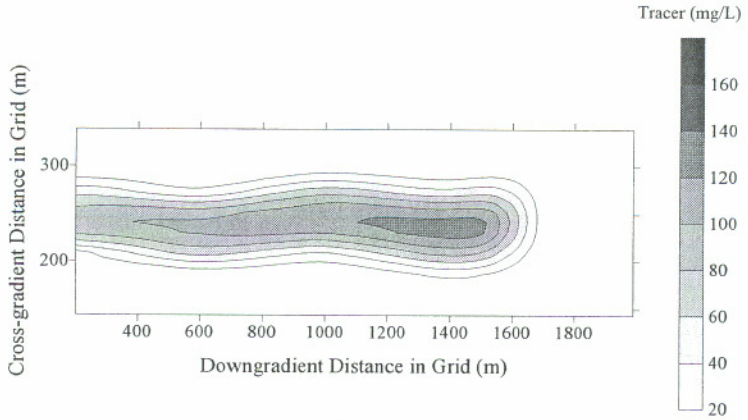

(a)

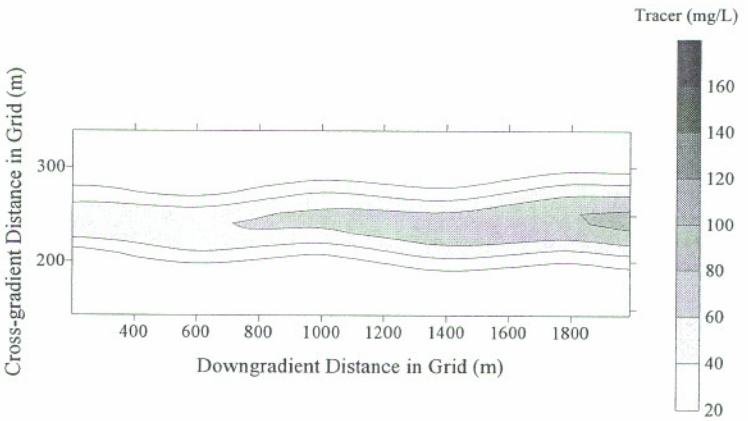

(b)

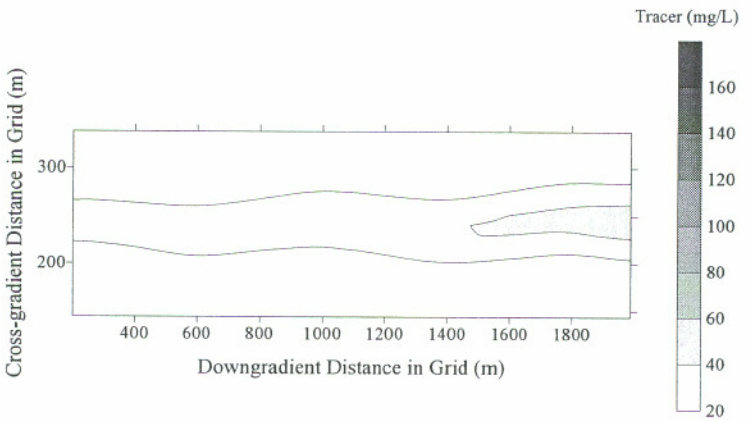

(c)

Figure 3.15: Case 3 Tracer Footprints at (a) t = 1080 Days, (b) 2070 Days, (c) 3060 Days

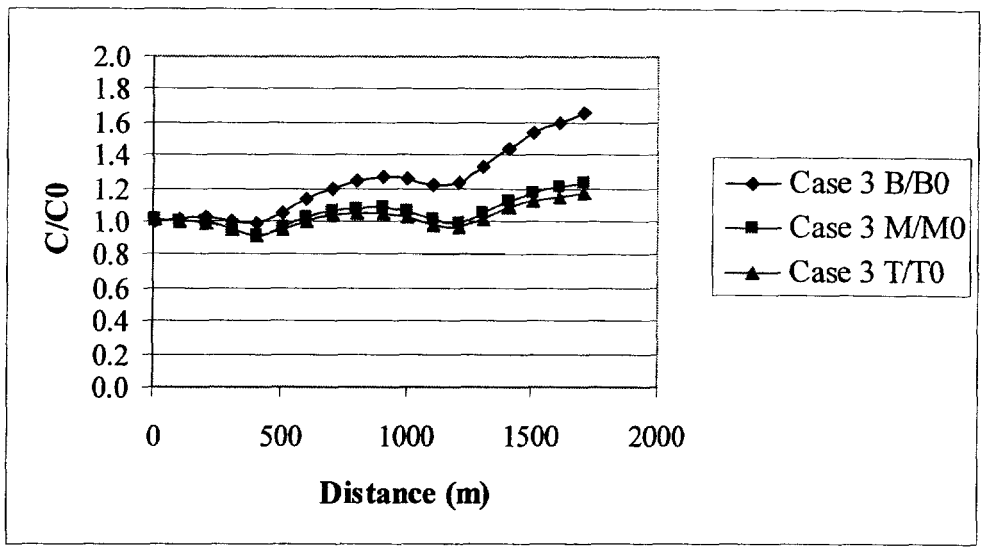

(a)

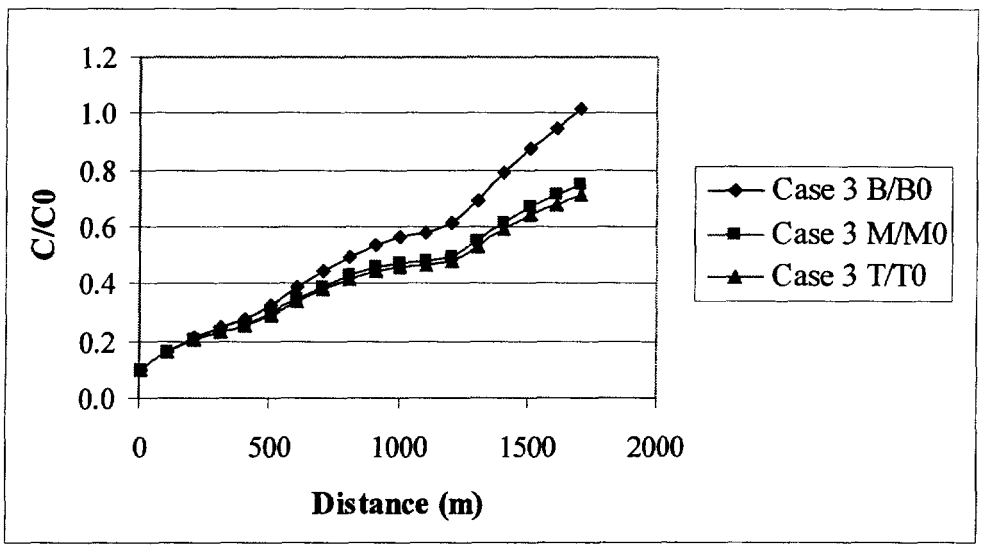

(b)

Figure 3.16: Benzene, MTBE, and Tracer Concentration Profiles along the Longitudinal Transect Resulting from an Exponential Source Function in (a) Upper 2-m Wells and (b) Lower 2-m Wells at t = 3060 Days

the profile along the transect showed a decrease in concentration with distance and similar behavior among the species. Normalizing to C_{max}, which removed the propagated effect of the source function, allowed a clearer understanding of attenuation due to dispersion. Figure 3.17 shows the profiles after accounting for the source function. Although using C_{max} would require explicit knowledge of the source function, a condition rarely met at field sites, the exercise showed the potential impact of the source function on interpreting downgradient concentrations.

Dispersion as well as the decreasing flux from the source with time caused the attenuation of species' concentrations in the plume. Attenuation rates calculated from C vs. d data at 3060 days are shown in Table 3.5. Rates based on data that were not adjusted for the source function (C/C_0) are low positive numbers. The C/C_{max} rates, however, are more consistent with the dispersion-only rates from Case 2-1 (Table 3.2). The use of C_{max} rather than C_0 also improved the R^2 value for the linear regression from 0.31 to 0.91 for the tracer and MTBE and 0.88 to 0.92 for benzene.

Because the mass flux from the source was changing with time in Case 3, a corresponding change in mass flux with time was expected at each of the fences. Since no degradation occurred in this experiment, changes in flux between the source fence and the downgradient fences were attributable to dispersion and sorption. Table 3.6 presents time series flux data assuming that the flux is measured at all four fences at the same time: that is, at different travel times. The change in mass flux with time observed in downgradient fences became more negative with distance from the source zone corresponding to greater mass losses with increasing distance and, therefore, residence time. This suggested that some change in source function was being measured since a constant source would be expected to cause increases with time (if the plume was expanding) or a constant mass flux in the absence of degradation. In addition, the changes in mass flux at each fence were more negative in the 2070 days-1080 days comparison than the 3060 days-2070 days comparison. This also suggested a non-linear loss of mass with time. It was unclear from these mass flux data, however, which mechanism(s) accounted for these observations.

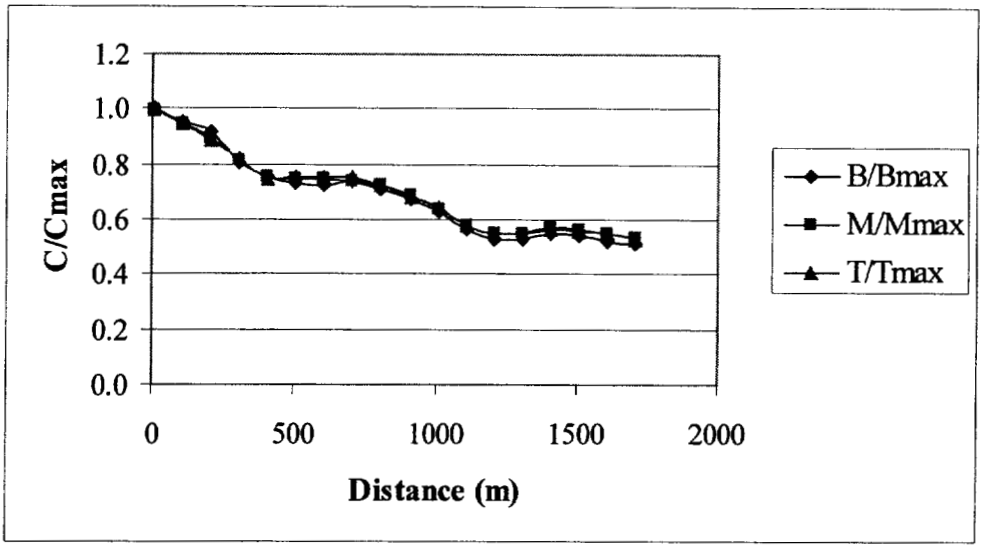

Figure 3.17: Benzene, MTBE, and Tracer Concentration Profiles along the Longitudinal Transect Corrected for the Exponential Source Function in the Upper 2-m Wells at t = 3060 Days

Table 3.5: First-Order Attenuation Rates (day^{-1}) for Exponential Source Function Based on t = 3060 Days C versus Distance Data in Case 3

Case	Calculated by:	Benzene	MTBE	Tracer	Attributed to:
3	C/C_0	9E-5 R^2=0.88	2E-5 R^2=0.31	2E-5 R^2=0.31	Dsp, Src
3	C_{corr}/C_0	8E-5 R^2=1.00	2E-5 R^2=1.00	NA	Src
3	C/C_{max}	-0.0002 R^2=0.92	-0.0002 R^2=0.91	-0.0002 R^2=0.91	Dsp
3	C_{corr}/C_{max}	-9E-6 R^2=0.57	NS	NA	Sorption (Benzene)

NS = Not Significant; NA = Not Applicable
Dsp = Dispersion; Src = Source Function; Deg = Degradation

Table 3.6: Mass Fluxes (g/day) Through the Cross-Gradient Fences at t = 1080 Days, t = 2070 Days, and t = 3060 Days for Case 3

		XS			X1			X3			X4		
Time (days)	Spacing/K Scenario	B	M	T	B	M	T	B	M	T	B	M	T
1080	15-m/average	482	14435	14432	534	15972	15967	858	23026	22622	270	27925	27117
2070	15-m/average	266	7967	7966	295	8816	8813	474	12717	12492	618	15418	14976
3060	15-m/average	146	4399	4398	162	4868	4866	262	7020	6897	341	8514	8268
F_{2070}-F_{1080}	*15-m/average*	*-216*	*-6468*	*-6466*	*-239*	*-7156*	*-7154*	*-384*	*-10309*	*-10130*	*348*	*-12507*	*-12141*
F_{3060}-F_{2070}	*15-m/average*	*-120*	*-3568*	*-3568*	*-133*	*-3948*	*-3947*	*-212*	*-5697*	*-5595*	*-277*	*-6904*	*-6708*
1080	30-m/average	362	10817	10813	444	13262	13254	858	23033	22628	270	27922	27115
2070	30-m/average	199	5971	5968	245	7321	7316	474	12720	12496	618	15417	14975
3060	30-m/average	110	3297	3295	135	4042	4040	262	7021	6899	341	8513	8268
F_{2070}-F_{1080}	*30-m/average*	*-163*	*-4846*	*-4845*	*-199*	*-5941*	*-5938*	*-384*	*-10313*	*-10132*	*348*	*-12505*	*-12140*
F_{3060}-F_{2070}	*30-m/average*	*-89*	*-2674*	*-2673*	*-110*	*-3279*	*-3276*	*-212*	*-5699*	*-5597*	*-277*	*-6904*	*-6707*
1080	15-m/measured	707	21182	21178	784	23438	23430	1259	33789	33196	396	40889	39707
2070	15-m/measured	390	11691	11689	432	12937	12932	695	18660	18331	904	22576	21928
3060	15-m/measured	215	6456	6454	238	7143	7141	384	10301	10121	499	12466	12130
F_{2070}-F_{1080}	*15-m/measured*	*-317*	*-9491*	*-9489*	*-352*	*-10501*	*-10498*	*-564*	*-15129*	*-14865*	*508*	*-18313*	*-18021*
F_{3060}-F_{2070}	*15-m/measured*	*-175*	*-5235*	*-5235*	*-194*	*-5794*	*-5791*	*-311*	*-8359*	*-8210*	*-405*	*-10110*	*-9798*

Table 3.6 continued

		XS			X1			X3			X4		
Time (days)	Spacing/K Scenario	B	M	T	B	M	T	B	M	T	B	M	T
1080	30-m/measured	531	15874	15867	652	19461	19450	1259	33799	33204	395	40814	39635
2070	30-m/measured	293	8761	8757	360	10743	10736	695	18666	18337	902	22535	21889
3060	30-m/measured	161	4838	4836	198	5932	5928	384	10303	10124	498	12443	12128
F_{2070}-F_{1080}	*30-m/measured*	*-238*	*-7113*	*-7110*	*-292*	*-8718*	*-8714*	*-564*	*-15133*	*-14867*	*507*	*-18279*	*-17746*
F_{3060}-F_{2070}	*30-m/measured*	*-132*	*-3923*	*-3921*	*-162*	*-4811*	*-4808*	*-311*	*-8363*	*-8213*	*-404*	*-10092*	*-9761*

Table 3.7(a) through (c) shows the change in mass flux at each downgradient fence with the corresponding change in mass flux at the source fence accounting for travel times based on benzene, MTBE, and tracer velocities of 0.87 m/d, 1.25 m/d, and 1.31 m/d, respectively. The influence of the change in source flux on downgradient changes in mass flux was most evident at the nearest fence, where it accounted for 82-92% of the changes, depending on the monitoring configuration. This dropped to 63-88% at the farther distances. The data also show that percentages due to the source function were consistent across sampling times and species. The source influence was consistently more noticeable with the 15-m well spacing.

The impact of the exponential source function on total mass in the system is evident in Table 3.8. The data from Case 2-1 are included in the table to show the change from the constant source scenario. At 1080 days, the plume appeared to be expanding, particularly based on the positive benzene kg/day value. Sorption was believed to account for the differences between MTBE and the tracer as lower source concentrations move farther into the grid for the tracer than MTBE. The change in MTBE and tracer mass between 2070 days and 3060 days are now –4.1 kg/day and –4.0 kg/day, respectively, showing that outflow was replaced with inflow at a lower concentration.

3.3.3 Cases 4 and 5 – Assessment of Degradation in a Complex Flow Field

The last set of results address how degradation is assessed in a complex flow field with an exponential source function. Case 4 served as the control, i.e. no degradation, for Case 5. Figures 3.18 through 3.22 show the footprints for benzene, MTBE and the tracer. In a natural attenuation demonstration, figures such as these would serve as the primary line of evidence that attenuation, and specifically degradation, was occurring. For benzene, the effect of degradation was evident at the 1080-day snapshot. This would be reasonable at a "real world" field site given a half-life for total BTEX ranging from 0.14 to 1.4 days based on degradation rates in groundwater (Suarez and Rifai 1999). The plume shortened with time and concentrations became noticeably lower with distance from the source in Case 5

Table 3.7(a): Comparison of Changes in Mass Flux (g/day) with Time Between XS and X1 Accounting for Travel Time Between Fences in Case 3

		XS				X1			% due to source		
Spacing/K Scenario	Time (days)	B	M	T	Time (days)	B	M	T	B	M	T
15-m/avg.	1050	490	14695	14692	1080	534	15972	15967			
15-m/avg.	2040	271	8110	8109	2070	295	8816	8813			
15-m/avg.	3030	149	4483	4482	3060	162	4868	4866			
15-m/avg.	F_{2040}-F_{1050}	*-219*	*-6585*	*-6583*	F_{2070}-F_{1080}	*-239*	*-7156*	*-7154*	*91.6*	*92.0*	*92.0*
15-m/avg.	F_{3030}-F_{2040}	*-122*	*-3627*	*-3627*	F_{3060}-F_{2070}	*-133*	*-3948*	*-3947*	*91.7*	*91.9*	*91.9*
30-m/avg.	1050	368	11012	11008	1080	444	13262	13254			
30-m/avg.	2040	202	6078	6075	2070	245	7321	7316			
30-m/avg.	3030	112	3360	3358	3060	135	4042	4040			
30-m/avg.	F_{2040}-F_{1050}	*-166*	*-4934*	*-4933*	F_{2070}-F_{1080}	*-199*	*-5941*	*-5938*	*83.4*	*83.0*	*83.1*
30-m/avg.	F_{3030}-F_{2040}	*-90*	*-2718*	*-2717*	F_{3060}-F_{2070}	*-110*	*-3279*	*-3276*	*81.8*	*82.9*	*82.9*
15-m/meas.	1050	719	21563	21559	1080	784	23438	23430			
15-m/meas.	2040	397	11901	11899	2070	432	12937	12932			
15-m/meas.	3030	219	6579	6577	3060	238	7143	7141			
15-m/meas.	F_{2040}-F_{1050}	*-322*	*-9662*	*-9660*	F_{2070}-F_{1080}	*-352*	*-10501*	*-10498*	*91.5*	*92.0*	*92.0*
15-m/meas.	F_{3030}-F_{2040}	*-178*	*-5322*	*-5322*	F_{3060}-F_{2070}	*-194*	*-5794*	*-5791*	*91.8*	*91.9*	*91.9*
30-m/meas.	1050	540	16160	16153	1080	652	19461	19450			
30-m/meas.	2040	298	8919	8923	2070	360	10743	10736			
30-m/meas.	3030	164	4930	4928	3060	198	5932	5928			
30-m/meas.	F_{2040}-F_{1050}	*-242*	*-7241*	*-7230*	F_{2070}-F_{1080}	*-292*	*-8718*	*-8714*	*82.9*	*83.1*	*83.0*
30-m/meas.	F_{3030}-F_{2040}	*-134*	*-3989*	*-3995*	F_{3060}-F_{2070}	*-162*	*-4811*	*-4808*	*82.7*	*82.9*	*83.1*

Table 3.7(b): Comparison of Changes in Mass Flux (g/day) with Time Between XS and X3 Accounting for Travel Time Between Fences in Case 3

		XS				X3			% due to source		
Spacing/K Scenario	Time* (days)	B	M	T	Time (days)	B	M	T	B	M	T
15-m/avg.	600	745	19663	19243	1080	858	23026	22622			
15-m/avg.	1590	410	10829	10639	2070	474	12717	12492			
15-m/avg.	2580	227	5977	5860	3060	262	7020	6897			
15-m/avg.	F_{1590}-F_{600}	*-335*	*-9024*	*-8604*	F_{2070}-F_{1080}	*-384*	*-10309*	*-10130*	*87.2*	*87.5*	*84.9*
15-m/avg.	F_{2580}-F_{1590}	*-183*	*-4852*	*-4779*	F_{3060}-F_{2070}	*-212*	*-5697*	*-5595*	*86.3*	*85.2*	*85.4*
30-m/avg.	600	559	14735	14417	1080	858	23033	22628			
30-m/avg.	1590	307	8115	7970	2070	474	12720	12496			
30-m/avg.	2580	170	4479	4391	3060	262	7021	6899			
30-m/avg.	F_{1590}-F_{600}	*-252*	*-6620*	*-6447*	F_{2070}-F_{1080}	*-384*	*-10313*	*-10132*	*65.6*	*64.2*	*63.6*
30-m/avg.	F_{2580}-F_{1590}	*-137*	*-3636*	*-3579*	F_{3060}-F_{2070}	*-212*	*-5699*	*-5597*	*64.6*	*63.8*	*63.9*
15-m/meas.	600	1093	28854	28238	1080	1259	33789	33196			
15-m/meas.	1590	601	15890	15611	2070	695	18660	18331			
15-m/meas.	2580	333	8767	8599	3060	384	10301	10121			
15-m/meas.	F_{1590}-F_{600}	*-492*	*-12964*	*-12627*	F_{2070}-F_{1080}	*-564*	*-15129*	*-14865*	*87.2*	*85.7*	*84.9*
15-m/meas.	F_{2580}-F_{1590}	*-268*	*-7123*	*-7012*	F_{3060}-F_{2070}	*-311*	*-8359*	*-8210*	*86.2*	*85.2*	*85.4*
30-m/meas.	600	820	21623	21156	1080	1259	33799	33204			
30-m/meas.	1590	451	11908	11696	2070	695	18666	18337			
30-m/meas.	2580	250	6570	6443	3060	384	10303	10124			
30-m/meas.	F_{1590}-F_{600}	*-369*	*-9715*	*-9460*	F_{2070}-F_{1080}	*-564*	*-15133*	*-14867*	*65.4*	*64.2*	*63.6*
30-m/meas.	F_{2580}-F_{1590}	*-201*	*-5338*	*-5253*	F_{3060}-F_{2070}	*-311*	*-8363*	*-8213*	*64.6*	*63.8*	*64.0*

* Based on tracer velocity; $t_{Benzene}$ = 360, 1350, 2340 days, t_{MTBE} = 570, 1560, 2550 days

Table 3.7(c): Comparison of Changes in Mass Flux (g/day) with Time Between XS and X4 Accounting for Travel Time Between Fences in Case 3

		XS				X4			% due to source		
Spacing/K Scenario	Time* (days)	B	M	T	Time (days)	B	M	T	B	M	T
15-m/avg.	300	0	23468	23041	1080	270	27925	27117			
15-m/avg.	1290	536	12954	12718	2070	618	15418	14976			
15-m/avg.	2280	296	7154	7024	3060	341	8514	8268			
15-m/avg.	F_{1290}-F_{300}	*536*	*-10514*	*-10323*	F_{2070}-F_{1080}	*348*	*-12507*	*-12141*		*84.1*	*85.0*
15-m/avg.	F_{2280}-F_{1290}	*-240*	*-5800*	*-5694*	F_{3060}-F_{2070}	*-277*	*-6904*	*-6708*	*86.6*	*84.0*	*84.9*
30-m/avg.	300	0	17587	17263	1080	270	27922	27115			
30-m/avg.	1290	402	9708	9528	2070	618	15417	14975			
30-m/avg.	2280	222	5361	5262	3060	341	8513	8268			
30-m/avg.	F_{1290}-F_{300}	*402*	*-7879*	*-7735*	F_{2070}-F_{1080}	*348*	*-12505*	*-12140*		*63.0*	*63.7*
30-m/avg.	F_{2280}-F_{1290}	*-180*	*-4347*	*-4266*	F_{3060}-F_{2070}	*-277*	*-6904*	*-6707*	*65.0*	*63.0*	*63.6*
15-m/meas.	300	0	34438	33811	1080	396	40889	39707			
15-m/meas.	1290	787	19008	18663	2070	904	22576	21928			
15-m/meas.	2280	434	10498	10307	3060	499	12466	12130			
15-m/meas.	F_{1290}-F_{300}	*787*	*-15430*	*-15148*	F_{2070}-F_{1080}	*508*	*-18313*	*-18021*		*84.3*	*84.1*
15-m/meas.	F_{2280}-F_{1290}	*-353*	*-8510*	*-8356*	F_{3060}-F_{2070}	*-405*	*-10110*	*-9798*	*87.2*	*84.2*	*85.3*
30-m/meas.	300	0	25808	25331	1080	395	40814	39635			
30-m/meas.	1290	590	14245	13982	2070	902	22535	21889			
30-m/meas.	2280	326	7867	7722	3060	498	12443	12128			
30-m/meas.	F_{1290}-F_{300}	*590*	*-11563*	*-11349*	F_{2070}-F_{1080}	*507*	*-18279*	*-17746*		*63.3*	*64.0*
30-m/meas.	F_{2280}-F_{1290}	*-264*	*-6378*	*-6260*	F_{3060}-F_{2070}	*-404*	*-10092*	*-9761*	*65.3*	*65.3*	*64.1*

* Based on tracer velocity; $t_{Benzene}$ = -74, 900, 1890 days, t_{MTBE} = 270, 1260, 2250 days

Table 3.8: Total Mass (kg) of Benzene, MTBE, and Tracer in the Plume at t=1080 Days, 2070 Days, and 3060 Days for the Exponential Source Compared to the Constant Source

	Experiment 3			Experiment 2-1		
Time (Days)	B	M	T	B	M	T
1080	259	10651	11316	367	15101	16408
2070	362	9095	8829	677	20529	20527
3060	203	5022	4875	684	20529	20527
Kg/day 2070-1080	*0.10*	*-1.6*	*-2.5*	*0.31*	*5.5*	*4.5*
Kg/day 3060-2070	*-0.16*	*-4.1*	*-4.0*	*0.01*	*0.0*	*0.0*

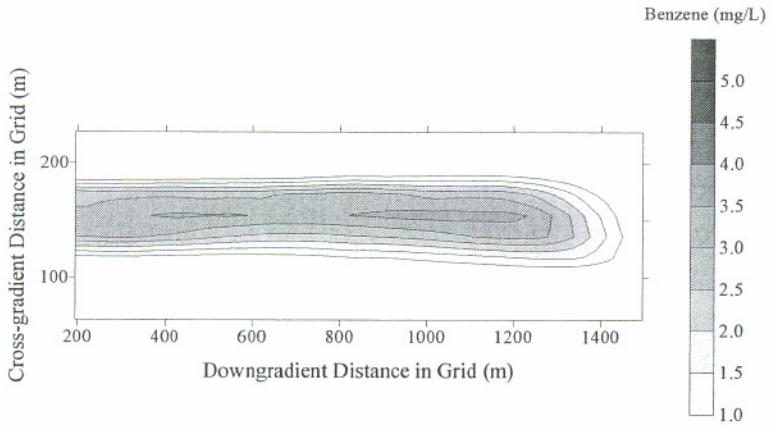

(a)

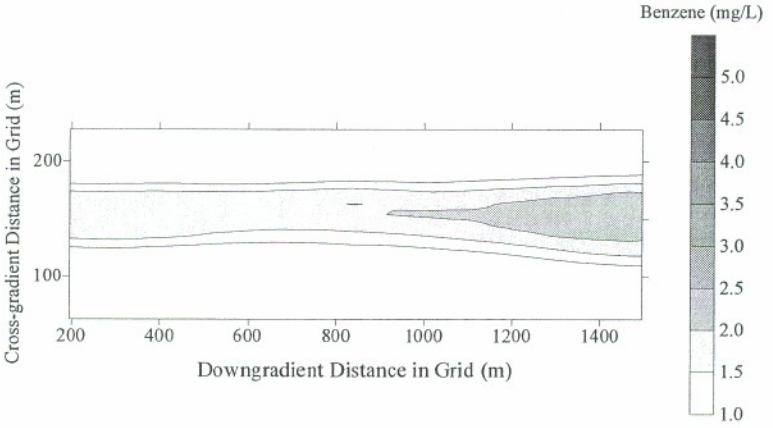

(b)

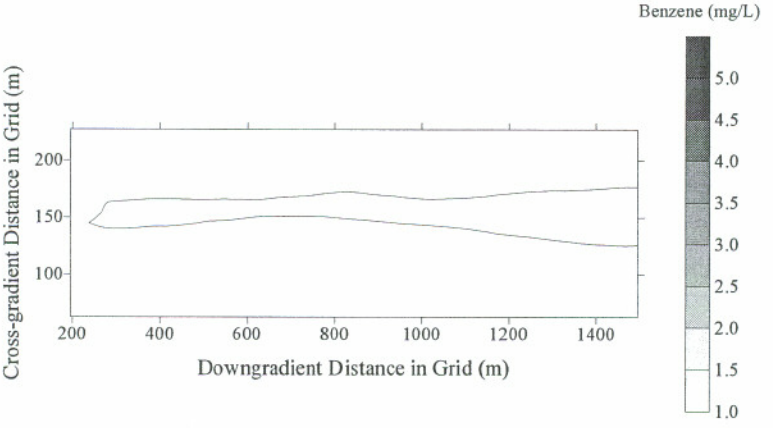

(c)

Figure 3.18: Case 4 Benzene Footprints at (a) t = 1080 Days, (b) 2070 Days, (c) 3060 Days with No Degradation

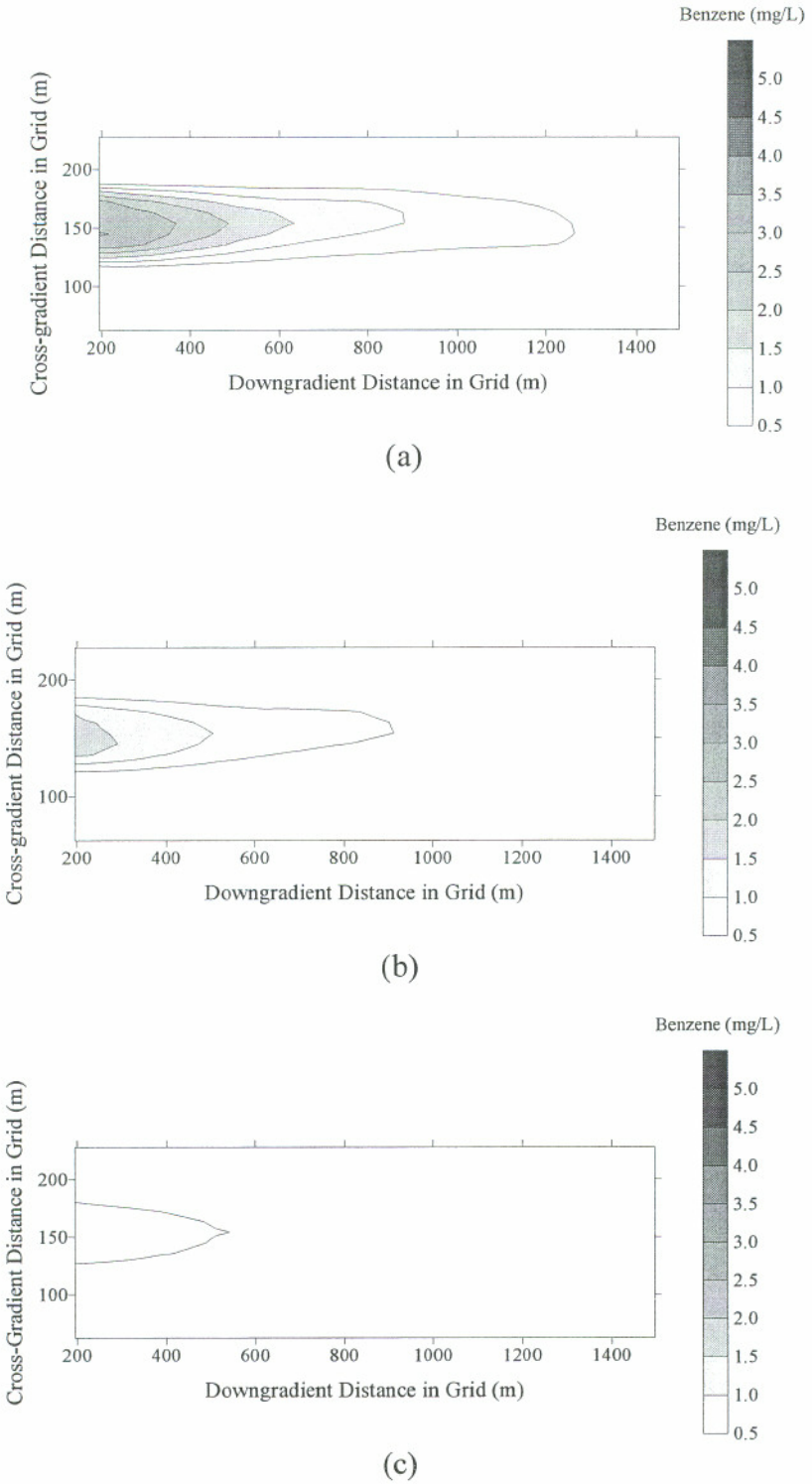

Figure 3.19: Case 5 Benzene Footprints at (a) t = 1080 Days, (b) 2070 Days, (c) 3060 Days with Degradation

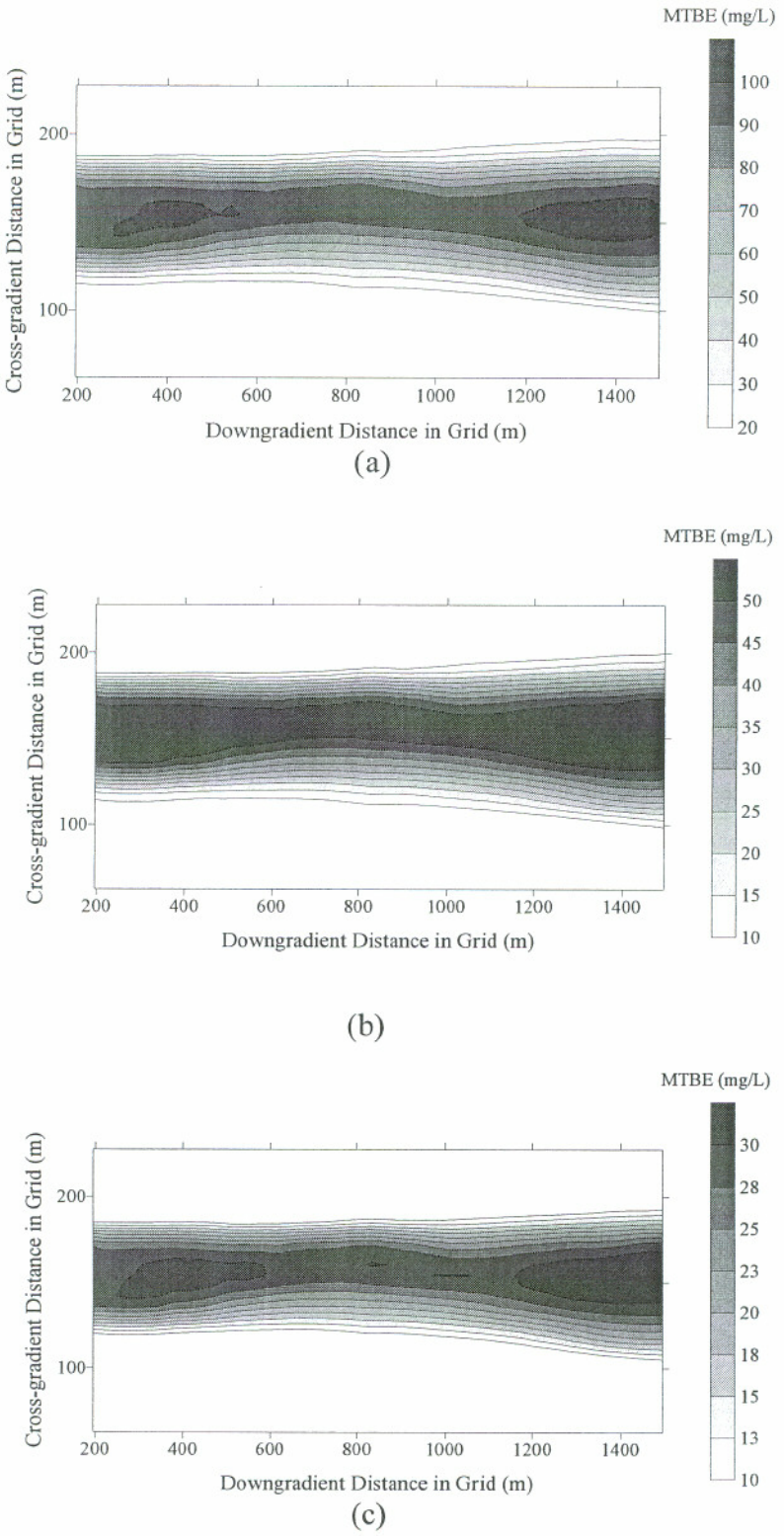

Figure 3.20: Case 4 MTBE Footprints at (a) t = 1080 Days, (b) 2070 Days, (c) 3060 Days with No Degradation

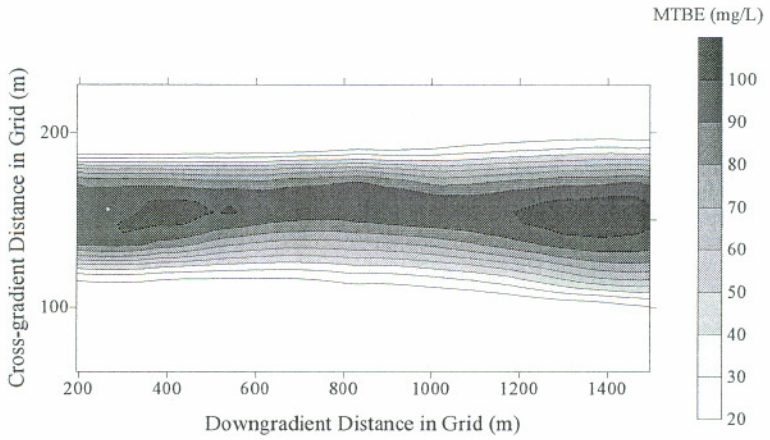

(a)

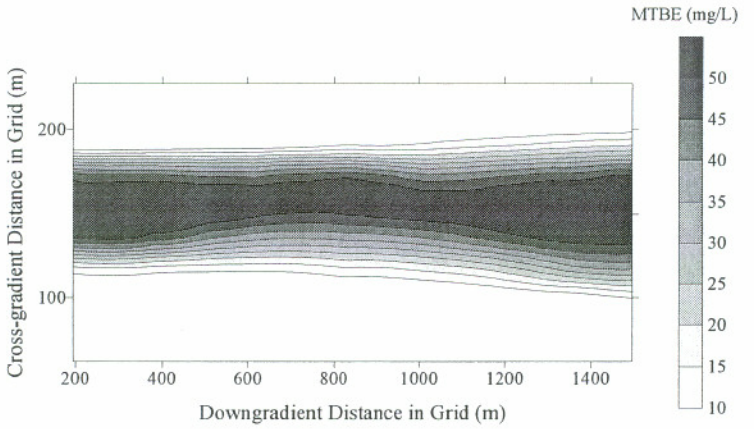

(b)

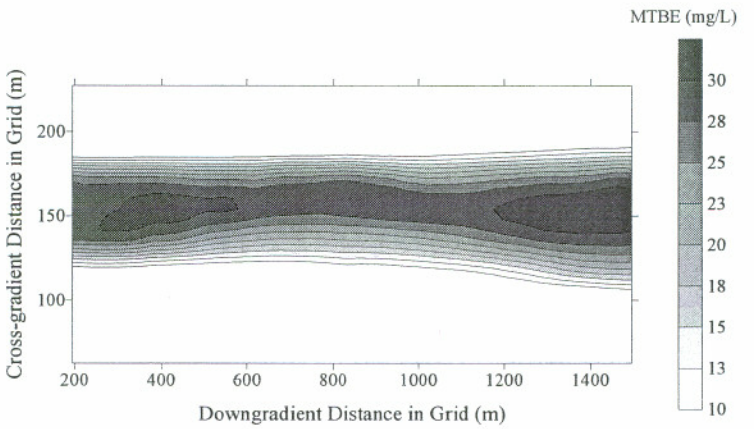

(c)

Figure 3.21: Case 5 MTBE Footprints at (a) t = 1080 Days, (b) 2070 Days, (c) 3060 Days with Degradation

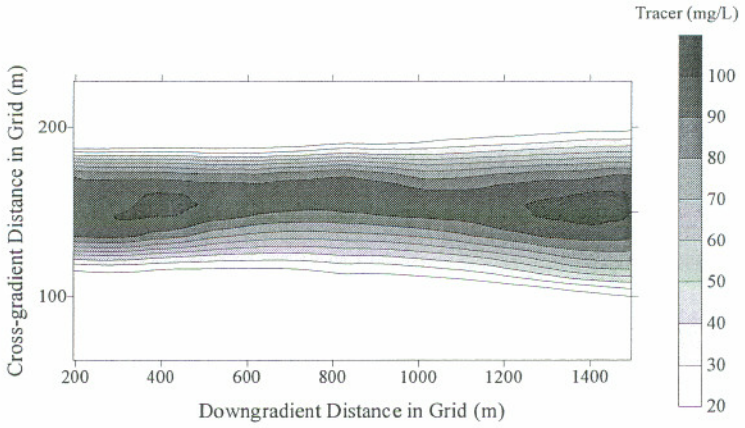

(a)

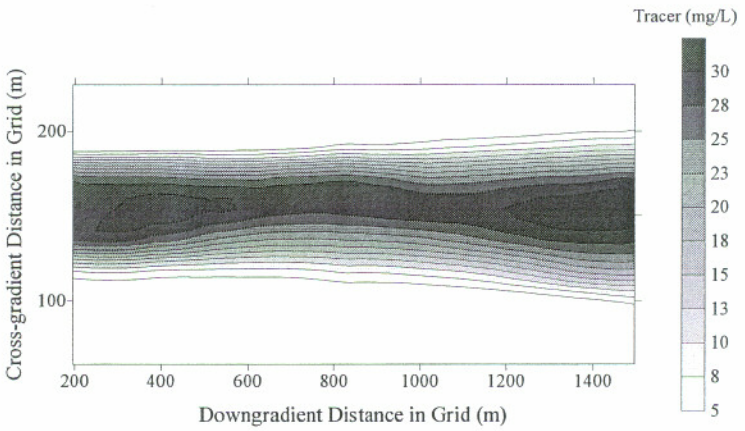

(b)

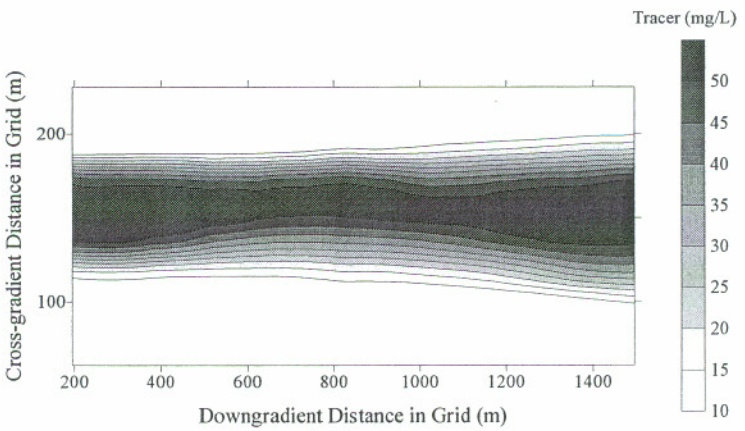

(c)

Figure 3.22: Case 4 Tracer Footprints at (a) t = 1080 Days, (b) 2070 Days, (c) 3060 Days

compared to Case 4. For MTBE, however, the footprints remained similar in the two experiments. There were subtle differences in the degradation scenario compared to the control that suggested that degradation could be occurring. At 1080 days, the higher concentration area from 300 to 600 m into the grid separated into two pieces in the degradation case. At 3060 days, the small areas of higher concentration at 850 m and 1000 m into the grid disappeared in the degradation case. None of these features in the control MTBE footprints were present in the tracer footprints for comparison. The footprints, while providing evidence of benzene degradation, could not be considered definitive proof of MTBE degradation.

The species profiles with time at X = 5 m, X = 605 m, and X = 1005 m gave some additional evidence of degradation and are shown in Figures 3.23 through 3.28. The Case 4 profile is presented before the Case 5 profile for each distance. Evidence of benzene degradation was seen in the lower wells immediately downgradient of the source zone as soon as oxygen or the anaerobic electron acceptor became available. Benzene was largely depleted in both the upper and lower wells at 605 m and completely gone at 1005 m. By contrast, MTBE concentrations remain at the same level as the tracer in the upper and lower wells at all three locations.

The Case 4 and 5 concentration profiles along the transect are presented in Figures 3.29 through 3.32. As in the time series figures, the data showing degradation follow immediately after the corresponding control scenario. The data for 1080 days and 3060 days were selected to show the control versus degradation behavior while the plume was moving down the transect and after it had migrated the length of the domain. Again, benzene degradation was seen after 1080 days. MTBE showed no degradation after 1080 days; however, the 3060 days plot showed some subtle evidence of degradation in the lower wells as the position of the MTBE line was shifted slightly with respect to the tracer line.

Attenuation rates for Cases 4 and 5 were calculated in a similar manner to those in Case 3 so that concentrations along the transect were corrected for and

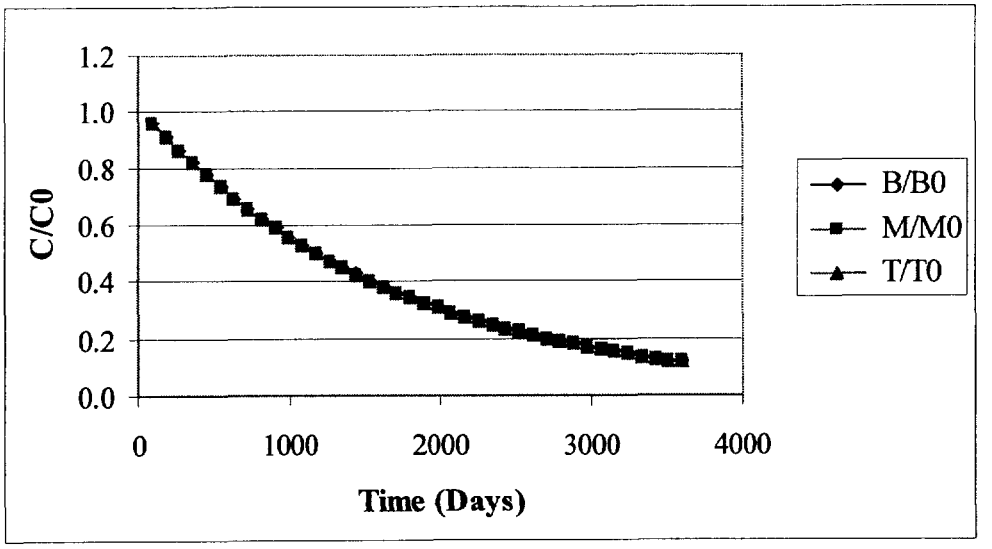

(a)

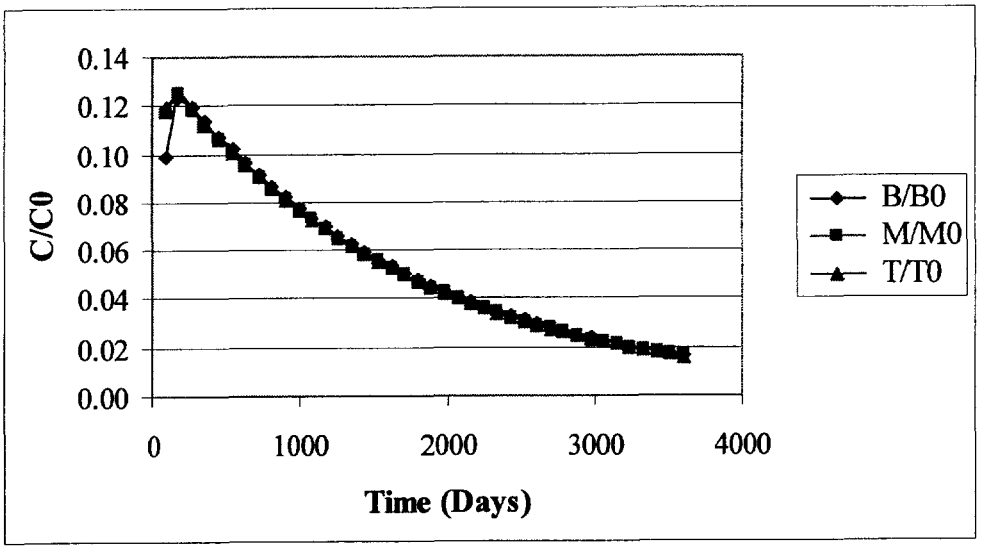

(b)

Figure 3.23: Case 4 (No Degradation) Benzene, MTBE, and Tracer Profiles with Time at 5 m from the Source Zone along the Longitudinal Transect Observed in (a) Upper 2-m Wells and (b) Lower 2-m Wells

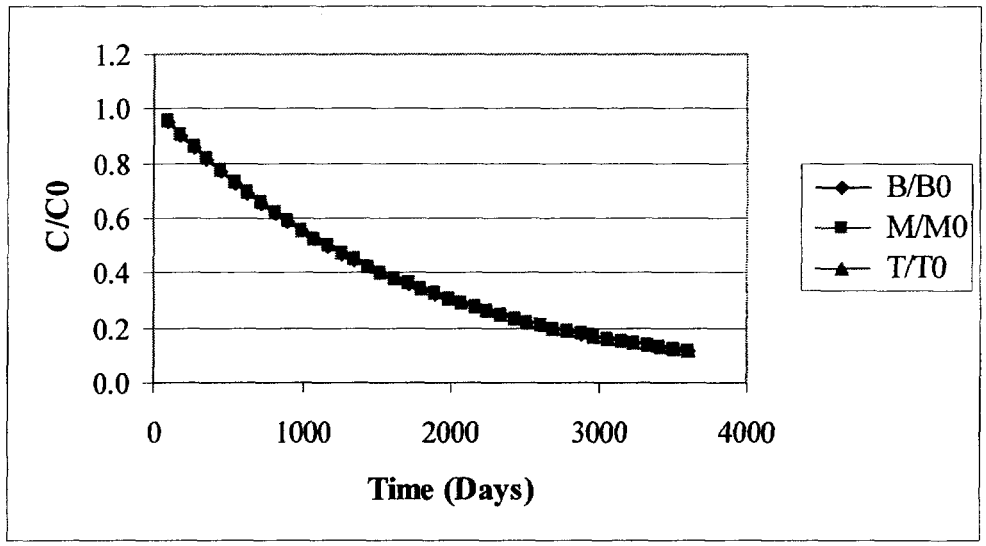

(a)

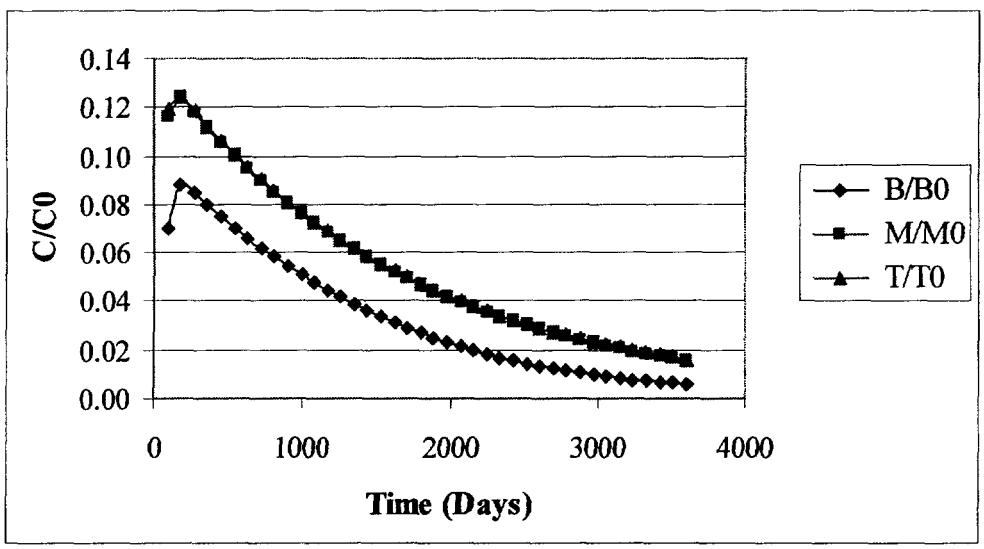

(b)

Figure 3.24: Case 5 (Degradation) Benzene, MTBE, and Tracer Profiles with Time at 5 m from the Source Zone along the Longitudinal Transect Observed in (a) Upper 2-m Wells and (b) Lower 2-m Wells

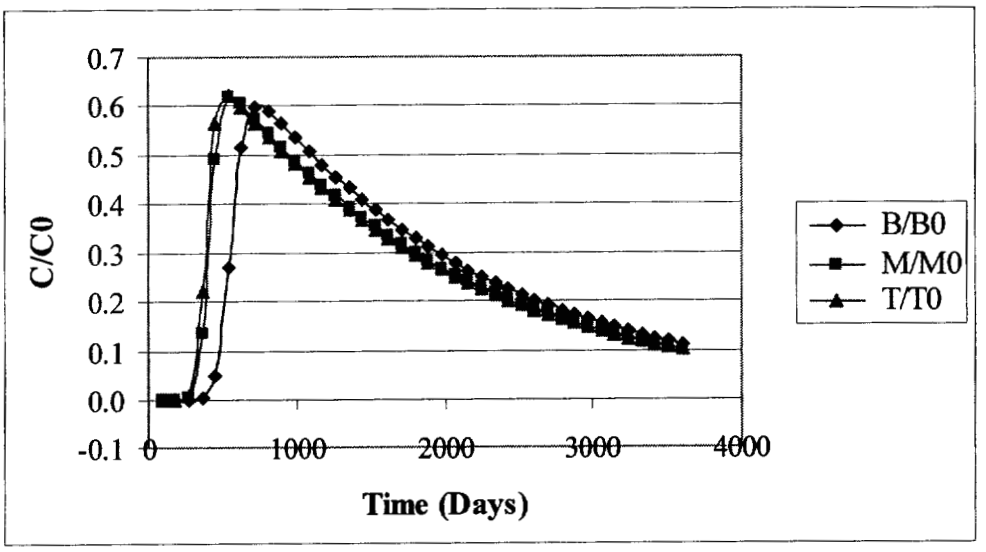

(a)

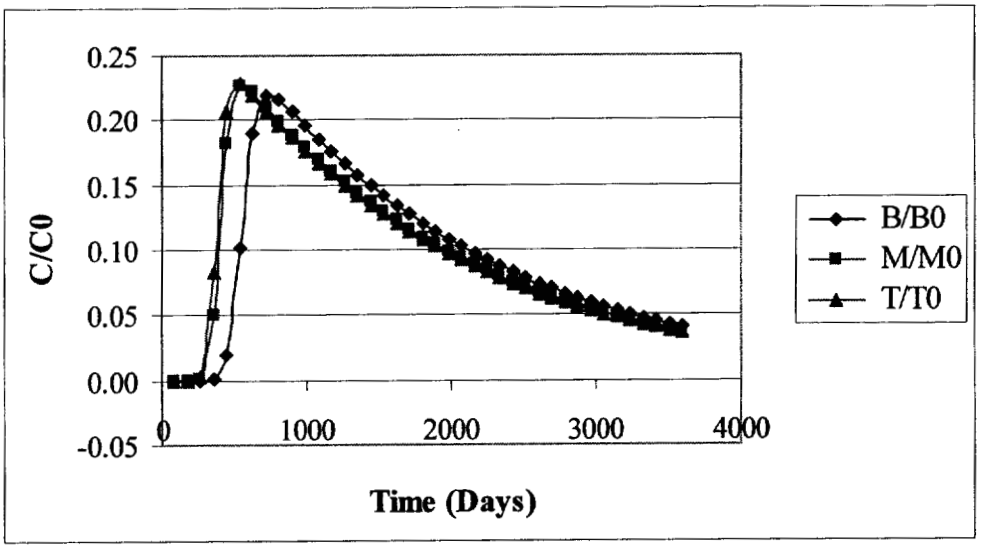

(b)

Figure 3.25: Case 4 (No Degradation) Benzene, MTBE, and Tracer Profiles with Time at 605 m from the Source Zone along the Longitudinal Transect Observed in (a) Upper 2-m Wells and (b) Lower 2-m Wells

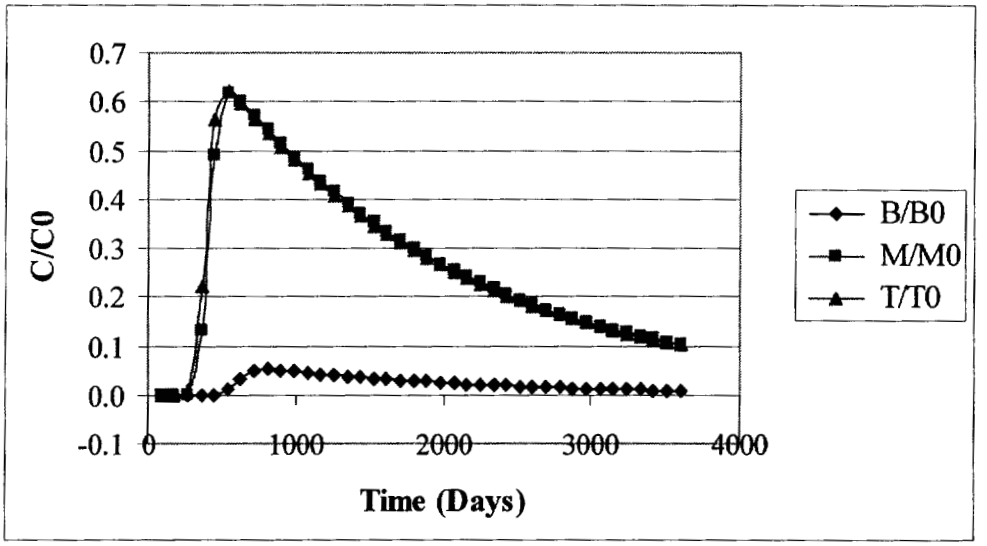

(a)

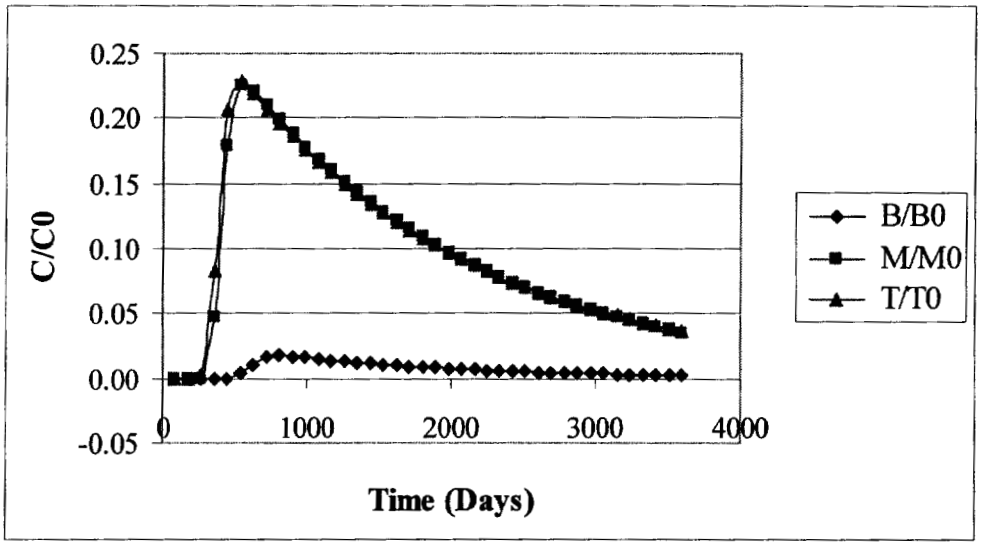

(b)

Figure 3.26: Cases 5 (Degradation) Benzene, MTBE, and Tracer Profiles with Time at 605 m from the Source Zone along the Longitudinal Transect Observed in (a) Upper 2-m Wells and (b) Lower 2-m Wells

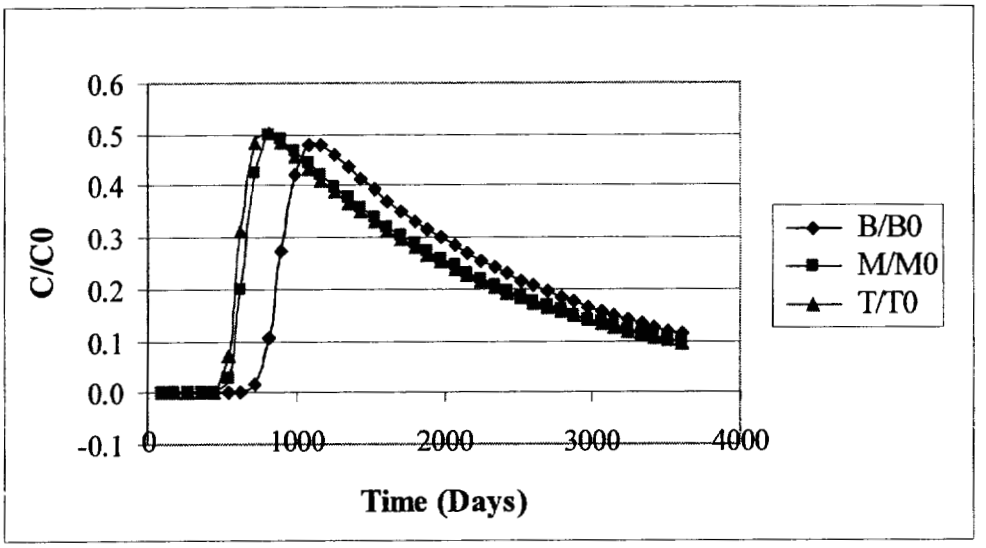

(a)

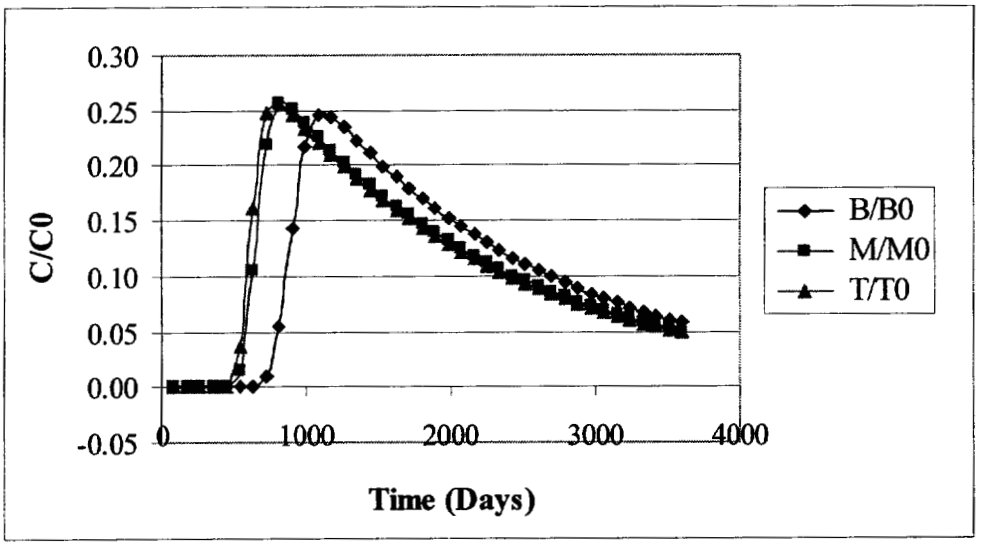

(b)

Figure 3.27: Case 4 (No Degradation) Benzene, MTBE, and Tracer Profiles with Time at 1005 m from the Source Zone along the Longitudinal Transect Observed in (a) Upper 2-m Wells and (b) Lower 2-m Wells

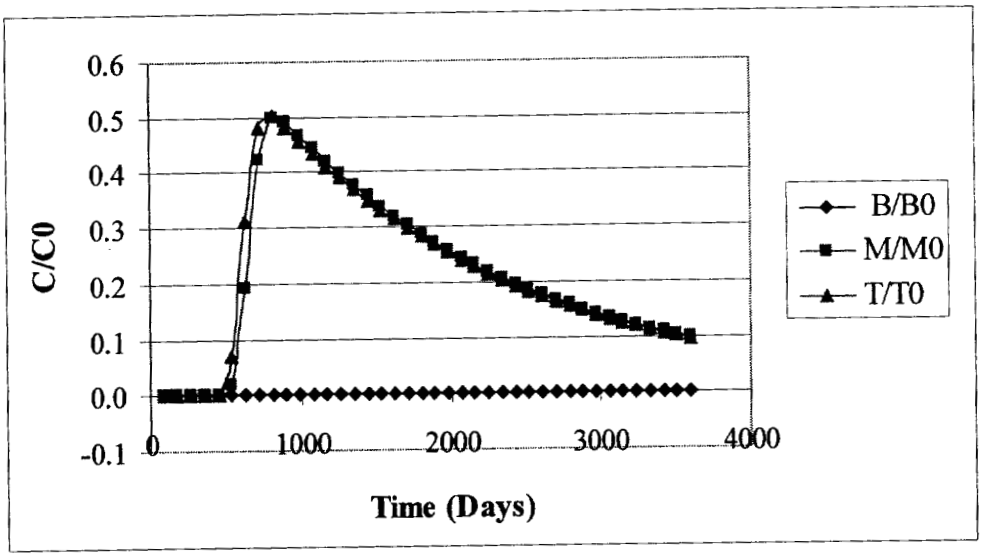

(a)

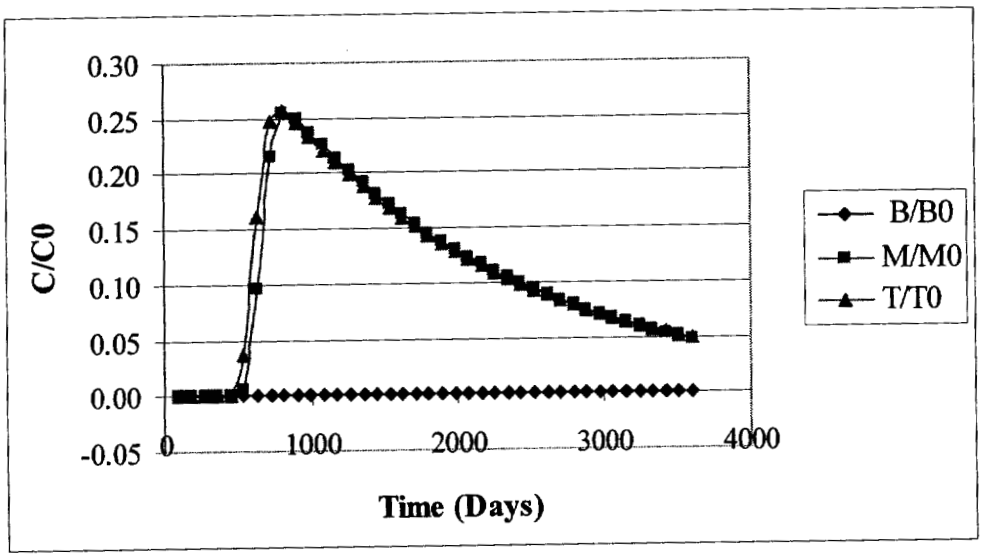

(b)

Figure 3.28: Case 5 (Degradation) Benzene, MTBE, and Tracer Profiles with Time at 1005 m from the Source Zone along the Longitudinal Transect Observed in (a) Upper 2-m Wells and (b) Lower 2-m Wells

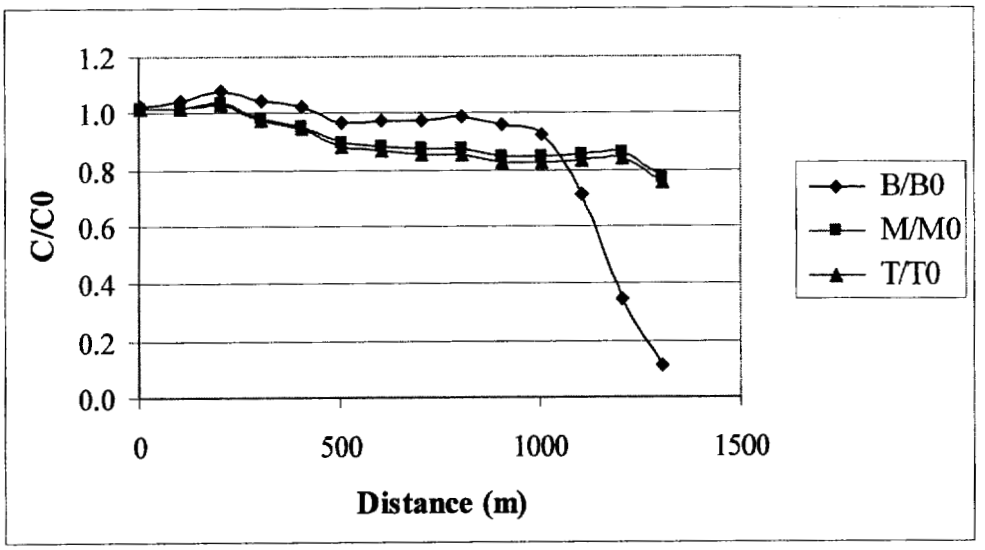

(a)

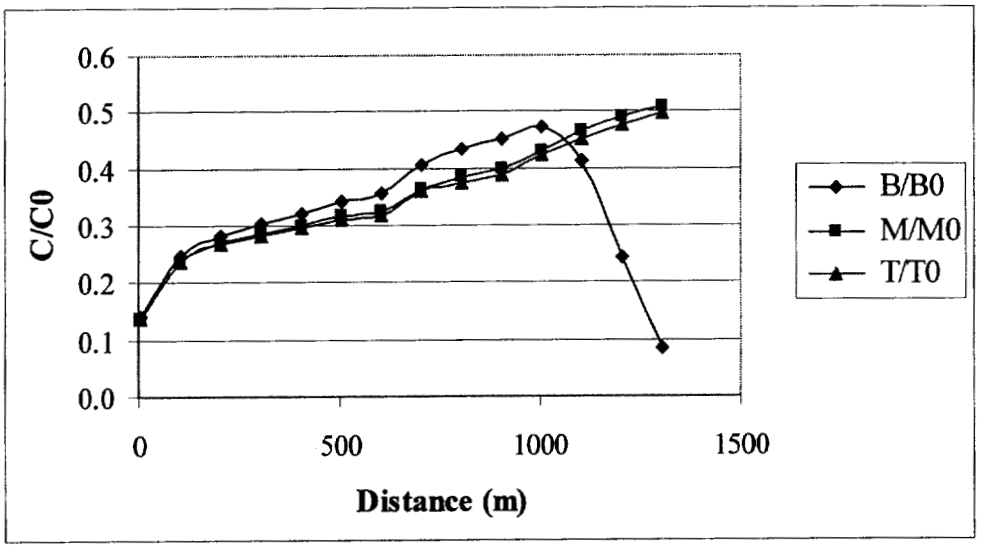

(b)

Figure 3.29: Benzene, MTBE, and Tracer Concentration Profiles along the Longitudinal Transect with No Biodegradation in (a) Upper 2-m Wells and (b) Lower 2-m Wells at t = 1080 Days

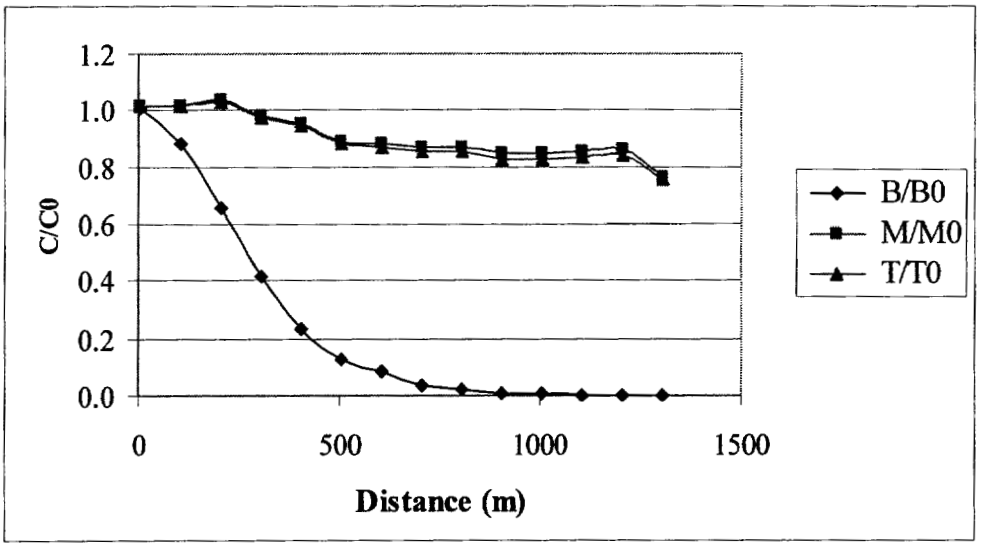

(a)

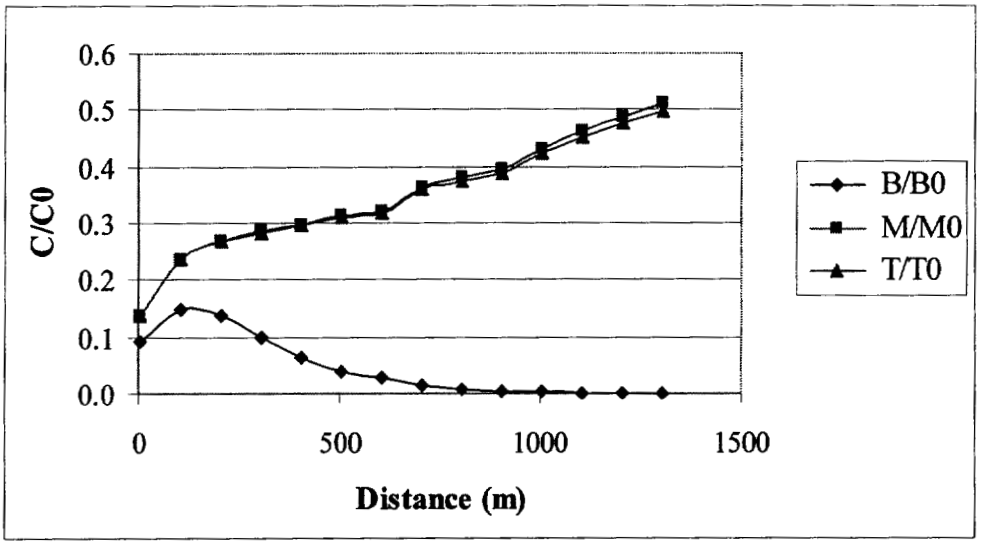

(b)

Figure 3.30: Benzene, MTBE, and Tracer Concentration Profiles along the Longitudinal Transect with Biodegradation in (a) Upper 2-m Wells and (b) Lower 2-m Wells at t = 1080 Days

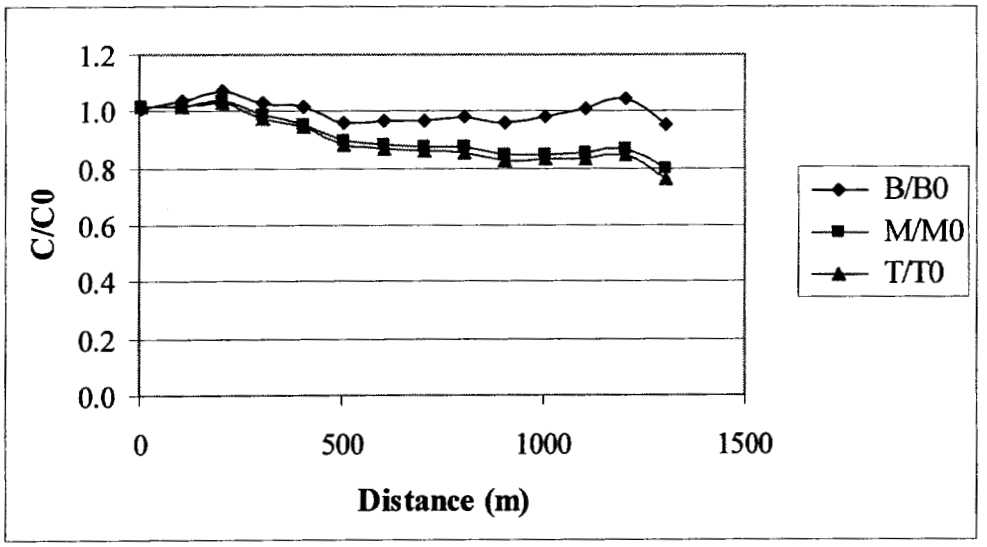

(a)

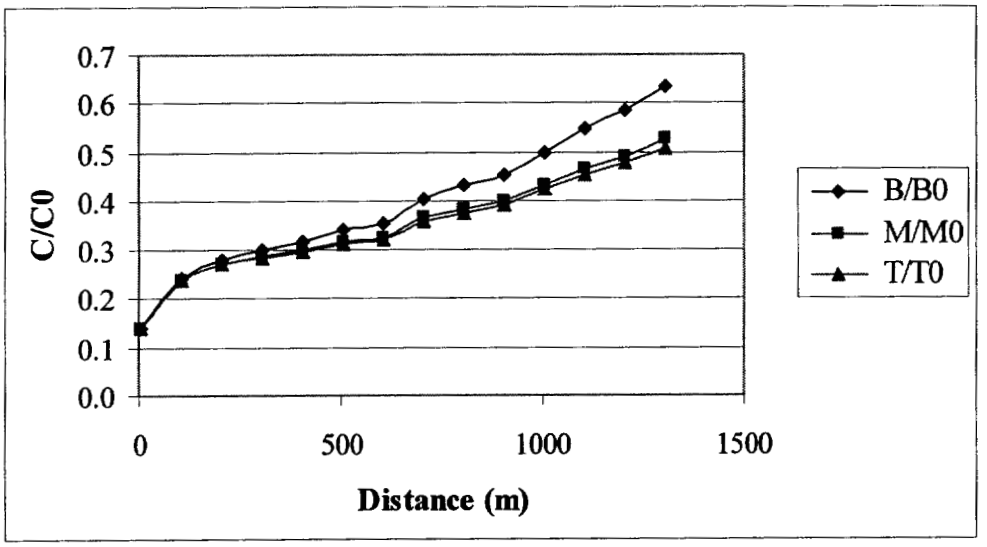

(b)

Figure 3.31: Benzene, MTBE, and Tracer Concentration Profiles along the Longitudinal Transect with No Biodegradation in (a) Upper 2-m Wells and (b) Lower 2-m Wells at t = 3060 Days

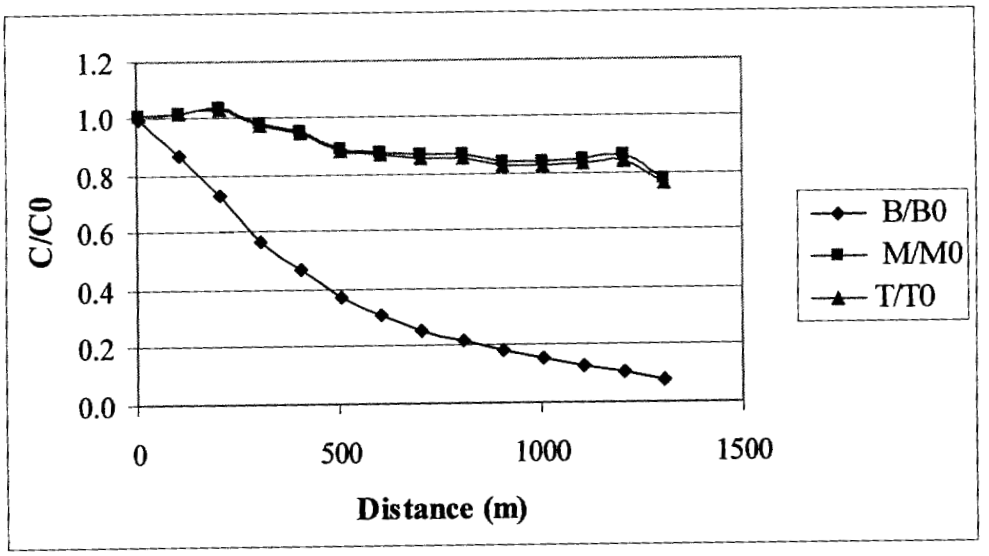

(a)

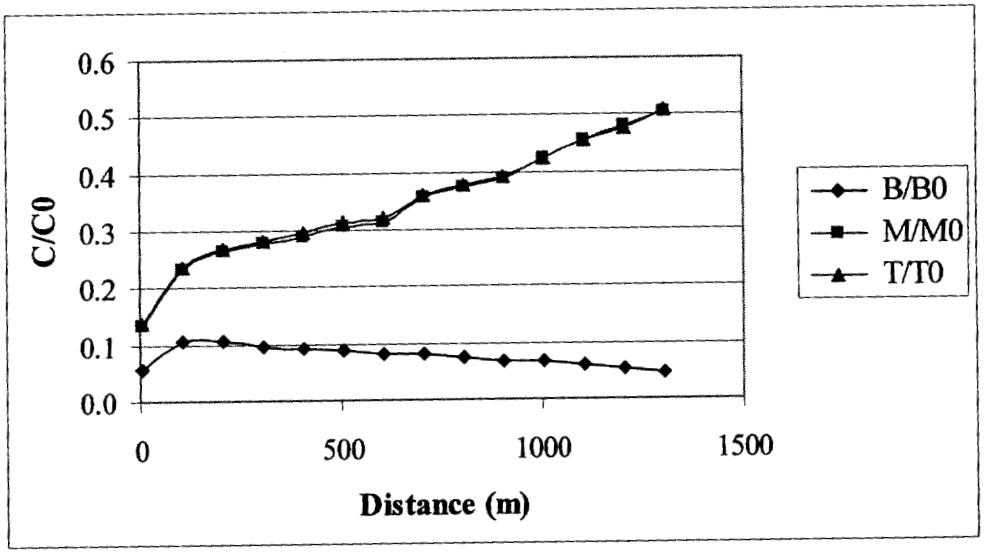

(b)

Figure 3.32: Benzene, MTBE, and Tracer Concentration Profiles along the Longitudinal Transect with Biodegradation in (a) Upper 2-m Wells and (b) Lower 2-m Wells at t = 3060 Days

compared to C_0 and C_{max}. In both cases, attenuation rates based on three velocities were evaluated since the true velocity along the transect was not known. Attenuation rates for Cases 4 and 5 can be found in Tables 3.9 and 3.10, respectively. Benzene attenuation rates in the degradation scenario (Case 5) were consistently faster than in the control scenario (Case 4), providing another indication that degradation is occurring. Furthermore, when the measured benzene concentrations were corrected for source function and dispersion, a downward trend was observed, giving evidence of degradation without the need for comparison with the control. Lastly, all of the benzene attenuation rates calculated at a given velocity were similar, suggesting that the correction factors were not critical for the benzene rate calculations. Conversely, the Case 5 MTBE data were closely related to both the control MTBE data and the Case 5 tracer data, providing little evidence of degradation.

Mass flux calculations in Cases 4 and 5 looked at the change in fluxes between the source and downgradient fences and the change in fluxes between downgradient fences as methods of assessing natural attenuation. In addition to evaluating how well spacing across a fence impacts the assessment of natural attenuation, data for these cases also evaluated how 0.5-m vertical sampling intervals differed from 2-m sampling intervals.

Differences in mass fluxes between the source fence and downgradient fences yielded evidence of degradation for both compounds; however, the three-dimensional hydraulic conductivity field and overlaid curvature complicated the flux data obtained from the comparison. Data from Cases 4 and 5 are given in Tables 3.11 and 3.12, respectively. Travel times were accounted for using benzene, MTBE, and tracer velocities of 0.81 m/d, and 1.16 m/d, and 1.22 m/d, respectively. As seen in previous experiments, the dispersive mass flux led to positive changes with distance if the fences adequately captured the plume behavior. The Case 4 data showed that the positive values occurred primarily in the 15-m well spacing, measured hydraulic conductivity data. Negative values reflected missed contaminant mass across the fence and illustrated the potential for missed data to mistakenly indicate degradation has occurred. The Case 5 benzene data showed

Table 3.9: Case 4 First-Order Attenuation Rates (day^{-1}) for an Exponential Source in a Complex Hydraulic Conductivity Field Based on Concentration versus Distance Data at t = 3060 Days

Case	Calculated by:	Benzene	MTBE	Tracer	Attributed to:
4 High V	C/C_0	-8E-6 R^2=0.07	-0.0001 R^2=0.84	-0.0002 R^2=0.87	Dsp, Src
4 High V	C_{corr}/C_0	0.0001 R^2=1.00	2E-5 R^2=0.96	NA	Src
4 High V	C/C_{max}	-0.0003 R^2=0.95	-0.0004 R^2=0.98	-0.0004 R^2=0.98	Dsp
4 High V	C_{corr}/C_{max}	NS	NS	NA	
4 Average V	C/C_0	-4E-6 R^2=0.07	-8E-5 R^2=0.84	-0.0001 R^2=0.87	Dsp, Src
4 Average V	C_{corr}/C_0	6E-5 R^2=1.00	1E-5 R^2=0.96	NA	Src
4 Average V	C/C_{max}	-0.0003 R^2=0.99	-0.0003 R^2=0.99	-0.0004 R^2=0.99	Dsp
4 Average V	C_{corr}/C_{max}	-3E-5 R^2=0.87	NS	NA	Sorption (Benzene)
4 Low V	C/C_0	-1E-6 R^2=0.07	-2E-5 R^2=0.84	-2E-5 R^2=0.87	Dsp, Src
4 Low V	C_{corr}/C_0	1E-5 R^2=1.00	3E-6 R^2=0.96	NA	Src
4 Low V	C/C_{max}	-0.0003 R^2=1.00	-0.0003 R^2=1.00	-0.0003 R^2=1.00	Dsp
4 Low V	C_{corr}/C_{max}	-0.0001 R^2=1.00	-2E-5 R^2=0.57	NA	Sorption (Benzene)

NS = Not Significant; NA = Not Applicable
Dsp = Dispersion; Src = Source Function; Deg = Degradation

Table 3.10: Case 5 First-Order Attenuation Rates (day^{-1}) for an Exponential Source in a Complex Hydraulic Conductivity Field with Degradation Based on Concentration versus Distance Data at t = 3060 Days

Experiment	Calculated by:	Benzene	MTBE	Tracer	Attributed to:
4 High V	C/C_0	-0.0012 R^2=1.00	-0.0001 R^2=0.85	-0.0002 R^2=0.87	Dsp, Src, Deg
4 High V	C_{corr}/C_0	-0.0011 R^2=1.00	2E-5 R^2=0.97	NA	Src, Deg
4 High V	C/C_{max}	-0.0015 R^2=1.00	-0.0004 R^2=0.98	-0.0004 R^2=0.98	Dsp, Deg
4 High V	C_{corr}/C_{max}	-0.0012 R^2=1.00	NS	NA	Deg
4 Average V	C/C_0	-0.0007 R^2=1.00	-8E-5 R^2=0.85	-0.0001 R^2=0.87	Dsp, Src
4 Average V	C_{corr}/C_0	-0.0006 R^2=1.00	9E-6 R^2=0.97	NA	Src, Deg
4 Average V	C/C_{max}	-0.0009 R^2=1.00	-0.0003 R^2=0.99	-0.0004 R^2=0.99	Dsp, Deg
4 Average V	C_{corr}/C_{max}	-0.0007 R^2=1.00	NS	NA	Deg
4 Low V	C/C_0	-0.0002 R^2=1.00	-2E-5 R^2=0.85	-2E-5 R^2=0.87	Dsp, Src
4 Low V	C_{corr}/C_0	-0.0002 R^2=1.00	2E-6 R^2=0.97	NA	Src, Deg
4 Low V	C/C_{max}	-0.0004 R^2=1.00	-0.0004 R^2=1.00	-0.0003 R^2=1.00	Dsp, Deg
4 Low V	C_{corr}/C_{max}	-0.0002 R^2=1.00	-2E-5 R^2=0.62	NA	Deg (Benzene)

NS = Not Significant; NA = Not Applicable
Dsp = Dispersion; Src = Source Function; Deg = Degradation

clear mass loss with distance, such that the influence of the dispersive flux and/or missed contaminant mass would have affected the calculated degradation rate but not the conclusion that degradation occurred. The MTBE data showed greater mass loss with distance using any of the sampling strategies, which would have indicated degradation if no other data were available. The tracer data, however, showed a corresponding change in mass flux in many instances. Only the comparison with the Case 4 results gave a strong indication that significant mass loss occurred that was attributable to degradation. For example, the 15-m, measured hydraulic conductivity data set showed losses of –577 g/d, -560 g/d, -590 g/d at t = 1080 days, t = 2070 days, and t = 3060 days, respectively.

Data from Cases 1 and 2 indicated that changes in mass flux unrelated to degradation could be minimized by using only fences beyond the source zone and reducing the distance between them. Changes in mass fluxes between fences X4 and X1 or X3 were calculated to determine whether or not this approach was equally valid in a more complex scenario. Because the travel time to X4 from either of the other fences required data from a time that was not sampled, bracketing values were calculated with the actual change in mass flux falling somewhere between the two. The results are presented in Table 3.13 and 3.14. Decreasing the spacing between fences mitigated nondegradative changes in mass flux for benzene and the tracer in the control case but exacerbated the problem for MTBE. Furthermore, changes in mass flux between fence pairs were different in the degradation case but interpreting those changes as degradation was not straightforward. The interaction of a complex hydraulic conductivity field, individual contaminant transport properties, and the relationship of the fence sampling points to the hydrogeology made a comparison of mass fluxes between fences difficult.

The complex hydrogeology built into Cases 4 and 5 featured a long correlation length in the longitudinal direction; that is, long, narrow channels of similar hydraulic conductivity were present. The mass flux comparisons often showed that the 15-m average velocity values minimized non-degradative changes more than the 15-m measured values. The main exception was between the source fence and X4. This could be significant because at this spacing the highest

Table 3.11: Case 4 Change in Mass Fluxes (g/day) Between XS and Downgradient Fences Accounting for Travel Time

			X1-XS			X3-XS			X4-XS		
Spacing/K Scenario	Vertical Interval	Time (days)	B	M	T	B	M	T	B	M	T
15-m/avg.	0.5 m	1080	37	1088	1080	-60	-4067	-4413	941	-6394	-7062
15-m/avg.	2.0 m	1080	33	957	949	-52	-3845	-4193	937	-6443	-7108
15-m/avg.	0.5 m	2070	21	601	597	-32	-2249	-2440	-38	-3520	-3892
15-m/avg.	2.0 m	2070	19	528	524	-28	-2127	-2318	-40	-3548	-3917
15-m/avg.	0.5 m	3060	11	325	324	-18	-1235	-1340	-21	-1942	-2148
15-m/avg.	2.0 m	3060	10	285	284	-16	-1167	-1273	-22	-1957	-2162
30-m/avg.	0.5 m	1080	-285	-8570	-8580	-302	-11307	-11649	946	-14951	-15622
30-m/avg.	2.0 m	1080	-286	-8589	-8599	-285	-10838	-11185	945	-14844	15514
30-m/avg.	0.5 m	2070	-156	-4730	-4735	-166	-6248	-6436	-197	-8244	-8617
30-m/avg.	2.0 m	2070	-157	-4741	-4746	-157	-5989	-6179	-195	-8164	-8558
30-m/avg.	0.5 m	3060	-87	-2619	-2622	-92	-3442	-3546	-109	-4551	-4758
30-m/avg.	2.0 m	3060	-87	-2625	-2628	-87	-3299	-3404	-108	-4519	-4725
15-m/meas.	0.5 m	1080	63	1854	1845	285	5241	4741	1204	15	-831
15-m/meas.	2.0 m	1080	63	1854	1845	285	5241	4741	1204	15	-831
15-m/meas.	0.5 m	2070	35	1024	1019	158	2890	2615	102	19	-451
15-m/meas.	2.0 m	2070	35	1024	1019	158	2890	2615	102	19	-451
15-m/meas.	0.5 m	3060	19	559	557	87	1605	1452	57	13	-248
15-m/meas.	2.0 m	3060	19	559	557	87	1605	1452	57	13	-248
30-m/meas.	0.5 m	1080	-218	-6573	-6585	39	-1975	-2450	1261	-5271	-6150
30-m/meas.	2.0 m	1080	-218	-6573	-6585	39	-1975	-2450	1261	-5271	-6150
30-m/meas.	0.5 m	2070	-119	-3628	-3634	22	-1095	-1356	8	-2900	-3388
30-m/meas.	2.0 m	2070	-119	-3628	-3634	22	-1095	-1356	8	-2900	-3388
30-m/meas.	0.5 m	3060	-66	-2011	-2014	12	-595	-740	5	-1598	-1869
30-m/meas.	2.0 m	3060	-66	-2011	-2014	12	-595	-740	5	-1598	-1869

Table 3.12: Case 5 Change in Mass Fluxes (g/day) Between XS and Downgradient Fences Accounting for Travel Time

			X1-XS			X3-XS			X4-XS		
Spacing/K Scenario	Vertical Interval	Time (days)	B	M	T	B	M	T	B	M	T
15-m/avg.	0.5 m	1080	13	1058	1080	-757	-5259	-4413	143	-6856	-7062
15-m/avg.	2.0 m	1080	10	927	949	-753	-5033	-4193	143	-6904	-7108
15-m/avg.	0.5 m	2070	0	581	597	-418	-3033	-2440	-637	-3969	-3892
15-m/avg.	2.0 m	2070	-1	508	524	-416	-2909	-2318	-636	-3996	-3917
15-m/avg.	0.5 m	3060	-3	307	324	-235	-1782	-1340	-352	-2415	-2148
15-m/avg.	2.0 m	3060	-4	267	284	-234	-1714	-1273	-352	-2430	-2162
30-m/avg.	0.5 m	1080	-343	-8607	-8580	-1054	-12696	-11649	144	-15381	-15622
30-m/avg.	2.0 m	1080	-344	-8626	-8599	-1045	-12220	-11185	144	-15275	15514
30-m/avg.	0.5 m	2070	-199	-4773	-4735	-583	-7130	-6436	-847	-8711	-8617
30-m/avg.	2.0 m	2070	-199	-4783	-4746	-578	-6866	-6179	-844	-8652	-8558
30-m/avg.	0.5 m	3060	-113	-2664	-2622	-326	-4049	-3546	-468	-5094	-4758
30-m/avg.	2.0 m	3060	-113	-2670	-2628	-323	-3902	-3404	-467	-5061	-4725
15-m/meas.	0.5 m	1080	32	1817	1845	-676	3935	4741	184	-562	-831
15-m/meas.	2.0 m	1080	32	1817	1845	-676	3935	4741	184	-562	-831
15-m/meas.	0.5 m	2070	10	997	1019	-377	1999	2615	-636	-541	-451
15-m/meas.	2.0 m	2070	10	997	1019	-377	1999	2615	-636	-541	-451
15-m/meas.	0.5 m	3060	2	534	557	-214	953	1452	-352	-577	-248
15-m/meas.	2.0 m	3060	2	534	557	-214	953	1452	-352	-577	-248
30-m/meas.	0.5 m	1080	-291	-6619	-6585	-936	-3414	-2450	194	-5783	-6150
30-m/meas.	2.0 m	1080	-291	-6619	-6585	-936	-3414	-2450	194	-5783	-6150
30-m/meas.	0.5 m	2070	-172	-3680	-3634	-520	-2047	-1356	-800	-3459	-3388
30-m/meas.	2.0 m	2070	-172	-3680	-3634	-520	-2047	-1356	-800	-3459	-3388
30-m/meas.	0.5 m	3060	-99	-2065	-2014	-293	-1293	-740	-443	-2254	-1869
30-m/meas.	2.0 m	3060	-99	-2065	-2014	-293	-1293	-740	-443	-2254	-1869

Table 3.13: Change in Mass Fluxes (g/day) Between Fences X4 at 2070 Days and X1 or X3 in Case 4

		X4 – X1@ t_1			X4 – X1@ t_2			X4 – X3 @ t_1			X4 – X3 @ t_2		
Spacing/K Scenario	Vertical Interval	B	M	T	B	M	T	B	M	T	B	M	T
15-m/avg.	0.5 m	-256	-4879	-5244	-211	-3812	-4179	-32	-5295	-193	2	-4199	615
15-m/avg.	2.0 m	-252	-4783	-5146	-207	-3725	-4090	-39	-5508	-368	-5	-4405	445
30-m/avg.	0.5 m	-80	-675	-1040	-44	173	-192	-19	-4882	125	14	-3805	918
30-m/avg.	2.0 m	-76	-596	-961	-40	246	-118	-29	-5217	-130	4	-4124	674
15-m/meas.	0.5 m	-151	-2066	-2528	-103	-929	-1392	-149	-10287	-2875	-101	-8710	-1712
15-m/meas.	2.0 m	-151	-2066	-2528	-103	-929	-1392	-149	-10287	-2875	-101	-8710	-1712
30-m/meas.	0.5 m	50	-2815	2336	89	3737	3258	-68	-7791	-839	-23	-6302	256
30-m/meas.	2.0 m	50	-2815	2336	89	3737	3258	-68	-7791	-839	-23	-6302	256

X1: benzene t_1 = 810 days; benzene t_2 = 900 days; MTBE t_1 = 1200 Days; MTBE t_2 = 1290 Days;
tracer t_1 = 1230 Days; tracer t_2 = 1320 Days
X3: benzene t_1 = 1560 days; benzene t_2 = 1650 days; MTBE t_1 = 1710 Days; MTBE t_2 = 1800 Days
tracer t_1 = 1740 Days; tracer t_2 = 1830 Days

Table 3.14: Change in Mass Fluxes (g/day) Between Fences X4 at 2070 Days and X1 or X3 in Case 5

		X4 – X1@ t_1			X4 – X1@ t_2			X4 – X3 @ t_1			X4 – X3 @ t_2		
Spacing/K Scenario	Vertical Interval	B	M	T	B	M	T	B	M	T	B	M	T
15-m/avg.	0.5 m	-530	-5307	-5244	-497	-5011	-4179	-54	-599	-193	-46	239	615
15-m/avg.	2.0 m	-526	-5211	-5146	-493	-4917	-4090	-56	-780	-368	-48	64	445
30-m/avg.	0.5 m	-372	-1101	-1040	-346	-865	-192	-50	-334	125	-42	490	918
30-m/avg.	2.0 m	-369	-1024	-961	-343	-789	-118	-53	-601	-130	-45	235	674
15-m/meas.	0.5 m	-543	-2598	-2528	-507	-2282	-1392	-93	-3452	-2875	-81	-2245	-1712
15-m/meas.	2.0 m	-543	-2598	-2528	-507	-2282	-1392	-93	-3452	-2875	-81	-2245	-1712
30-m/meas.	0.5 m	-376	2304	2336	-348	2561	3258	-73	-1407	-839	-62	-268	256
30-m/meas.	2.0 m	-376	2304	2336	-348	2561	3258	-73	-1407	-839	-62	-268	256

X1: benzene t_1 = 810 days; benzene t_2 = 900 days; MTBE t_1 = 1200 Days; MTBE t_2 = 1290 Days;
tracer t_1 = 1230 Days; tracer t_2 = 1320 Days
X3: benzene t_1 = 1560 days; benzene t_2 = 1650 days; MTBE t_1 = 1710 Days; MTBE t_2 = 1800 Days
tracer t_1 = 1740 Days; tracer t_2 = 1830 Days

concentrations were being measured in the same hydraulic conductivity channel. At the 30-m spacing the average versus measured results depended on the spacing between fences, particularly when both fences were downgradient of the source. In the source to downgradient fence comparisons, the 15-m spacing using a given velocity profile always resulted in smaller non-degradative changes in mass flux than the associated 30-m spacing. In the downgradient to downgradient fence comparisons the opposite was true. These results suggested that in complex hydrogeology with dominant flow paths not only well spacing but well positioning must be considered to minimize changes unrelated to degradation. There were no significant differences in the results for 0.5-m and 2-m vertical intervals, which may have been linked to the way the velocity profile was handled in the calculations.

Total mass calculations for Cases 4 and 5 confirmed that degradation had occurred for both benzene and MTBE in Case 5. The mass balance calculations are shown in Table 3.15. Attenuation rates that were calculated as the change in total mass in the domain with time for each experiment reflected the effects of reduced mass loading from the source and degradation (Case 5). The results for benzene showed different loss rates in Cases 4 and 5 using this evaluation method while those for MTBE remained the same for both experiments. In addition, rates for MTBE were comparable to those for the tracer. When total mass in Cases 4 and 5 were compared at each snapshot in time there were ~100 kg changes for MTBE at each time, indicating that degradation had occurred. These results suggested that the effects of the source function and dispersion masked the evidence of degradation for both benzene and MTBE but the effect was more pronounced for MTBE.

3.4 Conclusions

The step-by-step progression through increasingly complicated scenarios revealed several factors key for demonstrating natural attenuation in general and of MTBE in particular.

- Dominant features in the hydrogeology such as the zigzag channel were reflected in longitudinal transect data, the importance of those features

Table 3.15: Total Mass (kg) of Benzene, MTBE, and Tracer in the Plume at t=1080 Days, t=2070 Days, and t=3060 Days for Case 4 (No Degradation) and Case 5 (Degradation)

	Case 4			Case 5			Degradation (kg/day)	
Time (Days)	B	M	T	B	M	T	B	M
1080	249	8057	7937	87	7947	7937	*-0.15*	*-0.10*
2070	166	4463	4386	48	4363	4386	*-0.06*	*-0.05*
3060	92	2465	2423	25	2361	2423	*-0.02*	*-0.03*
Kg/day 2070-1080	*-0.08*	*-3.6*	*-3.6*	*-0.04*	*-3.6*	*-3.6*		
Kg/day 3060-2070	*-0.08*	*-2.0*	*-2.0*	*-0.02*	*-2.0*	*-2.0*		

depended on the source location relative to the feature, and it was important to understand the combined effect to interpret the concentration versus difference profile. The effect was more pronounced for MTBE than for benzene.

- Comparison of contaminant concentrations to a tracer was critical in differentiating degradation from dispersion and dilution when calculating attenuation rates from the longitudinal transect. The effectiveness of the tracer decreases if its tendency to sorb differs significantly from the contaminant of interest as seen in the benzene data.
- Knowing the source function and accounting for maximum possible concentrations along the longitudinal transect resulted in improved estimates of attenuation and degradation rates from the transect data for both compounds.
- Closer well spacing in cross-gradient fences generally resulted in measuring less mass flux due to dispersion and reducing the mass "lost" between fences.
- Understanding the mass flux from the source and accounting for contaminant travel time improved the interpretation of changes in mass flux between fence pairs.
- In complex hydrogeology, sampling from the same flow path at each fence improved interpretation of changes in mass flux between fence pairs.
- Accounting for the source function and dispersion was critical to interpreting MTBE loss in the mass balance.

3.5 References

ASTM. 1998. Standard Guide for Remediation of Ground Water by Natural Attenuation at Petroleum Release Sites. ASTM E 1943 – 98. American Society for Testing and Materials, West Conshohocken, PA.

Borden, R.C., R.A. Daniel, L.E. LeBrun, IV, and C.W. Davis. 1997. Intrinsic Biodegradation Rates of MTBE and BTEX in a Gasoline-Contaminated Aquifer. *Water Resources Research.* 33(5):1105-1115.

Mormile, M.R, S. Liu, and J.M. Suflita. 1994. Anaerobic Biodegradation of Gasoline Oxygenates: Extrapolation of Information to Multiple Sites and Redox Conditions. *Environmental Science and Technology*. 28(9): 1727-1732.

Church, C.D., P.G. Tratnyek, J.F. Pankow, J.E. Landmeyer, A.L. Baehr, M.A. Thomas, and M. Schirmer. 1999. Effects of Environmental Conditions on MTBE Degradation in Model Column Aquifers. *Proceedings*, U.S. Geological Survey, Toxic Substances Hydrology Program Technical Meeting, Charleston, SC, March 7-12, 1999. pp. 93-101. Borden et al. (1997)

Clement, T.P. 1997. A Modular Computer Code for Simulating Reactive Multi-Species Transport in 3-Dimensional Groundwater Systems. PNNL –SA-11720.

Deeb, R.A., H.Y. Hu, J.R. Hanson, K.M. Scow, and L. Alvarez-Cohen. 2001. Substrate Interactions in BTEX and MTBE Mixtures by an MTBE-Degrading Isolate. *Environmental Science and Technology*. 35(2): 312-317.

Harbaugh, A.W. and M.G. McDonald. 1996. User's Documentation for MODFLOW-96, An Update to the U.S. Geological Survey Modular Finite-Difference Ground-Water Flow Model. USGS Open-File Report 96-485.

Johnson, R.L. 2002. Hydcond – A Program to Multiply GMS Hydraulic Conductivity Files By a Constant Value. OGI School of Science & Engineering, Beaverton, OR.

Marsily, G. 1986. *Quantitative Hydrogeology*. Academic Press. San Diego, CA.

McDonald, M.G. and A.W. Harbaugh. 1988. A Modular Finite-Difference Ground-Water Flow Model. USGS Open-File Report TWI 6-A1.

National Research Council. 2000. *Natural Attenuation for Groundwater Remediation*. National Academy Press. Washington, DC.

Rehfeldt, K.R., J.M. Boggs, and L.W. Gelhar. 1992. Field Study of Dispersion in a Heterogeneous Aquifer, 3, Geostatistical Analysis of Hydraulic Conductivity. *Water Resources Research*. 28(12): 3309-3324.

Robin, M.J.L., A.L. Gutjahr, E.A. Sudicky, and J.L. Wilson. 1993. Cross-Correlated Random Field Generation with the Direct Fourier Transform Method. *Water Resources Research*. 29(7): 2385-2397.

Schirmer, M., B.J. Butler, J.F. Barker, C.D. Church, and K. Schirmer. 1999. Evaluation of Biodegradation and Dispersion as Natural Attenuation Processes of MTBE and Benzene at the Borden Field Site. *Physics and Chemistry of the Earth (B)*. 24(6): 557-560.

Squillace, P.J., J.F. Pankow, N.E. Korte, and J.S. Zogorski. 1997. Review of the Environmental Behavior and Fate of Methyl *tert*-Butyl Ether. *Environmental Toxicology and Chemistry*. 16(9): 1836-1844.

Suarez, M.P and H.S. Rifai. 1999.Biodegradation Rates for Fuel Hydrocarbons and Chlorinated Solvents in Groundwater. *Bioremediation Journal*. 3(4): 337-362.

Thoms, B. 2002. PostRT3D – Unformatted File Reader for RT3D.

Thoms, B. 2002. FGENCV – A Program for Converting FGEN Hydraulic Conductivity Fields to GMS Data File Format.

USEPA. 1999. Use of Monitored Natural Attenuation at Superfund, RCRA Corrective Action, and Underground Storage Tank Sites. Directive Number 9200.4-17P. U.S. Environmental Protection Agency, Office of Solid Waste and Emergency Response. Washington, DC.

USEPA. 2000. *Natural Attenuation of MTBE in the Subsurface under Methanogenic Conditions*. Research Report. EPA 600/R-00/006. U.S. Environmental Protection Agency, National Risk Management Research Laboratory, Office of Research and Development, Cincinnati, OH.

CHAPTER 4
A THREE-DIMENSIONAL STUDY OF THE DISSOLUTION OF MTBE FROM AN OXYGENATED FUEL SOURCE

4.1 Introduction

Researchers have attempted to describe contaminant dissolution from non-aqueous phase liquid (NAPL) with mass transfer models (Miller et al. 1990, Geller and Hunt 1993, Powers et al. 1994, Soerens et al. 1998, Sahloul et al. 2002), flow bypassing studies (Hunt et al. 1988), and mathematical modeling (Powers et al. 1991, Johnson and Pankow 1992, Zhu and Sykes 2000). Simple 1- and 2-dimensional experimental studies using glass beads, layered soils, and micromodels have been employed to acquire empirical data on the NAPL/aqueous phase relationship (Powers et al. 1994, Nambi and Powers 2000, Rixey and Joshi 2000, Sahloul et al. 2002). Rixey and Joshi looked at equilibrium and mass transfer limited dissolution of MTBE specifically in column studies using emplaced NAPL sources in glass beads and sand as well as modeling studies.

The results of the numerical modeling in Chapter 3 demonstrated the importance of accounting for the source function when quantifying attenuation rates in general and degradation rates in particular. In the model longitudinal transect, knowing the source function and the maximum concentrations that could be measured downgradient, allowed the influence of dispersion and degradation to be discerned from the concentration data. The data from the fence of wells across the plume showed how the changing mass flux from the source could be propagated downgradient. Consequently, an examination of the behavior of a developing source was warranted.

Following a spill of sufficient volume, the NAPL migrates downward through the vadose zone and capillary fringe to the water table. Gasoline, a light NAPL or LNAPL, collects and spreads laterally at the water table. During this process ganglia (blobs) of NAPL are left behind in the unsaturated zone and under the water table as residual

contamination. Because soils are composed of zones of higher and lower permeability, the residual NAPL becomes unevenly distributed, even in relatively homogeneous soils. The heterogeneity in NAPL distribution, as well as nonuniform flow, dilution with uncontaminated water, sorption, and mass transfer limitations, has been cited as the cause of observed concentrations in groundwater that are lower than theoretical equilibrium values (Hunt et al. 1988).

Fingers of residual NAPL in soil may form complex patterns in which tens of centimeters may separate fingers from each other. Furthermore, the result may be that the majority of the NAPL mass is in a small percentage of the soil in the source zone. Near the release point, the NAPL content is expected to be relatively high while only a small percentage of the pore space at the edges of the release would be occupied by NAPL. Because the soil permeability to water is reduced by the presence of NAPL in the pore space, water may bypass zones with higher residual NAPL, further complicating the dissolution process.

Vertical smearing of the gasoline results when the water table fluctuates. As the water table rises, water in equilibrium with the NAPL is pushed up out of the NAPL source. The upflow column experiment reported in Rixey and Joshi (2000) is analogous to this scenario and resulting aqueous MTBE concentrations in the 300-1000 mg/L range might be expected depending on the lateral distribution of the residual gasoline and mixing with relatively clean water that occurs during water table rise. More contaminant mass dissolves in the water flowing up through the source, resulting in lower concentrations than those in the first flush of water as MTBE is flushed from the residual gasoline. The first rise of the water table can also push the NAPL up leaving behind residual trapped beneath the water table as it rises. This distributes the residual NAPL more widely. In shallow aquifers, evaporation may cause the water table to drop again, transferring aqueous contaminants to the vapor phase and exposing residual NAPL to volatilization. Water table fluctuations as well as groundwater flow age the contaminant source, resulting in a change in NAPL composition. The Rixey and Joshi study (2000) showed a maximum MTBE concentration of ~100 mg/L for gasoline that had been aged for seven months.

Source zone MTBE concentrations observed at field sites are generally considerably lower than theoretical values. Landmeyer et al. (1998) reported concentrations exceeding 10,000 μg/L resulting from a mid-1980's release. Discrete direct-push samples taken prior to the natural gradient tracer test at Port Hueneme, CA revealed aqueous MTBE concentrations up to 270,000 μg/L near the source zone of a mid-1980's gasoline release. The highest concentration reported in USEPA 2000 at the Elizabeth City, NC site was 3,640 μg/L for a source of unknown age and volume. The range of values for these relatively old source zones suggested the possible complexity of the source function for MTBE.

A dissolution study was conducted as a prelude to an air sparging experiment in an OHSU Large Experimental Aquifer Program (LEAP) physical model. Although not specifically designed to look at MTBE dissolution from a gasoline source, the study provided an understanding of how an MTBE source zone develops from known initial conditions. Rather than use an emplaced source, this dissolution study employed an actual spill of gasoline immediately on top of the water table followed by smearing due to water table rise, with no constraints on subsequent NAPL migrations. The water table was allowed to fluctuate within controlled boundaries. Hydraulic gradient driven flow through the source was isolated from water table rise to assess the effects on the source and downgradient concentrations as independently as possible. Soil cores provided information on the NAPL distribution in a relatively homogeneous medium as well as a comparison of the initial MTBE distribution in the soil relative to a nearly insoluble compound (isooctane). Aqueous sampling tracked the development of the aqueous MTBE plume relative to the initial NAPL distribution.

4.2 Physical Model

The physical model is a 10-m long x 10-m wide x 5-m deep tank filled with a poorly sorted medium-to-coarse washed Columbia River Sand (MacPherson 1991). A plan view layout of the tank is shown in Figure 4.1. Because the surface of the sand was uneven, the rim of the tank was chosen as the datum against which all measurements

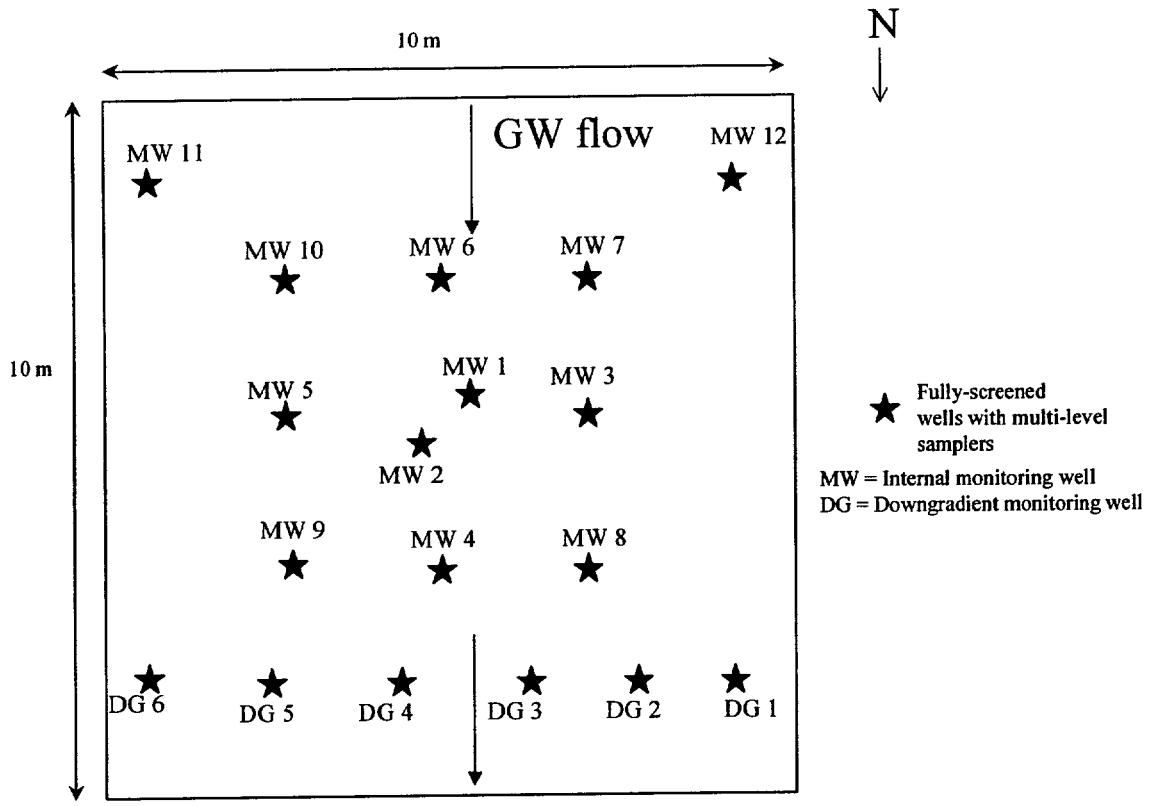

Figure 4.1: Schematic of the Physical Model Used in the Dissolution Study

were referenced. The datum was approximately 20 cm above the sand. A plywood deck was built over the entire tank area at the datum level.

A total of 18 groundwater monitoring wells were installed in the tank and were functionally divided into internal wells (MW) and downgradient wells (DG) as shown in Figure 4.1. Internal wells were used to monitor aqueous contaminant concentrations in and immediately surrounding the source zone. Downgradient wells monitored the contaminant concentrations resulting from flow through the source zone 1 m downgradient of the source. The wells were constructed of 1" slotted PVC pipe inserted without a filter pack. The wells were fully screened from the ground surface to 3 m in depth. Solid PVC risers attached to the slotted pipe allowed access at the deck level. A dedicated movable sampler was inserted into each well for sample collection. The samplers were built with inflatable packers that isolated four 25-cm sampling intervals inside the PVC well. The samplers were easily deflated, shifted up or down, and re-inflated to sample up to eight 25-cm intervals of interest per well from 0.5-2.5 m bd.

Water flow was accomplished using a series of 5 injection wells at the south end of the tank and 6 extraction wells at the north end of the tank. Water injection came from the city water supply while extraction was done using a series of peristaltic pumps. HP VEE (Agilent Technologies, Inc., Palo Alto, CA), a process control software package, was used to control the water level and flow in the tank using signals from calibrated pressure transducers. HP VEE was capable of controlling the water level within approximately four inches of fluctuation. During water flow, the pumps extracted water faster than it was introduced; therefore, HP VEE was set up to control the water level by switching the pumps on and off. Extracted water was collected in a 120-L reservoir where it was partially treated with an air bubbler before being pumped to a 2,000-L holding tank, further treated and discharged.

4.3 Experimental

4.3.1 Timeline

The experiment was started with the spill and subsequent smearing of approximately 200 L of MTBE- containing gasoline in December 1998. Water samples

and soil cores were collected and analyzed over the following 6 month period of source aging, water table fluctuations, and flow through the source zone as described below. Flow through the source for the dissolution study was conducted in four phases: June 6-8, June 15-16, June 19-22, and June 26-28, 1999. Water flow was turned on briefly prior to a sampling event on June 30, 1999. The flow rate was 5 m^3/d and the resulting groundwater velocity was 0.3 m/d.

4.3.2 Gasoline Spill and Smear

The gasoline spill and smear were completed in December 1998. The gasoline used for the dissolution experiment was American Petroleum Institute (API) research gasoline, identical to the gasoline used by Rixey and Joshi in their column studies of MTBE dissolution. MTBE was blended into the fuel to a final concentration of 11.09% by volume. A total of 200 L of gasoline was used in the experiment. A detailed chemical analysis of the gasoline was completed by Chevron Research and Technology Company (Richmond, CA), allowing the composition of the original gasoline to be known. Rhodamine dye was mixed into the gasoline before injection to allow visual observation of the residual gasoline distribution after the spill.

Prior to the spill, the water level in the tank was brought to 1 m below the datum (bd). Gasoline was introduced into the tank through ¼" copper tubing running from the 200-L drum into the ground at the center of the tank. A short piece of flexible tubing was placed in the spill line for the peristaltic pump used to introduce the gasoline. The end of the tubing terminated at the water table. The spill was completed in approximately 12.5 hours. The gasoline was smeared and trapped by raising the water table 0.5 m following the spill. To keep the water level as even as possible across the tank, water was introduced at both ends using garden hoses connected to a solenoid valve and flow splitter. HP VEE was set to stop water flow by closing the solenoid valve if the water level in any part of the tank exceeded the 0.5 m bd target and restart if the water level dropped. A steady water level of 0.5 m bd was achieved after 17.5 hours.

4.3.3 Soil Sampling for Residual Gasoline Distribution

Soil samples were collected on April 27, 1999 to help characterize the source zone. A downhole camera was used to look for gasoline immediately after the spill but very little gasoline was observed in the area of the access tubes. Because the tank was saturated to 0.5 m bgs at the time of soil sampling, much of the source was below the water table. To facilitate sampling a cryogenic technique was used to obtain the samples. A capped piece of stainless steel pipe was pushed into the ground at the sampling location. Liquid nitrogen was then introduced to the pipe, freezing the soil and water around the pipe. The pipe was then removed from the ground. Frozen soil samples were removed from the outside of the sampler at 0.25 m intervals from 0.5 – 1.5 m bd. Six soil cores were collected at 0.3 to 1 m from the spill location (Figure 4.2). Soil was placed in previously weighed 40 mL volatile organic analysis (VOA) vials with Teflon coated septa containing 20 mL of methanol to extract the gasoline from the soil. The vials were filled with soil to minimize the headspace and were placed in a 4°C cold room until analyzed. Samples were analyzed within a week of collection.

Soil samples were analyzed for gasoline components on an HP 5890/5971A GC/MS with a 50-m Petrocol column. The method details were similar to those described in Chapter 2 for the natural gradient tracer test with the exception that selective ion mode was not used for any of the tank samples. A stock standard solution was prepared using 1 mL of gasoline in 40 mL of methanol. Standards were prepared by adding 10 μL and 1 μL aliquots of stock to a helium purged 40 mL VOA vial. A blank was used to set the zero point since using a 0.1 μL aliquot did not result in reproducible peak areas. Samples were analyzed by injecting 3 μL of the gasoline in methanol sample (10 μL for soil core 2) into a helium-purged 40 mL VOA vial. A 1-μL aliquot of 20 g/L perdeuterated MTBE stock solution was added to all standards and samples as an internal standard.

4.3.4 Water Sampling for Aqueous MTBE Distribution

Water samples were collected to understand the impact of water table fluctuations on the source concentrations and subsequently the resulting downgradient concentrations after flow through the source. A summary of the sampling dates, the wells included and the purpose of each sampling event is presented in Table 4.1. Water samples were

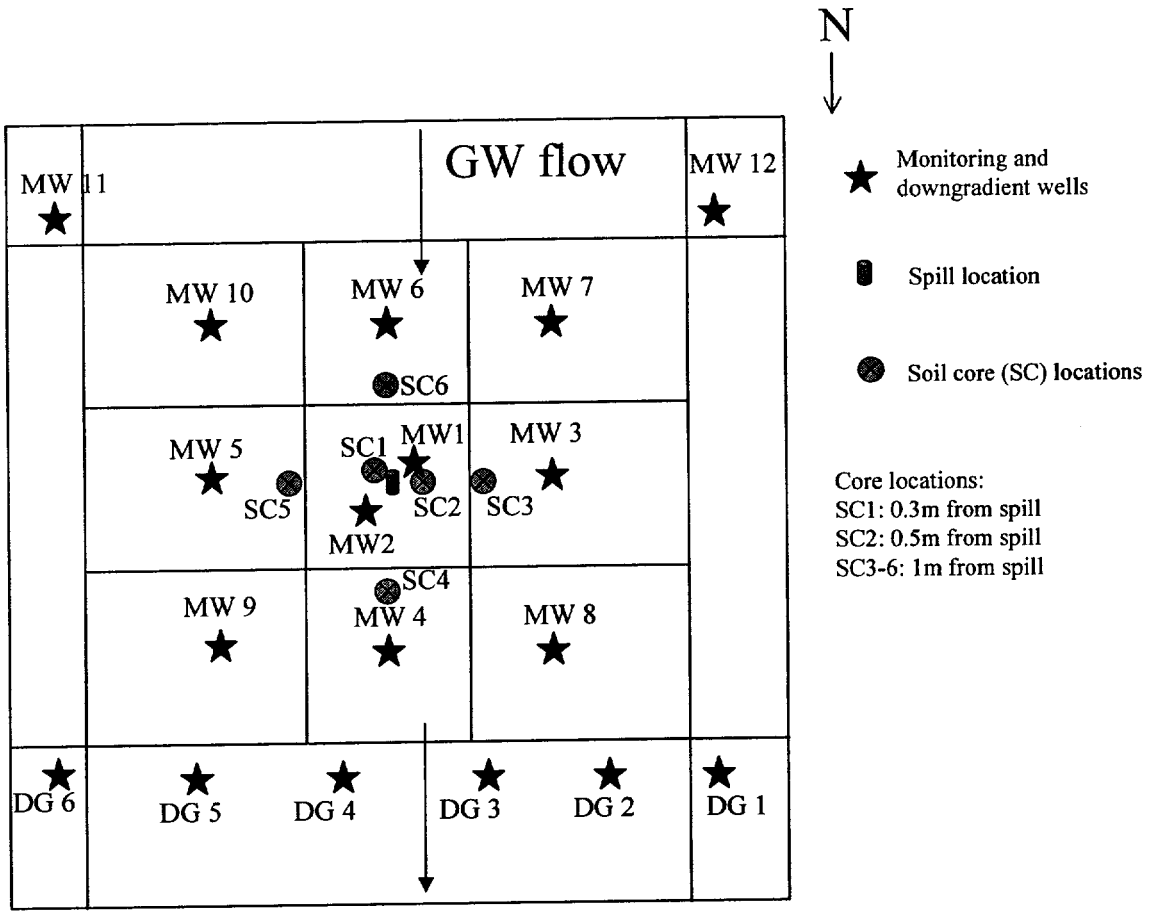

Figure 4.2: Dissolution Study Soil Core Locations

Table 4.1: Summary of Aqueous Sample Collection Events During the Dissolution Study

Date	Wells Samples	Depths Sampled (m below datum)	Purpose of Sampling Event
1/26/99	MW 1, 2, 3, 5	0.5-0.75; 0.75-1.0; 1.0-1.25; 1.25-1.5; 1.5-1.75; 2-2.25	Post-smear cross-section of source zone aqueous concentrations
5/12/99	MW 1-10	All intervals 0.75–2.5	Post-soil sampling assessment of aqueous distribution
6/6/99	MW 1-10 DG 2-6	1.0-1.25 1.0-1.25; 1.5-1.75; 2.0-2.25	Aqueous distribution immediately preceding first phase of water flow through source zone
6/19/99	MW 1, 3, 5, 7-10 MW 2, 4, 6 DG 2-6	1.0-1.25 1.0-1.25; 1.5-1.75; 2.0-2.25 1.0-1.25; 1.5-1.75; 2.0-2.25	Aqueous distribution between first and second phases of water flow through source zone
6/20/99	MW 1-10	0.75-1.0	Aqueous distribution between first and second phases of water flow through source zone
6/28/99	MW 1,3,5,7-10 MW 2, 4, 6 DG 2-6	1.0-1.25 1.0-1.25; 1.5-1.75; 2.0-2.25 1.0-1.25; 1.5-1.75; 2.0-2.25	Aqueous distribution after the last phase of water flow through source zone
6/30/99	MW 1-3, 5, 7-10 MW 2, 4 MW 2-4, 8, 10	0.75-1.0 1.25-1.5; 1.75-2.0 2.25 – 2.5	Aqueous distribution after the last phase of water flow through source zone

MW = Internal monitoring well
DG = Downgradient monitoring well

collected in duplicate in 40 mL VOA vials with Teflon septa and placed in a 4°C cold room until analyzed. Samples were analyzed within the week they were collected.

Water samples were analyzed using the same equipment and method as the soil core samples. A standard stock solution was prepared using 1 mL gasoline in 20 mL of methanol. Standard solutions were 1:10,000, 1:100,000, 1:1,000,000 dilutions in 40 mL VOA vials of nanopure water. A 1 mL aliquot of standard or sample was injected into a clean, helium-purged VOA along with 2 μL of 20 g/L perdeuterated MTBE stock solution as an internal standard.

4.4 Results and Discussion

4.4.1 Gasoline Distribution in Soil Cores

The gasoline distribution was evaluated from the isooctane concentration and its initial volume fraction in the gasoline. Because its solubility in water is limited, 1.14 mg/L (Montgomery 1996), isooctane was believed to best approximate the NAPL (as opposed to aqueous phase) distribution in the soil. The plan view in Figure 4.3 represented vertically-averaged concentrations and, therefore, masks the distribution with depth. Cross-sectional data through the center of the tank showing the vertical distribution in the direction of groundwater flow and perpendicular to groundwater flow are given in Table 4.2(a) and (b), respectively. There was evidence from soil core 1 (SC1), immediately adjacent to the spill location, that the gasoline depressed the water table somewhat during the spill, resulting in the maximum NAPL content at 1.1 m bd. Although the majority of residual gasoline was concentrated in the smear zone between 0.5 and 1.0 m bd, the irregular distribution of NAPL could be seen in the range of NAPL concentrations with distance. For example, cores SC6 and SC2, which are equidistant from the spill location, showed an order of magnitude difference in residual NAPL concentration. This typified the irregular distribution of NAPL flowing into a heterogeneous porous medium.

The distribution of MTBE in the soil cores was considerably different than the distribution of isooctane in soil on which the NAPL distribution was based. Figure 4.4 shows the vertical distribution of MTBE and isooctane in each of the soil cores. The component distributions in the soil cores were key results for MTBE. Isooctane was the

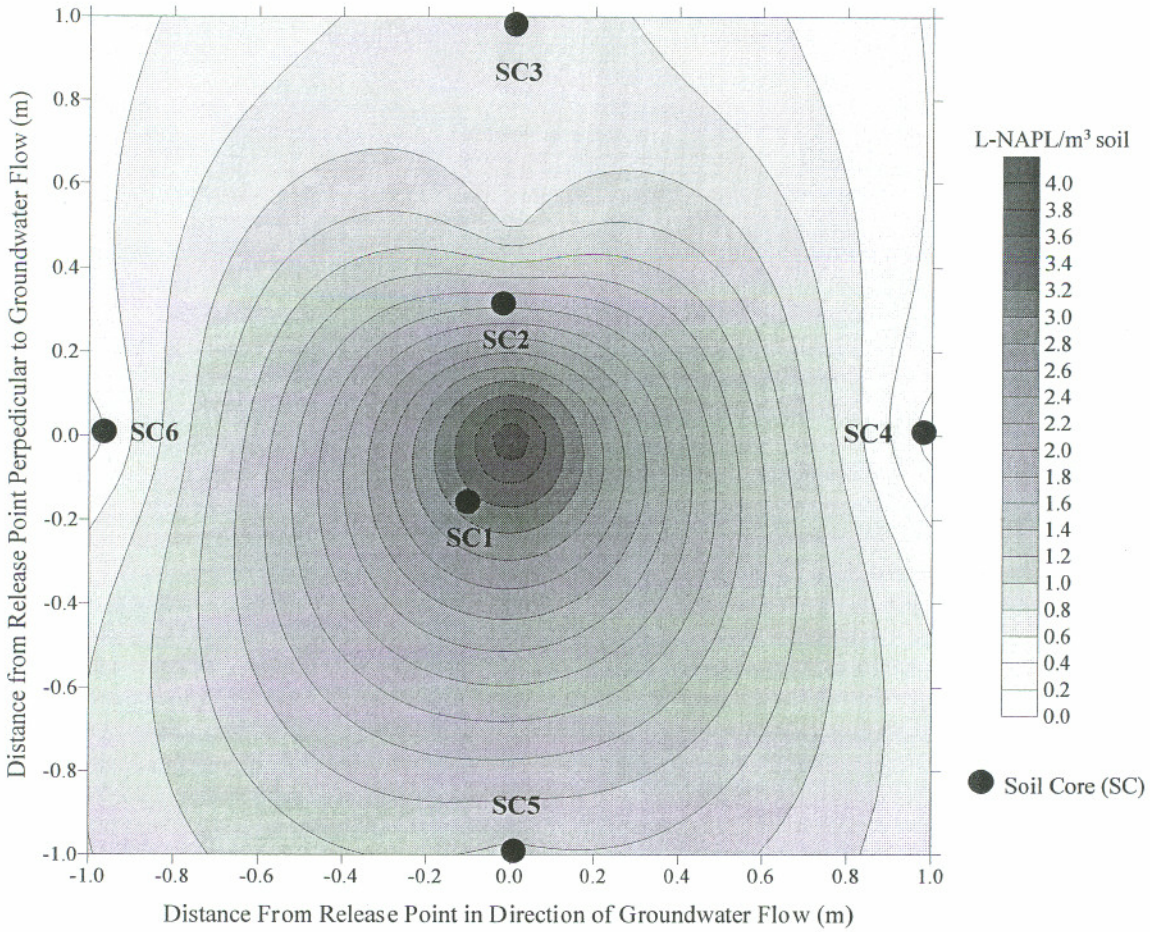

Figure 4.3: Plan View of NAPL Distribution Following the Gasoline Release (Concentration in L-NAPL/m^3 soil based on isooctane distribution and concentration)

Table 4.2: Concentration of NAPL in Vertical Cross-sections Based on Soil Cores (a) in the Direction of Groundwater Flow and (b) Perpendicular to Groundwater Flow. (Concentration in L-NAPL/m^3 soil based on isooctane distribution and concentration)

(a)

	Core and Downgradient Distance from Spill Location (m)		
Depth below datum (m)*	SC6: -1.2 m	SC1: -0.2 m	SC4: 1.2 m
0.4	0	NS	NS
0.6	0	1.49	0.17
0.9	1.24	4.65	0.12
1.1	0	5.27	0
1.4	0	0.87	0
1.6	0	NS	0

NS = No sample collected at this depth
SC = Soil core
*Reflects the midpoint of the sampled interval

(b)

	Core and Cross-gradient Distance from Spill Location (m)			
Depth below datum (m)*	SC5: -1.2 m	SC1: -0.2 m	SC2: 0.5 m	SC3: 1.2 m
0.4	0	NS	3.81	NS
0.6	2.57	1.49	0	0.13
0.9	2.01	4.65	0	2.72
1.1	0	5.27	0	0
1.4	0	0.87	0	0
1.6	0	NS	0.12	0

NS = No sample collected at this depth
SC = soil core
*Reflects the midpoint of the sampled interval

indicator compound for gasoline NAPL presence. It was significant, therefore, that in all of the soil cores MTBE occurred at depths above and occasionally below where little or no isooctane was present. The conceptual model presented in the introduction described the effect of smearing a gasoline spill on MTBE distribution. Due to its solubility in water MTBE is expected to preferentially dissolve from the NAPL and move upward with the rising water table. This was evident in the component distribution data.

4.4.2 Distribution of Aqueous MTBE Concentrations in the Source Zone

Aqueous MTBE concentrations in the source zone were measured at several points in time to observe how the distribution of MTBE changed with water table fluctuations and flow through the source. The January sampling occurred one month after the spill and smear. During that time, the water table had fallen about 0.1 m and was brought back up to 0.5 m bd. January data from a vertical cross-section through the center of the tank and perpendicular to the direction of groundwater flow are shown in Table 4.3. Concentrations near the source were lower than expected, which may have been, in part, a result of the water table rise before sampling. Clean water would have pushed more contaminated water up and possibly somewhat to the side resulting in the higher concentrations in adjacent wells (e.g. MW 5). Based on the NAPL distribution in the soil cores, MW1 and MW2 were expected to show the highest concentrations.

Subsequently, water samples were collected from all monitoring wells within the source zone to view the aqueous distribution of MTBE in and around the source. A plan view of the vertically-averaged May 12, 1999 MTBE concentrations is shown in Figure 4.5. The plan view showed a complex distribution of MTBE in the tank. The highest concentrations were in the vicinity of MW1, MW5, and MW6 with a pocket of higher concentration near MW4. Aqueous concentrations appeared to be unevenly distributed to one side of the tank, indicating either some preferential flow path or a distribution of the NAPL not discovered by soil sampling. The vertical distributions of aqueous MTBE concentrations through the center of the tank in the direction of groundwater flow and perpendicular to groundwater flow are shown in Table 4.4(a) and (b), respectively. Although the highest concentrations were measured at the depths directly impacted by the spill and subsequent smear, MTBE was distributed to all depths in the tank. This was

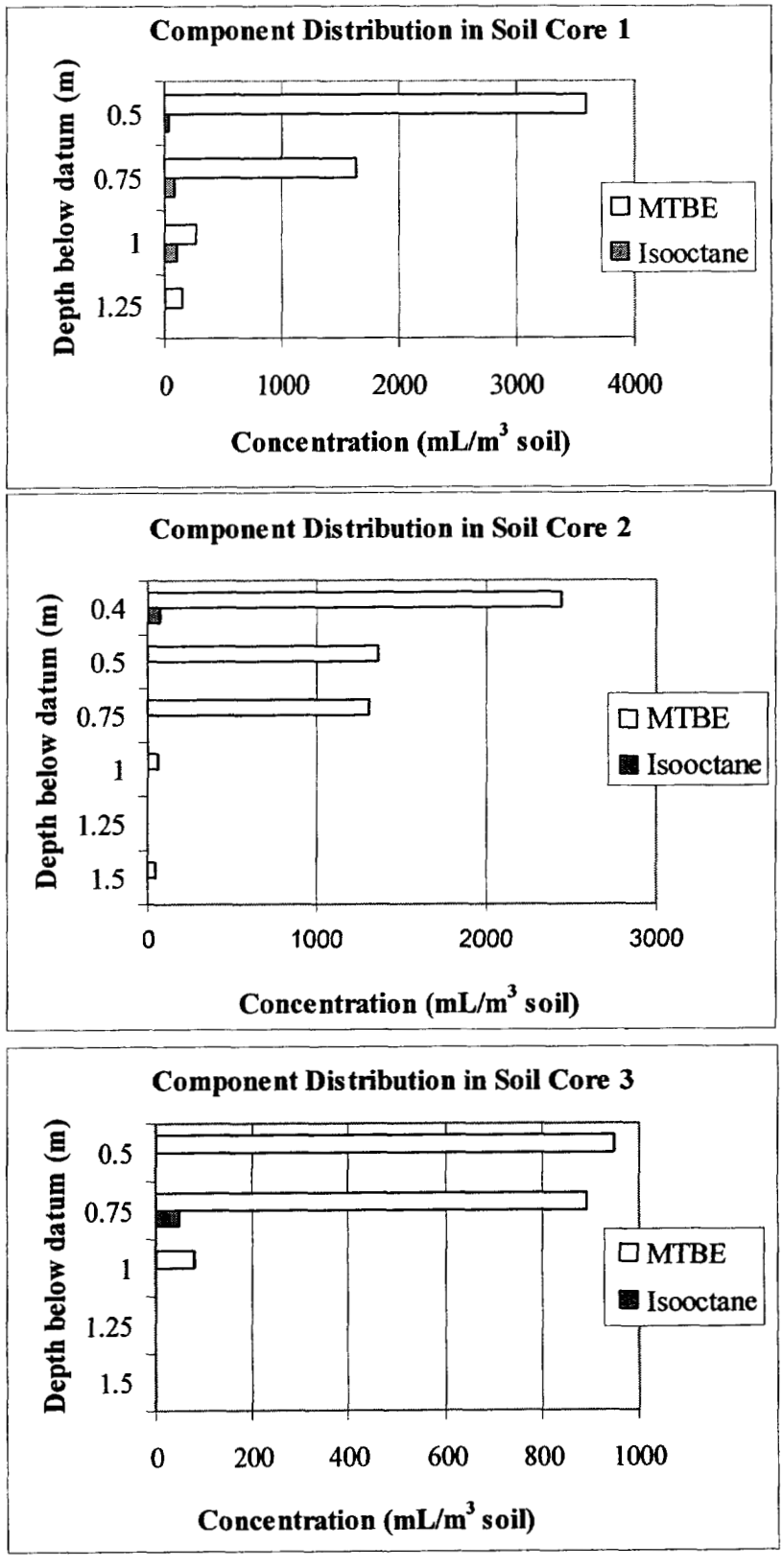

Figure 4.4: Comparison of MTBE and Isooctane Distributions in Soil Cores

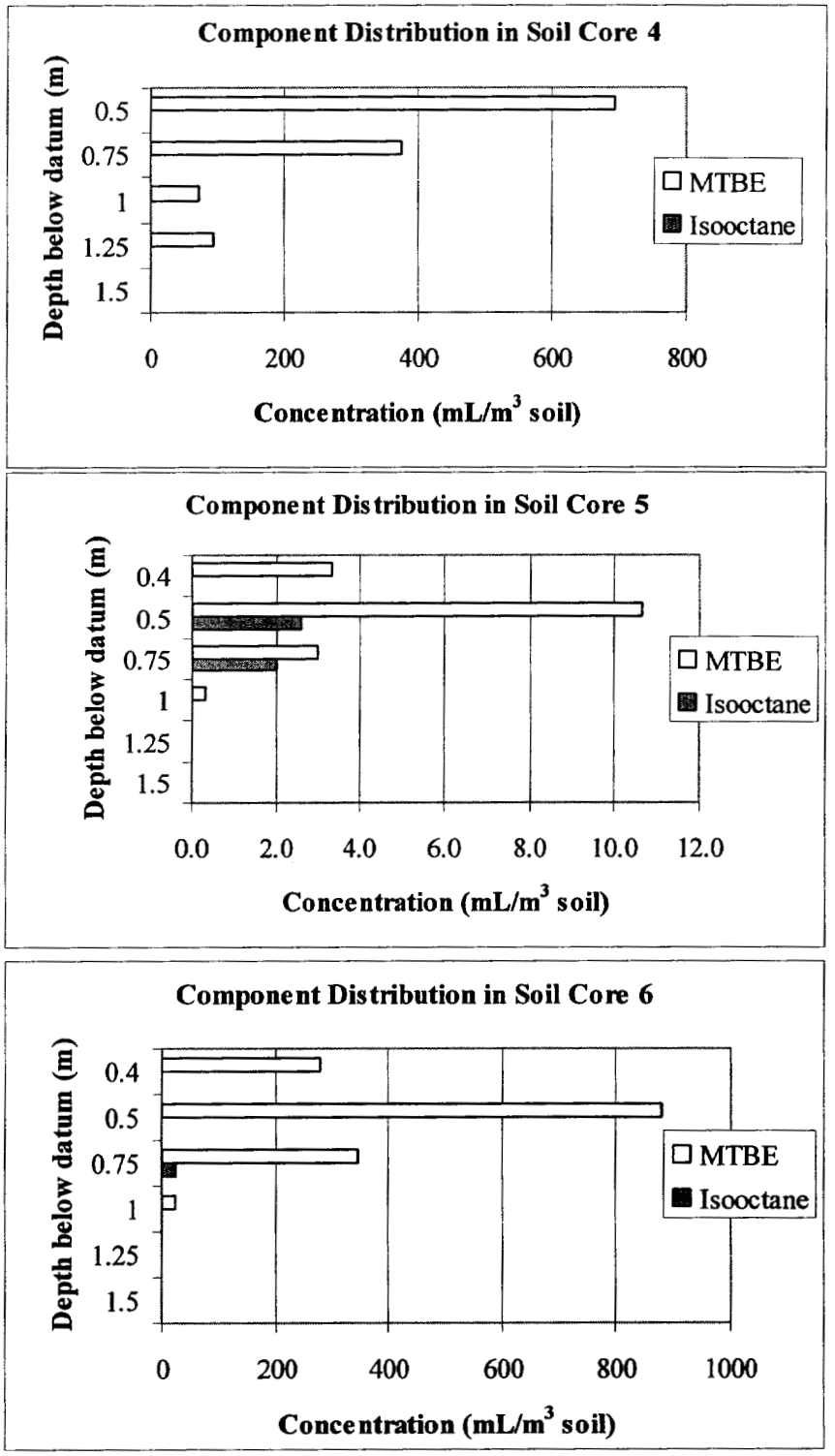

Figure 4.4(continued): Comparison of MTBE and Isooctane Distributions in Soil Cores

Table 4.3: Aqueous MTBE Concentrations (mg/L) in the Vertical Cross-Section Perpendicular to Groundwater Flow – January 1999.

	Well and Cross-gradient Distance from Spill Location (m)			
Depth below datum (m)	MW5: -1.5 m	MW2: -0.5 m	MW1: 0.4 m	MW3: 1.5 m
0.50-0.75	115	3.92	56.6	18.8
0.75-1.00	212	1.91	162	33.6
1.00-1.25	110	0.74	35.9	12.2
1.25-1.50	120	0.59	294	0.35
1.50-1.75	88.1	NS	26.2	0.49
2.00-2.25	67.1	NS	33.9	0.23

NS = No sample collected at this depth
MW = Internal monitoring well

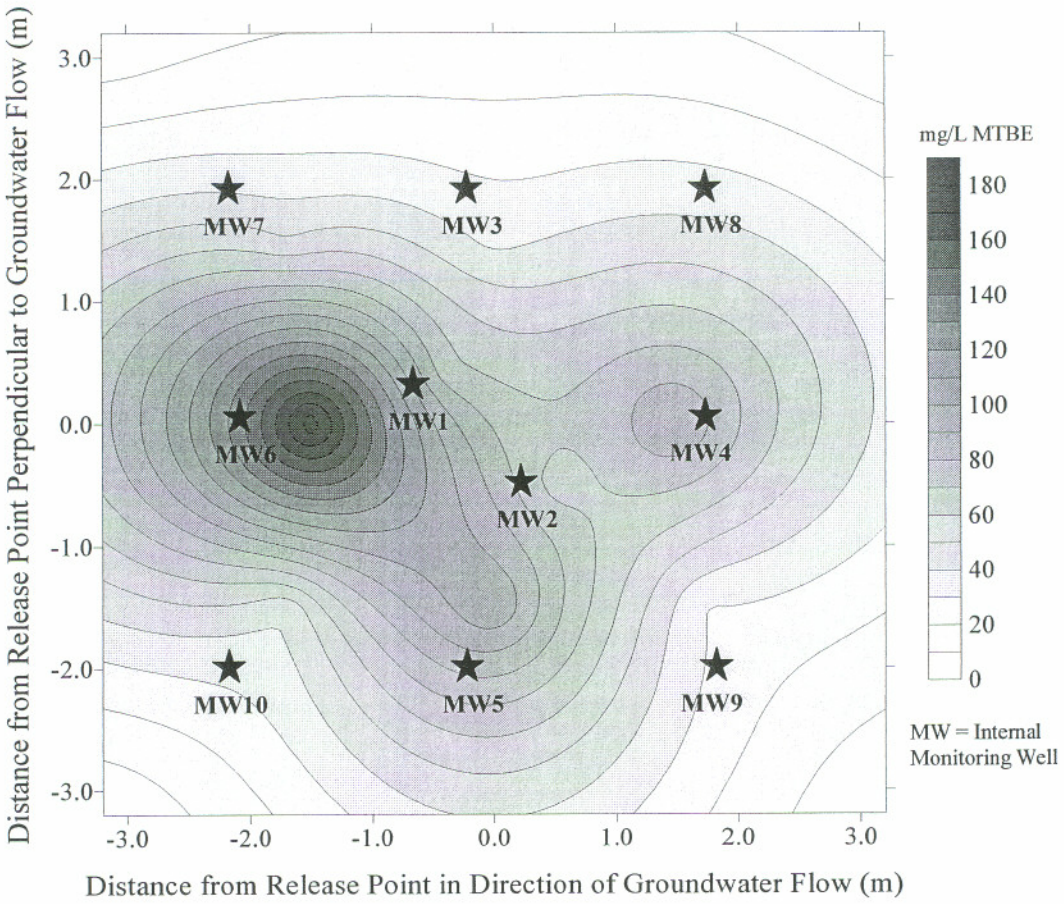

Figure 4.5: Plan View of Vertically-Averaged MTBE Concentrations 5 Months After the Spill

partially due to aqueous diffusion during the 5 months that the source was residing in the aquifer. It should be noted that the measured concentrations of MTBE in locations with high NAPL concentrations, i.e., MW1, MW2, MW5, show concentrations on the order of those observed in the Rixey and Joshi column studies. They are, however, significantly below the MTBE concentration in water that is in equilibrium with the original NAPL composition.

Groundwater flow through the source was initiated to evaluate the response at downgradient wells. Flow was intermittently stopped to collect samples from the interior wells to check the impact of water flow on the source zone. Plan views of aqueous MTBE concentrations in the 0.75-1.00 m bd and 1.00-1.25 m bd intervals during the June 19-20, 1999 sampling event are shown in Figures 4.6 and 4.7, respectively. The figures show different characteristics for the two depths. At the shallower depth, which is within the smear zone, the highest concentrations were near the spill location, though some spreading and preferential flow toward MW5 and MW9 seems to have occurred. Concentrations of MTBE were higher than in previous sampling data. In the 25-cm interval immediately below, high concentrations of MTBE were distributed from the upgradient to the downgradient end of the tank with some curvature to the flow path. This distribution may have reflected the spreading of the gasoline across the water table at the top of this interval. Although the gasoline had been in the tank for several months at this point and been subject to water table fluctuations, the highest MTBE concentrations still exceeded 500 mg/L at both depths. The vertical distribution of aqueous MTBE is shown for the center wells parallel to groundwater flow in Table 4.5. With the exception of MW6, concentrations dropped off quickly with depth during groundwater flow. During groundwater flow, MTBE mass may have been transferred to the lower depths by dispersion or preferential flow pathways, resulting in the low concentrations in water flowing under the source.

The last round of interior well sampling was conducted on June 28 and June 30, 1999 after the last phase of groundwater flow. At this point, water flow had occurred in the tank for a total of 12 days. Plan views the aqueous MTBE distribution in the 0.75-1.00m bd and 1.00-1.25 m bd intervals are shown in Figures 4.8 and 4.9, respectively. After "aging" for 6 months between January and June and a period of water flow through

Table 4.4: Aqueous MTBE Concentrations (mg/L) in the Vertical Cross-Section (a) Parallel to and (b) Perpendicular to Groundwater Flow – May 1999.

(a)

	Well and Cross-gradient Distance from Spill Location (m)			
Depth below datum (m)	MW6: -1.5 m	MW1: -0.5 m	MW2: 0.4 m	MW4: 1.5 m
0.50-0.75	NS	NS	NS	NS
0.75-1.00	467	95.8	126	72.5
1.00-1.25	NS	256	81.7	72.1
1.25-1.50	85.7	49.1	78.0	88.9
1.50-1.75	NS	48.7	49.0	90.7
1.75-2.00	77.0	24.4	37.8	90.9
2.00-2.25	NS	35.5	48.7	92.2
2.25-2.50	121	16.8	38.5	131

NS = No sample collected at this depth

(b)

	Well and Downgradient Distance from Spill Location (m)			
Depth below datum (m)	MW5: -1.5 m	MW2: -0.5 m	MW1: 0.4 m	MW3: 1.5 m
0.50-0.75	NS	NS	NS	NS
0.75-1.00	452	126	95.8	54.4
1.00-1.25	75.1	81.7	256	83.6
1.25-1.50	49.5	78.0	49.1	19.5
1.50-1.75	68.8	49.0	48.7	22.8
1.75-2.00	36.3	37.8	24.4	25.2
2.00-2.25	44.3	48.7	35.5	21.7
2.25-2.50	44.4	38.5	16.8	33.5

NS = No sample collected at this depth

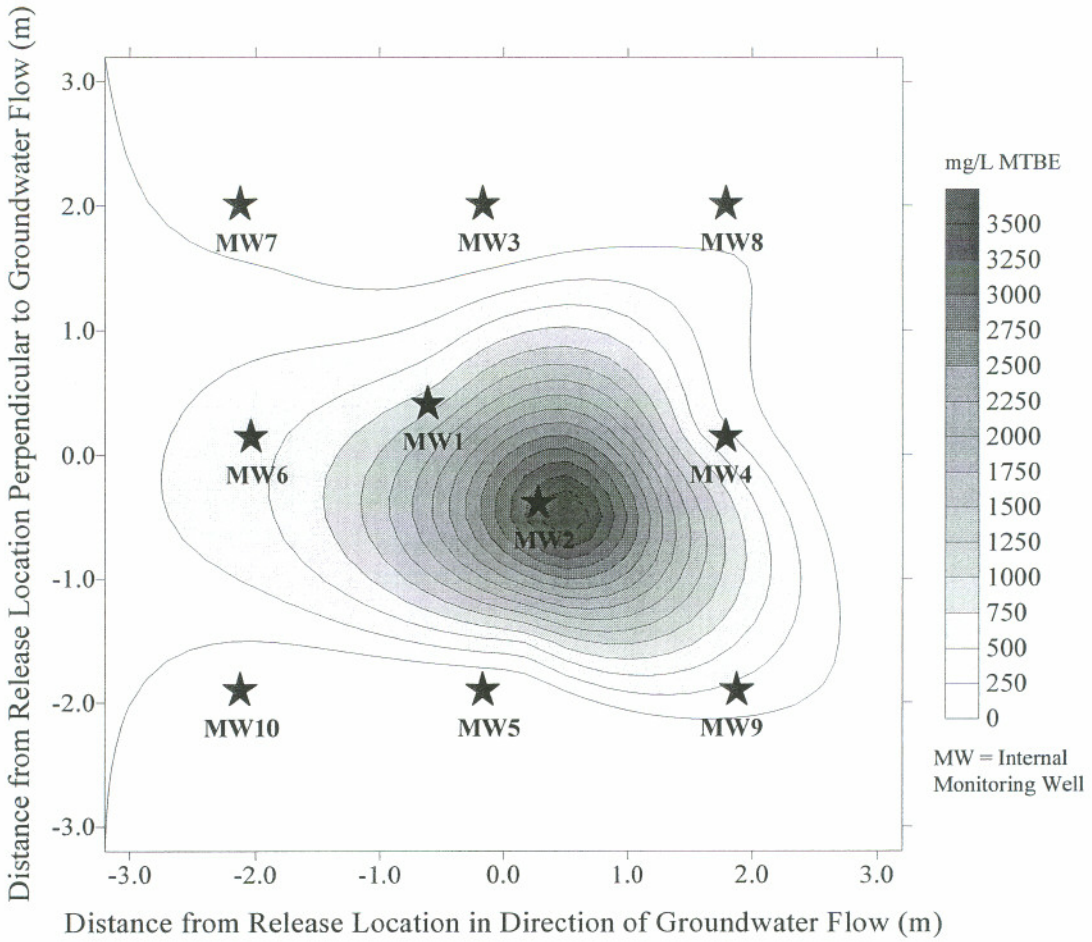

Figure 4.6: Plan View of Aqueous MTBE Concentrations 0.75 – 1.00 m Below Datum After 4 Days of Water Flow (June 19-20, 1999)

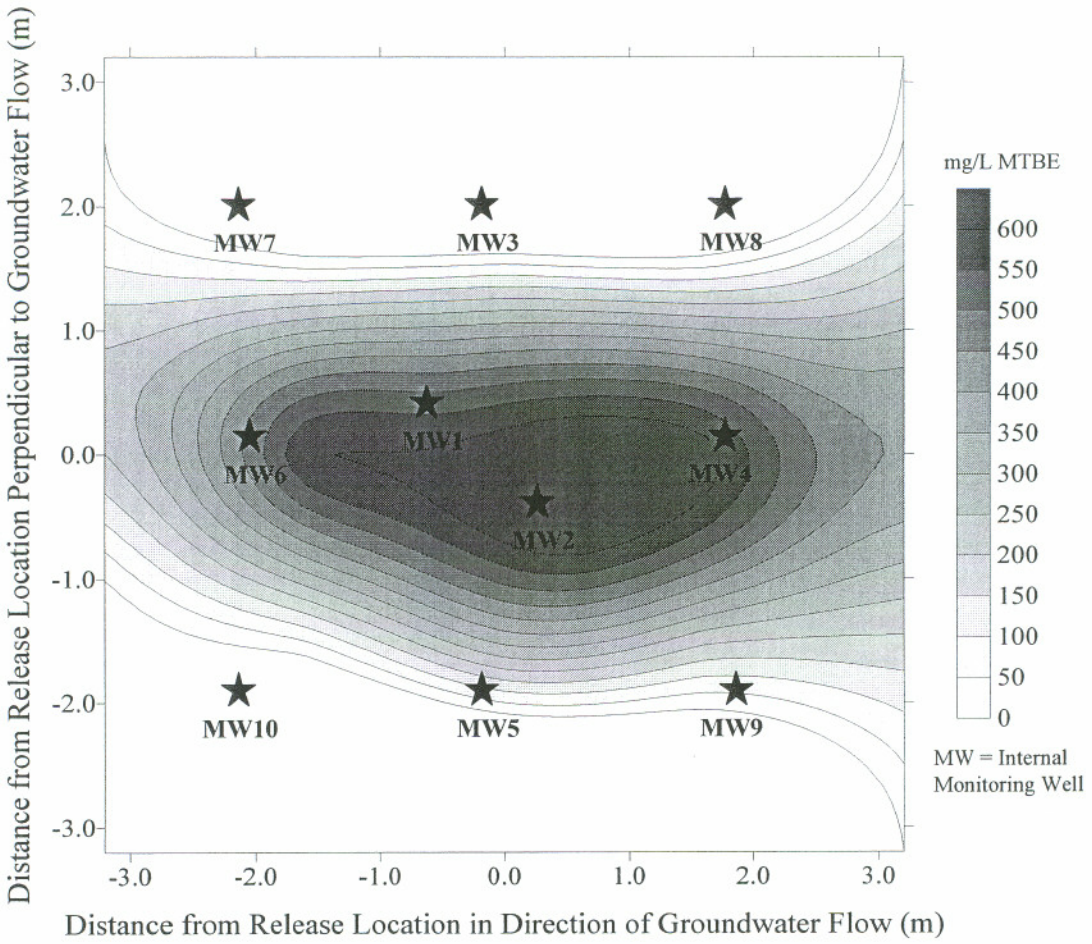

Figure 4.7: Plan View of Aqueous MTBE Concentrations 1.00-1.25 m Below Datum After 4 Days of Water Flow (June 19-20, 1999)

Table 4.5: Aqueous MTBE Concentrations (mg/L) in the Vertical Cross-Section Parallel to Groundwater Flow – June 19, 1999.

	Well and Cross-gradient Distance from Spill Location (m)		
Depth below datum (m)	MW6: -1.5 m	MW2: 0.4 m	MW4: 1.5 m
0.50-0.75	NS	NS	NS
0.75-1.00	NS	NS	NS
1.00-1.25	588	669	622
1.25-1.50	NS	NS	NS
1.50-1.75	336	11.7	3.83
1.75-2.00	NS	NS	NS
2.00-2.25	45.5	2.55	1.42
2.25-2.50	NS	NS	NS

NS = No sample collected at this depth

the source, high concentrations persisted in the center of the aqueous plume. A rapid drop in concentration with depth was observed. The maximum concentrations in the plume immediately below the spill depth were approximately one quarter of those in the smear zone. As in the previous round of sampling, the structure of the plume varied somewhat with depth.The vertical cross-section through the center wells in the direction of groundwater flow is shown in Table 4.6. The drop in concentration with depth was evident in the cross-section as well as the shift toward the downgradient end of the tank. Persistent, relatively low concentrations of MTBE were still present in MW6. The soil core data indicated some residual NAPL was present near this well, resulting in low level contamination at the upgradient end of the tank.

During water flow, uncontaminated water was introduced to that tank and flowed through the source zone. Table 4.7 summarizes the concentrations in the internal monitoring wells before and after water flow. In general, concentrations dropped in the internal monitoring wells; however, the magnitude of the changes depended on well locations. The highest aqueous concentrations observed at the end of the dissolution study correlated well to the residual NAPL footprint. MW4 was slightly downgradient of the residual source zone and reflected the influence of MTBE dissolving from the NAPL. The low concentrations in MW3 and high concentrations in MW9 may suggest a preferential flow pathway that moved contamination toward the left side of the tank, but the data were not conclusive.

Given the changes in aqueous distribution measured in the internal wells, it was of interest to see the corresponding response in the downgradient wells. Concentration versus time profiles for the downgradient wells are shown in Figure 4.10 (a)-(e). The maximum concentrations immediately downgradient of the spill location were an order of magnitude lower than the maximum concentrations measured in the internal wells. Based on the water velocity in the tank and the distance from the center of the tank to the downgradient wells, water from the spill location reached DG 3 and DG4 within the first 10 days of flow, suggesting that some mixing and dilution occurred during travel between the center of the source zone and the downgradient well locations. However, the data are consistent with the aged source concentrations measured by Rixey and Joshi in the one dimensional column studies using the same gasoline.

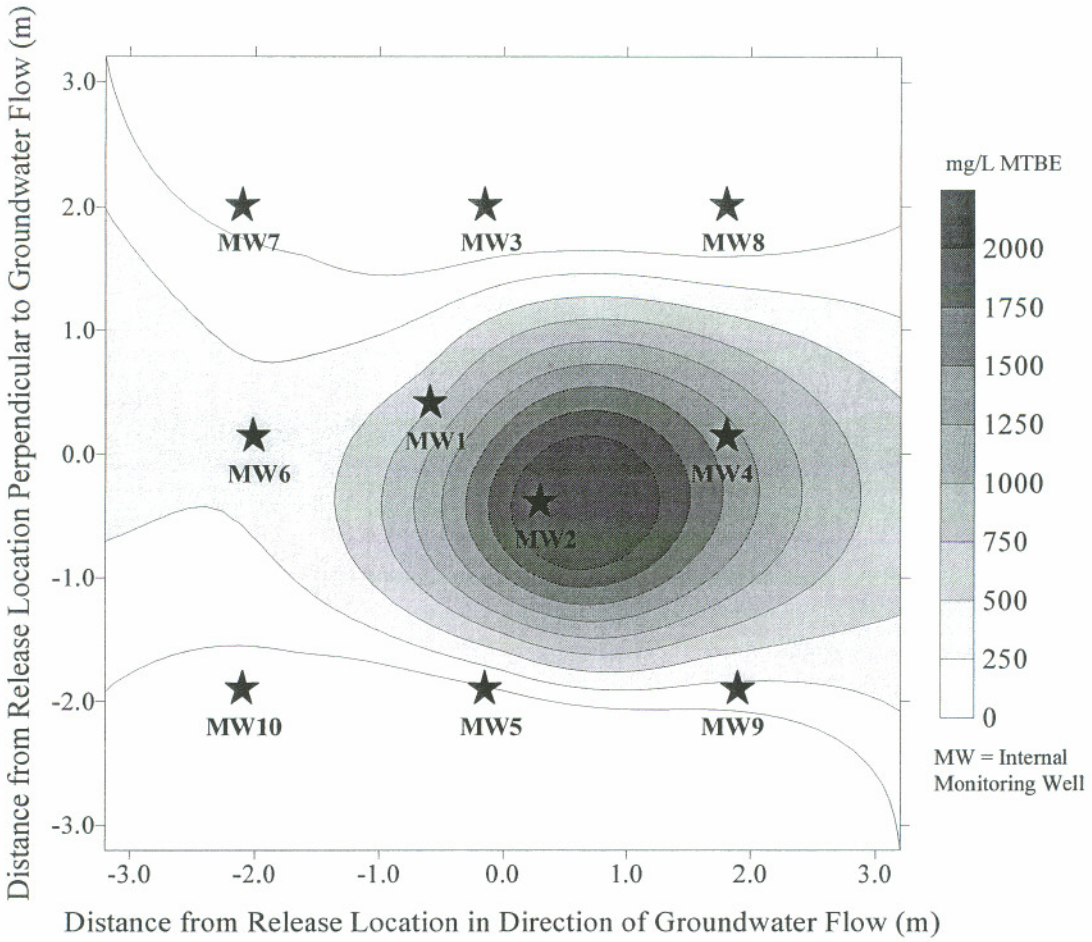

Figure 4.8: Plan View of Aqueous MTBE Concentrations 0.75 – 1.00 m Below Datum After 12 Days of Water Flow (June 28-30, 1999)

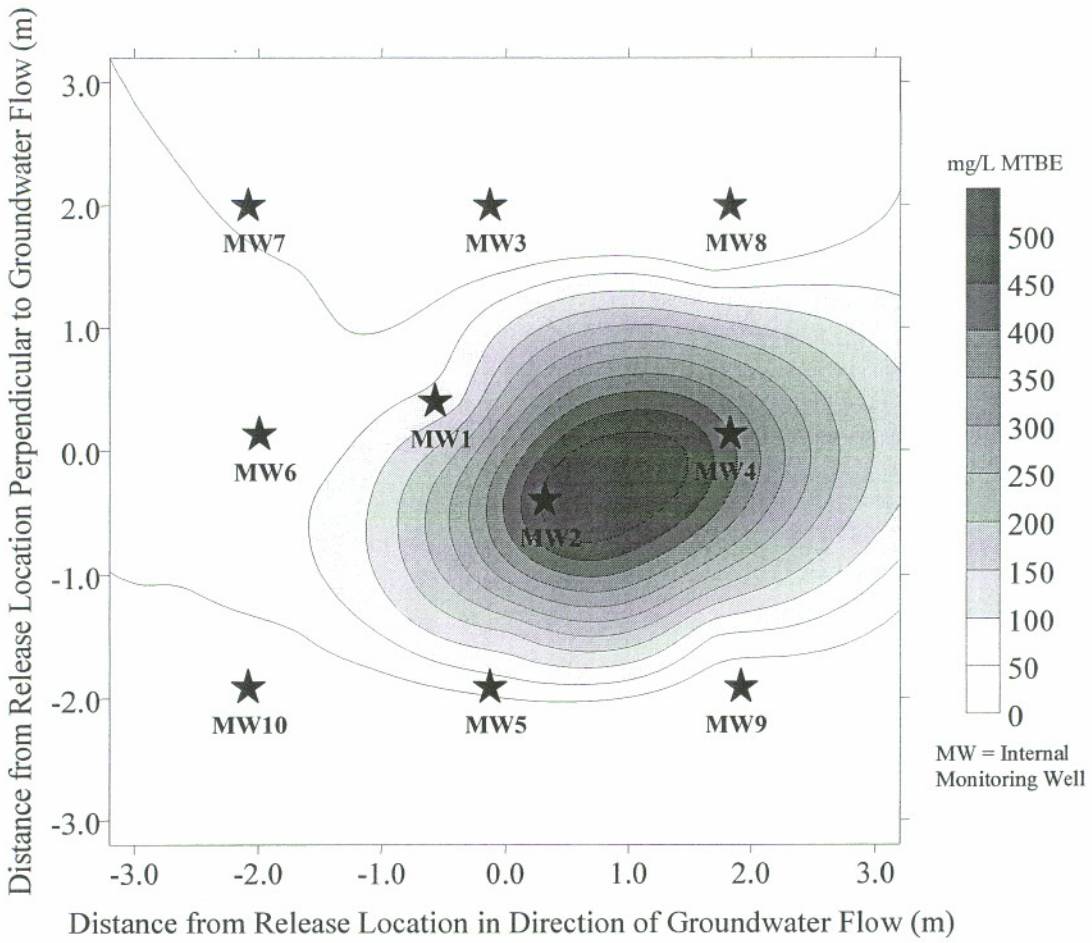

Figure 4.9: Plan View of Aqueous MTBE Concentrations 1.00-1.25 m Below Datum After 12 Days of Water Flow (June 28-30, 1999)

Table 4.6: Aqueous MTBE Concentrations (mg/L) in the Vertical Cross-Section Parallel to Groundwater Flow After 12 Days of Water Flow (June 28, 1999).

	Well and Cross-gradient Distance from Spill Location (m)		
Depth below datum (m)	MW6: -1.5 m	MW2: 0.4 m	MW4: 1.5 m
0.50-0.75	NS	NS	NS
0.75-1.00	NS	NS	NS
1.00-1.25	36.3	548	495
1.25-1.50	NS	NS	NS
1.50-1.75	10.7	0.21	4.5
1.75-2.00	NS	NS	NS
2.00-2.25	20.5	0.15	0.33
2.25-2.50	NS	NS	NS

NS = No sample collected at this depth

Table 4.7: Summary of Aqueous MTBE Concentrations Before and After 12 Days of Water Flow

Internal Monitoring Well	*Pre-Water Flow (mg/L)*	*Post-Water Flow (mg/L)*
MW1	759.8	380.3
MW2	1862.8	1516.1
MW3	35.1	3.5
MW4	655.9	494.6
MW5	464.7	320.8
MW6	505.4	36.3
MW7	7.1	0.66
MW8	55.2	0.59
MW9	31.6	317.7
MW10	91.9	0.23

In summary, the NAPL distribution in the tank was non-uniform, even without the presence of lenses and other forms of macroscale aquifer heterogeneity. The resulting aqueous MTBE plume changed in concentration and distribution with water table fluctuations and flow through the source. Despite 6 months of water table fluctuations followed by 12 days of water flow through the source zone, concentrations at several wells within the residual gasoline source zone remained in the 100-1,000 mg/L range; however, these concentrations were low enough to indicate contact with residual gasoline that was depleted in MTBE. The maximum downgradient concentration measured at the well immediately in line with the spill location was 298 mg/L, considerably lower than the >1000 mg/L that was measured in the internal wells but consistent with column studies performed with the same gasoline. The difference between the internal and downgradient concentrations suggests that concentrations in water flowing through the source do not necessarily reflect the significance of residual NAPL left in the source. Given that the source function could be a critical factor to demonstrating natural attenuation of MTBE, this begs consideration of source characterization and monitoring at field sites.

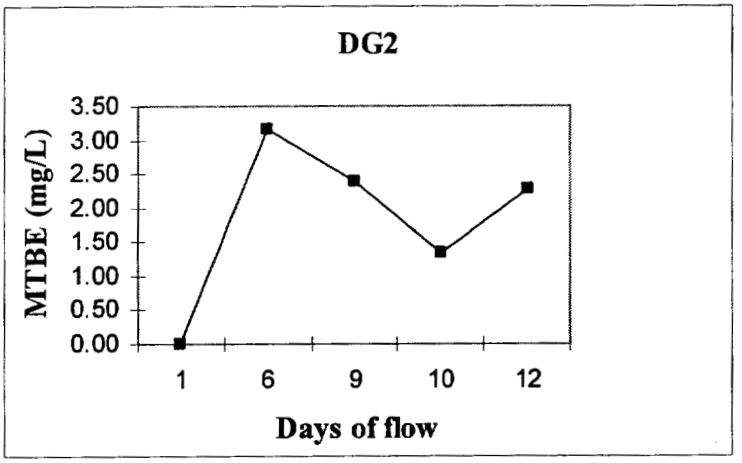

(a)

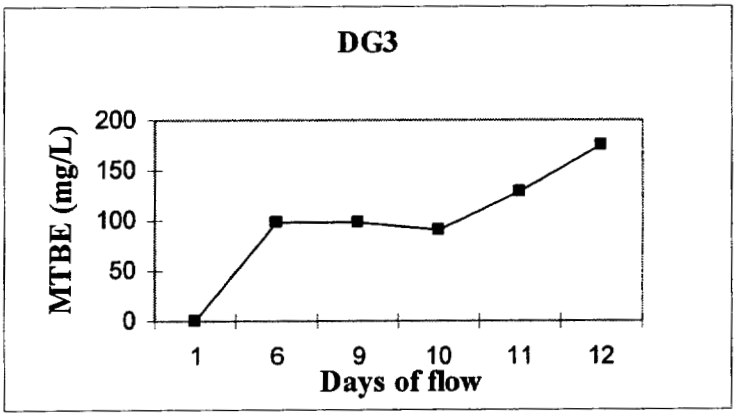

(b)

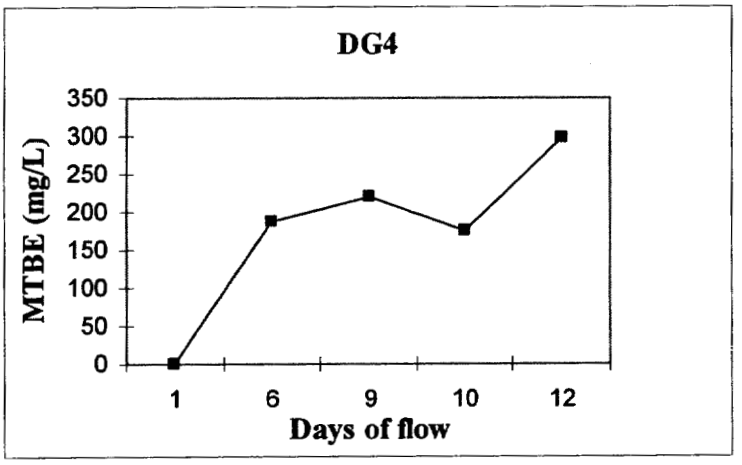

(c)

Figure 4.10: Concentration Versus Time Profiles in the Wells Downgradient from the Smear Zone

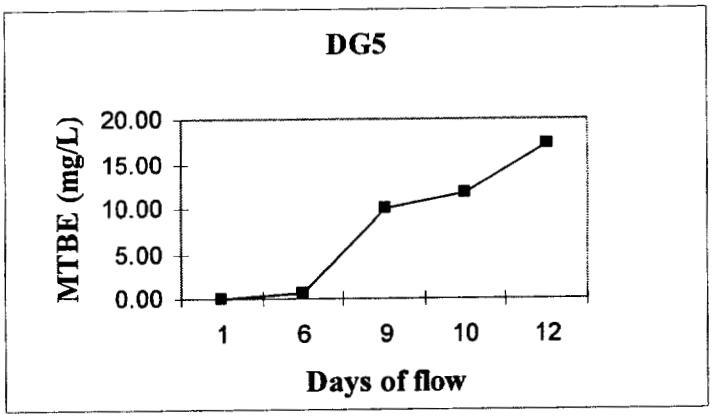

(d)

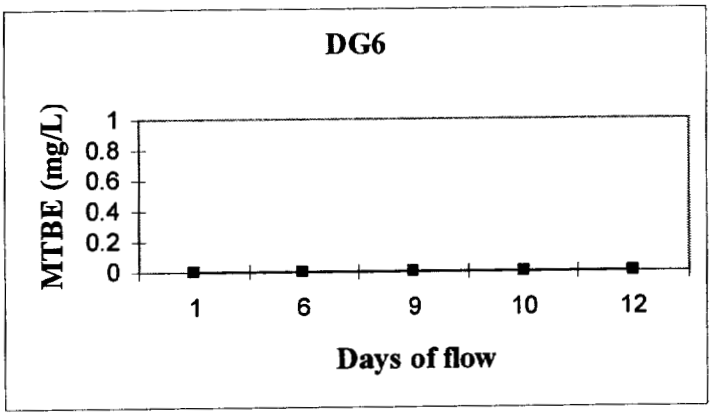

(e)

Figure 4.10 Continued: Concentration Versus Time Profiles in the Wells Downgradient from the Smear Zone

4.5 References

Geller, J.T. and J.R. Hunt. 1993. Mass Transfer From Nonaqueous Phase Organic Liquids in Water-Saturated Porous Media. *Water Resources Research.* 29(4): 833-845.

Hunt, J.R., N. Sitar, and K.S. Udell. 1988. Nonaqueous Phase Liquid Transport and Cleanup 1. Analysis of Mechanisms. *Water Resources Research.* 24(8): 1247-1258.

Johnson, R.L. and J.F. Pankow. 1992. Dissolution of Dense Chlorinated Solvents into Groundwater. 2. Source Functions for Pools of Solvent. *Environmental Science and Technology.* 26: 896-901.

Landmeyer, J.E., F.H. Chapelle, P.M. Bradley, J.F. Pankow, C.D. Church, and P.G. Tratnyek. 1998. Fate of MTBE Relative to Benzene in a Gasoline-Contaminated Aquifer (1993-98). *Ground Water and Monitoring Remediation.* Fall 1998: 93-102.

MacPherson, Jr., J.R. 1991. Gas Phase Diffusion of Organic Compounds in Porous Media: Physical and Numerical Modeling. Thesis (Ph.D.). Department of Environmental Science and Engineering, Oregon Graduate Institute of Science and Technology.

Miller, C.T., M.M. Poirier-McNeill, and A.S. Mayer. 1990. Dissolution of Trapped Nonaqueous Phase Liquids: Mass Transfer Characteristics. *Water Resources Research.* 26(11): 2783-2796.

Montgomery, J.H. 1996. *Groundwater Chemicals Desk Reference.* CRC Press, Inc., New York City, NY.

Nambi, I.M. and S.E. Powers. 2000. NAPL Dissolution in Heterogeneous Systems: An Experimental Investigation in a Simple Heterogeneous System. *Journal of Contaminant Hydrology.* 44: 161-184.

Powers, S.E., C.O. Loureiro, L.M. Abriola, and W.J. Weber, Jr. 1991. Theoretical Study of the Significance of Nonequilibrium Dissolution on Nonaqueous Phase Liquids in Subsurface Systems. *Water Resources Research.* 27(4): 463-477.

Powers, S.E., L.M. Abriola, and W.J. Weber, Jr. 1994. An Experimental Investigation of Nonaqueous Phase Liquid Dissolution in Saturated Subsurface Systems: Transient Mass Transfer Rates. *Water Resources Research.* 30(2): 321-332.

Rixey, W.G. and S. Joshi. 2000. Dissolution of MTBE from a Residually Trapped Gasoline Source. API Soil and Groundwater Research Bulletin. American Petroleum Institute. Washington, D.C.

Sahloul, N.A., M.A. Ioannidis, and I. Chatzis. 2002. Dissolution of Residual Non-Aqueous Phase Liquids in Porous Media: Pore-Scale Mechanisms and Mass Transfer Rates. *Advances in Water Resources.* 25: 33-49.

Soerens, T.S., D.A. Sabatini, and J.H. Harwell. 1998. Effects of Flow Bypassing and Nonuniform NAPL Distribution on the Mass Transfer Characteristics of NAPL Dissolution. *Water Resources Research.* 34(7): 1657-1673.

USEPA. 2000. Office of Research and Development. *Natural Attenuation of MTBE in the Subsurface under Methanogenic Conditions*, Research Report, EPA 600/R-00/006. Cincinnati, Ohio: U.S. E.P.A.

Zhu, J. and J.F. Sykes. 2000. The Influence of NAPL Dissolution Characteristics on Field-Scale Contaminant Transport in Subsurface. *Journal of Contaminant Hydrology.* 41: 133-154.

CHAPTER 5

NUMERICAL ANALYSIS OF MONITORED NATURAL ATTENUATION OF MTBE USING TRADITIONAL METHODS UNDER COMMON FIELD CONSTRAINTS

5.1 Introduction

Monitored natural attenuation (MNA) requires an accurate conceptual model for each site where it is applied. The goal of this chapter is to assess how uncertainties in site conceptual models can impact MNA estimates for MTBE. To develop the conceptual model used here, several experiments were conducted to examine components of contaminant behavior that influence natural attenuation and the importance of collecting the data that can illuminate that behavior. The natural gradient tracer test discussed in Chapter 2 showed the effects of hydrogeology on plume structure and how dominant flow paths or site features can cause deviations from the macroscopic direction of groundwater flow based on the hydraulic gradient or overall plume behavior. The dissolution experiment discussed in Chapter 4, although short in duration, illustrated the complexity of NAPL distribution and changes in aqueous concentration with water table fluctuations and flow through the source zone given a gasoline source of known volume and composition. The numerical modeling discussed in Chapter 3 provided insight on the effects of increasingly complex heterogeneity and the role of the source function using known initial conditions and an extensive monitoring network. At most field sites, however, these data are not available. The hydrogeology is not known a priori and is not ascertained using multiple long-term tracer tests. The release date and initial NAPL volume and composition are often not known and the source function is complex and largely unknown. At those sites, limited field measurements are often all that is available to develop the conceptual model. In light of these realities, the conceptual model

discussed here was developed as if natural attenuation were being assessed using traditional techniques and field constraints. The adequacy of the approach was evaluated the for MTBE as well as benzene, a representative BTEX compound.

The data used in this evaluation were taken from a modeling scenario with a high groundwater velocity, a simple source function compared to what would be expected at a field site, and known degradation characteristics. Comparing the level of effort necessary to demonstrate natural attenuation of benzene to that for MTBE *using only information that would be available at a real-world field site* yielded important considerations for demonstrations of natural attenuation for MTBE. Critical factors include tracer compounds, the source function, hydrogeology, and sampling networks. Each of these will be discussed below.

The site conditions reflected a release of gasoline containing MTBE, which resulted in benzene and MTBE plumes. Oxygen and sulfate were present as electron acceptors at concentrations of 4 mg/L and 600 mg/L, respectively, upgradient of the source zone; however, both have been depleted in the source zone. The source function was assumed to be unknown. Hydraulic conductivity data were limited to locations where monitoring wells had been placed and could, therefore, have been used for slug tests. The monitoring network consisted of either a longitudinal transect with three wells plus a source well or four fences of monitoring wells across the plume perpendicular to groundwater flow. The transect wells and fences were placed at the same distances from the source (5 m, 605 m, and 1005 m) as shown in Figure 5.1. All wells sampled a 2-m vertical interval. The fences consisted of wells placed at a 15-m spacing, although data were evaluated for both 15-m and 30-m intervals.

5.2 Evaluation Methods

Attenuation rates based on the longitudinal transect data were calculated by performing a linear regression on the change in concentrations with residence time. Data were corrected for the effects of dispersion and flow patterns using a conservative tracer as suggested by Wiedemeier et al. (1997). The Case 4 results were employed as the "ideal" tracer; that is, they reflected the same initial concentration, source function, retardation factor, and flow behavior as the corresponding contaminant of concern

without degradation. These data were included to determine the necessity of having tracer data to make the assessment of natural attenuation. Variations in groundwater velocity were accounted for by calculating the residence time using high, average, and low average velocities of 1.83 m/d, 1.51 m/d, and 1.20 m/d based on the variation in hydraulic conductivity "measured" at the fence well locations. Contaminant specific velocities were calculated using retardation factors of 1.5 and 1.05 for benzene and MTBE, respectively. These R values assumed organic-carbon-based partition coefficients (K_{oc}s) of 80 and 11 for benzene and MTBE (Squillace et al. 1997), respectively, and a soil organic fraction of 0.11%.

Mass flux calculations using fence data have the benefit of incorporating the full width of the plume, thus potentially removing the effects of non-uniform flow (Borden et al., 1997). At sites with complex heterogeneity, however, well spacing may be critical to the quality of the calculated attenuation rates (Barker et al. 2000). Both 15-m and 30-m well intervals were evaluated. In addition, fluxes based on uniform velocities and local velocities calculated from measured hydraulic conductivity data were both used to calculate attenuation rates. The common approach of assessing mass/time differences between fences is subject to the effects of dispersion, the source function, and inadequate well spacing. Because distance away from the source reflected residence time in the system, the mass flux data were evaluated in a similar fashion to the transect data. This approach was an attempt to minimize the complications with fence data and improve on the quality of the transect attenuation rates. Attenuation rates were calculated from fluxes through the source fence and the three downgradient fences after 3,060 days. Residence times were calculated using high, average, and low contaminant velocities based on the average and $\pm$ 1σ hydraulic conductivity values measured from the fence wells. The flux at each fence was normalized to the source fence flux (F/F_0) and plotted against residence time to obtain "tracer" and "contaminant" data. The contaminant data were corrected for the tracer values and a linear regression was performed to obtain first-order attenuation rates, presumably due only to degradation since tracer accounted for all other attenuation processes.

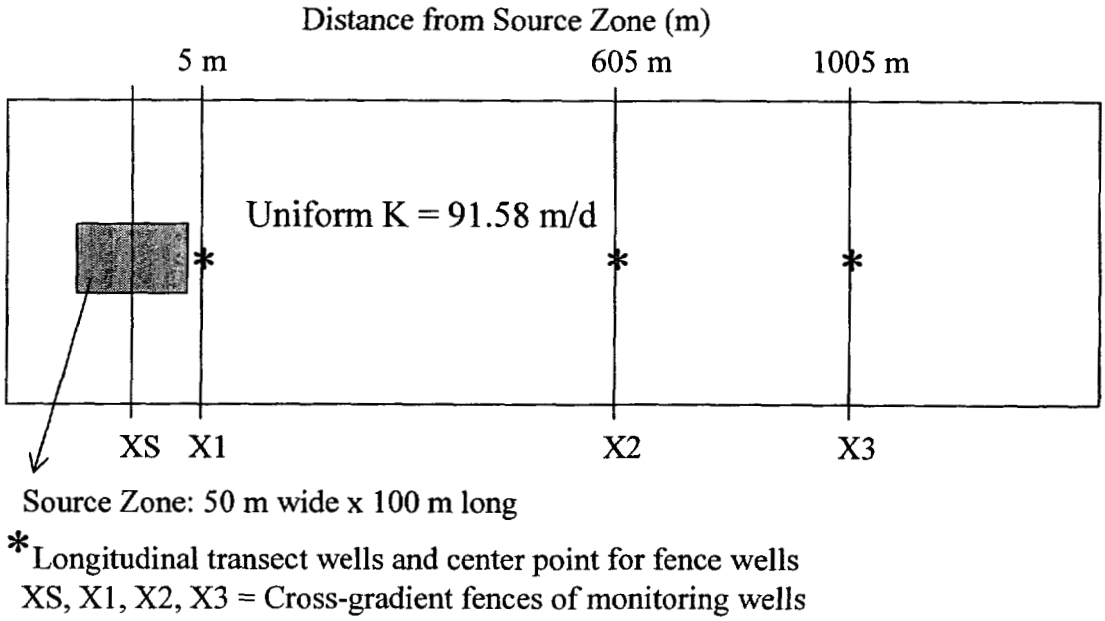

Figure 5.1: Schematic of Source Placement, Longitudinal Transect Wells, and Fences Used in the Numerical Analysis

5.3 Results and Discussion

The data in Figures 5.2 (a)-(c) and 5.3 (a)-(c) for the longitudinal transect show the ideal tracer attenuation rates, the contaminant attenuation rate before adjustment with the tracer values, and the contaminant attenuation rates after the ideal tracer data were used to correct for non-degrading mechanisms. Although the ideal MTBE tracer shows more attenuation due to non-degrading mechanisms, there was no obvious change in behavior between the tracer case and the degradation case. The change was readily apparent for benzene. Correction for the ideal tracer behavior yields degradation behavior for both compounds. Table 5.1 presents the apparent attenuation rates and 95% confidence levels for benzene and MTBE. While the benzene rates were significantly non-zero, the MTBE rates range from low negative values due to degradation to low positive values at the 95 percent confidence level; therefore, degradation could not be confirmed for MTBE based on the transect data with only three wells. The uncertainty decreases with increasing number of samples and increases with more scatter about the regression line. Assuming that additional data points would maintain approximately the same standard deviation from the regression line, the uncertainty in the apparent attenuation rates will decrease with additional wells. It is possible that additional wells could confirm degradation of MTBE.

Attenuation rates from a single longitudinal transect may not reflect the attenuation rate of the entire plume since transect data are sensitive to changes in the local hydraulic gradient (USEPA 2000). Fences may provide more representative attenuation rates when they encompass the full width of the plume. Figures 5.4 (a)-(c) through 5.7 (a)-(c) show plots analogous to those of the transect data for benzene attenuation rates calculated for 15-m and 30-m spacing with uniform velocities and 15-m and 30-m spacing with local velocities. Similar plots showing attenuation rates for the MTBE data are shown in Figures 5.8 (a)-(c) through 5.11 (a)-(c). The benzene plots show attenuation and specifically degradation without any normalization by the ideal tracer. The MTBE showed a rise in concentration with increasing distance from the source zone in the degradation case due to the exponentially decaying source function. Attenuation due to degradation in this case could only be extracted from the MTBE data once they were corrected by the corresponding ideal tracer data. In addition, the benzene

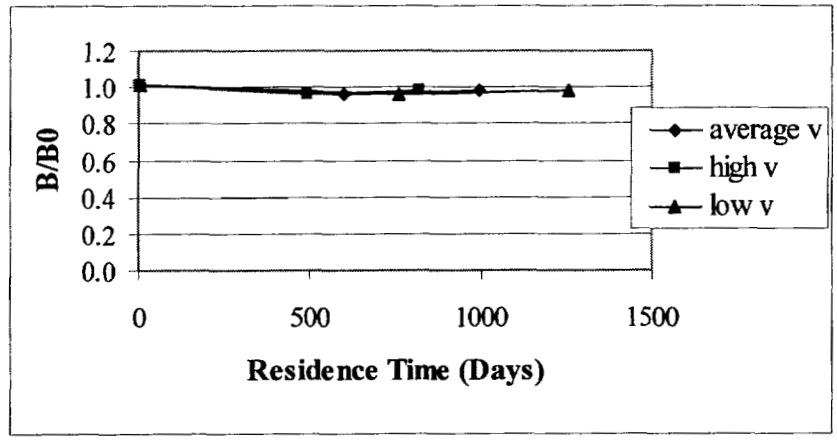

(a)

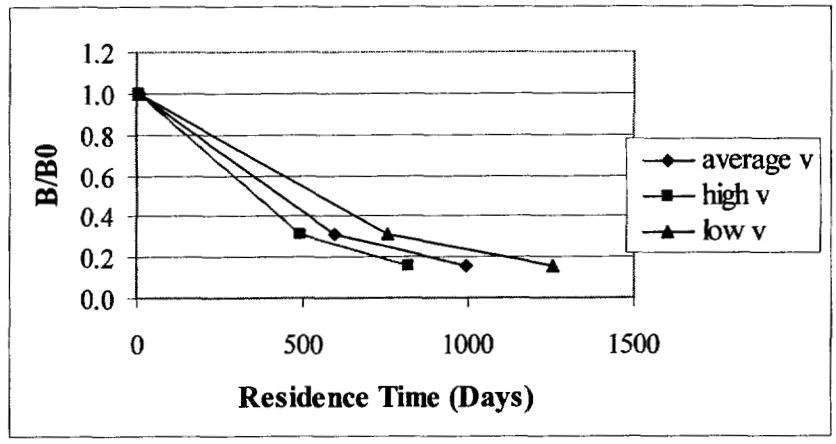

(b)

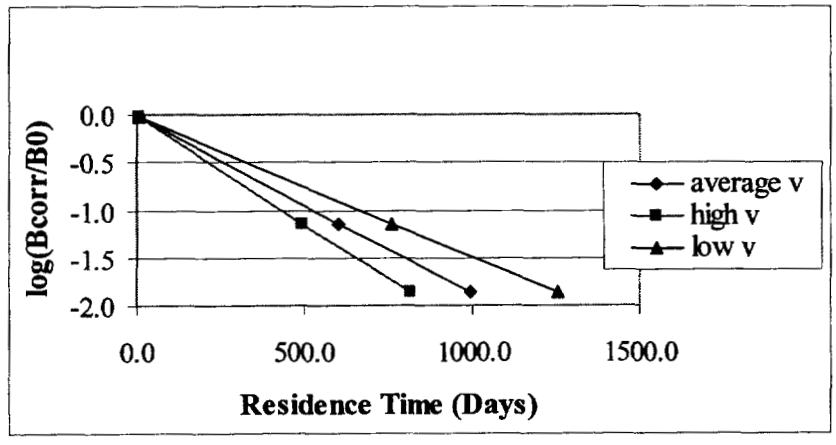

(c)

Figure 5.2: Contaminant Profiles for (a) Ideal Benzene Tracer (No Degradation), (b) Uncorrected Benzene (Degradation), and (c) Tracer-Corrected Benzene (Degradation)

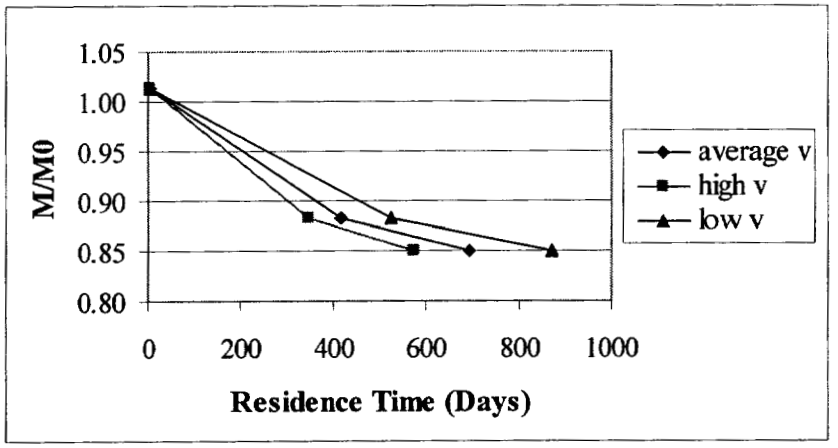

(a)

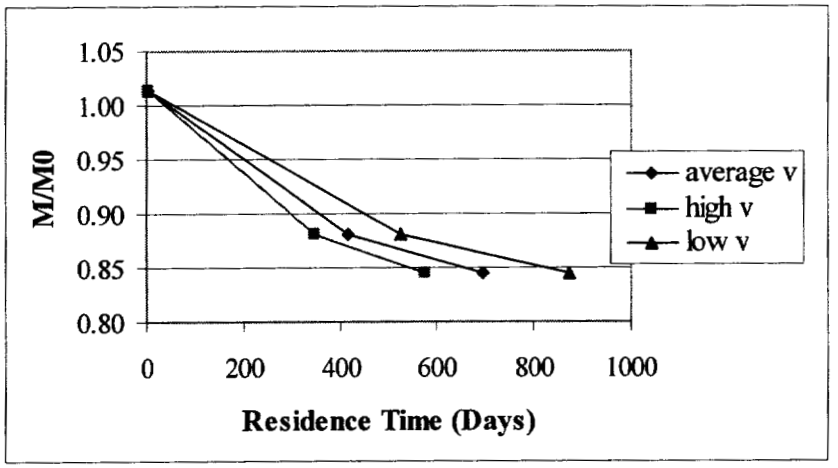

(b)

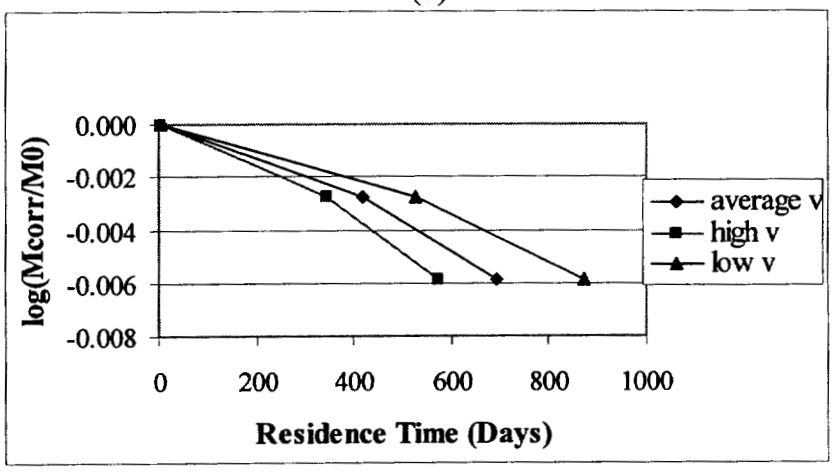

(c)

Figure 5.3: Contaminant Profiles for (a) Ideal MTBE Tracer (No Degradation), (b) Uncorrected MTBE (Degradation), and (c) Tracer-Corrected MTBE (Degradation)

Table 5.1: Apparent Attenuation Rates and Confidence Intervals from Transect Benzene and MTBE Measurements (a) Uncorrected and (b) Corrected with Ideal Tracer

(a)

	Benzene			MTBE		
	Upper 95%	Apparent K (d^{-1})	Lower 95%	Upper 95%	Apparent K (d^{-1})	Lower 95%
High V	-0.0029	-0.0023	-0.0017	-0.0009	-0.0003	0.0003
Average V	-0.0024	-0.0019	-0.0014	-0.0008	-0.0003	0.0003
Low V	-0.0019	-0.0015	-0.0011	-0.0006	-0.0002	0.0002

(b)

	Benzene			MTBE		
	Upper 95%	Apparent K (d^{-1})	Lower 95%	Upper 95%	Apparent K (d^{-1})	Lower 95%
High V	-0.0026	-0.0023	-0.002	-2E-5	-1E-5	5E-6
Average V	-0.0021	-0.0019	-0.0016	-2E-5	-8E-6	5E-6
Low V	-0.0018	-0.0015	-0.0012	-2E-5	-6E-6	1E-5

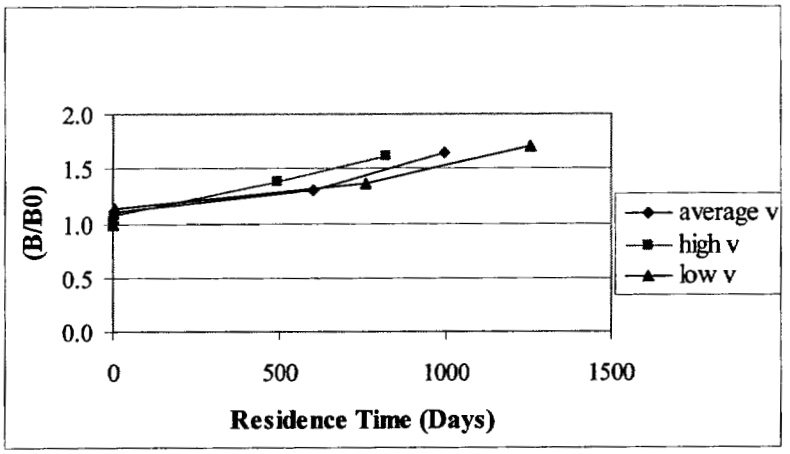

(a)

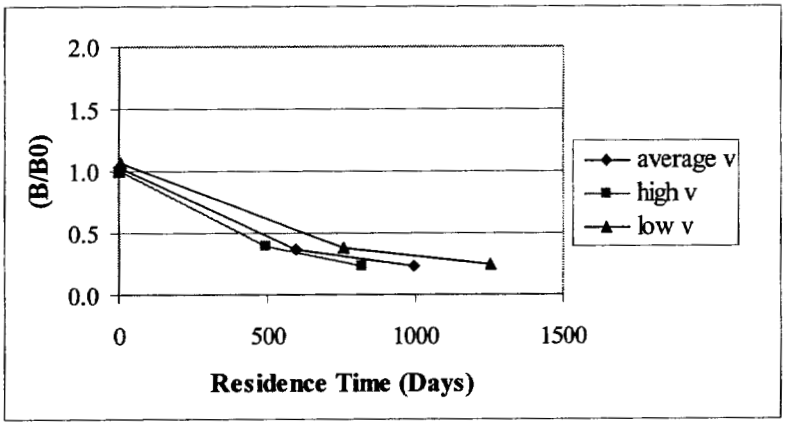

(b)

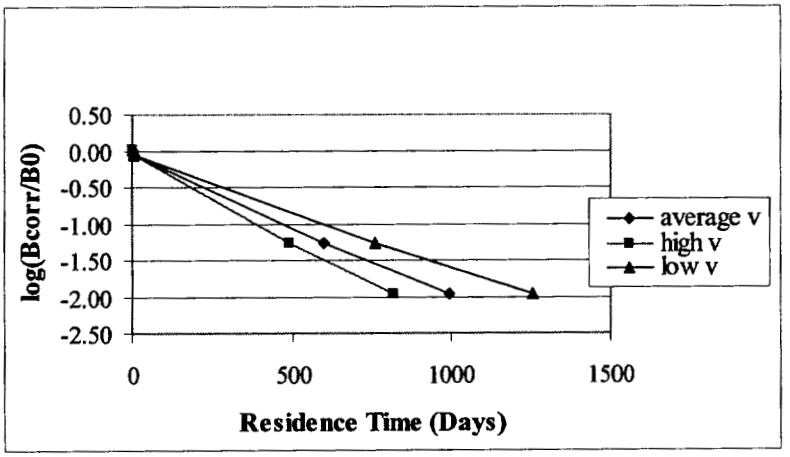

(c)

Figure 5.4: Contaminant Profiles for (a) Ideal Benzene Tracer (No Degradation), (b) Uncorrected Benzene (Degradation), and (c) Tracer-Corrected Benzene (Degradation) Using Fences with 15-m Spacing and Uniform Velocities

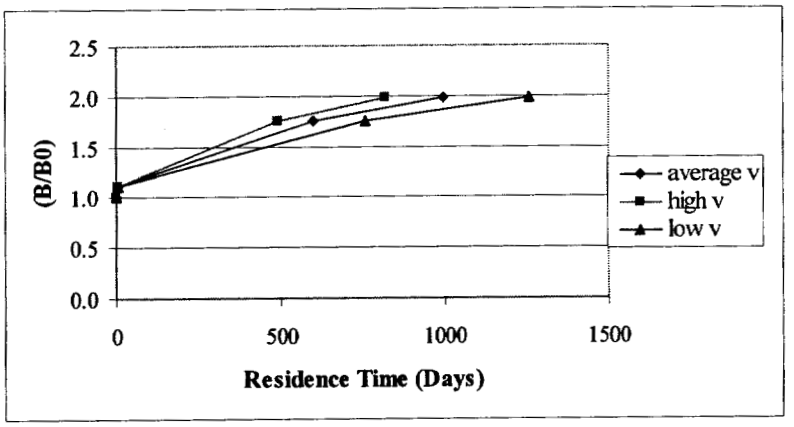

(a)

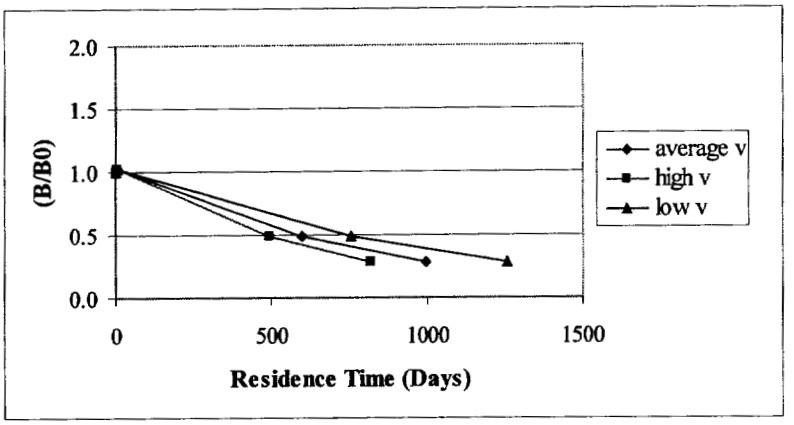

(b)

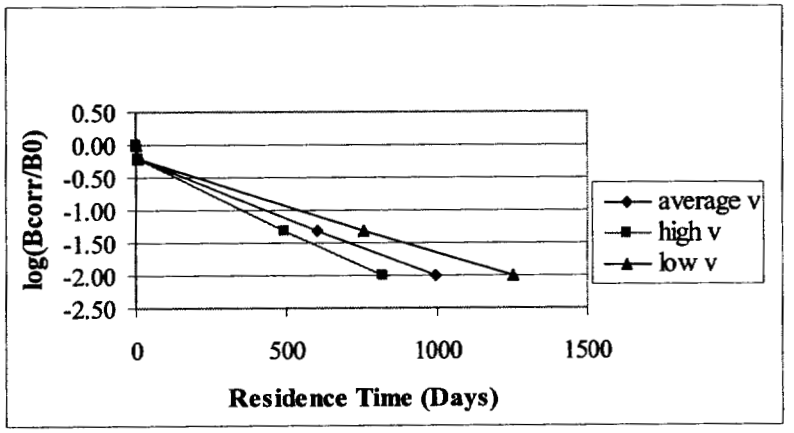

(c)

Figure 5.5: Contaminant Profiles for (a) Ideal Benzene Tracer (No Degradation), (b) Uncorrected Benzene (Degradation), and (c) Tracer-Corrected Benzene (Degradation) Using Fences with 30-m Spacing and Uniform Velocities

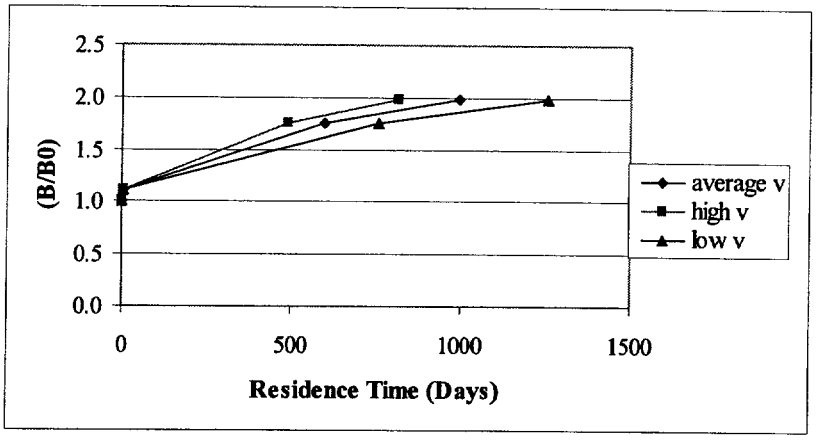

(a)

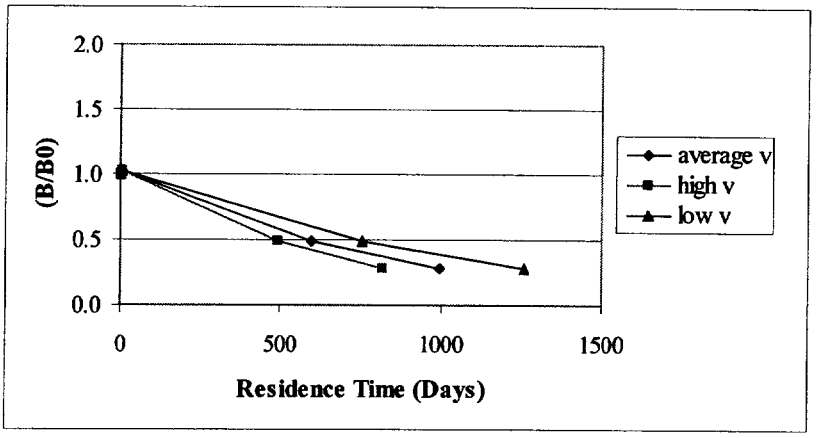

(b)

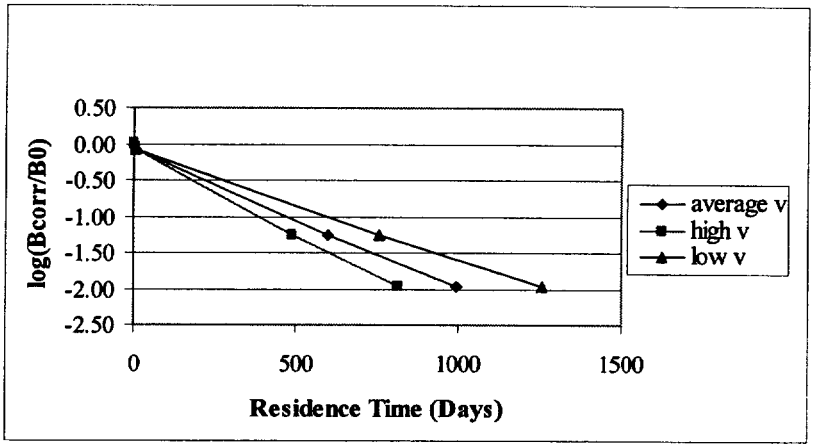

(c)

Figure 5.6: Contaminant Profiles for (a) Ideal Benzene Tracer (No Degradation), (b) Uncorrected Benzene (Degradation), and (c) Tracer-Corrected Benzene (Degradation) Using Fences with 15-m Spacing and Local Velocities

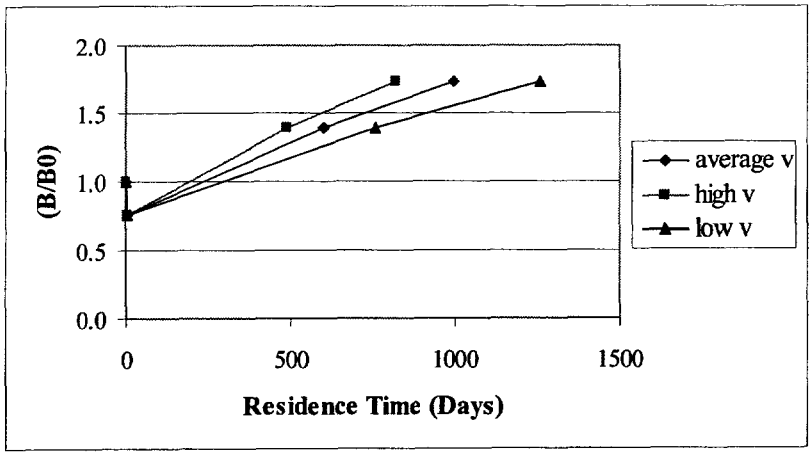

(a)

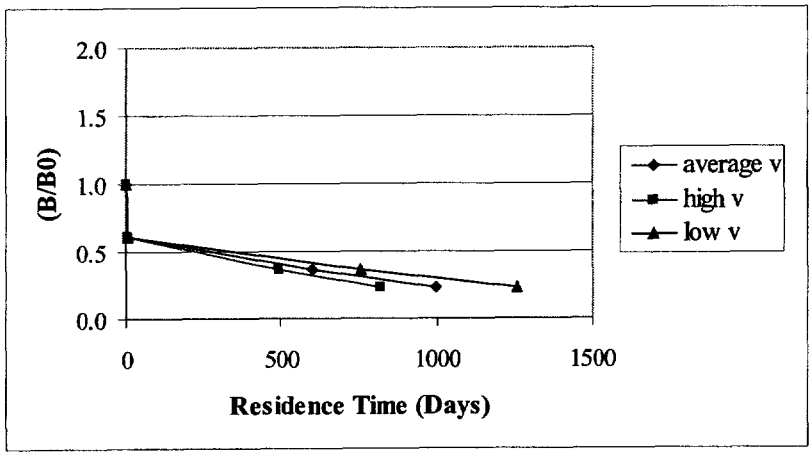

(b)

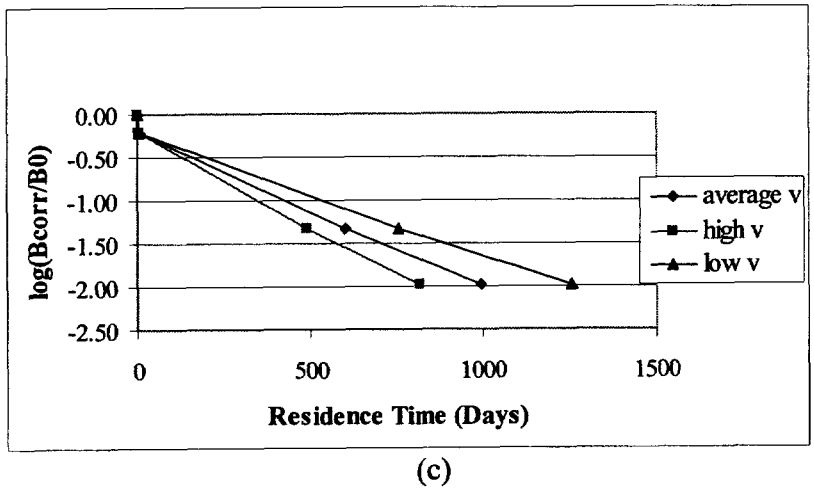

(c)

Figure 5.7: Contaminant Profiles for (a) Ideal Benzene Tracer (No Degradation), (b) Uncorrected Benzene (Degradation), and (c) Tracer-Corrected Benzene (Degradation) Using Fences with 30-m Spacing and Local Velocities

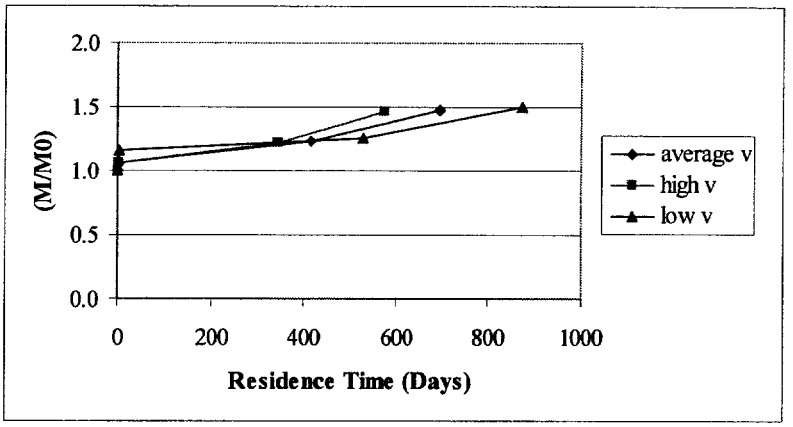

(a)

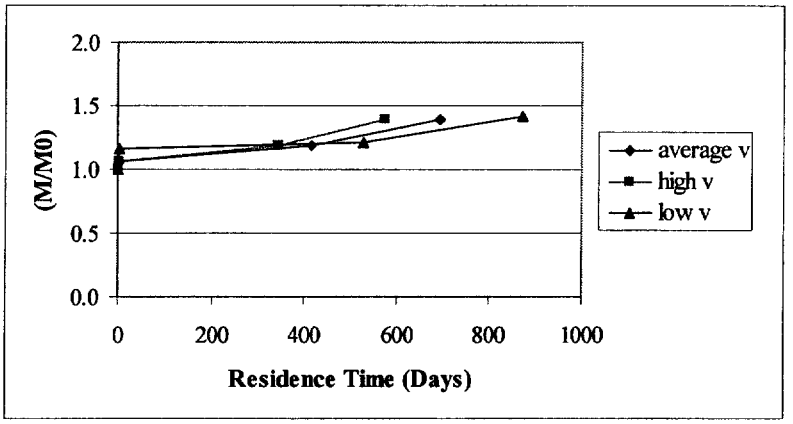

(b)

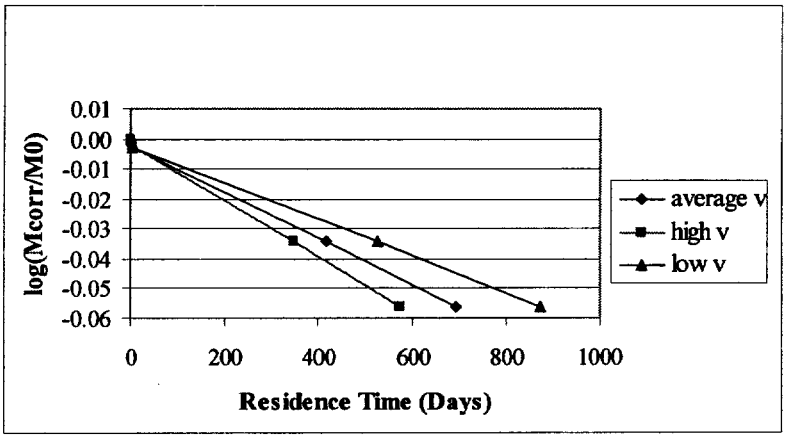

(c)

Figure 5.8: Contaminant Profiles for (a) Ideal MTBE Tracer (No Degradation), (b) Uncorrected MTBE (Degradation), and (c) Tracer-Corrected MTBE (Degradation) Using Fences with 15-m Spacing and Uniform Velocities

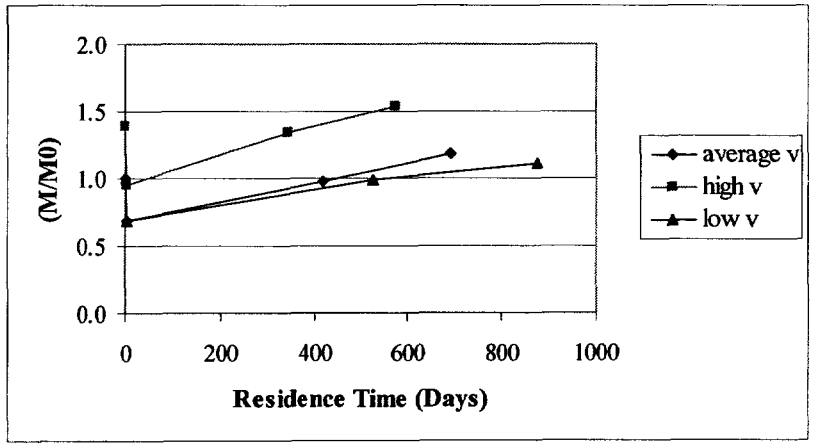

(a)

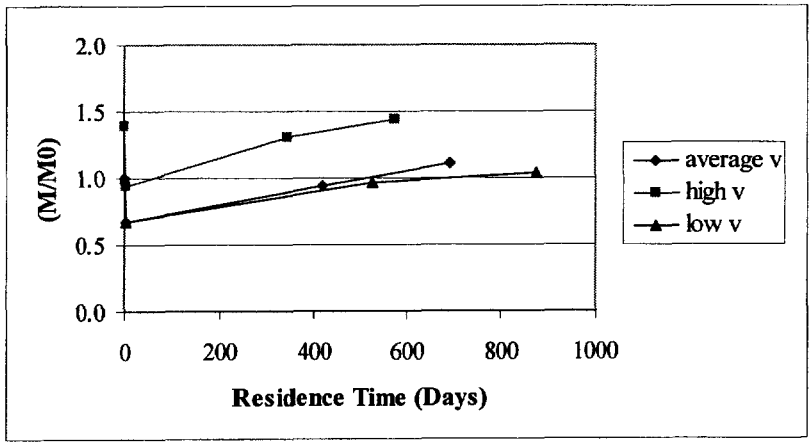

(b)

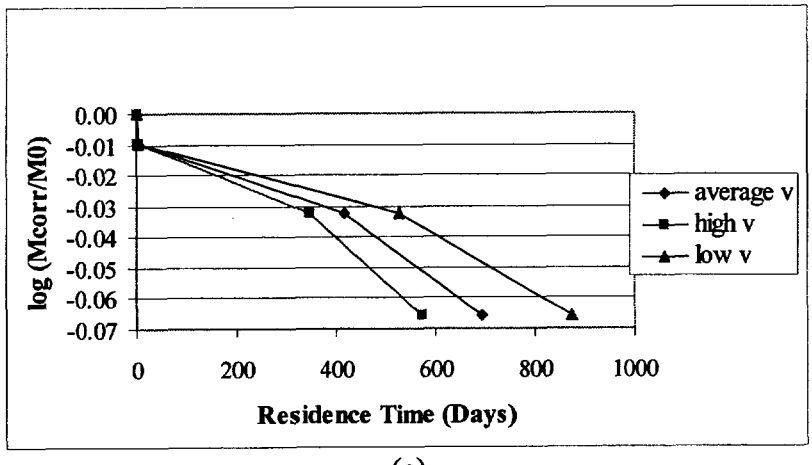

(c)

Figure 5.9: Contaminant Profiles for (a) Ideal MTBE Tracer (No Degradation), (b) Uncorrected MTBE (Degradation), and (c) Tracer-Corrected MTBE (Degradation) Using Fences with 30-m Spacing and Uniform Velocities

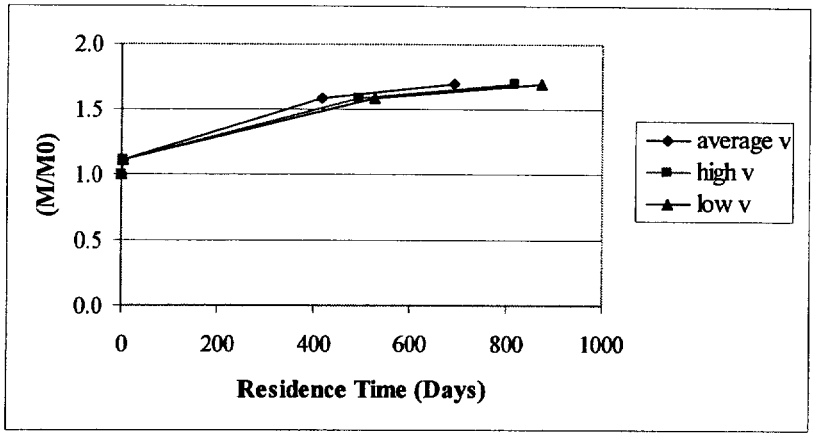

(a)

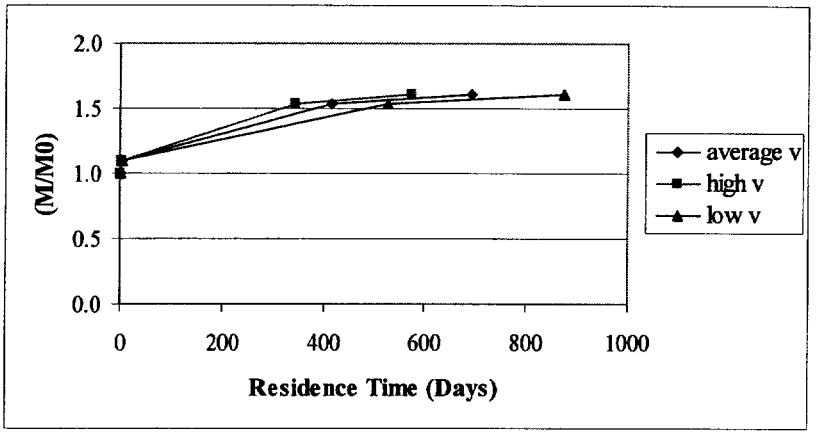

(b)

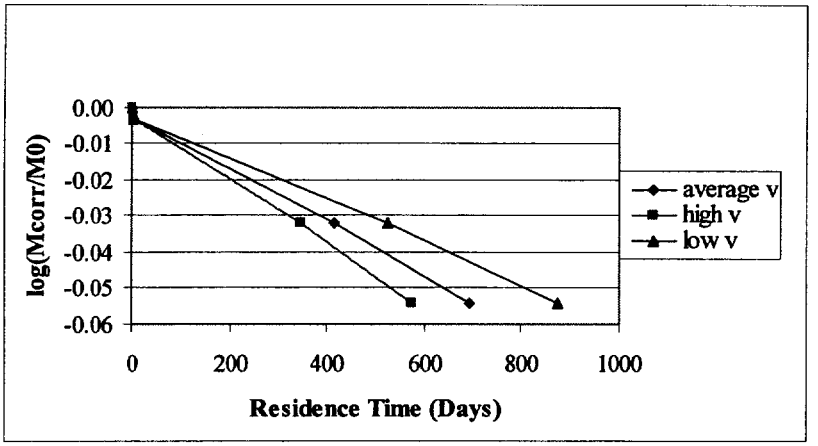

(c)

Figure 5.10: Contaminant Profiles for (a) Ideal MTBE Tracer (No Degradation), (b) Uncorrected MTBE (Degradation), and (c) Tracer-Corrected MTBE (Degradation) Using Fences with 15-m Spacing and Local Velocities

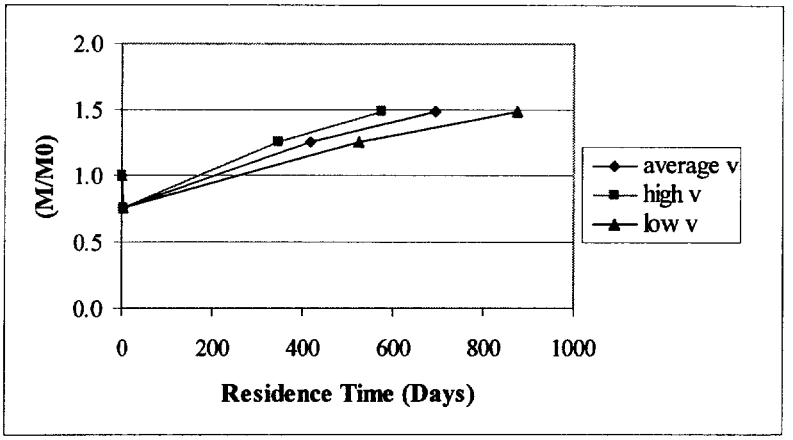

(a)

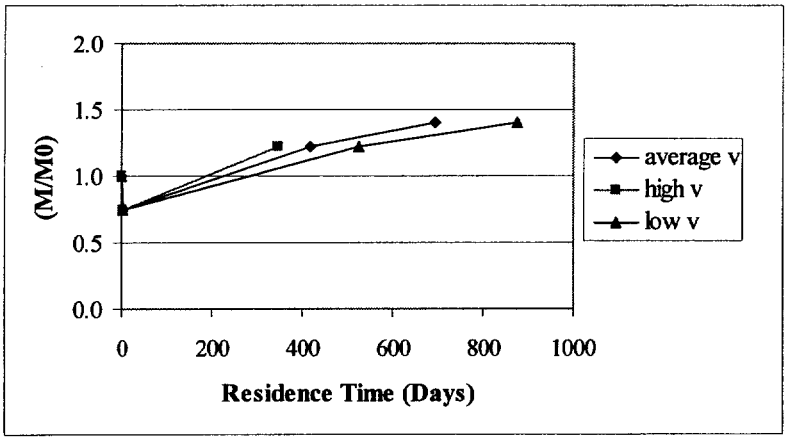

(b)

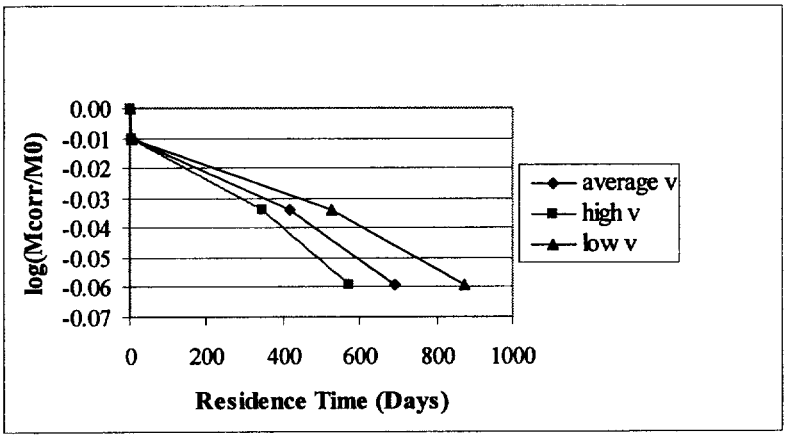

(c)

Figure 5.11: Contaminant Profiles for (a) Ideal MTBE Tracer (No Degradation), (b) Uncorrected MTBE (Degradation), and (c) Tracer-Corrected MTBE (Degradation) Using Fences with 30-m Spacing and Local Velocities

and MTBE plots show slightly different behavior for the 15-m and 30-m well spacing, suggesting that well spacing may have played a role in the quality of the attenuation-rate data. The significance of these observations were further investigated and are discussed below.

The calculated attenuation rates for all sets of benzene and MTBE data without and with correction by ideal tracer data are summarized in Figure 5.12 (a) and (b), respectively. The figure illustrates clearly the necessity of the tracer to extract a degradation rate from the MTBE data. Although the rates changed, the impact of degradation on benzene was evident even without the ideal tracer data.
Table 5.2 shows the upper and lower 95 percent confidence interval boundaries on the tracer-corrected attenuation rates calculated from the fence data. Non-zero attenuation rates were observed for both compounds. The calculated k values were similar for 15-m and 30-m well spacing; however, the range of the 95 percent confidence interval was wider for the 30-m spacing for both the uniform and local velocities. This suggested that while a degradation rate may be determined equally well with fewer wells, tighter well spacing will be needed to minimize the uncertainty. The calculated rates may still be insignificant for MTBE, however, because of very low apparent degradation rates and uncertainty attributable to the source function and velocity profile.

5.4 Implications

The analysis presented here incorporates a corresponding "no degradation" scenario to serve as the ideal conservative tracer in calculating degradation rates. In reality, the ideal tracer does not exist due to different fractions in the NAPL, solubilities, and retardation coefficients. Trimethylbenzenes (TMBs) and tetramethylbenzenes have been suggested as possible tracers for benzene (Weidemeier et al. 1995); however, the extent to which they are retarded due to sorption may be significantly different than for benzene. Given the plots of benzene concentration with time, incorporating the tracer data was not necessary to conclude that benzene degradation was occurring, although it changed the rate of observed degradation. Tracer data was critical to calculating

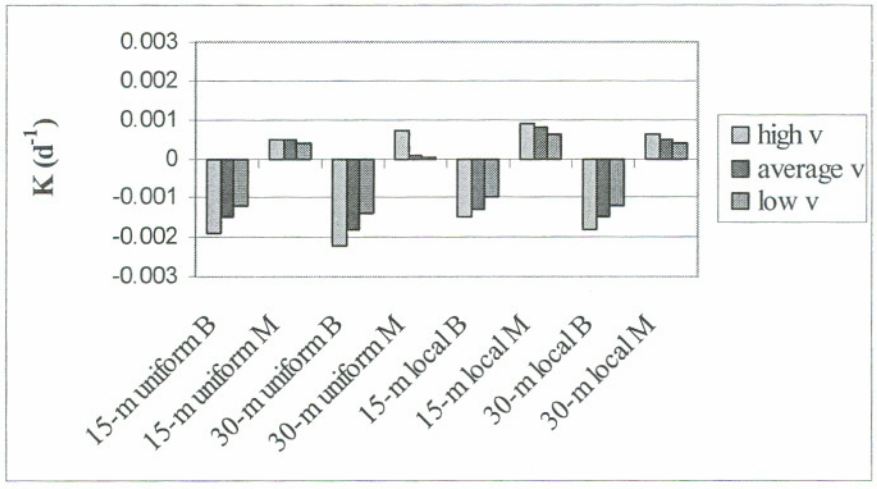

(a)

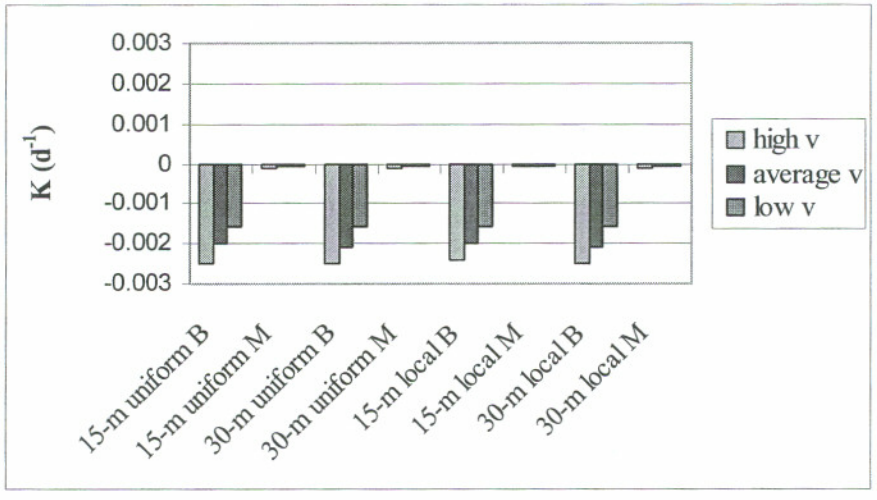

(b)

Figure 5.12: Benzene (B) and MTBE (M) Apparent Attenuation Rates Calculated from the Fence Data (a) Without Tracer Data Correction and (b) With Correction

Table 5.2: Apparent Attenuation Rates and Confidence Intervals from Fence Benzene and MTBE Measurements

15-m Spacing/Uniform Velocity Profile						
	Benzene			MTBE		
	Upper 95%	Apparent K (d^{-1})	Lower 95%	Upper 95%	Apparent K (d^{-1})	Lower 95%
High V	-0.0029	-0.0025	-0.0021	-0.0001	-0.0001	-9E-5
Average V	-0.0023	-0.002	-0.0017	-9E-5	-8E-5	-7E-5
Low V	-0.0019	-0.0016	-0.0013	-7E-5	-6E-5	-5E-5
30-m Spacing/Uniform Velocity Profile						
	Benzene			MTBE		
	Upper 95%	Apparent K (d^{-1})	Lower 95%	Upper 95%	Apparent K (d^{-1})	Lower 95%
High V	-0.0034	-0.0025	-0.0015	-0.0002	-0.0001	-3E-5
Average V	-0.0029	-0.0021	-0.0013	-0.0001	-9E-5	-3E-5
Low V	-0.0022	-0.0016	-0.001	-0.0001	-7E-5	-2E-5
15-m Spacing/Local Velocity Profile						
	Benzene			MTBE		
	Upper 95%	Apparent K (d^{-1})	Lower 95%	Upper 95%	Apparent K (d^{-1})	Lower 95%
High V	-0.0028	-0.0024	-0.0020	-0.0001	-9E-5	-7E-5
Average V	-0.0023	-0.002	-0.0017	-0.0001	-8E-5	-6E-5
Low V	-0.0019	-0.0016	-0.0013	-7E-5	-6E-5	-5E-5
30-m Spacing/Local Velocity Profile						
	Benzene			MTBE		
	Upper 95%	Apparent K (d^{-1})	Lower 95%	Upper 95%	Apparent K (d^{-1})	Lower 95%
High V	-0.0036	-0.0025	-0.0015	-0.0002	-0.0001	-4E-5
Average V	-0.0030	-0.0021	-0.0012	-0.0001	-8E-5	-3E-5
Low V	-0.0023	-0.0016	-0.0009	-0.0001	-7E-5	-3E-5

degradation rates for MTBE in this analysis; however, an appropriate tracer compound for comparison to MTBE is not present in oxygenated fuels. This represents a significant complication for MTBE compared to benzene.

Part of the need for the tracer stemmed from the influence of the source function. The exponentially decaying source function incorporated into the modeling resulted in increasing concentrations with distance away from the source. The effect was masked somewhat as dispersion acted to reduce concentrations. The benzene data showed that degradation was rapid enough over the 10-year simulation period to cause a measurable reduction in downgradient concentrations, minimizing the effect of the source function. Unlike the benzene case, the MTBE data showed that the source function dominated over changes due to degradation. Without the tracer, natural attenuation of MTBE could not have been demonstrated in the absence of source function data. The dissolution results from the physical model study demonstrated that source behavior is more complicated than the exponential source used in the numerical model. Consequently, greater attention to residual non-aqueous phase gasoline distribution and source function characterization is required for MTBE.

Hydrogeology will influence the distribution of NAPL in the source zone as well as the flow characteristics of the contaminant plume. In this analysis, the most significant influences of hydrogeology were the high groundwater velocity and associated dispersion. Despite the evidence of degradation, physical processes dominated the MTBE behavior. Laboratory and field degradation rates for MTBE must be balanced against plume expansion due to advection and dispersion to determine whether or not natural attenuation will ultimately stabilize and shrink the contaminant plume.

The sampling network can also have an important impact on the demonstration of natural attenuation of MTBE. The complications associated with MTBE as illustrated by this analysis imply that monitoring networks at an oxygenated fuel site may have to address BTEX and MTBE independently. The transect data produced a degradation rate for benzene but none for MTBE. The fence data produced a narrower range of rates with smaller well spacing. Given the low MTBE degradation rates, well spacing in a fence may be the difference between reasonably concluding that degradation has (or has not) occurred and having rates ranging from degradation to production.

The techniques used to quantify attenuation due to degradation in this analysis are simple, straightforward approaches to demonstrating natural attenuation. Benzene degradation was readily demonstrated with or without the tracer data or knowledge of the source function. Although MTBE degradation did occur, tracer data was necessary to determine a degradation rate for MTBE. If the source function had been known, the downgradient impact could have been accounted for and an attenuation rate could have been calculated. Nonetheless, a conservative tracer would have been needed to extract a degradation rate from the overall attenuation rate due to physical processes. Based on this information, MNA for MTBE requires a much more sophisticated approach to demonstrating field degradation rates than what is needed for BTEX compounds.

5.5 References

Barker, J.F., C. Beland-Pelletier, F. Blaine, C.F. Devlin, M.W.G. King, M.Schirmer. 2000. Monitored Natural Attenuation- Can Mass Flux Through Monitoring Fences Document Mass Loss in Groundwater Plumes?Groundwater 2000: International Conference on Groundwater Research. Copenhagen, Denmark. June 6-8, 2000.

Borden, R.C., R.A. Daniel, L.E. LeBrun, IV, and C.W. Davis. 1997. Intrinsic Biodegradation Rates of MTBE and BTEX in a Gasoline-Contaminated Aquifer. *Water Resources Research.* 33(5):1105-1115.

Squillace, P.J., J.F. Pankow, N.E. Korte, and J.S. Zogorski. 1997. Review of the Environmental Behavior and Fate of Methyl *tert*-Butyl Ether. *Environmental Toxicology and Chemistry.* 16(9): 1836-1844.

USEPA. 2000. Office of Research and Development. *Natural Attenuation of MTBE in the Subsurface under Methanogenic Conditions*, Research Report, EPA 600/R-00/006. Cincinnati, Ohio: U.S. E.P.A.

Wiedemeier, T.H, J.T. Wilson, D.H. Kampbell, R.N. Miller, and J.E. Hansen. 1995. Technical Protocol for Implementing Intrinsic Remediation with Long-Term Monitoring for Natural Attenuation of Fuel Contamination Dissolved in Groundwater. Air Force Center for Environmental Excellence, Brooks Air Force Base, San Antonio, TX.

BIOGRAPHICAL SKETCH

Illa Amerson was born in Sacramento, California on February 7, 1970. She was raised in Sacramento until 1983, when she left to attend high school at Santa Catalina School in Monterey, California. She attended Massachusetts Institute of Technology and graduated with a Bachelor of Science degree in Chemical Engineering in 1991. Illa moved to Phoenix, Arizona in 1991 where she worked as a hydrologist and environmental engineer at the Arizona Department of Environmental Quality and EMCON Consultants (now part of IT Group) while working on her Masters degree. She earned a Master of Science in Civil and Environmental Engineering from Arizona State University in 1997. Illa's Masters research was with Dr. Paul C. Johnson and involved developing innovative tools for monitoring and optimizing in-situ air sparging systems for groundwater remediation.

Illa met Rick Johnson while working on her Masters degree and eventually came to OGI to work with him in 1998. While at OGI, Illa continued her work with in-situ air sparging by evaluating its potential to remediate groundwater contaminated with methyl tert-butyl ether (MTBE). Her doctoral work ultimately focused on critical data requirements for demonstrating natural attenuation of MTBE. In addition to her research, Illa was an active member of the OGI Student Council and a team leader with the Advocates for Women in Science, Engineering, and Mathematics (AWSEM) program. Her research, leadership, and service earned her the Oregon Graduate Institute of Science and Technology's "Student Achievement Award" in 2000. In March of 2002, Illa became the American Geophysical Union's 2002-2003 Congressional Science Fellow, earning the opportunity to work in a Congressional office for a year after finishing her Ph.D. Illa completed her degree requirements in August of 2002.

PUBLICATIONS

Amerson, I. L., Johnson, R. L. A Natural Gradient Tracer Test to Evaluate Natural Attenuation of MTBE Under Anaerobic Conditions. *Ground Water Monitoring and Remediation* (accepted)

Amerson, I. L., Bruce, C. L., Johnson, P. C., Johnson, R. L. 2001. A Multi-Tracer Push-Pull Diagnostic Test for In Situ Air Sparging Systems. *Bioremediation Journal* 5(4): 349-362.

Bruce, C. L., Amerson, I. L., Johnson, R. L., Johnson, P. C. 2001. Use of an SF_6-Based Diagnostic Tool for Assessing Air Distributions and Oxygen Transfer Rates during IAS Operation. *Bioremediation Journal* 5(4): 337-347.

Johnson, R. L., Johnson, P. C., Amerson, I. L., Johnson, T. L., Bruce, C. L., Leeson, A., Vogel, C. M. 2001. Diagnostic Tools for Integrated In Situ Air Sparging Pilot Tests. *Bioremediation Journal* 5(4): 283-298.

Johnson, P. C., Leeson, A., Johnson, R. L., Vogel, C. M., Hinchee, R. E., Marley, M., Peargin, T., Bruce, C. L., Amerson, I. L., Coonfare, C. T., Gillespie, R. D. 2001. A Practical Approach for the Selection, Pilot Testing, Design, and Monitoring of In Situ Air Sparging/Biosparging Systems. *Bioremediation Journal* 5(4): 267-281.

Amerson, I. L. and Johnson, R. L. 2000. Evaluation of *In Situ* Air Sparging for MTBE Removal from a Gasoline Source. *Preprints of Extended Abstracts 219th ACS National Meeting*, San Francisco, CA, Division of Environmental Chemistry, American Chemical Society, Vol. 40, No. 1, pp. 247-250.